

ADVERTIMENT. L'accés als continguts d'aquesta tesi queda condicionat a l'acceptació de les condicions d'ús establertes per la següent llicència Creative Commons:  <https://creativecommons.org/licenses/?lang=ca>

ADVERTENCIA. El acceso a los contenidos de esta tesis queda condicionado a la aceptación de las condiciones de uso establecidas por la siguiente licencia Creative Commons:  <https://creativecommons.org/licenses/?lang=es>

WARNING. The access to the contents of this doctoral thesis it is limited to the acceptance of the use conditions set by the following Creative Commons license:  <https://creativecommons.org/licenses/?lang=en>

UAB

Universitat Autònoma de Barcelona

Facultat de Biociències

Departament de Genètica i de Microbiologia

Grup de Mutagènesi

Environmentally representative true-to- life nanoplastics as model test materials for human health risk evaluation.

DOCTORAL DISSERTATION

Aliro Villacorta

2024

UAB

Universitat Autònoma de Barcelona

Facultat de Biociències

Departament de Genètica i de Microbiologia

Grup de Mutagènesi

Environmentally representative true-to-life nanoplastics as model test materials for human health risk evaluation.

To Universitat Autònoma de Barcelona in partial fulfillment of the requirements for the degree of Doctor of Philosophy, as per the Doctorate Program in Genetics

Under the supervision of Dra. Alba Hernández Bonilla

**Dra. Alba
Hernández Bonilla**

**Aliro
Villacorta Villacorta**

AKNOWLEDGMENT

I would like to begin this section by expressing my heartfelt thanks to Ricard Marcos for his endless patience and always thoughtful advice, for his guidance along this journey, which has been as short as it has been intense and enriching. I also want to thank Alba Hernandez, who, together with Ricard, has not only imparted scientific knowledge but has also taught me how to navigate the path of becoming a functional scientist in the demanding times we face.

I am deeply grateful to Catalunya for welcoming and embracing us during this period, and for playing an integral part in the growth of our little Lilith, giving her a unique personality, distinct from my own and from Camila's—my best life companion, who, in ways I neither understand nor expect to, chose to walk this path together with me. I also thank Kimbo for bringing us joy and companionship. Additionally, I hold Catalunya responsible for bringing Glòria Umbert into my life—someone I was warned about, with remarkable accuracy, as someone I would grow to deeply cherish. I must also thank this land for leading me to Cristian Valiente, who, along with Glòria, is the heart of the space where, in my opinion, good science is made. You both breathe life into the space we share.

I am grateful to my lab colleagues—without you, everything this work represents would be nothing more than words on paper. My fellow predocs, Joan and Javi, who taught me the difference between helping and collaborating. To those who, through proximity, shared experiences, battling the same daily challenges, or simply by choice, I grew closer to during this time. I'd like to highlight Lourdes Vela, whose presence always sharpened the focus of everyone fortunate enough to have her nearby. To Michelle Morataya-Reyes, who, as I mentioned during a conference, has been crucial in helping me maintain mental peace. To Alireza and Gooya, with whom I've shared countless moments over coffee, ice cream, and tea. And to Bala, who was kind enough to invite me into his home, introduce me to his family, and share his outlook on life.

I am also deeply grateful to those who, despite the distance, have never ceased to be present. To my wonderful family—Claudio, Fernanda, Limbert, and little Agustín—and especially to my mother Mariela, who as always with just a glance has reminded me countless times of the reason behind everything I do.

To those who have been fundamental to my professional development and who, without seeking it, have earned a permanent place in my heart and have instilled in me a deep appreciation for public education—Jose Delatorre, Felipe Carevic,

Erico Carmona, Miguel Zarzar, Eduardo Peña, and Ricardo Tejos. To Álvaro Carevic, for not letting me go, and to Pedro Buc, for his unwavering support.

To my friends, I am incredibly grateful for your constant presence—Jose Pablo and Cristofer I truly have no words for you guys.

I also wish to extend my gratitude to all the members of the Universitat Autònoma de Barcelona, the Institut Català de Nanociència i Nanotecnologia (ICN2), the Institut de Ciència de Materials de Barcelona (ICMAB), and especially to the teams at the Servei de Microscòpia i Difracció de Raigs X (SMIDRX) and the Servei de Cultius Cel·lulars, Producció d'Anticossos i Citometria (SCAC). I also want to thank to the Chilean Government particularly to the CONICYT (currently ANID) Becas Chile program (PFCHA/DOCTORADO BECAS CHILE/2020–72210237) and extend this to my beloved Universidad Arturo Prat along with the countless students who have passed through the classrooms where I've had the privilege to teach. They are the driving force behind all of this.

To the European project PlasticHeal (*Innovative tools to study the impact and mode of action of micro and nanoplastics on human health: towards a knowledge base for risk assessment* H2020-965196), to the Generalitat de Catalunya and the Spanish Ministry of Science and Innovation for partially finance this research 2021-SGR-00731 and PID2020-116789, RB-C43, respectively.

Finally, to anyone who has taken the time to read this far, I want to say that everyone who has been part of this journey should be included in this expression of gratitude. However, if you know me, you'll understand that I lack the gift of finding the perfect words at the right moment, and now is not the time for that to change. But know that you have all shaped the person who is writing these words today.

ABSTRACT

The pervasive presence of micro- and nanoplastics (MNPLs) in the environment has recently emerged as a critical issue. The global population is unavoidably exposed to these plastic particles, making it essential to define the hazards and risks posed by MNPL exposure to ensure the health and wellbeing of the population. However, this task remains unfeasible due to significant scientific knowledge gaps. One of the most prominent gaps is the lack of realistic reference materials for conducting hazard and risk assessments. As a result, the vast majority of studies have used pristine plastics, such as polystyrene beads, which differ significantly from the nanoplastics found in nature. This limits the reliability of the evidence generated. Thus, there is an urgent need for environmentally relevant test materials to improve MNPL health hazard and risk assessments.

In this context, the present work aims to generate and validate the usefulness of in house made true-to-life nanoplastics, derived from the degradation and fragmentation of larger plastic materials, as realistic models of secondary nanoplastics found in the environment. To achieve this, the proposed approach is based on mechanical degradation processes that mimic environmental conditions, ensuring that the resulting nanoparticle models closely resemble those present in ecosystems. Consequently, this allows for more meaningful assessments of uptake, distribution, and toxicity in toxicological studies, facilitating subsequent risk assessment evaluations.

Three sub-objectives were defined for this work. The first objective was to develop a reliable method for the production and characterization of micro- and nanoplastics derived from commercially available polyethylene terephthalate (PET) water bottles. PET was chosen due to its ubiquity, ease of access, and its status as one of the most widely distributed single-use plastics, making it a common pollutant in landfills and water bodies.

The nanoplastic particles generated using the proposed method exhibited a wide range of sizes, consistent with what would be expected in real environmental samples. Additionally, initial toxicity assessments were conducted on human-derived THP1 and TK6 cells, showing no detectable signs of DNA damage at the studied concentrations or endpoints. However, a trend in reactive oxygen species (ROS) induction was observed, indicating the need for refined methodologies or

endpoints to accurately assess the risks associated with exposure to true-to-life PET MNPLs.

The second objective focused on the production of titanium-doped PET (PET-Ti) MNPLs from opaque PET milk bottles. Titanium serves as a useful marker for tracking MNPLs in complex biological systems due to its high electron density and visibility through techniques like electron microscopy. PET-Ti MNPLs were successfully produced and characterized, with titanium content demonstrating consistent distribution throughout the nanoplastics, although minor variability in titanium levels was observed, which may have implications for response-related outcomes. Toxicological assessments revealed that PET-Ti MNPLs did not significantly affect the viability of human-derived hematopoietic cells at sub-lethal concentrations, supporting their potential use as a model for future studies on MNPL interactions in biological systems.

The third and final objective was to develop a simplified and cost-effective method for labeling micro- and nanoplastics (primarily true-to-life) for use in biological applications. This was an adaptation of existing methodologies, with a specific focus on true-to-life nanoplastics, ensuring that the physicochemical properties of the original particles were minimally altered. Various dyes were tested, with iDye PolyPink proving to be the most suitable and reliable for staining both commercially available and in-house-produced plastic nanoparticles. The staining process was validated through confocal microscopy, confirming the presence of labeled nanoparticles in human-derived THP1 cells. For true-to-life PET-Ti MNPLs, experimental approaches were conducted in human-derived hepatocyte cell lines, demonstrating the technique's versatility and compatibility with biological models and more complex polymeric matrices. The particles maintained their structural integrity while enabling clear visualization in biological matrices, reducing the likelihood of false positives.

In conclusion, this dissertation presents significant advancements in the production and application of true-to-life nanoplastics for evaluating the health risks associated with MNPL exposure. The methodologies developed here provide a solid foundation for current and future research, highlighting the importance of extensive MNPL characterization for both *in vitro* and *in vivo*

studies aimed at understanding the complex interactions between nanoplastics and human health.

ABBREVIATION LIST

ABS	Acrylonitrile butadiene styrene
AF4	Asymmetric flow field flow fractionation (AF4)
ASTM	American Society for Testing and Materials
DHE	Dihydroethidium
DLS	Dynamic light scattering
EDS	Energy dispersive X-ray microscopy
ENPs	Engineered nanoparticles
ENPLs	Engineered nanoplastics
FBS	Fetal bovine serum
FTIR	Fourier transmission infrared spectroscopy
HDPE / PE-HD	High density polyethylene
HUH-7	Human derived epithelial-like tumorigenic cell line
LDPE / PE-LD	Low density polyethylene
MADLS	Multi-angle dynamic light scattering
MMS	Methyl methanesulfonate
MNPLs	Micro and nanoplastics
MPLs	Microplastics
Mt	Metric tones
NPs	Nanoparticles
NPLs	Nanoplastics
PA	Polyamides
PBT	Polybutylene terephthalate
PC	Polycarbonate
PDI	Polydispersity index
PE	Polyethylene
PET / PETE	Polyethylene terephthalate
POM	Polyacetal
PP	Polypropylene
PPE	Polyphenylene ether
PS	Polystyrene
PUR	Polyurethane
PVC / V	Polyvinylchloride
Raji-B	Human derived lymphoblast-like cell line
RIC	Resin Identification Coding System
ROS	Reactive Oxygen Species
SDS	Sodium dodecyl sulfate
SEM	Scanning electron microscopy
SPI	Plastics Industry Association
TEM	Transmission electron microscopy
TFA	Trifluoroacetic acid
THP1	Human derived monocytic leukemia cell line
TK6	Human derived lymphoblast cell line

INDEX

1. INTRODUCTION.....	1
1.1. Plastic definition and classification.....	3
1.1.1. Plastic generation and fate	6
1.1.2. Additives.....	7
1.2. Micro and nanoplastics occurrence	8
1.2.1. Engineered nanoplastics	9
1.2.2. Reference materials	11
1.2.3. True-to-life nanoplastics	12
1.3. Health hazardous effects mediated by nanoplastics exposure	13
1.3.1. Exposure pathways	13
1.3.2. Health hazardous effects.....	15
2. OBJECTIVES	19
3. RESULTS	23
3.1. Chapter 1 (First Study).....	25
3.2. Chapter 2 (Second study).....	55
3.3. Chapter 3 (Third study)	83
4. DISCUSSION	113
4.1. Main objective brief.....	115
4.2. The need for true-to-life nanoplastic and the strategy for PET nanoplastic production	116
4.3. True-to-life PET MNPLs obtention	118
4.4. True-to-life titanium-doped PET MNPLs obtention	122
4.5. Research for a labelling efficient method for true-to-life MNPLs	125
4.6. Final remarks.....	127
5. CONCLUSIONS	131
6.- REFERENCES.....	135
7. ANNEXES	149
7.1. The pdf of the published paper entitled <i>A new source of representative secondary PET nanoplastics. Obtention, characterization, and hazard evaluation</i> . 151	
7.1.1. Supplementary material corresponding to the article entitled <i>A new source of representative secondary PET nanoplastics. Obtention, characterization, and hazard evaluation</i> (.....	163
7.2. Pdf of the article entitled <i>Titanium-doped PET nanoplastics of environmental origin as a true-to-life model of nanoplastic</i>	175

7.3. Pdf of the article entitled <i>Fluorescent labeling of micro/nanoplastics for biological applications with a focus on "true-to-life" tracking</i>	185
7.3.1. Supplementary material of the article entitled <i>Fluorescent labeling of micro/nanoplastics for biological applications with a focus on "true-to-life" tracking</i>	197

INTRODUCTION

1. INTRODUCTION

1.1. Plastic definition and classification

Plastic:

- “From the Greek word plastikos (πλαστικός), meaning "capable of being moulded or shaped," modern-day plastics are synthetic materials that can be shaped when soft and then hardened into shape. In Ancient Greece, the "plastic arts" referred to sculpture”. (Hales-Brittain, 2023)
- “'plæstɪk, 'plɑːstɪk) Also 7–8 -tick, -tique, (8 plaistic). [ad. L. plastic-us (Vitr.), a. Gr. πλαστικός that may be moulded, belonging to moulding or modelling, plastic, f. πλαστός formed, moulded, f. πλάσσειν to mould, form. So F. plastique (1556 in Hatz. - Darm.).] Also “A substance that is easily moulded or shaped under some conditions but that solidifies as it cools, dries, etc. Also, figurative.” (Oxford Ddictionary, 2024)
- An artificial substance that can be shaped when soft into many different forms and has many different uses.” (Cambridge Ddictionary, 2024)

Plastics are commonly referred to in literature as polymers, which are widely used in everyday life. Polymers in turn are macromolecules composed of smaller and simpler molecules called monomers (IUPAC, 2009), which can be described as the building blocks of these macromolecules. This distinction is important for understanding the extensive use of the terms nanoplastics (NPLs), microplastics (MPLs), or micro and nanoplastics (MNPLs) throughout this document.

Plastics can be classified in various ways based on their different characteristics:

- **Chemical Structure and Behavior Related to Temperature:** Plastics are commonly divided into two main categories—thermoplastics and thermosets (PlasticsEurope, 2019). However, elastomers are often included as a third category for rubbers. Thermoplastics can be melted and hardened repeatedly with temperature changes, whereas thermosets undergo chemical changes when heated and cannot be remelted and reformed.
- **Polarity:** Plastics can also be classified based on their polarity, which refers to the presence of different atoms that generate electron movement. Understanding this phenomenon is crucial because it influences the polymer's mechanical resistance, rigidity, and chemical resistance. As polarity increases, the polymer's resistance to weathering conditions improves, distinguishing among polyolefins, polyesters, halogenated polymers, and others.

- **Utility:** Exclusively for thermoplastics, a classification based on utility divides plastics into four subdivisions:
 - **Standard and Commodities:** These are produced in large quantities due to their low cost and desirable properties. Examples include polyethylene (PE), polypropylene (PP), polystyrene (PS), polyvinylchloride (PVC), and the copolymer acrylonitrile butadiene styrene (ABS).
 - **Engineering Plastics:** These polymers are notable for their transparency and good structural properties, such as polyamides (PA), polyacetal (POM), polycarbonate (PC), polyethylene terephthalate (PET), polyphenylene ether (PPE), and polybutylene terephthalate (PBT).
 - **Special plastics:** They possess a remarkable degree of a particular property, such as the excellent transparency and light stability of polymethyl methacrylate (PMMA), or the strong resistance to temperature and chemicals of polytetrafluoroethylene (Teflon).
 - **High-performance plastics:** Most of them are thermoplastic with excellent heat resistance. Specifically, they maintain strong mechanical properties at high temperatures, typically up to 150°C. Examples of high-performance plastics include polyimide (PI), polyethersulfone (PES), polysulfone (PSU), polyphenylene sulfide (PPS), polyarylsulfone (PAS), and liquid crystal polymers (LCP).
- **Carbon Source Origin:** Plastics can be categorized based on the origin of the carbon source—either from the petrochemical industry (fossil-based) or from recently grown biomass (biobased). It is important to note that not all biobased nanoplastics are biodegradable.

In contemporary discourse, the classification of plastics emphasizes their end-of-life characteristics, rather than their origin or intended functional properties, due to their persistence in the environment. According to recent literature (Pilapitiya & Ratnayake, 2024), the widespread presence of plastics in daily life and the substantial increase in their production volumes can be attributed primarily to their effectiveness as alternatives to traditional materials. This trend has been further driven by significant demographic changes, with the global population expanding from approximately 2.5 billion to over 8.16 billion since plastics emerged as a viable material substitute. The situation is exacerbated by the ease of access to plastic materials and their derivatives in a consumer-driven society.

This context underscores the necessity of innovative approaches to managing plastic waste. To facilitate this process, the Society of the Plastics Industry, known as the

Plastics Industry Association (SPI), collaborated with the American Society for Testing and Materials (ASTM) to revise and update the nomenclature used by producers and recyclers of plastic materials. This collaboration culminated in the updated Resin Identification Coding System (RIC) introduced in recent years (ASTM, 2013, 2016) as summarized in **Fig. 1**.

The RIC classification has been employed to categorize the six most prevalent types of plastics in the market, thereby facilitating their identification for use and disposal. The correct application of this classification is crucial, as improper use can lead to significant issues in production lines, reintegration into the supply chain, or adverse effects on consumer well-being. The natural shift of markets toward greener and more sustainable economies, coupled with strict regulations on single-use plastics and the increasing societal preference, driven by necessity and choice, for more sustainable products, is likely to create an imbalance soon. This shift may alter the production landscape of the six primary plastics, enabling modern plastics, such as PLA (polylactic acid), to gain market share. This development may necessitate a revision of the classification codes, allowing these advanced plastics to move from category 7 into one of their own.















Type of Resin	Resin Identification Code-Option A	Resin Identification Code-Option B
Poli(ethylene terephthalate)	 PETE	 PET
High density polyethylene	 HDPE	 PE-HD
Poly(vinyl chloride)	 V	 PVC
Low density polyethylene	 LDPE	 PE-LD
Polypropylene	 PP	 PP
Polystyrene	 PS	 PS
Other resins	 OTHER	 O

Figure 1: Resin identification coding system consisting in an equilateral triangle, an identification number and an abbreviated term for polymeric material.

1.1.1. Plastic generation and fate

Plastics consumption, and therefore generation, is steadily growing and year by year reports indicate that the number is far from decreasing. Plastic production can be numbered in more than 400 million tons in 2022 (Garside, 2024). This story can be backdated as far as 1850 but in a more unnecessarily strict sense we can highlight the emergency of “Parkesine”, a slightly moldable ivory-like resin product of the dissolution of cotton initially used for the insulation of telegraph wires (Parkes, 1866) or celluloid as the first ever man-made plastic (Freinkel, 2011). And followed in 1907 by the first plastic entirely made from chemicals --phenol and formaldehyde—on an autoclave. A creation that was at the same time the first fully synthetic thermoset named bakelite after the Belgian-born chemist Leo Hendrik Baekeland (Bakelizer, 1993). PVC in turns, can be considered the first “modern plastic” with more complex additive-added formulations and the look for more “desirable characteristics” that make it in the decade of 1920 a more technological material than its predecessors (Mulder & Knot, 2001). Those early events have profoundly influenced the course of human history in ways that remain difficult to quantify even today.

The starting point of the plastic generation era is conveniently coincident with the dawn of a geological period named the Anthropocene and is backdated to the decade of 1950. At this point, it is important to highlight that the very definition of an age, implies the possibility of major changes though in this case the relationship between the human being and the planet, demonstration of the possibility to interfere and modify the geochemical cycles, climate and biosphere (Morand & Lajaunie, 2018). Some have made even balder declarations and socially and openly speak about a new *Plasticene* era (Reed, 2015). What is to be considered is that beyond any reasonable doubt, stratigraphically speaking, plastics have owned their place within sediments comprising a good indicator of the Anthropocene era strata (Zalasiewicz et al., 2016).

By 2017, the estimated global production of plastics was estimated at more than 348 Mt. By this date, the global production of plastic was comparable with the mass of 900000 Eiffel towers, 88 million blue whales or 1.2 billion elephants (Geyer, 2020). In 2018 the global production rise to 370.5 Mt, and by 2020 it already passes the 400.3 Mt. The geographical distribution of the plastic production, as well as the type of plastic produced are represented on **Figs. 2a & b**, respectively. On the other hand, according to the origin of the plastic represented on **Fig. 2c**, it is easy to observe that more than 90% of all plastic produced are fossil-based.

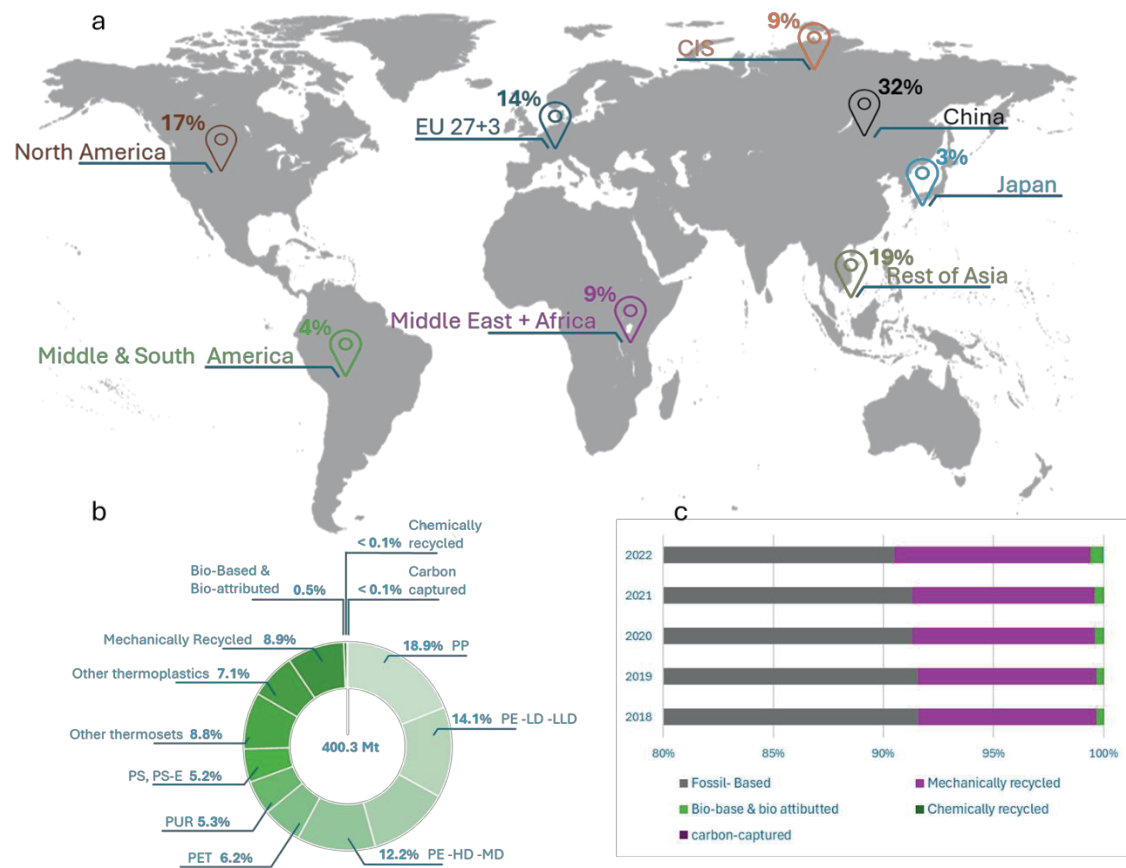


Figure 2: Global production of plastics by 2022 (a). Type of plastic produced (b) and origin of the raw material for plastic production (c).

1.1.2. Additives

Even considering that it is beyond the scope of the present Thesis, is important to keep in mind that an important part of the final product on modern plastics are additives that change, enhance or minimize some important characteristics of the final products. Among the most important there are plasticizers, and flame retardants that comprise more than 75% percent of the used additives. Plasticizers are applied to plastics and elastomers to improve their workability, distensibility and flexibility, among other characteristics, and are easily found in massively distributed devices from food packaging to complex medical devices though daily used cosmetic products (Gwenzi et al., 2022). The degradability of these products is rather short in a geological scale — generally ranging on weeks' time— but there are reports that warn about risk of some of these compounds for human, organisms, and ecosystems in general regardless the lack of persistency (Billings et al., 2021). In the other hand, related to flame retardants, there is very limited information in literature regarding its ecological impact, and even more

scarce when it comes to the biological impacts. The remarkable exception are the brominated compounds that are the most persistent, and more studies have been performed showing they are widely distributed.

It is relevant to remain vigilant on the true nature of the discarded plastic waste since plastic additives can represent a high proportion (7%) of its composition including compounds such as lubricants, colorants, antioxidants, and heat stabilizers.

1.2. Micro and nanoplastics occurrence

For the first time in literature, the concept of small sized plastic arises in 2004 (Thompson et al., 2004). At that time, it was already clear for the authors that the visible fraction or even the bigger portion of that, should be only a small proportion of what is out there. Moreover, it was already a matter of concern the possibility of these emergent pollutant to enter the food chain or the possibility or potential for this small fraction of plastics to carry different toxicants that was noted very early on and later confirmed and even differentiated between the type of polymer (Browne et al., 2008; Teuten et al., 2007). These are the first steps in a long road of discoveries that set the basis for the understanding of why the smaller fraction of plastic debris should be studied.

Microplastics or microlitter has been described extensively in the past. The definition that it is accepted the most, and with which the scientific community has shown more sympathy, seems to be the provided in 2003 by Gregory and Andrady, where they proposed microlitter or microplastics as the barely visible particles that pass through a 500 μm sieve but retained by a 67 μm sieve (Gregory & Andrady, 2003). Where the conversation gets more controversial is on the definition, or more specifically where are the limits for the correct use for the prefix nano. There is still no general agreement on what “nano” really means and it is not difficult to find different definitions even in different chapters of the same books. These differences range from those who define it as “minute fragments of matters that is less than 100 nm in diameter” using the definition of nanoparticle (Goh et al., 2016), to those who claim that plastic nanoparticles (NPs) are indeed “roughly defined as particles with a diameter smaller than 1 mm” (Attama et al., 2016). On a very strict sense one of these definitions the last contain the first and it seems that is more common to refer as nano, the otherwise known as submicrometric fraction. Nevertheless, and as can be assumed from the publication date these are old definitions submitted to multiple criticisms.

This is how there has been and still are scientific discussions on the correct use of the words and for the concrete case of nanoplastics the use of micro for particles ranging

from 1 to 1000 μm is beyond discussion. The term nano for those particles ranging from 1 to 100 nm is widely accepted but there is still a big proportion of the submicrometric range that remains undefined. The European Union has given some recommendations on the use of terminology, and it stand for the use of a looser that may contain the previous definitions in which at least 50% of the material must be on a scale of 1 to 100 nm in at least one of its dimensions (European Commission, 2022). Nevertheless, we consider that micro- and nanoplastics would be defined by their units (μm and nm). Thus, microplastics are those with an average range between 1 and 1000 μm , while nanoplastics are those with an average range between 1 and 1000 nm.

Nanoparticles, and particularly the nanoplastics, whether commercially available and in house made ones, are produced by two main means to be used as model materials to mimic what is in the environment. Those two methodologies are top-down or bottom-up (Pradel et al., 2023; Reynaud et al., 2022). Briefly, these two approaches consist in the breaking down of larger pieces until the required nanoscale is reached and in the assembly of molecules and atoms into larger nanostructures respectively.

From this conception, it is relatively easy to infer that there are two different types of nanoplastics according to the origin. Primary nanoplastics are those that are intentionally designed and manufactured and therefore their occurrence is intentional. In contrast, secondary nanoplastics result from the fragmentation of larger plastics due to weathering, which can be mechanical, physical, chemical, biological or more likely, a combination of these factors among others. For all the above, and due to the differences from one particle to the other is that we can summarize the relevant differences on nanoplastic.

1.2.1. Engineered nanoplastics

Engineered nanoplastics (ENPLs) are of anthropogenic nature and therefore engineered nanoplastics are necessarily primary nanoplastics. It has been stated by that nanoplastics differs from microplastics due to several characteristics as a) the Brownian movement that prevent its sedimentation or buoyancy, b) the interaction with light and its wave-like nature that allows the analysis though characteristics as the diffraction, c) the surface area volume ratio and its consequent molecule interactions, it is also relevant to remark the compatibility in terms of interaction with biota as it may be the uptake or the ability to penetrate though biological barriers or the accumulation. Derived from this it may result detrimental for living organisms due to the release of additives or substances that are constituent or carried by the nanomaterial. Nanoplastics also differs from engineered nanoplastics in several characteristics as just for start it is the particle

heterogeneity not only in composition as may result logical but also in terms of size distribution and geometry which at time may result from the degradation of the ENPLs itself. Therefore, the unique or distinct characteristics of NPLs will largely influence their environmental behavior, fate and of course interactions in contact with biological systems (Gigault et al., 2021), which may result in complex outcomes in terms of hazard evaluation or toxicity determination among others. And this is not going to deep into particle aggregation dynamics which is a whole topic on its own.

From 1965, with the first reports of polystyrene engineered nanoplastics (Matsumoto & Ochi, 1965), until the control on the size of the generated particles (Yun et al., 2010) polystyrene nanoparticles have been the most distributed nanoparticles for toxicology or hazard evaluation studies and have been increasingly defined as “nanoplastics” instead of nanoparticles (**Fig. 3**). This name discrepancy may result in data loss or result masking and, therefore, it is relevant that this lexical misunderstanding is at least considered when plastic nanoparticles and nanoplastics are studied. Less selective databases, like the one used here, have shown a similar trend (Gigault et al., 2021). Understanding the language limitations and considering the nature of the predominant materials used in the present work, the term nanoplastics will be used. To avoid any inconvenience the reference material used on the third study will be referred as well as polystyrene nanoplastics (PSNPLs) knowing that the term is both true and imprecise.

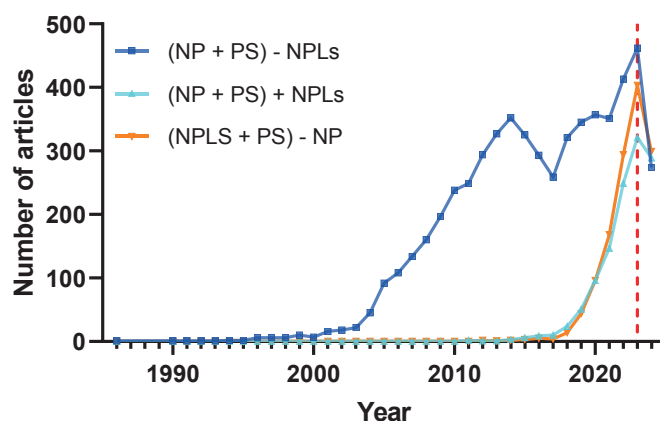


Figure 3: Number of articles related to the use of the terms nanoparticles and polystyrene used together in articles without the term nanoplastics (**blue**) and with the term (**turquoise**). The search was repeated using nanoplastic and polystyrene together, this time excluding the term nanoparticle (**orange**), and the result is similar with a slight increase in the last years. The search was carried out on PubMed using the terms "**Nanoparticle***" or "**Nano particle***" for **NP**; "**polystyrene***" for **PS**; and "**nanoplastic***" OR "**nano plastic***" for **NPLs**. As noticed the connectors were **AND (+)** and **NOT (-)** and the criteria was to include the whole text [**tw**]. On the graph, a red dashed line was added on 2024 since not all articles are included or indexed since the data was accessed during the course of the year 2024.

1.2.2. Reference materials

As previously stated, it is relevant for appropriate discussion and coherent conclusions to properly define the terms to be used. When it comes to size, nanoplastics upper limit have been widely discussed and seems that the limit is selected according to the study convenience. However, to set the ground we will consider a widely accepted definition that lies in ISO normative (Hartmann et al., 2019; ISO/TR 21960, 2020; Mitrano et al., 2021). Is important to highlight that nanoparticles are a subset of nanomaterials, and the common characteristic is the nano range being present in all three dimensions (Rist & Hartmann, 2018). However, as it is in this text, the term is also used to describe the particulate nature of the material, and the ranges are described in **Fig. 4**.

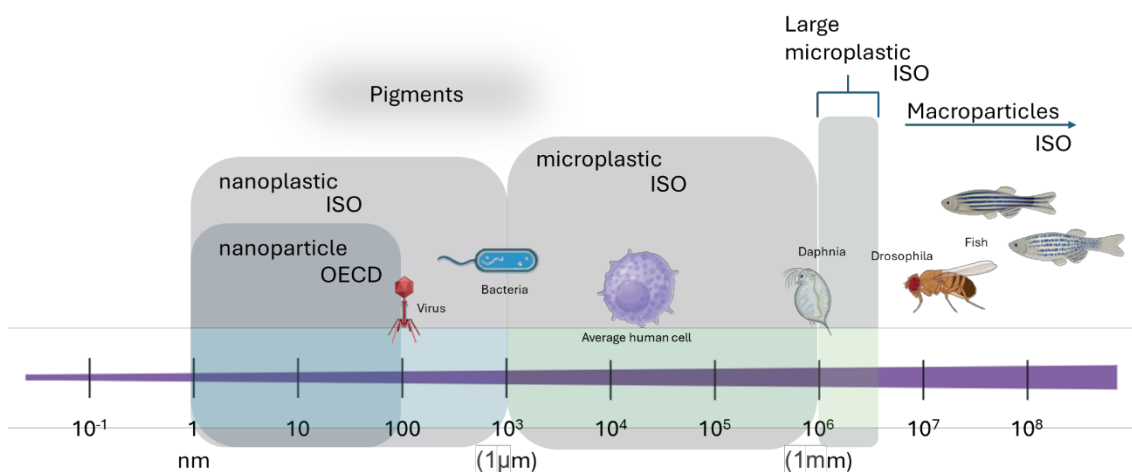


Figure 4: Description of the reference sizes for materials of anthropogenic origin compared with organisms and pigment pollutants according to ISO/TR 21960, and microplastic and nanoparticle according to ISO/TC 61 and OECD, respectively.

In a strict sense nanoplastics and reference materials are the most difficult combination since the production is usually not generating materials that are at the same time stable in terms of suspension and consistent in terms of repeatability. Efforts have been made on the look for reference materials and good results have been recently obtained for PP (Hildebrandt & Thünemann, 2023). There are also reports of representative nano PET which has a more realistic size distribution comparable with what is expected to be the degradation product of primary and secondary microplastics (Lionetto et al., 2021). The efforts in the hereby works goes precisely in this direction, trying to recreate the wide range of characteristics of environmentally present plastic nanomaterials and therefore to have more true-to-life particles for toxicology studies.

1.2.3. True-to-life nanoplastics

Understanding the concept of nanoplastics, it may seem redundant to emphasize the representativeness of nanoplastics compared to engineered plastic nanoparticles. However, it is also important to recognize the limitations of these materials and acknowledge that this is merely a necessary step toward increasing the verisimilitude of tested materials. This, in turn, helps reduce artifacts or potential misinterpretations in future toxicity studies. These steps are graphically depicted in **Fig. 5**, which illustrates the natural evolution in terms of the complexity of plastic nanoparticles used to achieve more accurate outcomes. These outcomes are intended to better represent the interactions between living organisms and plastic nanoparticulate materials.

It has been discussed how engineered nanomaterials—specifically, reference plastic materials or engineered plastic nanoparticles—have driven the modification of testing methods for assessing toxicity (Hartmann et al., 2019; Petersen et al., 2021, 2022). The literature clearly documents this transition, starting from the use of perfectly shaped and sized polystyrene nanoparticles (Rubio et al., 2020) to more complex models that simulate interactions with environments, such as the digestive tract (Vela et al., 2023). These evaluations can also be conducted using complex particles without environmental interactions, by simply altering the characteristics of the particles themselves, such as surface modifications (Martín-Pérez et al., 2024).

Thus, natural progress will converge toward increasingly complex models, such as the one proposed in this Thesis. These models are refined methods based on previous attempts (Rodríguez-Hernández et al., 2019), featuring tested purity and unaltered characteristics that better represent what is expected in environmental samples. This contrasts with surface modifications introduced through different and more technologically challenging production processes (Magrì et al., 2018). There is also the combination of production of true-to-life nanoplastics with the surface modification that better cover the possible differences of the less realistic plastic nanoparticles (Ducoli et al., 2022). These complex true-to-life nanoplastics are as far as we have arrived so far in science and the next steps are not only to try the toxicity outcome of combined pollutants that seems logic, but in recent years there have been efforts to isolate and measure nanoplastics on waterbodies and air (Materić et al., 2022; Kau et al., 2024), that may be a good starting point on the way to first, have a first glimpse on the rates and proportion of combined pollutant to test, but even more relevant, to have a correct amount of realistic samples to conduct hazard evaluation studies.

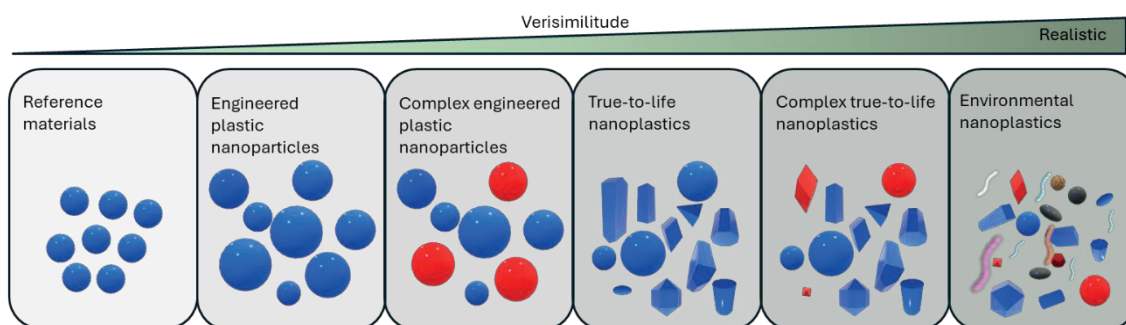


Figure 5: Progression that illustrate the increase in verisimilitude from engineered plastic nanoparticles to environmental nanoplastics. This figure depicts the evolution in complexity moving from well-defined synthetic particles with narrow size distribution through those that better represent the diverse characteristics of nanoplastics until what the gold standard for toxicology tests will be.

1.3. Health hazardous effects mediated by nanoplastics exposure

1.3.1. Exposure pathways

Information for nanoplastics compared to microplastics is rather limited, and by extension the toxicological or risk assessment data is also scarce (Hildebrandt & Thünemann, 2023). Before going into much deeper detail, it is important to remark that the occurrence of nanoplastics is relevant for human health because we are inevitably exposed to plastic nanoparticles, regardless the incidental or intentional origin, the constituent material, the size, the surface modification and the additives that carries. Exposure to nanoplastics will almost inevitably end up in plastic penetration into the human body which can be by two principal ways that are by ingestion and inhalation. However, it is important to highlight that dermal contact should not be underestimated (Domenech & Marcos, 2021). The relevant characteristics of plastic at the nanoscale, and the exposure pathways are summarized in **Fig. 6**.

Food and drinking water have been identified as the primary sources through which ingestion is considered one of the main pathways of exposure to nanoplastics. The direct consequences of this exposure, along with the potential degradation of these materials mediated by the intestinal juices/microbiota, and the resulting by-products from this interaction as the production of reactive monomers or oligomers as well as metabolites as oxidative products, or the dysbiosis caused by nanoplastic exposure, may have significant implications for health (Tsochatzis et al., 2024). Furthermore, there is still very limited knowledge regarding the actual levels of ingestion or exposure to nanoplastics.

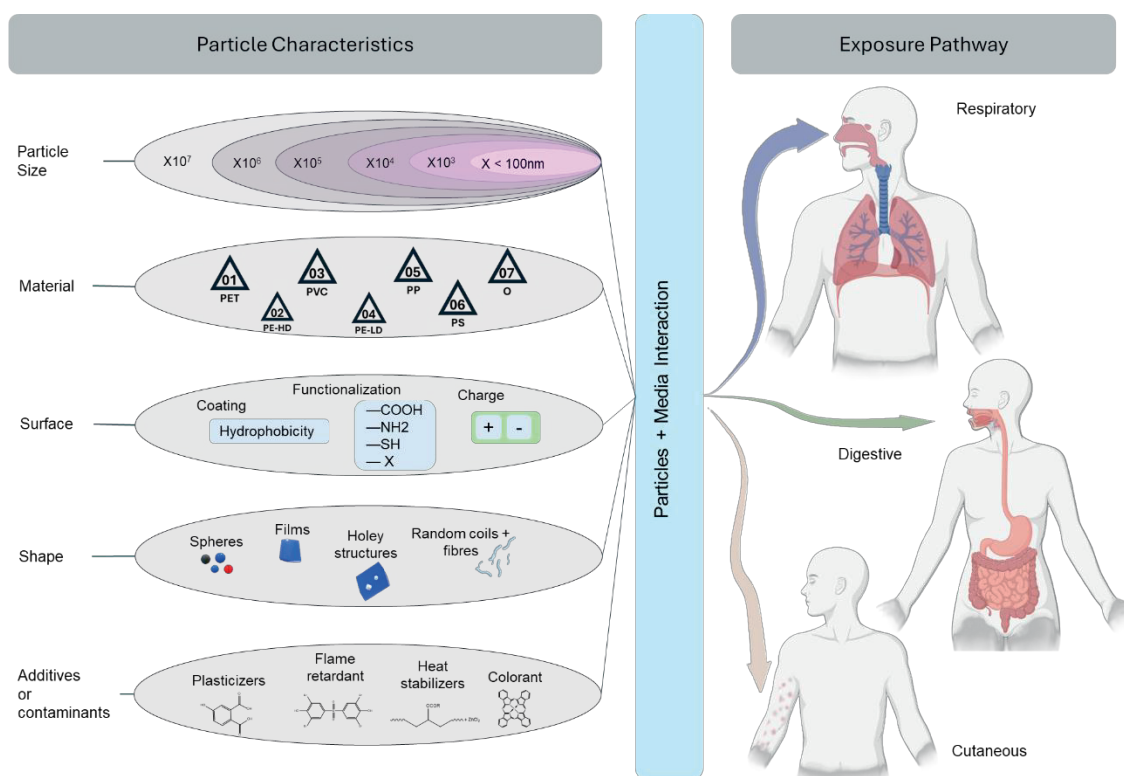


Figure 6: summary of nanoplastic main characteristics related with their behavior and the human exposure pathways.

Despite the extensive documentation of their ability to cross biological barriers, the precise mechanisms by which this occurs remain unknown. This lack of understanding, along with insufficient information on toxicokinetic and the scarcity of long-term studies related to exposure, represents significant gaps in current research (Sánchez et al., 2022). However, the presence of micro and nanoplastic in human stool has confirmed the oral intake (Schwabl et al., 2019), and the contamination in food has been largely reported. This inclusion in the food chain, or accumulation through biomagnification process, poses a threat to all trophic levels (Liu et al., 2024).

As persistent as in the soil, micro and nanoplastics have been described as airborne air pollutants, pervasive even in areas where human activity is usually considered minimal, negligible or non-existent at all like in the poles (Bergmann et al., 2022). Therefore, it is crucial to study exposure to micro- and nanoplastics not only through traditional gastrointestinal pathways but also via airborne routes, which require thorough investigation (Banaei et al., 2023; García-Rodríguez et al., 2024). Through this route, several distinctions have been made, ranging from indoor exposure to outdoor environments, urban settings, and even occupational sources, including the use of face masks, and have been described as the principal route of human exposure to nanoplastics (Woo et al., 2023). The diversity of plastics found in human lungs varies not

only in composition—with polypropylene (PP) being the most dominant, closely followed by polyethylene terephthalate (PET)—but also in shape and size (Jenner et al., 2022). We must also acknowledge that current reports are limited by the available techniques and technology. Therefore, the inability to detect smaller materials in more complex matrices at present does not imply that these materials do not exist or are not present. Rather, it reflects our current limitations in detecting them. This is a classic case where the absence of evidence is not evidence of absence.

1.3.2. Health hazardous effects

This knowledge gap is a challenging field that have led many different research groups to investigate the possible health implications of nanoplastic exposure such as heart abnormalities in animal models as it is cardiomyocytes senescence and important oxidative stress (Wang et al., 2024) and how not only the plastics but also the polymer additives used on its production may have a detrimental effect on human health as toxicants, endocrine or metabolic disruptors that can finally increase the risk of diabetes, cardiovascular disease, or strokes (Landrigan, 2024). Additionally, oxidative stress and inflammatory response mediated lung damage have been reported in animal models (Ji et al., 2024) as well as ferroptosis, an autophagy dependent process that has been linked to nanoplastic exposure. As remarked, there are effects at many levels, systemic and cellular, and a nice example of it is the use of primary human nasal cells that have been used to describe how autophagy driven effects can affect human epithelia by using primary nasal epithelial cells exposed to engineered polystyrene plastic particles and true-to-life PET nanoplastics (Annangi et al., 2023a; 2023b).

From the logical considerations—such as the ease with which smaller particles can enter a cell, to the fact that exposure ultimately depends on the time of exposure—it has been observed that these factors also hold true at the level of biological effects. Intestinal barrier cell models have shown increased reactivity, as evidenced by elevated reactive oxygen species (ROS) production, depending on particle size, cell type, and exposure time. However, it is important to note that no significant reduction in cell viability has been observed at concentrations up to 100 µg/mL (Y. Zhang et al., 2022). This is particularly relevant in the context of exposure to environmentally representative nanoplastics, as the use of simple pristine particle models, such as polystyrene, has laid the foundation for New Approach Methodologies (NAMs), a set of old/new methods aiming to detect important biological effects at sub-toxic levels, as i.e. generating differential levels of oxidative stress. Within these NAMs, the use of complex barrier models, such as Caco-2 based previously reported (Domenech, et al., 2020; Domenech et al., 2021) stand out.

This model, in combination with the use of true-to-life nanoplastics, has highlighted the need to push the boundaries of current techniques. These studies have revealed several critical findings, including the role of proteins like mucins in influencing particle kinetics. For example, goblet cell models, such as HT29 cells, have shown greater affinity for PLA nanoplastics compared to other cell types (Banaei et al., 2023). Additionally, there is a clear need to extend exposure times to investigate how prolonged overexposure to these plastics might cause damage at levels that may not be immediately evident but have been shown to be significant, particularly in the context of DNA damage. This includes disruptions in all hallmarks of carcinogenesis, which have been observed when exposed to simple nanoplastic models (Barguilla et al., 2022). The potential health effect of MNPLs exposure is a topic receiving an increasing relevance by the scientific and regulatory community, as supported by the large number of studies published in the two last years. Despite the high variability of *in vitro/in vivo* models and biological endpoints evaluated, there is a big problem when such data need to be used for risk assessment studies. This problem is the lack of representative environmental models of MNPLs. Most of the studies have been conducted using commercial pristine polystyrene MNPLs, which are far away from the secondary MNPLs present in the environment as consequence of plastic goods degradation. There are large differences between the commercial pristine PS MNPLs and secondary MNPLs mainly in the shape, size and chemical composition. Thus, while commercial PSMNPLs are uniform in size, with spherical shape, and without the presence of plastic additives, the secondary MNPLs found in the environment present completely different characteristics. Due to the impossibility of obtaining enough amount of environmental MNPLs to carry out the large number of biological assays required for a sound characterization of the toxicological profile of such samples, the idea of creating in the laboratory MNPLs from the degradation of plastic goods raised. These “secondary MNPLs” are denominated “true-to-life” MNPLs and are considered to present all the characteristics of the secondary MNPLs resulting from the “natural” environmental degradation of plastic waste.

Thus, according to the relevance of the obtention/use of true-to-life MNPLs, the aim of this Thesis was to establish methods for their obtention, as well as methods to mark them to determine their internalization in cells and organisms. Accordingly, MNPLs from transparent PET water bottles and from opaque PET milk bottles were obtained and characterized from the physicochemical and biological point of view. In addition, different dyes were evaluated to determine which of them present more advantages to be used to stain “true-to-life” MNPLs. The results indicate that the denominated iDye poly pink meet the requirements needed.

The Thesis is presented in the format of compendium of publications, including three publications i) one regarding the obtention/characterization of MNPLs resulting from the degradation of transparent PET water bottles (PETNPLs), ii) a second including the obtention/characterization of MNPLs resulting from the degradation of opaque PET milk bottles (PET-Ti_MNPLs), and iii) the third including all the studies carried out to choose iDye poly pink as the dye selected to stain the obtained “true-to-life”.

OBJECTIVES

2. OBJECTIVES

The main objective of this Thesis is to obtain true-to-life nanoplastics as model test materials representative of secondary environmental nanoplastics, useful to determine their hazards and risks posed by MNPLs human exposure.

This main objective has been divided into three sub-objectives, each one corresponding to each one of the scientific publications of this Thesis, presented as a compendium of publications.

1. To develop a reliable method for PET MNPLs production (from PET plastic water bottles) and to fully characterize the obtained PET nanoparticles from the physicochemical point of view. Additionally, to determine their kinetics and toxicity in human derived cells.
2. To develop a reliable method for titanium-doped PET MNPLs production (from opaque PET plastic milk bottles) and to fully characterize the obtained nanoparticles focusing on their quantification in biological samples. Additionally, to determine their kinetics and toxicity in human derived cells.
3. To develop a reliable, yet simple and cost-effective method for the staining of true-to-life MNPLs that enable the assessment of the particles' internalization in both *in vitro* and *in vivo* systems.

RESULTS

3. RESULTS

3.1. Chapter 1 (First Study)

A new source of representative secondary PET nanoplastics. Obtention, characterization, and hazard evaluation

3. RESULTS

3.1. Chapter 1 (First Study)

A new source of representative secondary PET nanoplastics.
Obtention, characterization, and hazard evaluation

Journal: [Journal of Hazardous Materials](#)
Year: [2022](#)
Volume: [439](#)
Doi: [10.1016/j.jhazmat.2022.129593](#)
Impact Factor: [13.6](#)

This chapter is a verbatim of the mentioned article that is fully cited as:

Villacorta et al., 2022

A. Villacorta, L. Rubio, M. Alaraby, M. López-Mesas, V. Fuentes-Cebrian, O.H. Moriones, R. Marcos, A. Hernández. A new source of representative secondary PET nanoplastics. Obtention, characterization, and hazard evaluation. J. Hazard. Mater., 439 (2022), 129593, Doi: 10.1016/j.jhazmat.2022.129593.

(The original *pdf* version is included in the Annexes, as well as the Supplementary material)

A new source of representative secondary PET nanoplastics. Obtention, characterization, and hazard evaluation

Aliro Villacorta^{a,b}, Laura Rubio^{a,c}, Mohamed Alaraby^{a,d}, Montserrat López-Mesas^e, Victor Fuentes-Cebrian^e, Oscar H. Moriones^{f,g}, Ricard Marcos^{a,*}, Alba Hernández^{a,*}

^a*Group of Mutagenesis, Department of Genetics and Microbiology, Faculty of Biosciences, Universitat Autònoma de Barcelona, Cerdanyola del Vallès, Barcelona, Spain*

^b*Facultad de Recursos Naturales Renovables, Universidad Arturo Prat, Iquique, Chile*

^c*Nanobiology Laboratory, Department of Natural and Exact Sciences, Pontificia Universidad Católica Madre y Maestra, PUCMM, Santiago de los Caballeros, Dominican Republic*

^d*Zoology Department, Faculty of Sciences, Sohag University, 82524 Sohag, Egypt*

^e*GTS-UAB Research Group, Department of Chemistry, Faculty of Science, Universitat Autònoma de Barcelona, 08193 Bellaterra, Cerdanyola del Vallès, Spain*

^f*Institut Català de Nanociència i Nanotecnologia (ICN2-UAB-CSIC-BIST), Campus UAB, Bellaterra, 08193 Barcelona, Spain*

^g*Universitat Autònoma de Barcelona (UAB), Campus UAB, Bellaterra, 08193 Barcelona, Spain*

* Correspondence to: Group of Mutagenesis, Department of Genetics and Microbiology, Faculty of Biosciences, Universitat Autònoma de Barcelona, Campus of Bellaterra, 08193 Cerdanyola del Vallès, Barcelona, Spain.

E-mail addresses: ricard.marcos@uab.cat (R. Marcos), alba.hernandez@uab.cat (A. Hernández).

<https://doi.org/10.1016/j.jhazmat.2022.129593>.

Received 10 March 2022; Received in revised form 4 July 2022; Accepted 11 July 2022

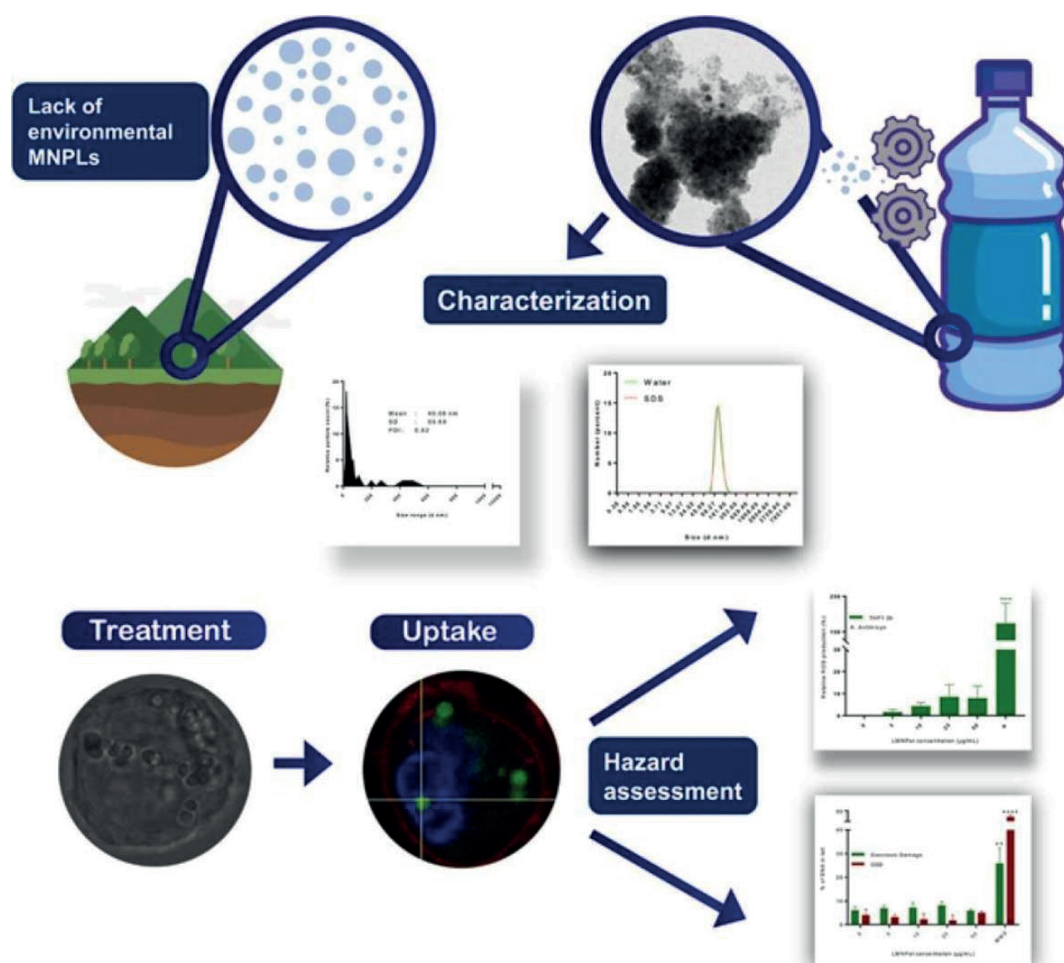
Available online 14 July 2022

0304-3894/© 2022 The Author(s). Published by Elsevier B.V. This is an open access article under the CC BY license (<http://creativecommons.org/licenses/by/4.0/>).

HIGHLIGHTS

- A proposed method to get PET nano- plastic samples from plastic bottles is presented.
- Completed physicochemical characterization is provided.
- Cell uptake was evaluated following different methods.
- Different Hazard effects were determined.
- The method is extrapolated to other plastic and avoids metal contamination.

GRAPHICAL ABSTRACT



ARTICLE INFO

Editor: Dr. T Meiping

Keywords:

Nanoplastics
Polyethylene terephthalate
Physicochemical characterization
Cell uptake
Cytotoxicity

ABSTRACT

Micro and nanoplastics (MNPLs) are emergent environmental pollutants requiring urgent information on their potential risks to human health. One of the problems associated with the evaluation of their undesirable effects is the lack of representative samples, matching those resulting from the environmental degradation of plastic wastes. To such end, we propose an easy method to obtain polyethylene terephthalate nanoplastics from water plastic bottles (PET-NPLs) but, in principle, applicable to any other plastic goods sources. An extensive characterization indicates that the proposed process produces uniform samples of PET-NPLs of around 100 nm, as determined by using AF4 and multi-angle and dynamic light scattering methodologies. An important point to be highlighted is that to avoid the metal contamination resulting from methods using metal blades/burrs for milling, trituration, or sanding, we propose to use diamond burrs to produce metal-free samples. To visualize the toxicological profile of the produced PET-NPLs we have evaluated their ability to be internalized by cells, their cytotoxicity, their ability to induce oxidative stress, and induce DNA damage. In this preliminary approach, we have detected their cellular uptake, but without the induction of significant biological effects. Thus, no relevant increases in toxicity, reactive oxygen species (ROS) induction, or DNA damage -as detected with the comet assay- have been observed. The use of representative samples, as produced in this study, will generate relevant data in the discussion about the potential health risks associated with MNPLs exposures.

1. Introduction

Despite the multiple advantages of plastic materials, a very dramatic side-effect resulting from this big success is the increased presence of plastic wastes in the environment. Unfortunately, and considering the present capacities of recycling such wastes, this environmental catastrophe will still be increasing and remain for a long (Borrelle et al., 2020).

Once into the environment, plastic wastes degrade due to different abiotic (i.e., photodegradation, physical abrasion, or hydrolysis) and biotic mechanisms (Ali et al., 2021a), generating a new source of contaminants: the micro/nanoplastics (MNPLs). With a size between less than 10 nm and a few mm, MNPLs can be highly mobilized by water and air and, consequently, they can be found in all the environmental niches on a global scale (Evangelidou et al., 2020, Batool et al., 2021). Another characteristic linked to the MNPLs' size is their potential to enter the food web as they can be easily uptaken by living organisms, including humans. In this way, they have become a new group of emergent contaminants with a potential human health risk. In fact, it has been demonstrated that at the nanoscale level MNPLs could exert important biological effects such as reactive oxygen species (ROS) generation, the activation of the immune system by inflammatory responses, and even more, genotoxic DNA damage (Rubio et al., 2020, Ballesteros et al., 2020, Rai et al., 2021).

It should be noted that environmental MNPLs have two different origins. One is associated with the abiotic/biotic degradation of big plastic sizes (macroplastics), as above indicated. In this case, these MNPLs are denominated secondary MNPLs. On the contrary, some MNPLs are synthesized at these small size ranges for specific purposes and are denominated primary MNPLs. One typical example of primary MNPLs is the micro/nanobeads used in exfoliating hand cleansers and facial scrubs. In fact, they are also intentionally added to other many products such as paints, coatings, and inks, or in construction, agriculture/horticulture, and medical products, among others. For these MNPLs, the estimated used amount in Europe is around 145,000 tons per year, and to minimize their impact on the environment and potentially on human health, a restriction on the intentionally-added-microplastic use has been proposed (ECHA, 2018). Regarding the environmental levels of secondary MNPLs they are very difficult to estimate. Nevertheless, it must be remembered that the world production of plastics on 2019 was 368 million tons, that its production is exponentially growing over time, that about 40 % was used for packaging (or single-use), and about 80 % is not properly recycled ending into the environment or landfills (PlasticsEurope 2019; Ali et al., 2021b). Studies aiming to determine the potential hazard of MNPLs enface big challenges, one being the selection of environmentally representative MNPLs to be used as reference materials. Due to the impossibility of collecting real MNPLs from the environment, especially at the nano range, practically all available studies have used the only MNPLs type that is commercially available in a wide range of sizes, surface modifications, and labeling, which is polystyrene (PS) MNPLs. Hence, all our present knowledge on the potential risk of MNPLs for human health is basically limited to one polymer type. To avoid this bias, some recent alternatives have been proposed aiming at artificially

degrade plastic items to obtain new sources of secondary MNPLs to be included in the hazard assessment studies. The pioneering study used the UV-laser ablation process to obtain PET-NPLs (Magrì et al., 2018). Others have used mechanical milling followed by sieve fractionation into MPLs fractions applied to agricultural plastics (a mulch film prepared biodegradable polymer polybutyrate adipate-co-terephthalate and low-density polyethylene (Astner et al., 2019). As well as the trituration of a few millimeters' of industrial PET pellets (Pignattelli et al., 2021). The use of mechanical ground approaches was also proposed to obtain PET-NPLs (Rodríguez-Hernández et al., 2019).

Two important aspects need to be pointed out regarding the so-far proposed alternative protocols to obtain MNPLs. First, polyethylene terephthalate (PET) is used in most of these approaches. This is because, as a thermoplastic polymer, PET do not undergo chemical reactions when heated, and can re-ground several times, what it is very useful for recycling purposes. This, among other reasons, is why PET is one of the major contributors to worldwide plastic wastes (Gwada et al., 2019). Second, many of the proposed methods to obtain degraded MNPLs, such as mechanical milling, allows only to obtain MPLs, but not NPLs. This is very relevant from the toxicological point of view, since it is considered that NPLs have the ability to cross biological primary barriers and, consequently, reach the different organs and tissues after an exposure (Zitouni et al., 2021).

According to the above indicated, it is clear that there is an urgent need to generate new representative MNPLs samples for further use in hazard evaluations (Balakrishnan et al., 2019). In this study, we thoroughly describe our in-house method to obtain PET-NPLs, provide exhaustive characterization of the obtained materials, and assess its usefulness in hazard assessment approaches by analyzing the cellular uptake, cytotoxicity, reactive oxygen (ROS) production, and DNA damage induction in human lymphoblastic cell line models after an acute exposure.

2. Materials and methods

2.1. PET-NPLs obtention

The PET raw material used to produce PET-NPLs was obtained from commercially available water plastic bottles. The developed procedure was adapted from the previously reported by Rodríguez-Hernández et al. (2019). A schematic overview of the used protocol is outlined in Fig. 1. Briefly, pieces of about 12 cm² from the bottom part of the water bottles were initially sanded with aluminum oxide/silicon carbide rotary burrs. Due to the observed metal-contamination (as explained in the Results section) a diamond rotary burr sander accessory, attached to a flexible shaft powered by a multitool Dremel 3000, was choose for the sanding process. The obtained PET debris was passed through a 0.20 mm sieve (CISA R-92), and 4 g of the resulting material were dispersed in 40 mL of pre-heated (50 °C) trifluoroacetic acid (TFA, 90% v/v), in a proportion of 10 mL TFA per gram of sieved PET, on a stirring plate at 100 rpm for 2 h. After a complete dispersion, the mixture was kept at room temperature overnight in continuous agitation. Next day, 40 mL of TFA 20% (v/v) was added to the sample and the mixture was kept

under constant and vigorous stirring for 24 h. After that, the obtained dispersion was distributed on six 10 mL glass tubes and centrifuged at 2500 RCF for 1 h. Once the supernatants were discarded, the obtained pellets were resuspended on 400 mL of 0.50% sodium dodecyl sulfate (SDS) solution, vigorously mixed, and distributed into two 200 mL beakers, for ultrasonication on an SSE-1 Branson sonicator. Sonication lasted for 2 min at 25% amplitude, in 9/9 s sonication/break cycles. The volume of each beaker was transferred to a graduated cylinder, where sedimentation of larger particles took place for 1 h. The top 100 mL of the suspension (from each graduated cylinder) was collected and centrifuged as before for SDS elimination, and further washed twice with Milli-Q water and twice with pure ethanol and let to dry. Pellets were then resuspended on Milli-Q at the desired final concentration and sonicated at 10% amplitude for 16 min in a cold-water bath, aliquoted, and immediately frozen on cryotubes in liquid nitrogen and stored at -80°C for further use. Each one of the cryotubes contains 1 mL of a concentration of 12.50 mg/mL.

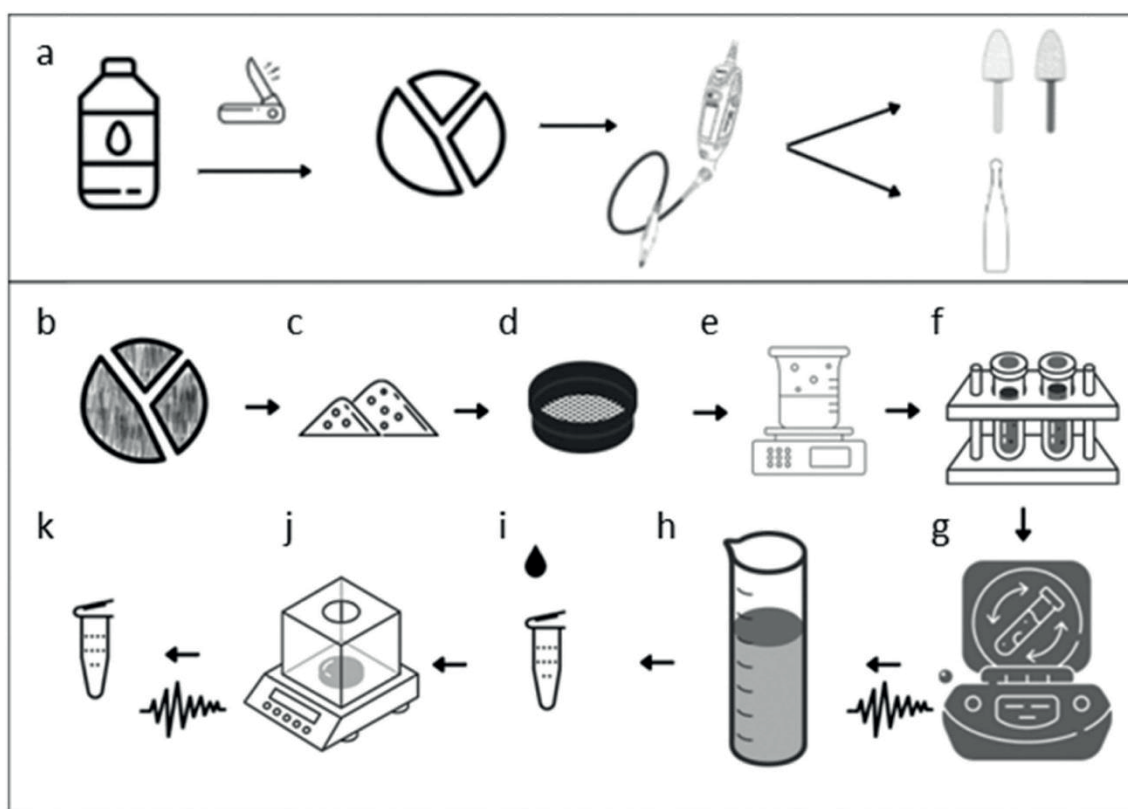


Fig. 1. Schematic representation of the fragmentation and grind process with the mixed burrs or the diamond covered burr (a). Representation of the fractioned pieces (b), PET powder obtained (c) that will be passed through the sieve (d), stirred, suspended, and heated at different concentrations of TFA (e), distributed on glass tubes (f) and centrifuged (g), washed and then resuspended on SDS, sonicated, and transferred to a cylinder for sedimentation (h) and then collected, washed (i), weighted (j), resuspended, sonicated and stored frozen until needed (k).

2.2. Characterization of particle suspension

2.2.1. Scanning electron microscopy/Energy dispersive X-ray microscopy (SEM-EDS)

The stock solution was thawed on a warm bath at 37 °C, and a working solution of 200 µg/mL was prepared on Milli-Q water. A holey carbon grid was dipped into the working solution and water was allowed to evaporate overnight; additionally, a drop was placed on the Si holder. Then, particles in the grid were examined on a SEM Zeiss Merlin (Zeiss, Oberkochen, Germany) coupled with an X-Max 20 mm EDS system (Oxford Instruments, Oxford, UK). In addition to collecting SEM images, for the EDX analysis an area including the nanoparticle surface was selected, and the sample signal was collected and analyzed by the INCA Energy software.

2.2.2. Transmission electron microscopy (TEM)

A working solution of 200 µg/mL was prepared on Milli-Q water and mounted on a holey carbon grid as described above. Particles in the grid were examined by TEM on a JEOL JEM 1400 instrument (JEOL LTD, Tokyo, Japan) operated at 120 kV. TEM imaging was analyzed for particle size distribution using ImageJ software 1.8.0_172 processing and analysis software.

2.2.3. Fourier transform infrared spectroscopy (FTIR)

To detect the functional groups, and to identify the samples as PET, these were analyzed by Fourier-transform infrared spectroscopy (FTIR), as briefly indicated. A drop of particle suspension at a concentration of 1 mg/mL was placed on a gold mirror and let dry for one week inside a petri dish. Analysis was carried out on a Hyperion 2000 micro-spectrometer using the gold mirror as reference. This analysis was carried out at the Molecular Spectroscopy and Optical Microscopy facility at the Institut Català de Nanociència i Nanotecnologia (ICN2). To assess the composition, interferograms were analyzed and contrasted with previous reports.

2.2.4. Multi angle and dynamic light scattering (DLS-MADLS) and zeta potential

The indicative size of the colloid structures in suspension of the hypothetical hard sphere that behave similarly to the particle suspension of the PET-NPLs was analyzed using a Zetasizer® Ultra from Malvern Panalytical. A working solution of 1 mg/mL of PET-NPLs suspension was thawed and then diluted on Milli-Q water for further analysis at a concentration of 200 µg/mL. To investigate better the fraction on the nanoscale, avoiding the masking generated by agglomerates or particles bigger in size, a sonication for 16 min at 10% amplitude (as described above), and a filtration step with a 450 µm PES membrane Millex®-HP from Millipore express® was included. To visualize the influence of anionic surfactant as a dispersant of the sample the same procedure described was carried out maintaining the SDS 0.5% v/v original concentration. Once prepared, the samples were placed on DTS1070 cuvette for surface charge determination by zeta potential measurements, for both water and SDS 0.5% dispersant. DLS, MADLS and particle concentration measurement were carried out by placing 1.5 mL of the prepared solutions on DTS0012 cuvettes.

2.2.5. Asymmetric flow field flow fractionation (AF4)

The PET nanoparticles separation was performed using the AF2000 Asymmetric Flow FFF system from Postnova Analytics GmbH (Landsberg, Germany) with two PN1130 Isocratic Pumps, a Kloehe V6 Pump, a PN5300 Autosampler, a PEEK AF4 Channel with a 10 kDa regenerated cellulose membrane and a 350 μ m height spacer. The mobile phase and the PET suspension were prepared in NovaChem Surfactant 100 (IESMAT, Madrid, Spain) at 0.20% (v/v). The size data (gyration radius, R_g) was obtained using a PN3609 MALS Detector (9 angles), calibrated with a 125 nm NIST Polystyrene Latex standard (Postnova Analytics GmbH), using the software AF2000 Software and used to calculate the geometric diameter (D_{geo}) by dividing $2 \cdot R_g$ by the typical form factor of a sphere (0.78) (Lohrke et al., 2008). The method consisted in three steps, used a constant detector flow of 0.50 mL/min and injections of 20 μ L of samples of 1 mg/mL of PET-NPLs suspended in NovaChem 0.20% were performed. The first step was a focusing step of 3 min with an injection flow of 0.20 mL/min, a cross-flow of 2.00 mL/min and a focus flow of 2.30 mL/min, the second was a separation step, with focus-flow of 0 mL/min, cross-flow from 2.00 mL/min exponential to 0.10 mL/min in 40 min and a final step at a constant flow of 0.10 mL/min of cross-flow during 20 min

2.3. Cell culture

Two human lymphoblastic cell lines were used to detect the potential biological effects of the obtained PET-NPLs, the THP-1 (monocytes) and the TK6 (lymphoblasts). Both cell lines were obtained from Sigma Aldrich (MO, USA) and grown in T-25 flasks containing Roswell Park Memorial Institute (RPMI) medium (Biowest, France) supplemented with 10% fetal bovine serum (FBS), 1% glutamine (Biowest, France), and 2.5 μ g/mL of Plasmocin™ (InvivoGen, CA, USA). Cultures, with a density ranging from 5×10^5 and 1×10^6 cells were maintained at 37 °C in a humidified atmosphere of 5% CO₂.

2.4. Cell uptake determination

To confirm the cell uptake of the obtained PET-NPLs, three different approaches have been used: flow cytometry (internal complexity), TEM (internalization), and confocal microscopy (Nile red staining).

2.4.1. Internal complexity

As an indicator of structural complexity of THP1 cells, once the PET-NPLs uptake takes place the orthogonal light scattering -commonly known as Side Scatter (SSC)- was evaluated at concentrations ranging from 0 to 50 μ g/mL after exposures lasting for 3 h. The highest concentration (50 μ g/mL) was tested in different scenarios in which PET-NPLs were added directly after being rapidly thawed from - 80 °C on a 37 °C water bath, then vortexed and resuspended on RPMI media with or without FBS, vortexed again and applied directly to the culture and compared with regular culture conditions with and without FBS. Cells were analyzed by flow cytometry on a CytoFlex s and CytExpert software was used to properly collect means from 10,000 events on the live cell population. Data were analyzed using GraphPad Prism 7.0.

2.4.2. TEM analysis

Exposed cells were fixed in 2% (w/v) paraformaldehyde and 2.5% (v/v) glutaraldehyde (Merck, Darmstadt, Germany) in 0.10 M cacodylate buffer (Sigma-Aldrich, Steinheim, Germany) at pH 7.4. After that, cells were processed as already published ([Rubio et al., 2016](#)). Briefly, samples were post-fixed with osmium, dehydrated in ethanol, embedded in Epon, polymerized at 60 °C, and cut with an ultramicrotome. Finally, ultrathin sections placed in copper grids, were contrasted with conventional uranyl acetate and Reynolds's lead citrate solutions and observed using a Jeol 1400 (Jeol LTD) transmission electron microscope equipped with a CCD GATAN ES1000 W Erlangshen camera.

Nile Red stained particles and confocal visualization. Nile red staining of PET-NPLs was carried out following the procedure described in [Rodríguez-Hernández et al. \(2019\)](#) with some important modifications. Briefly, an aliquot (1 mg/mL) was centrifuged for 25 min at 16100 RCF. The supernatant was removed, and 1 mL of Nile red solution (0.50% in DMSO) was added to the PET-NPLs pellet. The mixture was stirred at room temperature for 24 h (protected from light) at 200 rpm. Successive washes, at least twelve times, with ethanol in 0.10 M PBS, pH 7.40 and resuspended on RPMI supplemented media, prior to cell exposure. For confocal visualization, nuclei were stained using Hoechst 33342 (excitation of 405 nm and emission collected at 415–503), cell membranes were dyed using Cellmask (excitation of 633 nm and emission collected at 645–786). For PET-NPLs labeled with Nile red, an excitation wavelength of 514 nm and emission collected at 546–628 was used. Images of each sample were obtained using a Leica TCS SP5 confocal microscope and processed using ImageJ processing and analysis software. version 1.8.0_172.

2.5. Cell viability assay

Cell viability after exposure to PET-NPLs, was determined using the Beckman counter method. To proceed, cells were seeded at a cell density of 5×10^5 cells/mL on 96 well plates and exposed to a range of concentrations from 0 up to 200 µg/mL of PET-NPLs (200 µg/mL per well). After the exposure time, cells were mixed and diluted 1:100 in ISOFLOW and counted with a ZTM series coulter-counter (Beckman Coulter Inc., CA, USA). The average number of cells counted in each treatment was compared with the average number of the untreated control cells. The results from the viability assay permit to determine the non-cytotoxic concentrations to be used in further experiments.

2.6. Reactive oxygen species (ROS) quantification

Due to the combined capacity of passively diffuse into the cell and being highly reactive, the reduced form of ethidium bromide (dihydroethidium, DHE) was used to detect cytosolic superoxide. Cellular suspensions were seeded on 96 U-type well plates at a cell density of 5×10^5 and treated with concentrations of 5, 10, 25, and 50 µg/mL of PET-NPLs for 3 and 24 h. After the exposure, cells were centrifuged at 1000 rpm for 5 min, resuspended on 10 µM DHE diluted on PBS 1X, to a final cell density of 1×10^6 , and incubated for 30 min at 37 °C. Cells were kept on ice for immediate analysis by using a flow cytometer (Beckman Coulter CytoFLEX S). A total number of 20000 events (single cells) were scored and evaluated using the CytExpert software.

2.7. DNA damage detection: The comet assay

The levels of DNA damage (DNA breaks) in both selected cell lines were evaluated using the published protocol ([García-Rodríguez et al., 2019](#)). Both, the overall DNA damage, and the oxidized DNA base levels were determined with the absence/presence of formamidopyrimidine DNA glycosylase (FPG) enzyme. This enzyme detects oxidized DNA bases, excise them, and generate a transient single-strand DNA break detected by the comet assay and denominated as specific oxidative DNA damage (ODD). THP1 cells were exposed to concentrations of 5, 10, 25, and 50 µg/mL of PET-NPLs for 3 h. Treated cells were centrifuged at 0.30 RCF for 8 min at 4 °C. The obtained pellet was washed and resuspended on cold PBS 1x to get 10⁶ cell density per mL. Cells were mixed 1:10 with 0.75% low melting point agarose at 37 °C and dropped on triplicates onto GelBond® films (GBFs) (Life Sciences, Lithuania). GBFs containing the samples were treated overnight on cold lysis buffer at 4 °C and washed on successive 5 and 50 min of enzyme buffer immersion, immediately followed by 30 min incubation at 37 °C with FPG for the detection of ODD, or without FPG for the detection of general genotoxic damage. GBFs were subjected to electrophoresis (20 V, 300 mA, 4 °C), washed twice with cold PBS 1X, fixed in absolute ethanol, and air-dried overnight at room temperature. After staining with SYBR Gold, GBFs were visualized in an epifluorescent microscope (Olympus BX50, Hamburg, Germany). The levels of DNA damage, as percentage of DNA in the tail, was quantified with the Komet 5.5 Image analysis system (Kinetic Imaging Ltd, Liverpool, UK). A total of 100 comet images randomly selected were analyzed per sample.

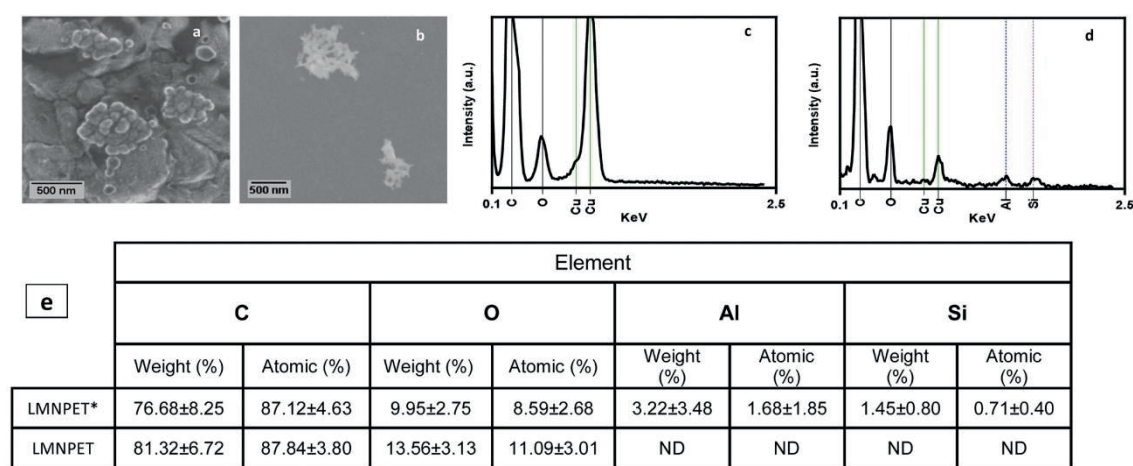
3. Results and discussion

3.1. Characterization of the obtained PET-NPL samples

3.1.1. Morphology and composition

To identify size, shape, and composition of the obtained PET-NPLs, SEM-EDS was used. In Figs. 2a and 2b (as well as in Fig. S1) SEM morphology of the obtained PET-NPLs is visualized. Surface irregularities of the produced particles can be easily observed on the copper and on the carbon sections of the holder. Not only the differences in size are noticeable, but also the holey structures that can be appreciated. This means that not only the particles are on the nanoscale, but also their surface/volume ratios are different than in a solid body. Interestingly, when energy dispersive X-ray microscopy was used, metal contamination resulting from the sanded process was detected. Thus, in the samples obtained using aluminum oxide/silicon carbide rotary burrs such elements were detected. This metal contamination was not present when a diamond rotary burr was used. This can be observed on Figs. 2c and 2d, and it is summarized on the included table (Fig. 2e). These findings raise an important alarm regarding the abrasive methods to be used in the case of mechanically produced MNPLs, mostly when the potential hazard of the obtained MNPLs need to be evaluated. Surprisingly, this potential metal contamination of the obtained samples is not taken into consideration in neither of the recent published papers using mechanical milling or the trituration of few millimeters' industrial pellets ([Astner et al., 2019](#), [Parolini et al., 2020](#), [Lionetto et al., 2021](#), [Pignattelli](#)

et al., 2021). The contamination by metals, as consequence of the mechanical milling of other polymers pellets, has also been detected by us, as indicated in Fig. S2, where the results of milling polylactic acid plastic' pellets are indicated. Therefore, from this point forward all the results presented in this study corresponds to the PET-NPLs produced with the diamond burr rotating tool.



*Produced with aluminum oxide and silicon carbide burrs.

Fig. 2. Scanning electron microscopy results. Amorphous particle structures from a diverse range of geometry can be observed as aggregates metallic section of the holder (a) as in the polymer, where differences in sizes and shapes as well as holey structures can also be detected (b). Notorious differences on the EDS spectra are noticed according to the type of rotating burr utilized where only the diamond covered (c) was able to produce not contaminated samples (d). Aluminum contamination is marked on blue and silica on violet dashed lines, while copper signal marked with green solid lines corresponds to background signal produced by the cooper grid holder. Summary of EDS for both conditions on the table at the bottom (e).

From our data, a warning signal must be put to all the hazard data generated using MNPLs obtained using milling procedures, due to the potential metal associated contamination. It is well-know the toxic effects of metals, including those included during the manufacture of plastics (Turner and Filella, 2021).

3.1.2. Dry state size distribution and shape

The TEM images of PET-NPLs reveal a polydisperse anisodiametric particles population with notorious lack of shape regularity. The Martin diameter was measured, and the relative percentage of particle size is represented in Fig. 3a using GraphPad Prism 7.0. The obtained average size of 40.08 nm presents a standard deviation of 55.68 nm and a polydispersity index of 0.52 evidencing the heterogeneity of the PET particles on the suspension produced by this method. Interestingly, the graphic shows a bimodal distribution with a big peak around 50 mm and a second small peak around 500 nm. As an overall, this means that our protocol produces PET particles inside the nano range.

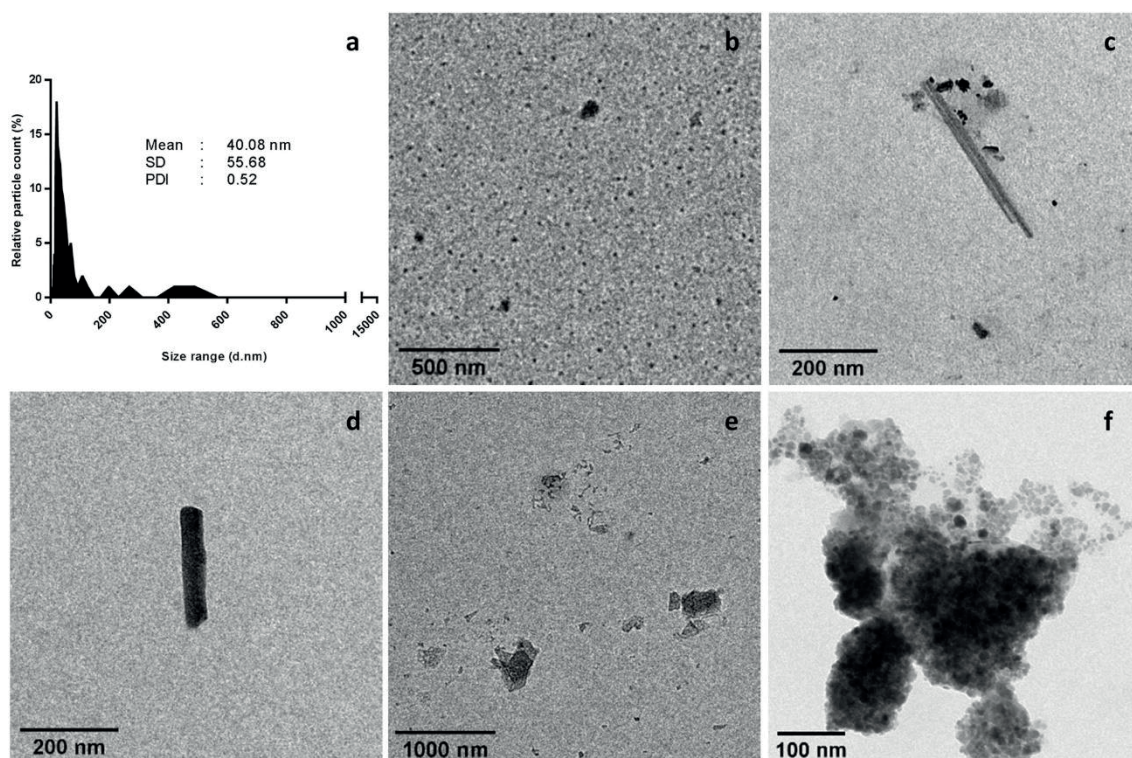


Fig. 3. PET-NPLs characterized by TEM. Size distribution of sizes was obtained from measures of more than 100 images showing a bimodal distribution, with the main peak with sizes around 50 nm, and a second peak with sizes around 400–500 nm (a). Fields with many small sized materials are observed (b), as well as some irregular shapes and fibers (c-e). Agglomerates permit to visualize the small sizes of their components (f).

Although the term MNPLs is increasingly used, no general agreement exists on the borders between microplastic and nanoplastic sizes. Engineered nanomaterials are classically considered to range between 1 and 100 nm, but this strict definition leaves out other sizes placed in the nano range. Although engineered materials are built at the desired size, secondary MNPLs are constituted by a wide range of sizes and shapes and some agreement is necessary to define the borders between MPLs and NPLs. At present, many authors consider that MNPLs range from few nm to several mm. To clarify the boundaries criteria, [Hartmann et al. \(2019\)](#) proposed to categorize MNPLs according to the conventional units of size: nano (1–1000 nm) and micro (1–1000 μ m). Nevertheless, to maintain the classical definition of nanomaterial/nanoplastic, they proposed to divide the nano range (1–1000 nm) between nanoplastics (1–100 nm) and submicron-plastics (100–1000 nm). Such classification needs to have the general agreement, mostly from those coming from the nanomaterials field. A close inspection of our TEM figures confirms the heterogeneity of the obtained material, which can be considered a realistic characteristic, thereby making it more representative from the environmental point of view. Thus, in addition of the small PET particles of around 50 nm (Fig. 3b), bigger sizes are also present, including rigid fibers (Figs. 3c, 3d), different large

shapes (Fig. 3e), and agglomerates (Fig. 3f). Interestingly in Fig. 3f, it is evident that a high amount of PET in the nano range is contained in the agglomerates; nevertheless, the potential biological effects discussed further in this section do not seem to be highly affected by the presence of such agglomerates.

3.1.3. Chemical composition

To confirm the chemical identity of the obtained PET-NPL samples, FTIR analysis was carried out at the premises of the ICN2. To assess the composition of our samples the obtained interferograms were analyzed and contrasted with previous reports of the representative bands present on PET spectrum (Andanson and Kazarian, 2008, Chen et al., 2013, Johnson et al., 2021), and then assigned as reported on Fig. 4. As observed, the obtained peaks match well with the expected, confirming the PET nature of our samples.

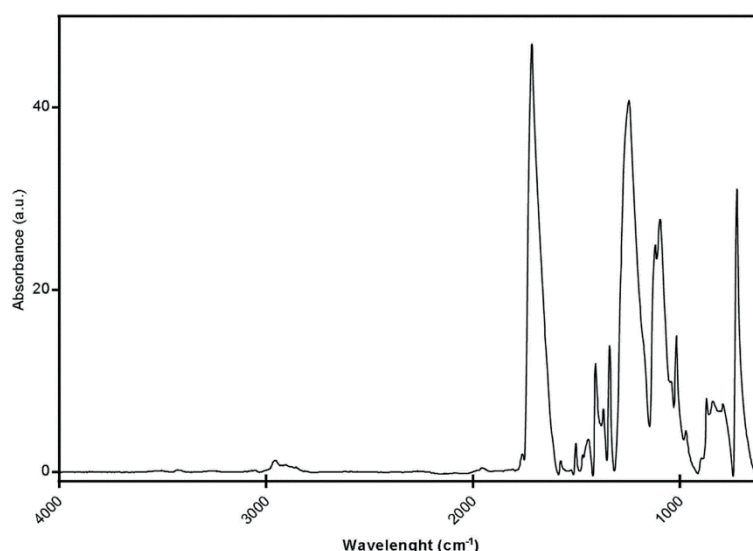


Fig. 4. FTIR spectra with the identity of principal peaks of the interferogram.

3.1.4. Aqueous solution size distribution and zeta potential

From the bimodal distribution observable by TEM, we tried to reduce the content of the higher-size peak (including agglomerates) by using sonication and/or filtration. This approach is schematized on the Supplementary Fig. S3. According to such approaches, we have observed that the best way to reduce agglomerates includes filtration and sonication. Thus, the characterization of such filtered/sonicated samples by a Zetasizer device is indicated in this section. Other combinations of filtration/sonication and dispersion procedures (Nanogenotox, 2011) are included in Fig. S3. Hydrodynamic diameter measurements by using dynamic light scattering shows mild differences in the average size (of around 30 nm) between the suspension of nanoparticles in water, or with the addition of SDS. The obtained diameter (161.01 ± 3.94 nm) and polydispersity index (PI, 0.22) for aqueous dispersions, slightly differ from those observed using SDS, 129.01 ± 0.94 nm and 0.21, respectively. The corresponding signals, expressed as the

mean of three independent measurements, are depicted in Fig. 5a. The correlograms for each condition by triplicates are observed in Fig. 5b. It is interesting to notice that for the mentioned measurements a fixed scattered collection angle of 174.7° was employed, but when the combination of three angles (174.7° , 90° , and 12.78°) are used, the differences or influence of the dispersion media is less noticeable. This can be observed on Fig. 5c, where the curves for both conditions, are almost overlapping. Thus, DLS and even better MADLS are excellent tools for the initial characterization of the obtained PET-NPLs. Another important approach to describe the relative behavior of the particles in suspension is the zeta potential (ZP), which indicates the charge on the surface of the PET-NPLs and the stability of the colloid dispersion. In both cases, summarized on the table (Fig. 5d), the obtained ZP values can be considered as indicative of moderately stable to highly stable suspensions. It is important to remark the important influence of the sample sonication, prior to the characterization, as can be observed in the Supplementary material (Figs. S3 and S4). It is also remarkable that it is possible to calculate the number of particles from the intensity values (Fig. 5d). The obtained values indicate that the used protocol permits to obtain highly concentrated samples.

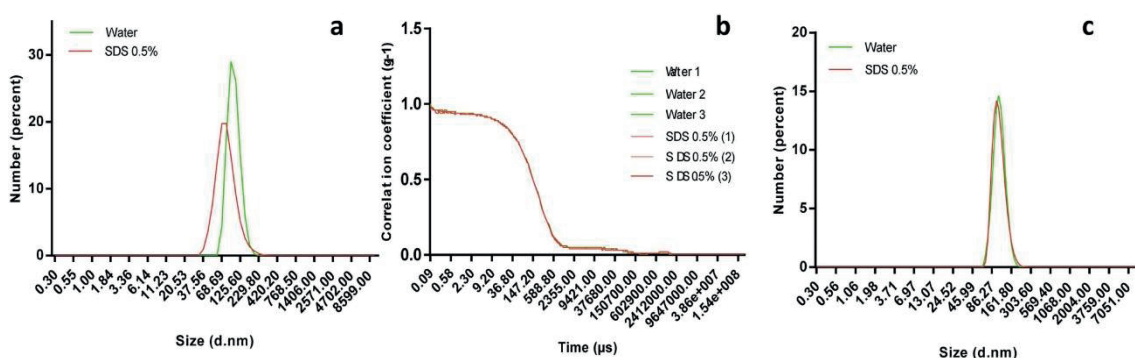


Fig. 5. Size distribution analysis by DLS. (a) Filtered and sonicated PET-NPLs samples were used with both water and SDS (0.5%) as dispersants, and 174.7° as the angle of scattering collection. (b) The correlation coefficients of the measurements. (c) Particle size distribution by using MADLS with three angles of scattering collection (174.7° , 90° , and 12.78°) with water or SDS (0.5 %) as dispersants.

From the results obtained by the analysis of PET by AF4-MALS, after the void peak at 5 min, a large peak appeared, from min 10–35 with an increase of gyration radius from 30 nm up to 600 nm (Fig. 6a). The 90% of PET size ranged from 40 nm up to 75 nm of gyration radius (103 up to 194 nm of Dgeo), being 5% from 75 nm to 100 nm and the rest of the sample above 100 nm (Dgeo above 258 nm), as it can be seen in the Cumulative tendency in Fig. 6b. Moreover, the differential distribution of the PET size, in Fig. 6b, indicated the highest number of particles at approximately 60 nm (155 nm of Dgeo), obtaining a weighted Dgeo of 145 ± 7 nm.

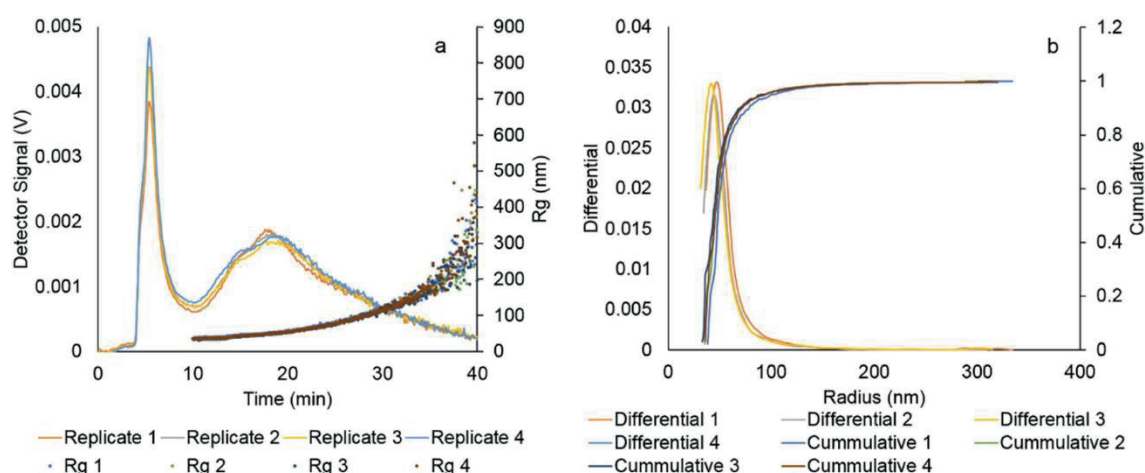


Fig. 6. AF4-MALS plots obtained for a 20 μ L injection of 1 mg/mL of PET, (a) Fractogram (left axis: MALS 90° detector signal (V); right axis: Gyration Radius (Rg, nm)) and (b) Differential and Cumulative graphics.

3.2. Cell uptake of PET-NPLs

To demonstrate the potential applicability of the obtained PET-NPLs, as a representative MNPLs material, it is important to find out whether it can be uptake by the cells after having applied a PET-NPLs dispersion and treatment protocol. Herein we have used three different approaches to confirm the cellular uptake in TK6 and THP1 cell models.

3.2.1. Internalization of PET-NPLs stained by Nile red by confocal microscopy

Nanoplastics, in opposition to metallic nanoparticles, are difficult to be visualized by confocal microscopy due to their lack of reflection. Hence, a staining is needed to explore its toxicokinetic behavior by imaging techniques. Among the different staining dyes available that can be applied to plastic particles after its synthesis/obtention, stand up the Nile red. It produced the best results when applied to virgin and weathered synthetic polymers and textile fibers, in comparison with other seven dyes (Prata et al., 2019). In fact, a recent review points out the main pros and cons of the use of the staining dye in the MNPLs context (Shruti et al., 2022). In our case, Nile red staining allowed us to visualize the internalized PET-NPLs inside cells. Due to its affinity for lipidic structures, Nile red signal could induce errors. Nevertheless, we have detected fluorescent signal into the nucleus (Fig. 7a-c) where not structures exist, confirming the usefulness of this staining. Further intracellular signals are indicated in Fig. 7g-j, confirming the cell uptake. In fact, the use of Nile red staining was previously found to be useful to detect the cell uptake of other sources of in-house produced PET-NPLs (Rodríguez-Hernández et al., 2019).

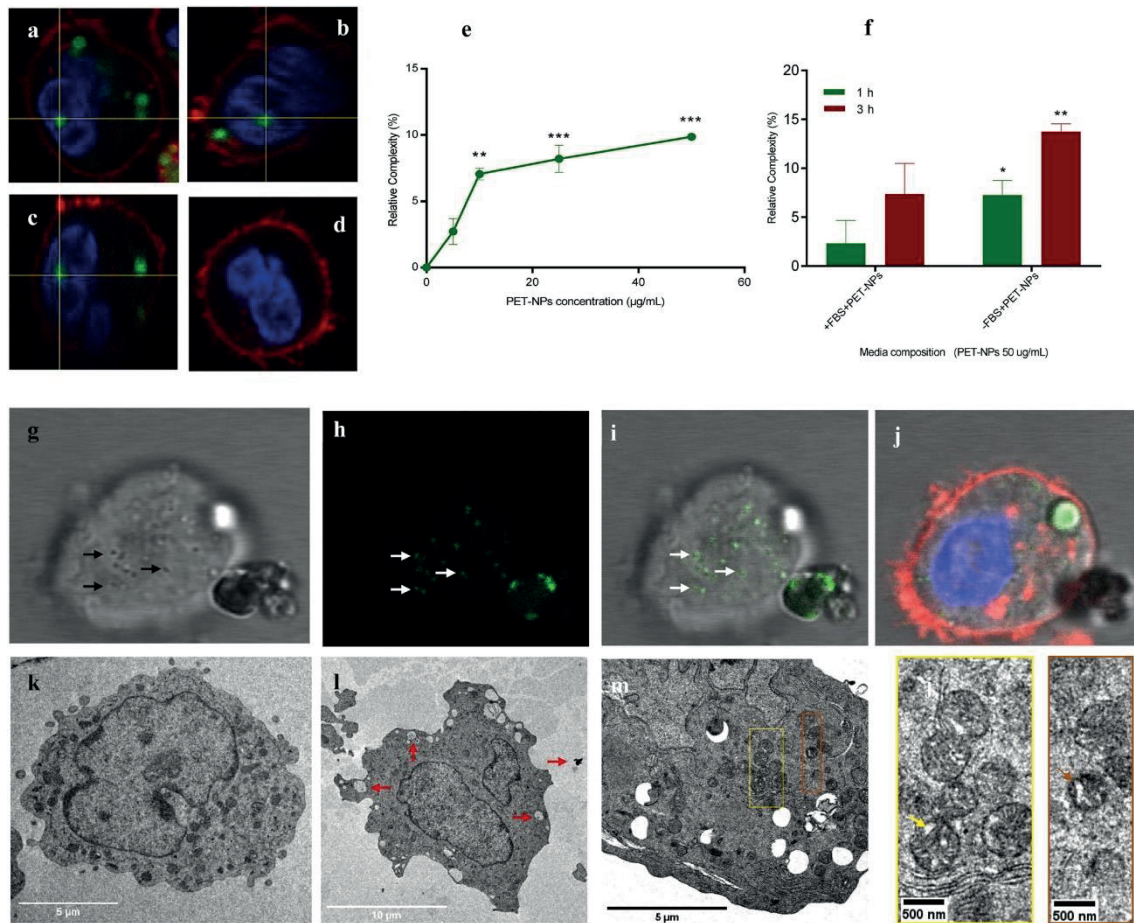


Fig. 7. Confocal orthogonal view of internalized Nile red stained PET-NPLs (green signal) on THP1 cells after 24 h exposure to 50 µg/mL is presented as XY, YZ and XZ (a, b and c respectively) three dimensional views and d is the control. Small dot-like structures is observed at the cytoplasm of THP1 cells (g) and fluorescence at 546–628 nm on h is collected on the same points. Merged images are visualized on i where also the big fluorescent structure corresponds to fluorescent agglomerates. Relative increment on complexity at early exposition to 50 µg/mL of PET-NP on THP1 cells is represented on e (** $p < 0.018$, *** $p < 0.0009$ and **** $p < 0.0004$) and influence FBS on the media composition (f) (* $p < 0.0162$ and ** $p < 0.0087$). For both cases One-way ANOVA with Dunnett's post-test was used for the statistical analysis. TEM images show an increment on vacuoles at 5 (l) or 50 (m) µg/mL of PET-NPs, relative to control (k), PET-NPs like structures are shown by the red arrows and mitochondrial abnormalities or holey mitochondrion are present only on PET-NPs treated cells (yellow and brown arrows).

3.2.2. Cell complexity as detected by flow cytometry

The first approach was an indirect one checking for structural cell changes due to PET-NPLs exposure. It is expected that cells internalizing PET-NPLs experience changes on their internal structures increasing their granularity, which can be assessed using flow cytometry. As cell granularity increases, an increment of side scattered light is expected, and this effect commonly known as cell-complexity can be observed on Fig. 7e,f. This methodology has shown to be useful in detection cell uptake of different nanomaterials (Vila et al., 2017). From our results, we show that cell uptake is modulated by two factors,

such as the exposure time and the presence/absence of FBS. As observed on Fig. 7b, cell uptake increases with the exposure time showing higher uptake after exposures lasting for 3 h regarding the observed after 1 h exposure. In addition, PET-NPLs dispersed in culture media with or without FBS are significantly different in terms of complexity, with a higher uptake in the absence of serum.

3.2.3. Cell uptake detection by TEM

TEM has successfully been applied to detect nanomaterials uptake by many cell types, including MNPLs (Vila et al., 2017, Cortés et al., 2020). Our TEM figures show substantial amounts of PET-NPLs incorporated into cytoplasmic vesicles (Fig. 7I). Although no specific studies have been addressed to understand the cell uptake of PET-NPLs, their presence in the lysosomes of Caco-2 cells (Magri et al., 2021) can suggest that their uptake is by endocytosis, as previously demonstrated for PS-NPLs where that was considered as the main cellular absorption pathway (Magri et al., 2018, Cortés et al., 2020). Interestingly, we detect PETNPLs into mitochondria inducing some alterations. These effects have been also reported for PSNPLs (Cortés et al., 2020, Trevisan et al., 2020).

Taking all three approaches together, it seems clear that cells can uptake our lab-produced PET-NPLs.

3.3. Cytotoxicity

Cell viability curves were studied to determine the cytotoxic effects of PET-NPLs exposure on THP1 and TK6 cell-lines. As shown in Fig. 8 no significant cytotoxicity was observed up to the concentration of 100 $\mu\text{g/mL}$. Only mild effects were observed at the high concentration of 200 $\mu\text{g/mL}$ of PET-NPLs on TK6, where the viability was compromised close to 80% for exposures lasting for 48 h. Since our aim is to work with non-cytotoxic doses, the following experiments were carried out at concentrations up to 50 $\mu\text{g/mL}$.

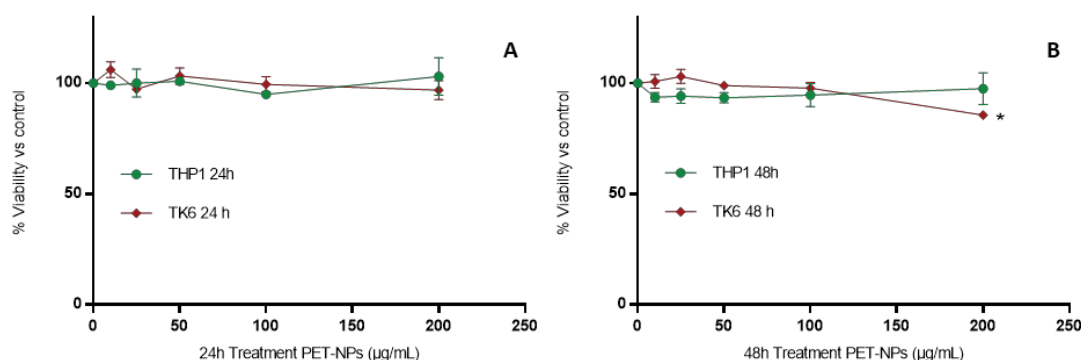


Fig. 8. Relative cell viability of THP1 (green) and TK6 (red) cell lines at concentrations ranging from 0 to 200 $\mu\text{g/mL}$, after PET-NPLs exposures lasting for 24 h (a) and 48 h (b). Data represented as percentage of living cells relative to the untreated control treatment at 24 (green) and 48 (blue) h of exposure. Data is expressed as percentage of cells relative to the untreated control \pm SEM.

One-way ANOVA with Dunnett's post-test was used for the statistical analysis. Statistical significance indicated on the graph as * $p < 0.01$.

This lack of toxicity of the obtained PET-NPLs agree with the reported for other secondary PET nanomaterials obtained using different methodological approaches (Magrì et al., 2018; Dhaka et al., 2022). Although the toxic effects of MNPLs can depend on distinctive characteristics, i.e., the size, most of the studies agree with their lack of acute toxic effects. This has been proved when the effects of different MPLs (polyethylene, polypropylene, polyvinylchloride, and PET) were evaluated in three different cell lines (Stock et al., 2021). This means that other milder, sub-toxic cellular effects, and not cell death, must be selected as biomarker when evaluating the harmful effects associated with MNPLs exposure. Further efforts looking for different exposure scenarios, considering acute exposure to higher concentrations, repeated doses, or long-term exposures, are necessary to decipher the toxic effects of PET-NPLs obtained from environmental plastic samples.

3.4. ROS induction by PET-NPLs

The ability of our PET-NPLs to increase the intracellular levels of ROS was evaluated using the DHE detection assay, in THP1 cells. The results indicated in Fig. 9 show that exposures lasting for 3 h were unable to induce statistically significant differences in the ROS levels when compared to untreated controls. Nevertheless, the positive control used (antimycin) induced important levels of ROS, confirming the goodness of the used protocol. Although one of the most recognized mechanisms of action of nanomaterials is the induction of ROS (Karkossa et al., 2021), MNPLs seem to have a different behavior. Recent results with real PET samples did not show ROS induction in human intestinal Caco-2 cells (Magrì et al., 2021). This inability of PET-NPLs to induce oxidative stress in vitro, agree with many studies using PSNPLs as a model of MNPLs where exposure did not increase ROS levels in Caco-2 cells after acute exposures (Domenech et al., 2020) or after long-term exposures (Domenech et al., 2021). Nevertheless, the potential induction of oxidative stress seems to be dependent on the cell type as demonstrated with different hematopoietic cell lines where ROS was clearly observable (Rubio et al., 2020), as well as dependent on the particle size (Kik et al., 2021).

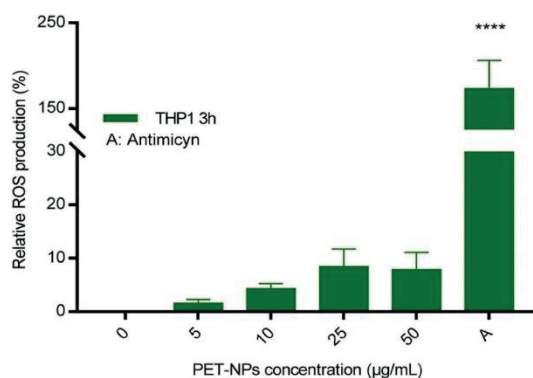


Fig. 9. Reactive oxygen species (ROS) induction in THP-1 cells after PET-NPLs exposures lasting for 3 h at concentrations ranging from 0 to 50 $\mu\text{g/mL}$ at 3 h exposition. Data is expressed as percentage of ROS production relative to the untreated control \pm SEM. One-way ANOVA with Dunnett's post-test was performed. Statistical significance indicated on the graph as **** $p < 0.0001$.

3.5. Genotoxic evaluation of PET-NPLs by using the comet assay

Among the different biomarkers evaluating health risk, those detecting genotoxicity stand out. This is because, due to the main role of DNA in cell functionality, DNA damage severely compromises human health (Carbone et al., 2020). Although the genotoxicity assays can evaluate both primary or fixed DNA damage, those detecting primary damage are much more sensitive. Thus, the comet assay is used to measures the induction of single/double DNA breaks as well as the induction of oxidative damage on the DNA bases. Its simplicity and sensitivity have spread its use in many fields, including the hazard assessment of nanomaterials (García-Rodríguez et al., 2019).

In our study, we have not been able to demonstrate the ability of our PET-NPLs to damage DNA, as indicated in Fig. 10. In addition to the lack of direct strand breaks (Fig. 10a) PET-NPLs exposure also did not induce oxidative damage on the DNA bases (Fig. 10b). These results agree with our previous data showing that PET-NPLs were unable to induce oxidative stress. No other studies are using PET where the genotoxic potential was evaluated. Nevertheless, a few studies on the genotoxic potential of polystyrene MNPLs have been reported showing contradictory results. In in vitro studies, negative findings using the micronucleus assay were observed in the intestinal/placenta barrier cells exposed to 50/500 nm polystyrene NPLs (Hesler et al., 2020). Negative results were also reported in human intestinal Caco-2 cells exposed to 50 nm polystyrene NPLs both as a component of an in vitro barrier (Domenech et al., 2020) or after long-term exposures (Domenech et al., 2021). Nevertheless, positive effects were observed in sh27 fibroblasts using the micronucleus assay (Poma et al., 2019). This would indicate differences between cell types in both MNPLs uptake and genotoxic effects as reported when different types of human hematopoietic cell lines were used (Rubio et al., 2020).

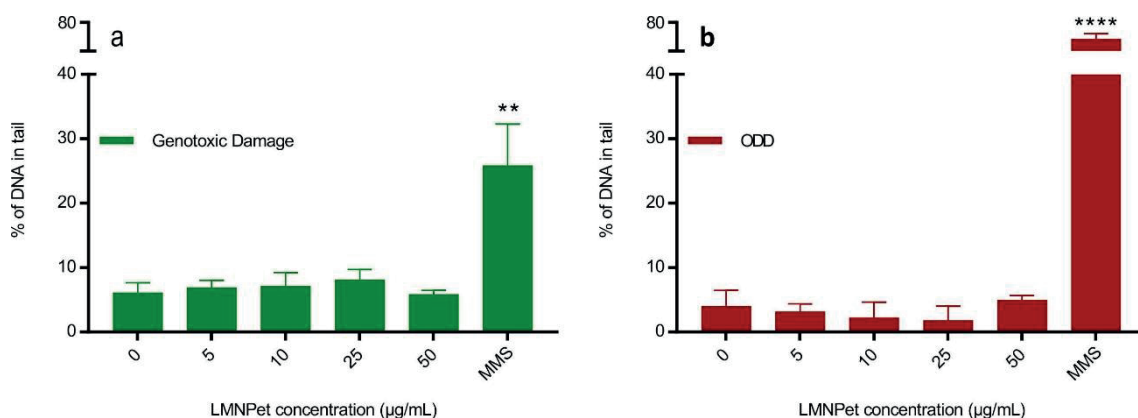


Fig. 10. THP1 genotoxic (a) and oxidative DNA damage (b) at concentrations ranging from 0 to 50 µg/mL and exposure lasting for 3 h. Damage is expressed as the percentage DNA in tail ± SEM. One-way ANOVA with Dunnett's post-test was performed. Statistical significance indicated on the graph as **P < 0.01 ****p < 0.0001. respectively. Methyl methanesulfonate (MMS) was used as a positive control.

As a summing up, we consider that the proposed method to obtain uniform and reproducible secondary NPLs from representative environmental plastic goods is adequate, since the nano sized fraction of the suspension is very high (about 95%). In addition, we consider that the obtained samples mimic the naturally occurring degradation phenomenon. The characterization of the working material by TEM showed a bimodal distribution in the nano range with most of the particles ranging around 50 nm. Simple filtering and sonication steps produce a uniform distribution around 100 nm when DLS and AF4 measurements are applied. We are confident that this methodology can be easily used to obtain NPLs from other plastics materials, escaping from the constrictions posed using pristine forms of commercial polystyrene NPLs. Materials resulting from environmentally representative plastics permit to answer the main open questions asking for the risks of environmental MNPLs resulting from degradation processes. As reported, our protocol using non-metallic burrs during the sanding process has a great advantage over those using metallic blades which contaminate the resulting MNPLs. Such metallic contamination would invalidate any approach aiming to evaluate the potential health risk of such types of MNPLs. It must be recalled that most of the studies evaluating the hazardous effects of MNPLs use sizes in the micro range. Although they can provide useful information, it must be remembered that plastic particles sized in the nano-range are more prone to cross epithelial barriers and, consequently, spread over the different tissues and organs. Accordingly, to be able to get nanoplastics -instead of microplastics- resulting from the degradation of representative environmental plastic pollutants can represent an important step to get more sound data answering about their potential effects on human health.

Although our hazard approach can be considered just as a preliminary one, it is important to highlight that the obtained PET-NPLs are easily internalized by the used cell models without important toxic or genotoxic effects. Due to the lack of gross biological effects, reported by many authors using different sized MNPLs, the use of methodological approaches detecting other types of milder cell effects, out of cell death, should be used when evaluating the harmful effects associated with MNPLs exposure ([Stock et al., 2021](#)). In such a context, having the facility of easily obtaining different types of MNPLs can result very helpful. It is obvious that the original sources of the environmental commercial PET plastics can differ in factors such as crystallinity and plasticizer content. This can suppose differences in the obtained samples, hence differences in their induced biological effects. However, this should not necessarily be considered a problem but rather a challenge, since the obtained/evaluated samples are more representative of the environmentally MNPLs pollutants.

CRedit authorship contribution statement

RM and AH planned the experiments. AV, LR, MA, MLM, VFC, and OHM carried out the experimental part. AV analyzed the data, carried out the statistical analysis, and prepared tables/figures. AV, RM, and AH wrote the final manuscript.

Declaration of Competing Interest

The authors declare that they have no known competing financial interests or personal relationships that could have appeared to influence the work reported in this paper.

Acknowledgments

A. Villacorta was supported by Ph.D. fellowships from the National Agency for Research and Development (ANID), CONICYT PFCHA / DOCTORADO BECAS CHILE / 2020 – 72210237. L. Rubio was supported by the Fondo Nacional de Innovación y Desarrollo Científico y Tecnológico (FONDOCYT) República Dominicana (Project 2018–2019-2B2–093). This project (PlasticHeal) has received funding from the European Union's Horizon 2020 research and innovation program under grant agreement No 965196. L. Rubio was supported by a contract Juan de la Cierva (IJC2020-2686I/AEI/10.13039/501100011033).

Environmental Implication

In spite of the intrinsic interest in understanding the potential hazards associated with the environmental micro-/nanoplastics exposure, most of the studies use pristine commercial samples. Thus, a challenge is to get/evaluate environmental representative samples. In this context, we propose a method to obtain real environmental samples of nanoplastics. Initially applied to PET water bottles, the proposed method is applicable to any source of environmental plastic goods. Interestingly, during the improvement of the method, we discover potential metal contamination resulting from other proposed milling procedures. Our method avoids such contamination, which benefits the ulterior hazard evaluations.

References

- Ali, M.U., Lin, S., Yousaf, B., Abbas, Q., Munir, M.A.M., Ali, M.U., Rasihd, A., Zheng, C., Kuang, X., Wong, M.H., 2021b. Environmental emission, fate and transformation of microplastics in biotic and abiotic compartments: global status, recent advances and future perspectives. *Sci. Total Environ.* 791, 148422 <https://doi.org/10.1016/j.scitotenv.2021.148422>.
- Ali, S.S., Elsamahy, T., Koutra, E., Kornaros, M., El-Sheekh, M., Abdelkarim, E.A., Zhu, D., Sun, J., 2021a. Degradation of conventional plastic wastes in the environment: a review on

- current status of knowledge and future perspectives of disposal. *Sci. Total Environ.* 771, 144719 <https://doi.org/10.1016/j.scitotenv.2020.144719>.
- Andanson, J.M., Kazarian, S.G., 2008. In situ ATR-FTIR spectroscopy of poly(ethylene terephthalate) subjected to high-temperature methanol. *Macromol. Symp.* 265, 195–204. <https://doi.org/10.1002/masy.200850521>.
- Astner, A.F., Hayes, D.G., O'Neill, H., Evans, B.R., Pingali, S.V., Urban, V.S., Young, T.M., 2019. Mechanical formation of micro- and nano-plastic materials for environmental studies in agricultural ecosystems. *Sci. Total Environ.* 685, 1097–1106. <https://doi.org/10.1016/j.scitotenv.2019.06.241>.
- Balakrishnan, G., Déniel, M., Nicolai, T., Chassenieux, C., Lagarde, F., 2019. Towards more realistic reference microplastics and nanoplastics: preparation of polyethylene micro/nanoparticles with a biosurfactant. *Environ. Sci. Nano* 6, 315–324. <https://doi.org/10.1039/C8EN01005F>.
- Ballesteros, S., Domenech, J., Barguilla, I., Cortés, C., Marcos, R., Hernández, A., 2020. Genotoxic and immunomodulatory effects in human white blood cells after ex vivo exposure to polystyrene nanoplastics. *Environ. Sci. Nano* 7, 3431–3446. <https://doi.org/10.1039/D0EN00748J>.
- Batool, I., Qadir, A., Levermore, J.M., Kelly, F.J., 2021. Dynamics of airborne microplastics, appraisal and distributional behaviour in atmosphere; a review. *Sci. Total Environ.* 14, 150745 <https://doi.org/10.1016/j.scitotenv.2021.150745>.
- Borrelle, S.B., Ringma, J., Law, K.L., Monnahan, C.C., Lebreton, L., McGivern, A., Murphy, E., Jambeck, J., Leonard, G.H., Hilleary, M.A., Eriksen, M., Possingham, H. P., De Frond, H., Gerber, L.R., Polidoro, B., Tahir, A., Bernard, M., Mallos, N., Barnes, M., Rochman, C.M., 2020. Predicted growth in plastic waste exceeds efforts to mitigate plastic pollution. *Science* 369, 1515–1518. <https://doi.org/10.1126/science.aba3656>.
- Carbone M, Arron ST, Beutler B, Bononi A, Cavenee W, Cleaver JE, Croce CM, D'Andrea A, Foulkes WD, Gaudino G, Groden JL, Henske EP, Hickson ID, Hwang PM, Kolodner RD, Mak TW, Malkin D, Monnat RJ Jr, Novelli F, Pass HI, Petrini JH, Schmidt LS, Yang H. Tumour predisposition and cancer syndromes as models to study geneenvironment interactions. *Nat Rev Cancer*, 2020, 20(9): 533-549. <https://doi.org/10.1038/s41568-020-0265-y>
- Chen, Z., Hay, J.N., Jenkins, M.J., 2013. The thermal analysis of poly(ethylene terephthalate) by FTIR spectroscopy. *Thermochim. Acta* 552, 123–130. <https://doi.org/10.1016/j.tca.2012.11.002>.
- Cortés, C., Domenech, J., Salazar, M., Pastor, S., Marcos, R., Hernández, A., 2020. Nanoplastics as a potential environmental health factor: effects of polystyrene nanoparticles on human intestinal epithelial Caco-2 cells. *Environ. Sci. Nano* 7, 272–285. <https://doi.org/10.1039/C9EN00523D>.
- Dhaka, V., Singh, S., Anil, A.G., Sunil Kumar Naik, T.S., Garg, S., Samuel, J., Kumar, M., Ramamurthy, P.C., Singh, J., 2022. Occurrence, toxicity and remediation of polyethylene terephthalate plastics. A review. *J. Environ. Chem. Lett.* 13, 1–24. <https://doi.org/10.1007/s10311-021-01384-8>.
- Domenech, J., Hernández, A., Rubio, L., Marcos, R., Cortés, C., 2020. Interactions of polystyrene nanoplastics with in vitro models of the intestinal barrier. *Arch. Toxicol.* 94 (9), 2997–3012. <https://doi.org/10.1007/s00204-020-02805-3>.
- Domenech, J., de Britto, M., Velázquez, A., Pastor, S., Hernández, A., Marcos, R., Cortés, C., 2021. Long-term effects of polystyrene nanoplastics in human intestinal Caco-2 cells. *Biomolecules* 11, 1442. <https://doi.org/10.3390/biom11101442>.
- ECHA, (2018) European Chemicals Agency. Background document on the Opinion on the Annex XV report proposing restrictions on intentionally added microplastics. <<https://echa.europa.eu/documents/10162/2ddaab18-76d6-49a2-ec46-8350dabf5dc>>.

- Evangelidou, N., Grythe, H., Klimont, Z., Heyes, C., Eckhardt, S., Lopez-Aparicio, S., Stohl, A., 2020. Atmospheric transport is a major pathway of microplastics to remote regions. *Nat. Commun.* 11 (1), 3381. <https://doi.org/10.1038/s41467-020-17201-9>.
- García-Rodríguez, A., Rubio, L., Vila, L., Xamena, N., Velázquez, A., Marcos, R., Hernández, A., 2019. The comet assay as a tool to detect the genotoxic potential of nanomaterials. *Nanomaterials* 9, 1385. <https://doi.org/10.3390/nano9101385>.
- Gwada, B., Ogendi, G., Makindi, S.M., Trott, S., 2019. Composition of plastic waste discarded by households and its management approaches. *Glob. J. Environ. Sci. Manag.* 5, 83–94. <https://doi.org/10.22034/gjesm.2019.01.07>.
- Hartmann, N.B., Hüffer, T., Thompson, R.C., Hassellöv, M., Verschoor, A., Daugaard, A. E., Rist, S., Karlsson, T., Brennholt, N., Cole, M., Herrling, M.P., Hess, M.C., Ivleva, N. P., Lusher, A.L., Wagner, M., 2019. Are we speaking the same language? Recommendations for a definition and categorization framework for plastic debris. *Environ. Sci. Technol.* 53 (3), 1039–1047. <https://doi.org/10.1021/acs.est.8b05297>.
- Hesler M, Aengenheister L, Ellinger B, Drexel R, Straskraba S, Jost C, Wagner S, Meier F, von Briesen H, Büchel C, Wick P, Buerki-Thurnherr T, Kohl Y. Multi-endpoint toxicological assessment of polystyrene nano- and microparticles in different biological models in vitro. *Toxicol In Vitro*, 2019, 61: 104610. <https://doi.org/10.1016/j.tiv.2019.104610>.
- Johnson, L.M., Mecham, J.B., Krovi, S.A., Moreno Caffaro, M.M., Aravamudhan, S., Kovach, A.L., Fennell, T.R., Mortensen, N.P., 2021. Fabrication of polyethylene terephthalate (PET) nanoparticles with fluorescent tracers for studies in mammalian cells. *Nanoscale Adv.* 3, 339–346. <https://doi.org/10.1039/D0NA00888E>.
- Karkossa, I., Bannuscher, A., Hellack, B., Wohlleben, W., Laloy, J., Stan, M.S., Dinischiotu, A., Wiemann, M., Luch, A., Haase, A., von Bergen, M., Schubert, K., 2021. Nanomaterials induce different levels of oxidative stress, depending on the used model system: comparison of in vitro and in vivo effects. *Sci. Total Environ.* 801, 149538 <https://doi.org/10.1016/j.scitotenv.2021.149538>.
- Kik, K., Bukowska, B., Krokosz, A., Sicińska, P., 2021. Oxidative properties of polystyrene nanoparticles with different diameters in human peripheral blood mononuclear cells (In vitro study). *Int J. Mol. Sci.* 22 (9), 4406. <https://doi.org/10.3390/ijms22094406>.
- Lionetto, F., Corcione, C.E., Rizzo, A., Maffezzoli, A., 2021. Production and characterization of polyethylene terephthalate nanoparticles. *Polymers* 13 (21), 3745. <https://doi.org/10.3390/polym13213745>.
- Lohrke, J., Briel, A., Mäder, K., 2008. Characterization of superparamagnetic iron oxide nanoparticles by asymmetrical flow-field-flow-fractionation. *Nanomedicine* 3 (4), 437–452. <https://doi.org/10.2217/17435889.3.4.437>.
- Magri, D., Veronesi, M., Sánchez-Moreno, P., Tolardo, V., Bandiera, T., Pompa, P.P., Athanassiou, A., Fragouli, D., 2021. PET nanoplastics interactions with water contaminants and their impact on human cells. *Environ. Pollut.* 271, 116262 <https://doi.org/10.1016/j.envpol.2020.116262>.
- Magri, D., Sánchez-Moreno, P., Caputo, G., Gatto, F., Veronesi, M., Bardi, G., Catelani, T., Guarnieri, D., Athanassiou, A., Pompa, P.P., Fragouli, D., 2018. Laser ablation as a versatile tool to mimic polyethylene terephthalate nanoplastic pollutants: characterization and toxicology assessment. *ACS Nano* 12 (8), 7690–7700. <https://doi.org/10.1021/acs.nano.8b01331>.
- Nanogenotox protocol. Final protocol for producing suitable manufactured nanomaterial exposure media. Nanogenotox, towards a method for detecting the potential genotoxicity of nanomaterials, 2011. https://www.anses.fr/en/system/files/nanogenotox_deliverable_5.pdf. Accessed on 15/01/2022.
- Parolini, M., Ferrario, C., De Felice, B., Gazzotti, S., Bonasoro, F., Candia Carnevali, M.D., Ortenzi, M.A., Sugni, M., 2020. Interactive effects between sinking polyethylene terephthalate (PET) microplastics deriving from water bottles and a benthic grazer. *J. Hazard. Mater.* 398, 122848 <https://doi.org/10.1016/j.jhazmat.2020.122848>.

- Pignattelli, S., Broccoli, A., Piccardo, M., Felling, S., Terlizzi, A., Renzi, M., 2021. Shortterm physiological and biometrical responses of *Lepidium sativum* seedlings exposed to PET-made microplastics and acid rain. *Ecotoxicol. Environ. Saf.* 208, 111718. <https://doi.org/10.1016/j.ecoenv.2020.111718>.
- PlasticsEurope, – The Facts 2018: An analysis of european plastics production, demand and waste data. <<https://plasticseurope.org/wp-content/uploads/2021/10/2018-Plastics-the-facts.pdf>> .
- Prata, J.C., Reis, V., Matos, J.T.V., da Costa, J.P., Duarte, A.C., Rocha-Santos, T., 2019. A new approach for routine quantification of microplastics using Nile Red and automated software (MP-VAT). *Sci. Total Environ.* 690, 1277–1283. <https://doi.org/10.1016/j.scitotenv.2019.07.060>.
- Rai, P.K., Lee, J., Brown, R.J.C., Kim, K.H., 2021. Environmental fate, ecotoxicity biomarkers, and potential health effects of micro- and nano-scale plastic contamination. *J. Hazard. Mater.* 403, 123910 <https://doi.org/10.1016/j.jhazmat.2020.123910>.
- Rodríguez-Hernández, A.G., Muñoz-Tabares, J.A., Aguilar-Guzmán, J.C., Vazquez-Duhalt, R., 2019. A novel and simple method for polyethylene terephthalate (PET) nanoparticle production. *Environ. Sci. Nano* 6 (7), 2031–2036. <https://doi.org/10.1039/c9en00365g>.
- Rubio, L., Annangi, B., Vila, L., Hernández, A., Marcos, R., 2016. Antioxidant and antigenotoxic properties of cerium oxide nanoparticles in a pulmonary-like cell system. *Arch. Toxicol.* 90, 269–278. <https://doi.org/10.1007/s00204-015-1468-y>.
- Rubio, L., Bargailla, I., Domenech, J., Marcos, R., Hernández, A., 2020. Biological effects, including oxidative stress and genotoxic damage, of polystyrene nanoparticles in different human hematopoietic cell lines. *J. Hazard. Mater.* 398, 122900 <https://doi.org/10.1016/j.jhazmat.2020.122900>.
- Shruti, V.C., Pérez-Guevara, F., Roy, P.D., Kutralam-Muniasamy, G., 2022. Analyzing microplastics with Nile Red: emerging trends, challenges, and prospects. *J. Hazard. Mater.* 423 (Pt B), 127171 <https://doi.org/10.1016/j.jhazmat.2021.127171>.
- Stock, V., Laurisch, C., Franke, J., Dönmez, M.H., Voss, L., Böhmert, L., Braeuning, A., Sieg, H., 2021. Uptake and cellular effects of PE, PP, PET and PVC microplastic particles. *Toxicol. Vit.* 70, 105021 <https://doi.org/10.1016/j.tiv.2020.105021>.
- Trevisan, R., Uzochukwu, D., Di Giulio, R.T., 2020. PAH sorption to nanoplastics and the Trojan horse effect as drivers of mitochondrial toxicity and PAH localization in zebrafish. *Front. Environ. Sci.* 8, 78. <https://doi.org/10.3389/fenvs.2020.00078>.
- Turner, A., Filella, M., 2021. Hazardous metal additives in plastics and their environmental impacts. *Environ. Int.* 156, 106622 <https://doi.org/10.1016/j.envint.2021.106622>.
- Vila, L., Rubio, L., Annangi, B., García-Rodríguez, A., Marcos, R., Hernández, A., 2017. Frozen dispersions of nanomaterials are a useful operational procedure in nanotoxicology. *Nanotoxicology* 11, 31–40. <https://doi.org/10.1080/17435390.2016.1262918>.
- Zitouni, N., Bousserhine, N., Missawi, O., Boughattas, I., Chèvre, N., Santos, R., Belbekhouche, S., Alphonse, V., Tisserand, F., Balmassiere, L., Dos Santos, S.P., Mokni, M., Guerbej, H., Banni, M., 2021. Uptake, tissue distribution and toxicological effects of environmental microplastics in early juvenile fish *Dicentrarchus labrax*. *J. Hazard. Mater.* 403, 124055 <https://doi.org/10.1016/j.jhazmat.2020.124055>.

3. RESULTS

3.2. Chapter 2 (Second Study)

Titanium-doped PET nanoplastics of environmental origin as a true-to-life model of nanoplastic

Titanium-doped PET nanoplastics of environmental origin as a true-to-life model of nanoplastic

Journal: [Science of The Total Environment](#)
Year: [2023](#)
Volume: [880](#)
Doi: [10.1016/j.scitotenv.2023.163151](#)
Impact Factor: [9.8](#)

This chapter is a verbatim of the mentioned article that is fully cited as:

Villacorta et al., 2023

A. Villacorta, L. Vela, M. Morataya-Reyes, R. Llorens-Chiralt, L. Rubio, M. Alaraby, R. Marcos, A. Hernández. Titanium-doped PET nanoplastics of environmental origin as a true-to-life model of nanoplastics. Sci. Total Environ., 880 (2023), 163151, Doi: 10.1016/j.scitotenv.2023.163151.

(The original *pdf* version is included in the Annexes, as well as the Supplementary material)

Titanium-doped PET nanoplastics of environmental origin as a true-to-life model of nanoplastic

Aliro Villacorta^{a,b}, Lourdes Vela^{a,c}, Michelle Morataya-Reyes^a, Raquel Llorens-Chiralt^d,
Laura Rubio^a, Mohamed Alaraby^{a,e}, Ricard Marcos ^{a,*}, Alba Hernández^{a,*}

^a*Group of Mutagenesis, Department of Genetics and Microbiology, Faculty of Biosciences, Universitat Autònoma de Barcelona, Cerdanyola del Vallès, Barcelona, Spain*

^b*Facultad de Recursos Naturales Renovables, Universidad Arturo Prat, Iquique, Chile*
Faculty of Health Sciences Eugenio Espejo, Universidad UTE, Quito, Ecuador

^d*AIMPLAS, Plastics Technological Centre, Gustave Eiffel, 4, 46980 Paterna, Valencia, Spain*

^e*Zoology Department, Faculty of Sciences, Sohag University, 82524 Sohag, Egypt*

* Corresponding authors at: Group of Mutagenesis, Department of Genetics and Microbiology, Faculty of Biosciences, Universitat Autònoma de Barcelona, Campus of Bellaterra, 08193 Cerdanyola del Vallès, Barcelona, Spain.

E-mail addresses: ricard.marcos@uab.cat (R. Marcos), alba.hernandez@uab.cat (A. Hernández).

<http://dx.doi.org/10.1016/j.scitotenv.2023.163151>

Received 30 January 2023; Received in revised form 13 March 2023; Accepted 25 March 2023

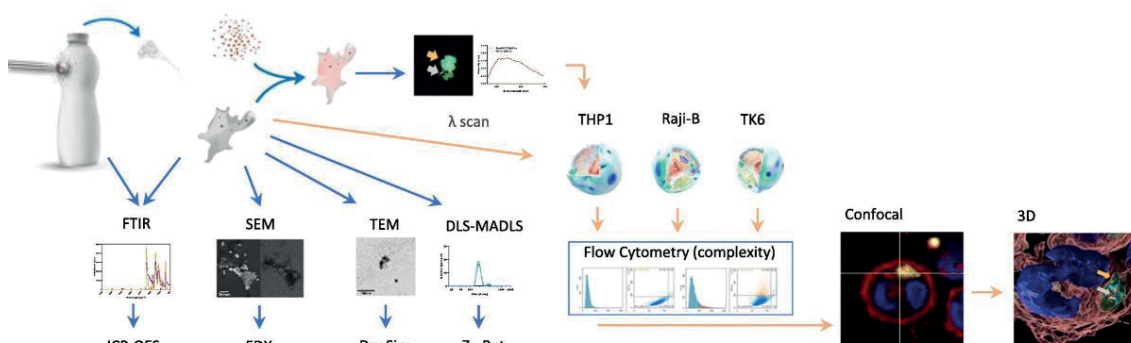
Available online 1 April 2023

0048-9697/© 2023 Published by Elsevier B.V.

HIGHLIGHTS

- Nanoplastics from opaque PET milk bottles have been obtained.
- The hybrid (PET/TiO₂NPs) nature of this material has been demonstrated.
- TEM/confocal microscopy showed the colocalization of both constituents.
- TEM(Ti)NPLs internalize differentially according to the used cell types.
- No toxic effects were observed for this true-to-life NPL.

GRAPHICAL ABSTRACT



ARTICLE INFO

Editor: Damià Barceló

Keywords:

PET(Ti) nanoplastics

Obtention

Characterization

Cell internalization

ABSTRACT

The increased presence of secondary micro/nanoplastics (MNPLs) in the environment requires urgent studies on their potentially hazardous effects on exposed organisms, including humans. In this context, it is essential to obtain representative MNPL samples for such purposes. In our study, we have obtained true-to-life NPLs resulting from the degradation, via sanding, of opaque PET bottles. Since these bottles contain titanium (TiO₂NPs), the resulting MNPLs also contain embedded metal. The obtained PET(Ti)NPLs were extensively characterized from a physicochemical point of view, confirming their nanosized range and their hybrid composition. This is the first time these types of NPLs are obtained and characterized. The preliminary hazard studies show their easy internalization in different cell lines, without apparent general toxicity. The demonstration by confocal microscopy that the obtained NPLs contain Ti samples offers this material multiple advantages. Thus, they can be used in in vivo approaches to determine the fate of NPLs after exposure, escaping from the existing difficulties to follow up MNPLs in biological samples.

1. Introduction

The extended use of plastic goods has results in global environmental pollution by plastic wastes, and their consequent environmental alarms ([Chang et al., 2022](#)). Although plastics have a relatively long life, degradation occurs through different physical-chemical-biological processes generating the so-called micro- and nanoplastics (MNPLs). At these sizes, and especially at the nano range, MNPLs can be easily internalized by organisms (including humans) following different routes, finally resulting in a potential health hazard ([Rubio et al., 2020a](#); [Gigault et al., 2021](#); [Wu et al., 2022](#)). Thus, determining the potential hazard risks associated with MNPLs exposure is a hot and current topic.

Although great efforts have been devoted to evaluating the hazards associated with MNPLs exposure, the lack of representative environmental MNPLs is a big barrier to overcome. Consequently, most of the studies have been carried out with pristine commercial polystyrene (PS) samples that, despite their advantages (uniformity, different sizes, surface functionalization, and fluorescent staining), are not fully representative of the environmental MNPLs ([Xu et al., 2022](#)). Although PSMNPLs have shown to be very useful for many purposes, the extrapolation of the obtained data is doubtful for human health risk assessment associated with MNPLs exposures ([Brachner et al., 2020](#); [Coffin et al., 2022](#)). Consequently, the obtention of environmentally relevant (true-to-life) MNPLs is an urgent challenge to be achieved.

Due to the impossibility of getting enough uniform MNPLs just by picking up environmental samples, different protocols have been proposed by using the physical degradation of plastic goods, followed by the collection of the different fractions (containing MPLs or NPLs), and their ulterior characterization. Interestingly, most of the published proposals have used polyethylene terephthalate (PET) goods as the original source. This is mainly due to the high demand for this plastic type that is mainly used for packaging, including bottles for multiple purposes, although it is also a polymer widely used in the textile industry (PlasticsEurope, n.d.). Consequently, and because of the deficient recycling mechanisms and the lack of awareness on the part of society, they finally end up in the environment as plastic waste. Among the different experimental approaches, the UV-laser ablation process was first used to obtain PET-NPLs ([Magrì et al., 2018](#)). Alternatively, mechanical milling is another fractionation process used to obtain mainly the MPLs fraction ([Astner et al., 2019](#); [Pignattelli et al., 2021](#); [Lionetto et al., 2021](#)). Furthermore, the use of mechanical ground approaches has also been proposed as an easy way to obtain PET-NPLs ([Rodríguez-Hernández et al., 2019](#); [Roursgaard et al., 2022](#); [Villacorta et al., 2022](#)).

Among the different types of PET bottles, we can distinguish between transparent and opaque PET ones. Opaque PET bottles are highly used many for packing milk because they provide the light protection that UHT milk requires and minimize gas permeability which, together with their low cost, are some of their advantages in front of other packaging options ([Tramis et al., 2021](#)). These characteristics of the opaque PET are due to the presence of titanium dioxide nanoparticles (TiO₂NPs) used as a filler, which also allows for reducing the bottle thickness. One of the common protocols to increase

the compatibility of the fillers introduced in the plastics intend to modify their surfaces by increasing their hydrophilicity or hydrophobicity. This compatibility critically depends on the particle size of the filler because that can increase/decrease viscosity affecting the physical and chemical properties of the final compound. Since surface treatments can decrease the viscosity of the compound or masterbatch, modifications of the surface of fillers are becoming important because of its improvement in adhesion (Mozetič, 2019). Surface modifications can be achieved by the chemical interaction of the fillers with compounds that possess functional groups, by chemical absorption on the surface of the particles of the filling material of some modifying agents, or by coating the filler particles with a suitable coupling agent (Fronza et al., 2019).

Aiming to obtain environmental representative MNPLs, we have used opaque PET bottles to obtain NPLs, following the protocol recently published (Villacorta et al., 2022). These true-to-life NPLs may help us to understand the complexity of the environmental MNPLs, while constituting unrivaled materials to be used to evaluate the potential health hazards of environmental MNPLs. Although different metals and metalloids like arsenic, cadmium, chromium (VI), and lead are normally used as plastic additives (Smith and Turner, 2020; Turner and Filella, 2021), they are present in amounts significantly less than TiO₂NPs in opaque PET bottles. The presence of such metals can suppose a potential concern from a toxicological perspective, not only for their possible leaching in environmental conditions but for their behavior in specific physicochemical conditions, such as the acidic environments encountered in the digestive tract of many animals, when MNPLs are unintentionally ingested. Beyond their potential toxicological profile, the obtention of titanium-doped MNPLs can represent a suitable true-to-life model to follow up their fate in complex matrices, including experimental *in vivo* models. Before determining the potential toxicity of MNPLs exposure, their cell uptake must be demonstrated and, if possible, quantified. These aspects have been the subject of recent reviews considering both the exposure route and the model organism used (Paul et al., 2020; Huang et al., 2022; Dusza et al., 2023).

Here we present our approach to obtain PET(Ti)NPLs, as well as their complete physicochemical characterization. In addition, preliminary data on their behavior in human cells under *in vitro* exposure conditions is also reported. It is important to point out that this is the first report getting and analyzing NPLs from opaque PET bottles.

2. Materials and methods

2.1. PET(Ti) nanoplastics obtention

We have used commercially available opaque-PET bottles to produce PET nanoplastics containing titanium [PET(Ti)NPLs]. The used procedure was based on the recently published method designed to get PETNPLs from water bottles (Villacorta et al., 2022). The process is schematized in Fig. 1. Briefly, pieces of about 12 cm² were cut from the original opaque PET bottle and sanded with a diamond rotary burr accessory, taking particular attention not to overheat the surface by passing in only one direction and only once on the same area. The obtained opaque PET debris was passed through a 0.20

mm sieve and 4 g of the resulting material was dispersed on 40 mL of trifluoroacetic acid pre-heated to 50 °C on a stirring plate at 100 rpm for 2 h and then kept under continuous agitation at room temperature overnight. The next day, 40 mL of TFA (20%, v/v) were added and the mixture was kept under constant stirring for 24 h more. The suspension was then passed through the 0.20 mm sieve, to eliminate the bigger pieces, and centrifuged at 2500 rcf for 1 h once distributed on six 10 mL glass tubes. The obtained pellets were resuspended on 400 mL of a 0.5% sodium dodecyl sulfate (SDS) solution, vigorously mixed, distributed into two 200 mL beakers, and ultrasonicated on an SSE-1 Branson sonicator (Branson Ultrasonics Co., Brookfield, CT, USA) for 2 min at 25% amplitude, in 9/9 s sonication/break cycles. The content of each beaker was transferred to a graduated cylinder to sediment for 1 h, to eliminate the bigger fraction. The top 100 mL of each cylinder were collected and centrifuged to eliminate SDS. Pellets were washed twice with Milli-Q water and twice with pure ethanol and dried under sterile air laminar flow. Pellets were then weighted and resuspended on Milli-Q water at concentrations of 10 mg/mL. Suspensions were then sonicated for 16 min at 10% amplitude in a cold-water bath and stock solution aliquots of 1 mL were immediately frozen on cryotubes in liquid nitrogen and stored at -80 °C for further use.

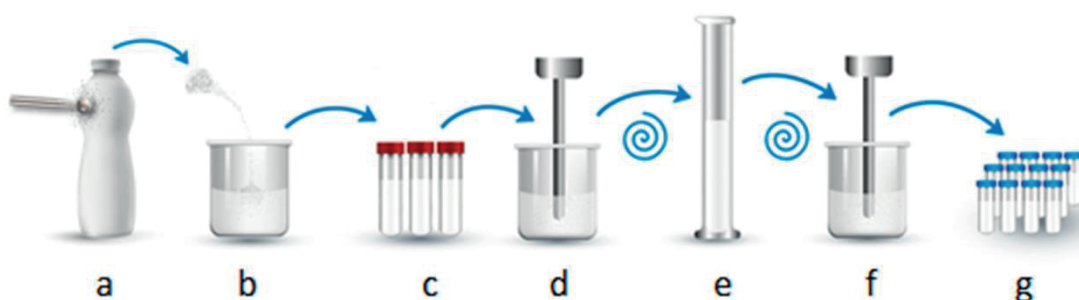


Fig. 1. Schematic representation of the PET(Ti)NPLs production. Opaque PET fragment from bottles were grinded until a powder is obtained, passed through the sieve (a), stirred, suspended, and heated at different concentrations of TFA (b), distributed on glass tubes and centrifuged (c), resuspended on SDS, sonicated (d), and transferred to a cylinder for sedimentation (e) and then collected, washed, weighted, resuspended and sonicated (f) and aliquots were prepared and stored frozen until needed (g).

2.2. PET(Ti)NPLs characterization by transmission electron microscopy (TEM)

A carbon-covered copper grid was dipped into the working solution (200 µg/mL) and allowed to evaporate overnight. Particles in the grid were examined by TEM using a JEOL JEM 1400 instrument (JEOL Ltd., Tokyo, Japan) operated at 120 kV. TEM images were analyzed for particle size distribution by measuring the Martin diameter using the ImageJ software 1.8.0_172 and processed with the GraphPad Prism 7.0 software (GraphPad, San Diego, CA). The Savitzky-Golay-like filter was applied to smoothen the curve.

2.3. PET(Ti)NPLs characterization by scanning electron microscopy (SEM) & energy dispersive X-ray spectroscopy (EDS)

From the stock solution, a working solution of 200 µg/mL was prepared by thawing in a warm bath at 37 °C and diluted in Milli-Q water. The working solution was vigorously vortexed and 10 µL of the suspension were deposited on a silica holder. Water was evaporated from the sample and examined on an SEM Zeiss Merlin (Zeiss, Oberkochen, Germany) coupled with an X-Max 20 mm EDS system (Oxford Instruments, Oxford, UK). In addition to collecting SEM images, an area including the nanoparticle surface was selected for the EDX analysis, the signal was collected and analyzed by the INCA Energy software (INCA, Grinnell, IA, USA).

2.4. PET(Ti)NPLs characterization by multi-angle and dynamic light scattering (DLS-MADLS), and zeta potential

The indicative size of the colloid structures in the suspension of the PET(Ti)NPLs was determined using a Zetasizer[®] Ultra device from Malvern Panalytical (Cambridge, United Kingdom). To such end, a working solution of 100 µg/mL of PET(Ti)NPLs was used. Additionally, to investigate the influence of the culture media in the nanoplastic dispersion, the same concentration was prepared by using the Nanogenotox dispersion protocol ([Nanogenotox, 2011](#)), and its behavior was evaluated on both Milli-Q water and on FBS supplemented RPMI (Roswell Park Memorial Institute) medium supplemented with 10% fetal bovine serum (FBS), 1% glutamine (Biowest, France), and 2.5 µg/mL of PlasmocinTM 226 (InvivoGen, CA, USA).

2.5. PET(Ti)NPLs characterization by Fourier transform infrared spectroscopy (FTIR)

To detect functional groups, and to identify samples as PET, materials at different stages of the production process were used. Thus, pieces of original materials (water- and opaque-bottles), midterm production sanded material before acid exposure, and final nanoparticle samples were analyzed and compared. For PET(Ti)NPLs from the stock solutions (10 mg/mL), a drop was placed on a gold mirror and let dry for one week inside a Petri dish. For the solid samples, 3 × 3 cm pieces for both PET bottle types were cut directly from bottles. For the above-described materials (suspension and solids original samples), the analysis was carried out on a Vertex 80 device, while the dust of polymer-metal obtained from the sanded material was analyzed by using a Tensor 27 device. Both types of equipment were from Bruker (Bruker Corporation, Billerica, Massachusetts, USA). To assess the composition, the obtained interferograms were analyzed and contrasted with previously reported data.

2.6. PET(Ti)NPLs characterization by mass spectroscopy

To determine the Ti content of the original PET source, 0.10 g of the PET(Ti) film was weighted on a Mettler Toledo XP205DR analytical balance (Mettler-Toledo S.A.E., Barcelona, Spain). This amount was dispersed in Milli-Q water to the same concentration

than the stock PET(Ti) (10 mg/mL). In an independent way, 0.25 mL of the two dispersions were vigorously agitated and digested in 5 mL of a mixture (4 mL HNO₃ 65% (p/v) and 1 mL of HF 40% (p/v)) in a microwave oven for 20 min at 260 °C (ramp 25 min to reach 260 °C). Samples were diluted on HNO₃ (1% v/v) before injection. The Ti content of the samples was determined on an inductively coupled plasma optical emission spectrometer ICP-OES Agilent 5900 (Agilent Technologies, Santa Clara, CA, USA).

2.7. PET(Ti)NPLs labeling and confocal visualization

To visualize/identify PET(Ti)NPLs on confocal microscopy, the reflection property was used for the detection of Ti. To visualize PET, separately from Ti, samples were labeled with iDye Poly Pink (iDye), following an adaptation of the published protocols to dye microplastics (Karakolis et al., 2019; Nguyen and Tufenkji, 2022). Briefly, a working solution of 1 mL of PET(Ti)NPLs at the concentration of 5 mg/mL was prepared from the stock dispersion (10 mg/mL) and transferred into a 1.5 mL tube containing previously weighed 0.01 g of the textile dye (iDye) used for synthetic fibers. The mixture was vigorously vortexed and incubated for 2 h at 70 °C on a glass tube. After cooling at room temperature, 9 mL of Milli-Q water was added to the suspension and then centrifuged at 4000 rpm on an Amicon® Ultra-15 centrifugal Ultracel®-100 K filter 1 × 105 MWCO for 15 min. This step was performed twice to remove the excess of iDye. The washed particles were then collected and suspended in the final volume of 1 mL of Milli-Q water and stored protected from light at 4 °C until needed. Here on, these stained PET(Ti)NPLs are named iDyePET(Ti)NPLs. For their visualization in the confocal microscope, the particle suspension was diluted on Milli-Q water at a final concentration of 400 µg/mL and two drops of 20 µL were placed on a slide, covered with a coverslip, and let dry inside the biosafety cabinet on air laminar flow. PET(Ti)NPLs were prepared similarly to be used as control. Both slides were examined by confocal microscopy using a Leica TCS SP5 confocal microscope. Excitation wavelength of 561 nm was set on an acousto-optic tunable filter (AOTF 561) and, emission spectra was collected between 580 and 700 nm (lambda scan begin bandwidth 575.00–585.00 nm to lambda scan end bandwidth 691.00–701.00 nm). Emission was analyzed using the Leica Application Suite X 3.7.5.24914 (Leica Microsystems CMS GmbH Wetzlar, Germany). Images were collected under the same conditions, further explained on Section 2.10.

2.8. Cell culture

To determine the cell internalization ability of PET(Ti)NPLs, three human hematopoietic cell lines were used. Thus, THP-1 monocytes, TK6 lymphoblasts, and Raji-B B-lymphocytes were selected as a widely distributed and accepted lymphoblastic human cell models. All three cell lines were purchased from Sigma Aldrich (MO, USA). Cells were grown in T-25 flasks on RPMI medium (Biowest, France) supplemented with 10% FBS, 1% glutamine (Biowest, France), and 2.5 µg/mL of Plasmocin (InvivoGen, CA, USA). Cultures, with a density ranging from 5×10^5 to 1×10^6 cells, were maintained at 37 °C in a humidified atmosphere of 5% CO₂.

2.9. PET(Ti)NPLs cell uptake (internal complexity), as determined by flow cytometry

To quantify cell internalization, the internal complexity of the exposed cells was used as an indicator of internal structural cell complexity and determined by flow cytometry. To proceed, the three selected cell lines (TK6, Raji-B, and HTP-1) were grown on U-bottom 96 well plate at a cell density of 5×10^5 cells/mL on a final volume of 0.20 mL and treated with concentrations of 25, 50, and 100 $\mu\text{g/mL}$ for a 24 h period. Once PET(Ti)NPLs uptake takes place, the orthogonal light scattering – commonly known as Side Scatter (SSC) – was evaluated using a flow cytometer Cytoflex S (Beckman Coulter CytoFLEX S). A total number of 10,000 events (single cells) were scored and evaluated using the CytExpert software and data was processed using GraphPad Prism Software 7.0. (GraphPad, San Diego, CA).

2.10. PET(Ti)NPLs cell uptake determination by confocal microscopy

For the visualization of internalized PET(Ti)NPLs into the cells, confocal microscopy was used using the protocol recently described ([Annangi et al., 2023](#)). Nuclei were stained using Hoechst 33342 (excitation of 405 nm and emission collected at 415–503), and cell membranes were dyed using Cellmask (excitation of 633 nm and emission collected at 645–786). For iDyePET(Ti)NPLs, an excitation wavelength of 561 nm and emission collected at 570–630 were used. For the localization of Ti, reflection images were obtained in parallel. Images of each sample were obtained using a Leica TCS SP5 confocal microscope and processed using ImageJ processing and analysis software, version 265 1.8.0_172.

2.11. Cell viability effects of PET(Ti)NPLs in the used cell lines

To assess the cell viability of the three hematopoietic cell lines after exposure, cells were seeded on the same conditions as previously described at a cell density of 5×10^5 cells/mL on a final volume of 0.20 mL on U-bottom 96 well plates and treated with concentrations ranging from 0 to 100 $\mu\text{g/mL}$ for a 24 h period at standard conditions. Cells were then mixed and diluted 1:100 on ISOFLOW and counted with a ZTM coulter counter (Beckman Coulter Inc., CA, USA). The average number of cells counted on each treatment was compared with the average number of the untreated control cells and data was evaluated using GraphPad Prism Software 7.0. (GraphPad, San Diego, CA).

3. Results and discussion

The PET(Ti)NPLs samples obtained according to the protocol outlined in Fig. 1 were used for further characterization. It should be remarked the large amount of material obtained in the extraction process above described. The resulting 10 vials of 1 mL of the stock dispersion (10 mg/mL) were stored at -80°C . Working solutions were prepared following the Nanogenotox protocol and aliquoted in 10 vials containing 0.2 mL of a

concentration of 5000 $\mu\text{g/mL}$. This means that a standard PET(Ti)NPLs production generate 100 vials of the working dispersion, which were stored at the same conditions until used. This is a large amount that permit to carry out several rounds of studies aiming to perform a complete characterization, and they hazard evaluation. The original process (Villacorta et al., 2022) has been used several times from PET water bottles to get more material to be spread among the PlasticHeal consortium, showing a very high repeatability.

3.1. Dry state size distribution and shape

TEM was used to determine the morphology and the size of the obtained PET(Ti)NPLs. The obtained figures were compared with those previously obtained from transparent PET bottles (Villacorta et al., 2022). In Fig. 2 it is indicated the morphology of PETNPLs (a) as compared with PET(Ti)NPLs (b and c). As observed, it is relatively easy to detect differences on the electrodensity of the sample when Ti is present. The presence of TiO_2NPs results in high-density points. Obviously, the degree of agglomeration can also be a factor modulating density. When the Martin diameter was measured for more than one hundred PET(Ti)NPLs figures, a mean size of 382.07 nm with a polydispersity index of 0.37 was obtained. Interestingly, the high electrodensity of TiO_2NPs also permitted to determine their size distribution inside the PET(Ti)NPLs complex, as indicated in Fig. 2d.

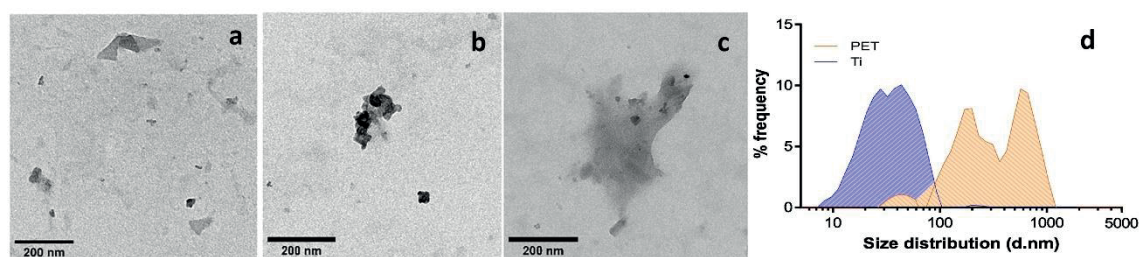


Fig. 2. TEM figures from in-house secondary PETNPLs (a) compared with PET(Ti)NPLs (b, c). The presence of TiO_2NPs is detected as a high density spots. Size distribution for PET(Ti)NPLs was determined, and a bimodal distribution was observed (orange). Due to the good detection of TiO_2NPs , their size distribution (Martin diameter) was also determined (blue).

From the size distribution it is obvious that the average exceeds the range of the nanoparticles (or by extension of a nanoplastic) definition. The last recommendation of the European Commission state that, at least the 50% of the particles contained in a dispersion must be in the nano-range, and at least one dimension must be in the 1–100 nm range (European Commission (EC), 2022). Nevertheless, this definition looks appropriated for the engineered nanomaterials, and by extension for the primary nanoplastics, but not seems adequate for secondary nanoplastics resulting from the degradation of macroplastic goods, where a large range of sizes and shapes are expected. To describe the new true-to-life obtained nanoplastics we propose to take into consideration the proposal of Hartmann et al. (2019). These authors propose to

categorize MNPLs according to the conventional units of size: nano (1–1000 nm) and micro (1–1000 μm). Although the authors divide the nano range between nanoplastics (1–100 nm) and submicron-plastics (100–1000 nm), this division add more darkness than light. Thus, from the operational point of view our sample of PET(Ti)NPLs distribution falls into the nano range.

3.2. Dry state morphology and composition

To better identify the PET(Ti)NPLs morphology and composition, SEM-EDS methodologies were used. Fig. 3a and b show the observed morphologies. It must be noted that due to the high electrodensity of Ti, the morphological visualization of PET is affected, and the figure definitions are not optimal. It is important to note the morphology of the TiO_2NPs showing their nanorod shape. Considering the average length of the TiO_2NPs nanorod present in the PET(Ti)NPLs it is assumable the size distribution determined by TEM, since it is difficult to find PET structures not associated to TiO_2NPs .

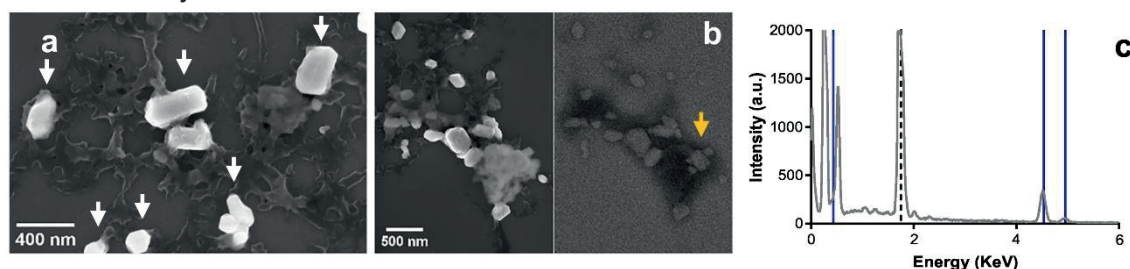


Fig. 3. SEM figures of PET(Ti)NPLs show TiO_2NPs embedded on nano-PET structures both on secondary electrons view (a), and both secondary (b, left) and backscattered (b, right) electrons. On (a) the white arrows indicate the TiO_2NPs , and on (b) the yellow arrow indicates the TiO_2NPs that are not easily visible due to the polymer covering. The EDS spectrum observed on (c), show the characteristic peaks of Ti remarked on blue, and the dashed line indicates the Si holder interference.

As previously indicated, different metals and metalloids like arsenic, cadmium, chromium (VI), and lead are normally used as plastic additives and, consequently, they can be found in their derived MNPLs (Turner and Filella, 2021). Nevertheless, the levels of titanium present in the MNPLs resulting from opaque bottles, like the obtained in this study, are very much high and impregnating the resulting MNPLs. This could suppose an associated hazard risk for such type of MNPLs. It should be remembered that Ti compound, and by extension TiO_2NPs , is a recognized food additive (E171), wide used in many food matrices (Cornu et al., 2022), were the E letter codes for substance that can be used as food additives. In addition to the multiple studies looking for potential hazards associated with E171 use, a recent publication from the panel on Food Additives and Flavorings from the European Food Safety Authority (EFSA) indicates that, “based on all the evidence available, E171 can no longer be considered as safe when used as a food additive” (EFSA Panel on Food Additives and Flavourings (FAF) et al., 2021).

Nevertheless, PET(Ti)NPLs samples can result very useful for specific purposes. The need to detect the fate of MNPLs in complex environmental matrices has been outlined as a special challenge. In the same way, to determine the fate of MNPLs in complex organisms like mammals is another important challenge. To overcome this problem, the use of metal-doped nanoplastics has been proposed (Mitrano et al., 2019; Clark et al., 2022). Nevertheless, these type of nanoplastics are far from the representative secondary MNPLs present in the environment. From this point of view our PET(Ti)NPLs would cover two main aspects, i) are MNPLs containing metal that can be used to determine their fate in experimental mammalian models, and ii) are true-to-life representative environmental MNPLs.

3.3. PET(Ti)NPLs size distribution and zeta potential in aqueous solution

The hydrodynamic behavior of PET(Ti)NPLs dispersed on Milli-Q water, or following the Nanogenotox protocol, shows mild differences among them. Independently of these mild differences, they show that there is a need of standardized procedures when it comes to nanoplastic dispersions. At this point is relevant to point out that, independently of the dispersion used, all obtained values do not differ importantly from the values obtained when TEM approaches were used (382.07 nm).

As observed on Fig. 4a–d, in terms of size distribution in number percentage, the curves whether on water or RPMI supplemented media almost overlap, and the Z-average shows no significant differences except for the behavior of PET(Ti)NPLs on supplemented RPMI, when compared with water dispersion using the one-way ANOVA with Dunnett multiple comparison test with a significance of 0.05. These data indicate that the surface coating of the particles is relevant in terms of hydrodynamic behavior when complex matrices must to be used. This not only apply for in vitro studies but mainly for in vivo studies, pointing out the need of stablish implemented dispersion protocols of nanoplastics as a good practice in terms of keeping the dispersed nanoplastics in the nanoscale range. This is a relevant key factor when different biological endpoints must be further tested. The differences in the Z-average when the BSA is added to the PET(Ti)NPLs dispersion and tested on supplemented RPMI culture medium may result in an electrosteric stabilization and this can be depicted not only in the already described changes but also in the Z-potential differences (Table 1) where the surface charge of the particle is dramatically shifted. In terms of significance, and regarding the Z-potential values, only PET(Ti)NPLs suspended on RPMI with or without the Nanogenotox protocol are not significantly different. When water dispersion values are compared with the other dispersion protocols, very significant differences for Z-potential values are observed. The particles dispersed in complex matrices tend to present a higher value of heterogeneity, which can be confirmed by observing that the values of this type of dispersion are above 0.40 in terms of the polydispersity index (PDI), while the dispersions in water do not exceed this value. In both cases, the values are not excessively low.

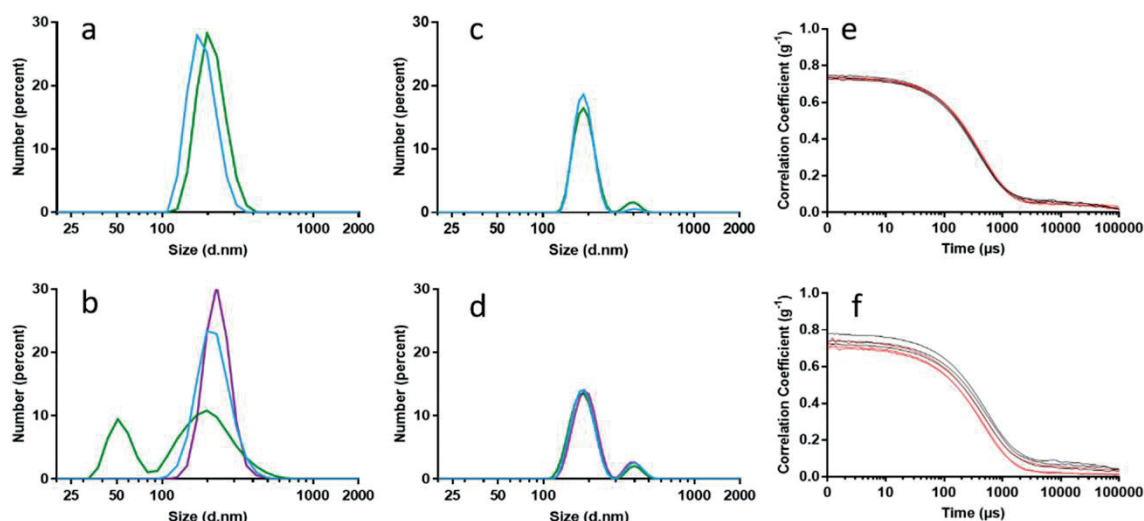


Fig. 4. Size distribution analysis of PET(Ti)NPLs on Milli-Q water (a, c) and on supplemented RPMI media (b, d) are shown by DLS (a, b) and (MADLS) (c, d) on Milli-Q water (light blue line on all charts) and on the Nanogenotox dispersion protocol (green line on all charts). Additionally multiple narrow measurements (purple lines on b and d) are shown. All correlation measurements are shown at the right side of the corresponding line (e, f, respectively).

Sample	Z-average	PDI	Z-potential*
PET(Ti)NPLs — Milli-Q	308.00 ± 6.10	0.36	- 33.10 (1)
PET(Ti)NPLs — Nanogenotox	320.00 ± 8.18	0.34	-18.23 (2)
PET(Ti)NPLs – RPMI - Nanogenotox	287.00 ± 16.10	0.40	-9.51 (3)
PET(Ti)NPLs — RPMI	357.00 ± 36.50 ^x	0.41	-6.96 (4)

*Significant differences in Z-potential values were determined by the one-way ANOVA analysis, with a Tukey's multiple comparison test. Comparisons were established between dispersion conditions (1–4) as follows: (1–2**), (1–3***), (1–4***), (2–3*), (2–4*), and (3–4ns). [ns: non-significant; *P < 0.05, **P < 0.01; ***P < 0.001]. ^x significant (P<0.05) in comparison with Milli-Q water dispersion.

3.4. Chemical determination of the PET(Ti)NPLs and Ti content quantification

As the FTIR methodology is suitable for the analysis of films, suspensions, and powders, we have used this tool to confirm the chemical identity of our PET(Ti)NPLS. This approach was used not only for the characterization of the final nanomaterial product, but also for the original commercial material (opaque PET films) and for the PET(Ti) powder obtained in the mid-step part of the process of our PET(Ti)NPLS generation. The main reason of this sequential analysis was to demonstrate that not changes in the original chemical (PET) nature was produced in the nano PET obtaining process. As observed in the Fig. 5 no significant differences in the obtained spectra are observed, confirming that the different steps carried out in the process does not modify the PET chemical nature. Thus, we can observe how the simultaneous determination of the

organic component of the sample are consistent and correspond with the spectra of PET previously reported on literature (Chen et al., 2013; Johnson et al., 2021), as well as in our previous work (Villacorta et al., 2022).

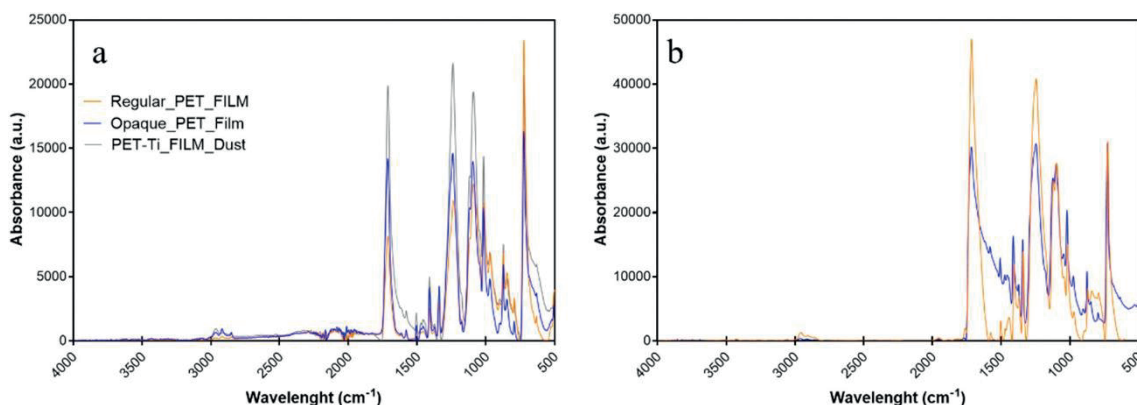


Fig. 5. FTIR spectra of the principal peaks of the interferogram. On the left chart (a) regular (orange), opaque PET (blue), and opaque PET dust produced from degradation process spectra are shown. On the right chart (b) PETNPLs (orange) from regular PET film and PET(Ti)NPLs (blue) from opaque PET are shown.

As a control, regular commercially available PET samples, as well as the nanoparticles produced from their degradation are also presented (Figs. 5a, b). We assume that during the degradation process, a fraction of the original material is lost. We specifically ask if part of the titanium content could be lost during the process. To such end we determined the percentage of titanium in the original film and in the resulting nanoplastic. Results indicate that the titanium content of the opaque PET films was 3.83%, which was reduced to 2.60% in the resulting PET(Ti)NPLs. Results for ICP-OES for the resulting PET(Ti)NPLs were very consistent and the variability among replicates was low, never been higher than 1 $\mu\text{g/mL}$, and the relative standard deviation (RSD) was never higher than 7%. On the other hand, for opaque PET film, the differences among replicates were never higher than 0.1 mg/g and the RSD was never higher than 0.6%. We assume that during the different ultracentrifugation steps, some titanium (possibly due to its high weight) is lost. Nevertheless, a very important fraction remains associated to the final product of the degradation process. Although no indications on the potential leakage of titanium from the opaque bottles have been found, such plastic can suppose many problems entering in the recycling processes (Tramis et al., 2021).

3.5. PET(Ti)NPLs labeling and confocal visualization

In this study we successfully dye PET(Ti)NPLs with the commercially available textile dye iDye Poly Pink by heating the nanoplastic/dye mixture allowing the swelling of the polymer at the time that allowing the dye entering the polymeric matrix, achieving that within the polymeric matrix we can find both the titanium and the iDye. Particles were

then resuspended and washed on Milli-Q water to remove the excess of pigment not attached to the particles, as previously described and depicted on Fig. 6a. iDyePET(Ti)NPLs shows a significant amount of fluorescence easily observed by confocal microscopy where fields with significant particle agglomerates were located and the emission collected (Fig. 6b, c, d). Consistent with previous reports (Karakolis et al., 2019) the fluorescence on PET was easily observed by this staining approach with the main difference that in our study we use nanoplastic instead of microplastics. In a recent study, authors shows that a commercially available dye (Atto 647N) can be used for similar approaches to stain different pristine NPLs (Nguyen and Tufenkji, 2022). It is necessary to remark that in our approach, in house made true-to-life nanoplastic have been used showing the suitability of our method not only for the type of polymer but also for size differences, due to the polydisperse nature of our material. As shown in Fig. 6d, signals corresponding to PET and Ti co-localize, demonstrating the mixed nature of PET(Ti)NPLs. Finally, no fluorescence signal for iDye was detectable on fields were PET(Ti)NPLs were the only component.

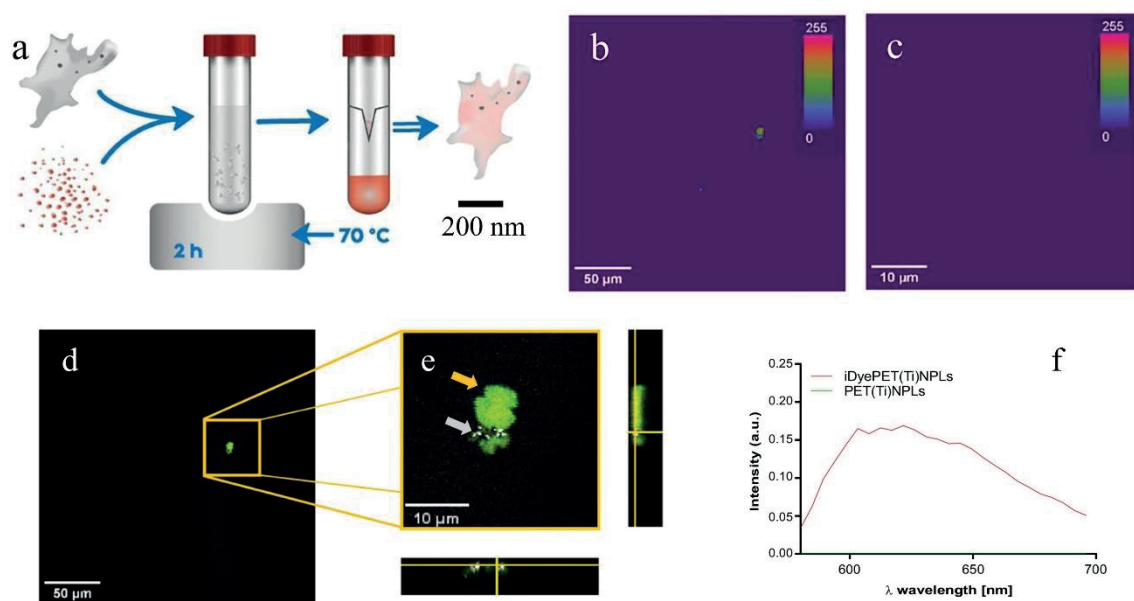


Fig. 6. a) Staining procedure: PET(Ti)NPLs were mixed with iDye Poly pink and heated at 70 °C for 2 h, then filtered, and finally resuspended. Labeling was evaluated by confocal microscopy acquiring images of the fluorescence where iDyePET(Ti)NPLs and PET(Ti)NPLs were observed agglomerated (b, c, respectively). d) When the signal for both iDye (yellow arrow) and Ti (grey arrow) were used, both signals appear together as indicative of the PET(Ti)NPLs identification. f) The emission spectra for both particles were collected and compared (green signal overlap the X-axis).

3.6. Cellular uptake evaluation

The potential harmful effects induced by MNPLs exposure require their previous internalization. There are different approaches to measure such uptake, and in this study we have used both flow cytometry and confocal microscopy. By using flow cytometry, the intensity of the side-scattered light revealed that the particles were taken up in the cells, as initially proposed (Suzuki et al., 2007). This method has been used to detect the uptake of different nanomaterials including titanium nanoparticles, by measuring the complexity of the BEAS-2B cells (Vales et al., 2015). In our study, this method has been applied to different hematopoietic cell lines to determine potential differences according to the used cell type. If MNPLs can cross the protective barriers, they move to the general compartment (blood), interacting with their respective components. Thus, blood cells can be considered as a general target to be used to determine the potential effects of any exposure including MNPLs and more specifically PET(Ti)NPLs. The obtained results are indicated in Fig. 7, for three well-known leukocytic cell lines: TK6 lymphoblastic, Raji-B lymphocytes, and THP-1 monocytic cells (Rubio et al., 2020b). As observed, the PET(Ti)NPLs uptake differs among the cell lines, leukemic monocytes (THP-1) showing the highest increase on cell complexity after exposures lasting for 24 h, and at all tested concentrations. Contrary, the lymphoblastic TK6 show practically no uptake. This differential uptake was also reported for polystyrene NPLs using the same leukocytic cells (Rubio et al., 2020b), as well as for three different white peripheral blood cells (lymphocytes, monocytes, and polymorphonuclear cells) (Ballesteros et al., 2020). Accordingly, the complexity of the uptake response must be considered in the selection of the cells to be used in any experiment aiming to evaluated hazardous effects of MNPLs.

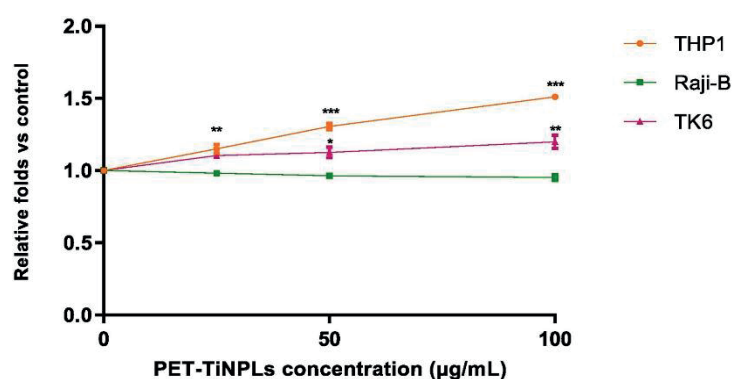


Fig. 7. Cellular internalization of PET(Ti)NPLs by Raji-B, TK6, and THP-1 cells after exposures lasting for 24 h. Graphs show the mean \pm SEM of three different experiments performed in duplicates. Complexity was compared with untreated cells using a One-way ANOVA analysis with Dunnett multiple comparisons post-test. (** $P < 0.01$; *** $P < 0.001$).

As indicated, cell uptake can also be determined by using confocal microscopy, as observed in Fig. 8. For this approach we focus our attention on THP-1 cells since this cell line showed the highest uptake in the flow cytometry approach. Interesting, we could

colocalize both the signal coming from the emission of the iDye on the iDyePET(Ti)NPLs and the signal from Ti. This is observed when Fig. 8b and c are compared, indicating the hybrid composition of the obtained PET(Ti)NPLs. The orthogonal views confirm the complex structures previously observed by using electronic microscopy (whether transmission or scanning) but this time inside a cell, as expected according to the complexity results obtained by flow cytometry. It is necessary to point out that not all the Ti remains attached to the PET MNPLs, since a fraction of the total is lost during the obtention process, as we describe on the Section 3.4, and quantify by ICP-OES. Nevertheless, the colocalization signals give relevant information supporting the mixed nature of the obtained true-to-life PET(Ti)NPLs.

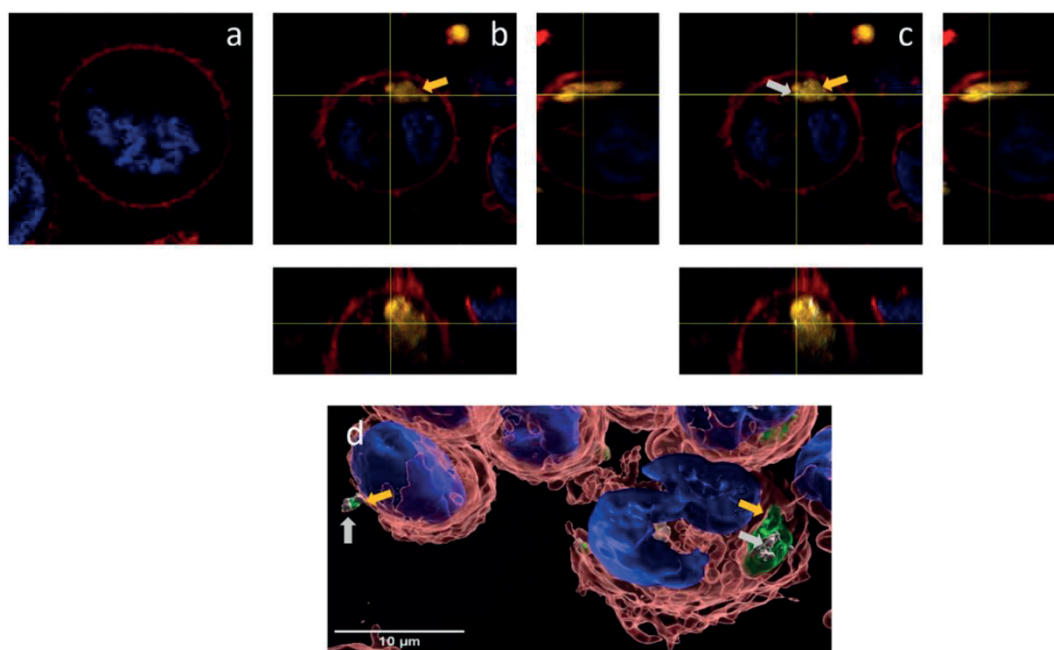


Fig. 8. Confocal microscopy uptake detection of iDyePET(Ti)NPLs in THP-1 cells, following 24 h exposure to 100 µg/mL. a) Control, untreated cells. b) Orthogonal view of THP1 cell with the Ti nanoparticles channel off and showing only iDye signal (yellow arrow). c) Co-localization of the Ti signal (grey arrow) with the PETNPLs emission. Arrows indicate both iDye and Ti signals. d) Imaris image reconstruction.

3.7. PET(Ti)NPLs effects on cell viability

As a final approach in the exhaustive evaluation of the characteristics of the obtained true-to-life PET(Ti)NPLs, the harmful effects in different human cell lines were determined in terms of cell survival. The obtained results are depicted in Fig. 9.

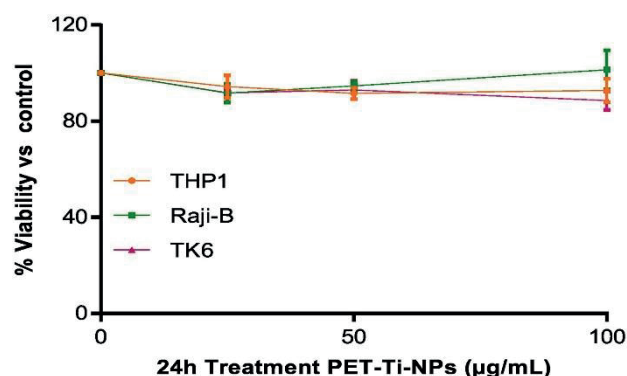


Fig. 9. Viability of hematopoietic THP-1, TK6, and Raji-B cells after exposures to PET(Ti)NPLs at concentrations ranging from 0 to 100 µg/mL for 24 h. The graph represents the viability relative to untreated cells. Graphs show the mean \pm SEM of three different experiments performed in duplicates. One-way ANOVA analysis with Dunnett multiple comparisons post-test with a confidence level of 95% was performed.

Despite the previous results, showing notorious differences on the uptake among the different selected cell lines, no significant decreases on cell viability were noticeable for any tested concentration nor cell line. This would confirm that the obtained true-to-life NPLs are not toxic, at least in the used hematopoietic cell lines and detecting effects on cell viability. This would agree with previous experiments exposing these cell lines to polystyrene nanoparticles, where not viability effects were observed in that range of exposures lasting for 24 h, and only mild effects when concentrations range to high levels such as 200 µg/mL (Rubio et al., 2020b). The lack of effects on cell viability of PET(Ti)NPLs is like our previous report using true-to-life PETNPLs obtained from sanding water bottles material (Villacorta et al., 2022), and from other secondary nano PET particles obtained following other degradation procedures (Magrì et al., 2018; Dhaka et al., 2022). Although the PET component is not considered as potentially toxic, what about the other component (TiO₂NPs)? It should be remembered that TiO₂NPs were authorized as a food additive (E171) in the EU, according to Annex II of Regulation (EC) No 1333/2008. A recent review conducted by the European Food Safety Authority (EFSA) on the safety of TiO₂NP used as food additive concluded that not toxic/harmful were identify, but a concern on their potential genotoxicity cannot be ruled out (EFSA Panel on Food Additives and Flavourings (FAF) et al., 2021). Accordingly, our data would agree with the assumed non-harmful effects of PET(Ti)NPLs exposure. It is obvious that cell viability is just the first step in the evaluation of the potential toxicity of PET(Ti)NPLs. Consequently, further extensive studies using a wide set of biomarkers are required to ruled out the existence of any type of harmful effects associated to the secondary MNPLs resulting from the degradation of opaque plastic goods.

4. Conclusions

True-to-life representative MNPLs, resulting from the degradation of environmental plastic waste, are urgently required to be used as a model for determining their potential hazards. In this context, the content of this study reports the obtention and

characterization of MNPLs resulting from the degradation of opaque milk plastic bottles [PET(Ti)NPLs] which contain TiO₂NPs. This is the first study reporting the obtention/characterization of this type of MNPLs. In addition to the multiple physicochemical assays determining the hybrid chemical nature of the obtained material, size and shape confirmed their nano range size. The preliminary studies on their biological effects show an important but variable cell uptake, depending on the used cell line. Although no significant cell viability effects were observed in any of the used cell lines, further and complex studies are necessary to have a clear view of their potential health hazards. It must be pointed out that confocal microscopy images reported that both, in the dispersion media or internalized inside the cells, PET and Ti signals colocalize. This offers an important advantage to the obtained NPLs since they can be used in in vivo studies to demonstrate their fate inside the organism, thanks to the easy identification/localization/quantification of internalized Ti.

CRedit authorship contribution statement

RM and AH planned the experiments. AV, LV, MMR, RLC, LR, and MA carried out the experimental part. AV analyzed the data, carried out the statistical analysis, and prepared tables/figs. AV, RM, and AH wrote the final manuscript.

Declaration of competing interest

The authors declare that they have no known competing financial interests or personal relationships that could have appeared to influence the work reported in this paper.

Acknowledgments

A. Villacorta was supported by PhD fellowships from the National Agency for Research and Development (ANID), CONICYT PFCHA/DOCTORADO BECAS CHILE/2020-72210237. L. Vela was supported by PhD fellowships from the Fundación Carolina. L. Rubio hold a postdoctoral Juan de la Cierva contract (IJC2020r2686I/AEI/10.13039/501100011033). M. Alaraby hold a Maria Zambrano postdoctoral contract (code 693063) from the Spanish Ministerio de Universidades, funded by the European Union-Next GenerationEU, at the UAB. M. Morataya-Reyes hold a Ph.D. FI fellowship from the Generalitat de Catalunya, A. Hernández was granted an ICREA ACADEMIA award.

This project has received funding from the European Union's Horizon 2020 research and innovation programme under grant agreement No 965196. This work was partially supported by the Spanish Ministry of Science and Innovation (PID2020-116789, RB-C43) and the Generalitat de Catalunya (2021-SGR-00731).

We thank the Molecular Inorganic Nanoparticles Group at the Institut Català de Nanociència i Nanotecnologia (ICN2-UAB-CSIC-BIST) at the UAB campus for using their premises.

References

- Annangi, B., Villacorta, A., López-Mesas, M., Fuentes-Cebrian, V., Marcos, R., Hernández, A., 2023. Hazard assessment of polystyrene nanoplastics in primary human nasal epithelial cells, focusing on the autophagic effects. *Biomolecules* 13, 220. <https://doi.org/10.3390/biom13020220>.
- Astner, A.F., Hayes, D.G., O'Neill, H., Evans, B.R., Pingali, S.V., Urban, V.S., Young, T.M., 2019. Mechanical formation of micro- and nano-plastic materials for environmental studies in agricultural ecosystems. *Sci. Total Environ.* 685, 1097–1106. <https://doi.org/10.1016/j.scitotenv.2019.06.241>.
- Ballesteros, S., Domenech, J., Barguilla, I., Cortés, C., Marcos, R., Hernández, R., 2020. Genotoxic and immunomodulatory effects in human white blood cells after ex vivo exposure to polystyrene nanoplastics. *Environ. Sci. Nano* 7, 3431–3446. <https://doi.org/10.1039/d0en00748j>.
- Brachner, A., Fragouli, D., Duarte, I.F., Farias, P.M.A., Dembski, S., Ghosh, M., Barisic, I., Zdzienbło, D., Vanoirbeek, J., Schwabl, P., Neuhaus, W., 2020. Assessment of human health risks posed by nano- and microplastics is currently not feasible. *Int. J. Environ. Res. Public Health* 17 (23), 8832. <https://doi.org/10.3390/ijerph17238832>.
- Chang, X., Fang, Y., Wang, Y., Wang, F., Shang, L., Zhong, R., 2022. Microplastic pollution in soils, plants, and animals: a review of distributions, effects and potential mechanisms. *Sci. Total Environ.* 850, 157857. <https://doi.org/10.1016/j.scitotenv.2022.157857>.
- Chen, Z., Hay, J.N., Jenkins, M.J., 2013. The thermal analysis of poly(ethylene terephthalate) by FTIR spectroscopy. *Thermochim. Acta* 552, 123–130. <https://doi.org/10.1016/j.tca.2012.11.002>.
- Clark, N.J., Khan, F.R., Mitrano, D.M., Boyle, D., Thompson, R.C., 2022. Demonstrating the translocation of nanoplastics across the fish intestine using palladium-doped polystyrene in a salmon gut-sac. *Environ. Int.* 159, 106994. <https://doi.org/10.1016/j.envint.2021.106994>.
- Coffin, S., Bouwmeester, H., Brander, S., Damdimopoulou, P., Guin, T., Hermabessiere, L., Khan, E., Koelmans, A.A., Lemieux, C.L., Teerds, K., Wagner, M., Weisberg, S.B., Wright, S., 2022. Development and application of a health-based framework for informing regulatory action in relation to exposure of microplastic particles in California drinking water. *Microplast. Nanoplast.* 2 (1), 12. <https://doi.org/10.1186/s43591-022-00030-6>.
- Cornu, R., Béduneau, A., Martin, H., 2022. Ingestion of titanium dioxide nanoparticles: a definite health risk for consumers and their progeny. *Arch. Toxicol.* 96 (10), 2655–2686. <https://doi.org/10.1007/s00204-022-03334-x>.
- Dhaka, V., Singh, S., Anil, A.G., Sunil Kumar Naik, T.S., Garg, S., Samuel, J., Kumar, M., Ramamurthy, P.C., Singh, J., 2022. Occurrence, toxicity and remediation of polyethyleneterephthalate plastics. A review. *Environ. Chem. Lett.* 20 (3), 1777–1800. <https://doi.org/10.1007/s10311-021-01384-8>.
- Dusza, H.M., van Boxel, J., van Duursen, M.B.M., Forsberg, M.M., Legler, J., Vähäkangas, K.H., 2023. Experimental human placental models for studying uptake, transport and toxicity of micro- and nanoplastics. *Sci. Total Environ.* 860, 160403. <https://doi.org/10.1016/j.scitotenv.2022.160403>.
- European Commission (EC), 2022. Recommendation on the nanoparticle definition. 10-6 https://ec.europa.eu/environment/chemicals/nanotech/pdf/C_2022_3689_1_EN_ACT_par_t1_v6.pdf.
- EFSA Panel on Food Additives and Flavourings (FAF) Younes, M., Aquilina, G., Castle, L., Engel, K.H., Fowler, P., Frutos Fernandez, M.J., Fürst, P., Gundert-Remy, U., Gürtler, R., Husøy,

- T., Manco, M., Mennes, W., Moldeus, P., Passamonti, S., Shah, R., Waalkens- Berendsen, I., Wölfe, D., Corsini, E., Cubadda, F., De Groot, D., FitzGerald, R., Gunnare, S., Gutleb, A.C., Mast, J., Mortensen, A., Oomen, A., Piersma, A., Plichta, V., Ulbrich, B., Van Loveren, H., Benford, D., Bignami, M., Bolognesi, C., Crebelli, R., Dusinska, M., Marcon, F., Nielsen, E., Schlatter, J., Vleminckx, C., Barmaz, S., Carfi, M., Civitella, C., Giarola, A., Rincon, A.M., Serafimova, R., Smeraldi, C., Tarazona, J., Tard, A., Wright, M., 2021. Safety assessment of titanium dioxide (E171) as a food additive. *EFSA J.* 19 (5), e06585. <https://doi.org/10.2903/j.efsa.2021.6585>.
- Fronza, B.M., Lewis, S., Shah, P.K., Barros, M.D., Giannini, M., Stansbury, J.W., 2019. Modification of filler surface treatment of composite resins using alternative silanes and functional nanogels. *Dent. Mater.* 35 (6), 928–936. <https://doi.org/10.1016/j.dental.2019.03.007>.
- Gigault, J., El Hadri, H., Nguyen, B., Grassl, B., Roweczyk, L., Tufenkji, N., Feng, S., Wiesner, M., 2021. Nanoplastics are neither microplastics nor engineered nanoparticles. *Nat. Nanotechnol.* 16 (5), 501–507. <https://doi.org/10.1038/s41565-021-00886-4>.
- Hartmann, N.B., Hüffer, T., Thompson, R.C., Hassellöv, M., Verschoor, A., Daugaard, A.E., Rist, S., Karlsson, T., Brennholt, N., Cole, M., Herrling, M.P., Hess, M.C., Ivleva, N.P., Lusher, A.L., Wagner, M., 2019. Are we speaking the same language? Recommendations for a definition and categorization framework for plastic debris. *Environ. Sci. Technol.* 53 (3), 1039–1047. <https://doi.org/10.1021/acs.est.8b05297>.
- Huang, D., Chen, H., Shen, M., Tao, J., Chen, S., Yin, L., Zhou, W., Wang, X., Xiao, R., Li, R., 2022. Recent advances on the transport of microplastics/nanoplastics in abiotic and biotic compartments. *J. Hazard. Mater.* 438, 129515. <https://doi.org/10.1016/j.jhazmat.2022.129515>.
- Johnson, L.M., Mecham, J.B., Krovi, S.A., Moreno Caffaro, M.M., Aravamudhan, S., Kovach, A.L., Fennell, T.R., Mortensen, N.P., 2021. Fabrication of polyethylene terephthalate (PET) nanoparticles with fluorescent tracers for studies in mammalian cells. *Nanoscale. Adv.* 3, 339–346. <https://doi.org/10.1039/D0NA00888E>.
- Karakolis, E.G., Nguyen, B., You, J.B., Rochman, C.M., Sinton, D., 2019. Fluorescent dyes for visualizing microplastic particles and fibers in laboratory-based studies. *Environ. Sci. Technol. Lett.* 6, 334–340. <https://doi.org/10.1021/acs.estlett.9b00241>.
- Lionetto, F., Corcione, C.E., Rizzo, A., Maffezzoli, A., 2021. Production and characterization of polyethylene terephthalate nanoparticles. *Polymers (Basel)* 13 (21), 3745. <https://doi.org/10.3390/polym13213745>.
- Magri, D., Sánchez-Moreno, P., Caputo, G., Gatto, F., Veronesi, M., Bardi, G., Catelani, T., Guarnieri, D., Athanassiou, A., Pompa, P.P., Fragouli, D., 2018. Laser ablation as a versatile tool to mimic polyethylene terephthalate nanoplastic pollutants: characterization and toxicology assessment. *ACS Nano* 12 (8), 7690–7700. <https://doi.org/10.1021/acs.nano.8b01331>.
- Mitrano, D.M., Beltzung, A., Frehland, S., Schmiedgruber, M., Cingolani, A., Schmidt, F., 2019. Synthesis of metal-doped nanoplastics and their utility to investigate fate and behaviour in complex environmental systems. *Nat. Nanotechnol.* 14 (4), 362–368. <https://doi.org/10.1038/s41565-018-0360-3>.
- Mozetič, M., 2019. Surface modification to improve properties of materials. *Materials (Basel)* 12 (3), 441. <https://doi.org/10.3390/ma12030441>. Nanogenotox, 2011. http://www.nanogenotox.eu/files/PDF/Deliverables/nanogenotox%20deliverable%203_wp4_%20dispersion%20protocol.pdf.
- Nguyen, B., Tufenkji, N., 2022. Single-particle resolution fluorescence microscopy of nanoplastics. *Environ. Sci. Technol.* 56 (10), 6426–6435. <https://doi.org/10.1021/acs.est.1c08480>.
- Paul, M.B., Stock, V., Cara-Carmona, J., Lisicki, E., Shopova, S., Fessard, V., Braeuning, A., Sieg, H., Böhmert, L., 2020. Micro- and nanoplastics -current state of knowledge with the focus on oral uptake and toxicity. *Nanoscale Adv.* 2 (10), 4350–4367. <https://doi.org/10.1039/d0na00539h>.

- Pignattelli, S., Broccoli, A., Piccardo, M., Felling, S., Terlizzi, A., Renzi, M., 2021. Short-term physiological and biometrical responses of *Lepidium sativum* seedlings exposed to PET-made microplastics and acid rain. *Ecotoxicol. Environ. Saf.* 208, 111718. <https://doi.org/10.1016/j.ecoenv.2020.111718>.
- PlasticsEurope. Plastics -The Facts 2021: An Analysis of European Plastics Production, Demand and Waste Data. (Accessed: on 13 September 2022); Available online <https://plasticseurope.org/wp-content/uploads/2021/12/Plastics-the-Facts-2021-web-final.pdf>.
- Rodríguez-Hernández, A.G., Muñoz-Tabares, J.A., Aguilar- Guzmán, J.C., Vazquez-Duhalt, R., 2019. A novel and simple method for polyethylene terephthalate (PET) nanoparticle production. *Environ. Sci. Nano* 6 (7), 2031–2036. <https://doi.org/10.1039/c9en00365g>.
- Roursgaard, M., Hezareh Rothmann, M., Schulte, J., Karadimou, I., Marinelli, E., Møller, P., 2022. Genotoxicity of particles from grinded plastic items in Caco-2 and HepG2 cells. *Front. Public Health* 10, 906430. <https://doi.org/10.3389/fpubh.2022.906430>.
- Rubio, L., Marcos, R., Hernández, A., 2020. Potential adverse health effects of ingested micro and nanoplastics on humans. Lessons learned from in vivo and in vitro mammalian models. *J. Toxicol. Environ. Health B. Crit. Rev.* 23 (2), 51–68. <https://doi.org/10.1080/10937404.2019.1700598>.
- Rubio, L., Barguilla, I., Domenech, J., Marcos, R., Hernández, A., 2020b. Biological effects, including oxidative stress and genotoxic damage, of polystyrene nanoparticles in different human hematopoietic cell lines. *J. Hazard. Mater.* 398, 122900. <https://doi.org/10.1016/j.jhazmat.2020.122900>.
- Smith, E.C., Turner, A., 2020. Mobilisation kinetics of Br, Cd, Cr, Hg, Pb, and Sb in microplastics exposed to simulated, dietary-adapted digestive conditions of seabirds. *Sci. Total Environ.* 733, 138802. <https://doi.org/10.1016/j.scitotenv.2020.138802>.
- Suzuki, H., Toyooka, T., Ibuki, Y., 2007. Simple and easy method to evaluate uptake potential of nanoparticles in mammalian cells using a flow cytometric light scatter analysis. *Environ. Sci. Technol.* 41, 3018–3024. <https://doi.org/10.1021/es0625632>.
- Tramis, O., Garnier, C., Yus, C., Irusta, S., Chabert, F., 2021. Enhancement of the fatigue life of recycled PP by incorporation of recycled opaque PET collected from household milk bottle wastes. *Waste Manag.* 125, 49–57. <https://doi.org/10.1016/j.wasman.2021.02.006>.
- Turner, A., Filella, M., 2021. Hazardous metal additives in plastics and their environmental impacts. *Environ. Int.* 156, 106622. <https://doi.org/10.1016/j.envint.2021.106622>.
- Vales, G., Rubio, L., Marcos, R., 2015. Long-term exposures to low doses of titanium dioxide nanoparticles induce cell transformation, but not genotoxic damage in BEAS-2B cells. *Nanotoxicology* 9 (5), 568–578. <https://doi.org/10.3109/17435390.2014.957252>.
- Villacorta, A., Rubio, L., Alaraby, M., López-Mesas, M., Fuentes-Cebrian, V., Moriones, O.H., Marcos, R., Hernández, A., 2022. A new source of representative secondary PET nanoplastics. Obtention, characterization, and hazard evaluation. *J. Hazard. Mater.* 439, 129593. <https://doi.org/10.1016/j.jhazmat.2022.129593>.
- Wu, P., Lin, S., Cao, G., Wu, J., Jin, H., Wang, C., Wong, M.H., Yang, Z., Cai, Z., 2022. Absorption, distribution, metabolism, excretion, and toxicity of microplastics in the human body and health implications. *J. Hazard. Mater.* 437, 129361. <https://doi.org/10.1016/j.jhazmat.2022.129361>.
- Xu, J.L., Lin, X., Wang, J.J., Gowen, A.A., 2022. A review of potential human health impacts of micro- and nanoplastics exposure. *Sci. Total Environ.* 17, 158111. <https://doi.org/10.1016/j.scitotenv.2022.158111>.

3. RESULTS

3.3. Chapter 3 (Third study)

Fluorescent labeling of
micro/nanoplastics for biological
applications with a focus on
“true-to-life” tracking

3.3. Chapter 3 (Third study)

Fluorescent labeling of micro/nanoplastics for biological applications with a focus on “true-to-life” tracking

Journal: [Journal of Hazardous Materials](#)
Year: [2024](#)
Volume: [476](#)
Doi: [10.1016/j.jhazmat.2024.135134](#)
Impact Factor: [13.6](#)

This chapter is a verbatim of the mentioned article that is fully cited as:

Villacorta et al., 2024

Villacorta, A., Cazorla-Ares, C., Fuentes-Cebrian, V., Valido, I. H., Vela, L., Carrillo-Navarrete, F., Morataya-Reyes, M., Mejia-Carmona, K., Pastor, S., Velázquez, A., Arribas Arranz, J., Marcos, R., López-Mesas, M., & Hernández, A. (2024). Fluorescent labeling of micro/nanoplastics for biological applications with a focus on “true-to-life” tracking. *Journal of Hazardous Materials*, 476, 135134. Doi: 10.1016/j.jhazmat.2024.135134

(The original *pdf* version is included in the Annexes, as well as the Supplementary material)

Fluorescent labeling of micro/nanoplastics for biological applications with a focus on “true-to-life” tracking

Aliro Villacorta^{a,b,#}, Camila Cazorla-Ares^{c,#}, Victor Fuentes-Cebrian^c, Lourdes Vela^{a,d}, Fernando Carrillo-Navarrete^e, Michelle Morataya-Reyes^a, Karen Mejia-Carmona^f, Susana Pastor^a, Antonia Velázquez^a, Jessica Arribas Arranz^a, Ricard Marcos^a, Montserrat López-Mesas^{c,*}, Alba Hernández^{a,*}

^a*Group of Mutagenesis, Department of Genetics and Microbiology, Faculty of Biosciences, Universitat Autònoma de Barcelona, Cerdanyola del Vallès, Barcelona, Spain.*

^b*Facultad de Recursos Naturales Renovables, Universidad Arturo Prat, Iquique, Chile.*

^c*GTS Research Group, Department of Chemistry, Faculty of Science, Universitat Autònoma de Barcelona, Cerdanyola del Vallès, 08193, Barcelona, Spain.*

^d*Faculty of Health Sciences Eugenio Espejo, Universidad UTE, Quito, Ecuador.*

^e*Institut d'Investigació Tèxtil i Cooperació Industrial de Terrassa (INTEXTER) and Department of Chemical Engineering, Universitat Politècnica de Catalunya, Terrassa, 08222, Barcelona, Spain.*

^f*Institut Català de Nanociència i Nanotecnologia (ICN2-UAB-CSIC-BIST), Cerdanyola del Vallès Spain.* # Both authors contributed equally

* Corresponding authors at Group of Mutagenesis, Department of Genetics and Microbiology, Faculty of Biosciences, and GTS Research Group, Department of Chemistry, Faculty of Science, both from Universitat Autònoma de Barcelona, Campus of Bellaterra, 08193 Cerdanyola del Vallès, Spain.

E-mail: alba.hernandez@uab.cat (A. Hernández)

montserrat.lopez.mesas@uab.cat (M. López-Mesas)

<https://doi.org/10.1016/j.jhazmat.2024.135134>

Received 28 March 2024; Received in revised form 24 June 2024; Accepted 5 July 2024

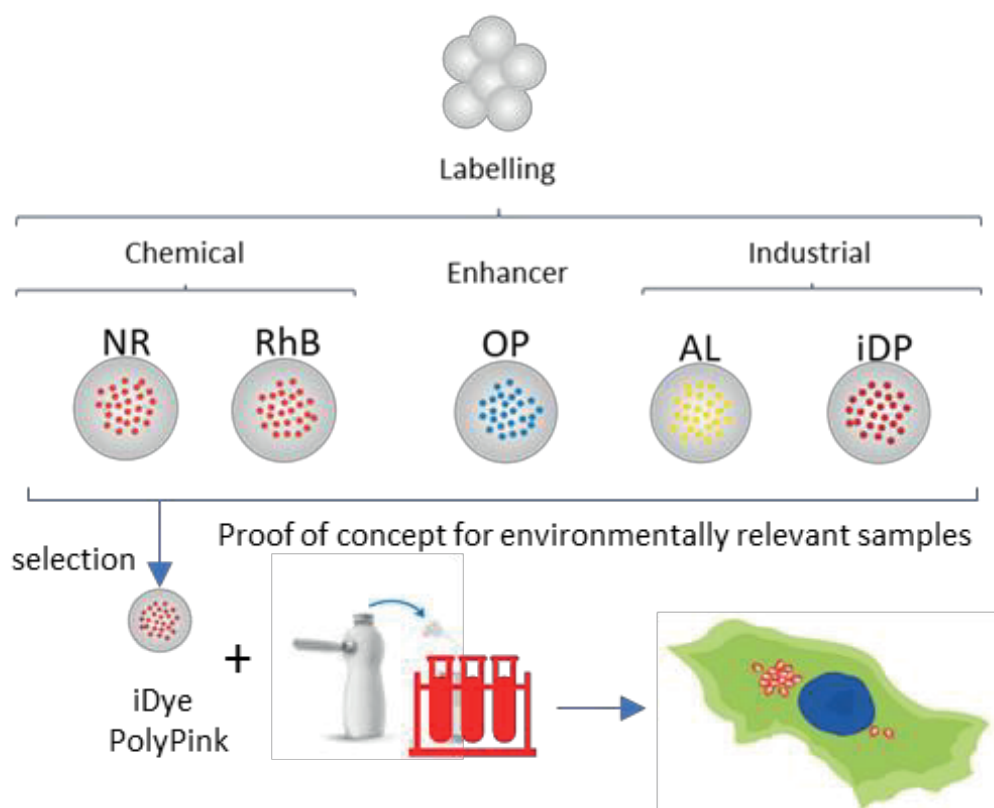
Available online 8 July 2024

0304-3894/© 2024 The Author(s). Published by Elsevier B.V.

HIGHLIGHTS

- Advantages/disadvantages of five dyes to label nanoplastics (NPLs) were evaluated.
- A wide battery of assays was used for such determinations.
- iDye PolyPink was the dye showing more advantages.
- The advantages of labeling nanopolystyrene were extended to true-to-life NPLs.
- iDye PolyPink succeeded in staining titanium-doped PET-NPLs.

GRAPHICAL ABSTRACT



ARTICLE INFO

Editor: Lingxin Chen,

Keywords:

Micro/nanoplastics
Staining; specificity
iDye PolyPink
Cell-internalization tracking.

ABSTRACT

The increased environmental presence of micro-/nanoplastics (MNPLs) and the potential health risks associated with their exposure classify them as environmental pollutants with special environmental and health concerns. Consequently, there is an urgent need to investigate the potential risks associated with secondary MNPLs. In this context, using “true-to-life” MNPLs, resulting from the laboratory degradation of plastic goods, may be a sound approach. These non-commercial secondary MNPLs must be labeled to track their presence/journeys inside cells or organisms. Because the cell internalization of MNPLs is commonly analyzed using fluorescence techniques, the use of fluorescent dyes may be a sound method to label them. Five different compounds comprising two chemical dyes (Nile Red and Rhodamine-B), one optical brightener (Opticol), and two industrial dyes (Amarillo Luminoso and iDye PolyPink) were tested to determine their potential for such applications. Using commercial standards of polystyrene nanoplastics (PSNPLs) with an average size of 170 nm, different characteristics of the selected dyes such as the absence of impact on cell viability, specificity for plastic staining, no leaching, and lack of interference with other fluorochromes were analyzed. Based on the overall data obtained in the wide battery of assays performed, iDye PolyPink exhibited the most advantages, with respect to the other compounds, and was selected to effectively label “true-to-life” MNPLs. These advantages were confirmed using a proposed protocol, and labeling titanium-doped PETNPLs (obtained from the degradation of milk PET plastic bottles), as an example of “true-to-life” secondary NPLs. These results confirmed the usefulness of iDye PolyPink for labeling MNPLs and detecting cell internalization.

1. Introduction

Large-scale production of synthetic organic polymers can be traced back to the 1950's. Since then, plastic production has progressively and steadily increased; consequently, a large amount of plastic waste has been continuously generated. Although environmental policies tend to reduce waste, a short-term scenario in which this situation could change is not feasible. In the environment, physicochemical or biologically mediated degradation processes of plastic waste produce secondary micro-/nanoplastics (MNPLs), which are considered environmental pollutants of emergent concern. Although the limits between microplastics (MPLs) and nanoplastics (NPLs) are still being investigated [2], [1], the smaller the size, the higher the probability of internalization into exposed organisms, including humans. As the definition of NPLs is a bit conflicting, this study considers NPLs in the range 1–1000 nm [3]. Multiple reviews have recently been published on the potential health risks associated with MNPL exposure, including oxidative stress, alterations in gene expression, genotoxicity, and carcinogenicity as potential effects associated with MNPL exposure [4], [5], [6]. However, the accurate determination of exposure (primarily at the NPLs level) requires further refinement and, consequently, the lack of exposure-effect information minimizes the relevance of the reported potential health risks [7]. In *in vitro/in vivo* experimental approaches, a growing interest exists in using “true-to-life” MNPLs resulting from the degradation of plastic goods because they are considered more representative of environmental plastic waste [3]. Accordingly, the use of these “true-to-life” MNPLs is a promising option, in opposition to the use of pristine polystyrene commercial MNPLs, to better define the potential risks associated with MNPL exposures owing to variations in their physicochemical properties. Notably, the confirmation that the used “*true-to-life*” (or any other used MNPLs) can internalize on cells/tissues should be a mandatory requirement in any published study. In this regard, significant advances have been made, pushing the boundaries of technology and techniques, demonstrating notable approaches such as the use of graphene oxide quantum dots to embed polystyrene (PS) microspheres by microemulsion polymerization [8] and hyperspectral imaging as a novel approach to studying the accumulation and distribution of NPs in human cells [9]. However, the development of techniques enabling three-dimensional (3D) analysis without detrimental or stressful effects at the cellular level and allowing, for instance, 3D reconstruction for future applications appears to be a secure path forward. Thus, it is necessary to “label” these “*true-to-life*” MNPLs in such a way that their presence can be easily detected to follow up on the presence of these plastics inside cell and /tissues. For such purposes, Nile Red staining has been extensively used to label MNPLs, showing multiple apparent advantages, including affordability and straightforward applications [10]. Although these advantages have been well-reported when environmental matrices are evaluated [11], problems arise with biological matrices [12], primarily because of the ability of Nile Red to stain intracellular lipid droplets/bodies. This ability to fluoresce strongly in lipophilic environments has been known for a long time and is why Nile Red was initially proposed to act as a lipid-specific stain [13]. In several cases, Nile Red has been used to detect propylene microplastics in crop plants; however, the protocol assumes the destruction/digestion of the plants, which prevents the detection of *in*

situ internalization [14]. Using Nile Red staining, polystyrene, polyethylene, and polyamide were detected in the bottled water samples. In addition, when zebrafish embryos were exposed to Nile red-stained polyethylene MPLs, their accumulation was observed in various organs [15]. Therefore, owing to the non-specific staining ability of Nile Red and its high cost, more specific MNPL staining is required.

Several studies have determined the potential usefulness of alternative dyes such as textile dyes. In a recent study, four textile dyes (Rit pink, Rit blue, iDye pink, and iDye blue) were compared with Nile Red using 17 different polymers [16]. The results indicated the low efficacy of blue dyes and similar efficacy of pink dyes for Nile Red. Another study compared the usefulness of fluorescein and Nile Red in detecting polystyrene, polypropylene, and polyethylene MNPLs [17]. Significant differences between dyes were observed, with fluorescein enabling the specific detection of polystyrene, whereas Nile Red showed the highest increase in fluorescence for polypropylene. Unfortunately, all of these studies were carried out in water dispersions, but did not use biological matrices, as required for biological studies. Furthermore, Rhodamine B has been demonstrated to successfully stain five types of microplastic polymers (polyethylene, polypropylene, polystyrene, polyvinyl chloride, and polyurethane) under laboratory conditions [18]. In addition, polyvinyl chloride MPLs were successfully stained, and their ingestion was demonstrated in the copepod (*Pseudocalanus spp*) gut [19]. All these studies highlight the relevance of staining MNPLs and the lack of consistent proposals for one of them.

The lack of harmonized and established protocols for MNPL labeling, to detect cell internalization, is an important inconvenience in the development and study of the effects of “true-to-life” MNPLs. To fill this gap, the present study was conducted using two textile dyes (Amarillo Luminoso Polyester GNH 400 for industrial use and iDye PolyPink for domestic use), an industrial optical brightener (Opticol UPR), and two chemical dyes (Nile Red and Rhodamine B) to determine their suitability. The study consisted of two parts. In the first step, a suitable protocol for staining commercial polystyrene nanoplastics (PSNPLs) is developed, avoiding interference from other typical labeling fluorescence compounds; the stained-PSNPLs are internalized into cells and their distribution is studied. In the second one, and as a *proof of concept*, the selected dye, following a simplified staining protocol, was evaluated for the labeling of titanium-labeled PET nanoplastics (PET-Ti-NPLs) resulting from the degradation of opaque PET plastic bottles, followed by the internalization into cells [20]. As a novelty, our proposal for the best labeling method for MNPLs is based on a deeper analysis of the pros and cons of the five selected dyes after analyzing their responses in a wide battery of assays.

2. Materials and methods

2.1. Reagents and standards

Commercial standards of polystyrene nanoplastics (PSNPLs) were obtained from Ted Pella Inc. (Redding, CA, USA). These nanospheres had an SEM/TEM certified size of 170 ± 9 nm and were provided in an aqueous stabilized suspension (for non-aggregation purposes) at a concentration of 0.1% (w/v). The selected compounds were Nile Red (NR), Rhodamine B (RhB) (Merck KGaA, Darmstadt, Germany), Amarillo Luminoso

Polyester GNH 400 (AL), Opticol UPR (Op) (Colorcenter, Terrassa, Spain), and iDye PolyPink (iDP) (Rupert, Gibbon & Spider, Inc., Healdsburg, CA, USA). For the second part of the study, “true-to-life” PET(Ti)-NPLs obtained as described below were used. Briefly, 12 cm² fragments from commercially available milk PET bottles were sanded using a diamond rotary burr to avoid overheating the surface of the polymer. The debris was sieved through a 0.20 mm mesh and 4 g of the fine material was dispersed in 40 mL of 90% (v/v) trifluoroacetic acid (TFA) pre-heated to 50 °C on a stirring plate at 100 rpm for 2 h, followed by continuous agitation at room temperature overnight. Particles in suspension were sieved through a 0.20 mm mesh, and the eluent was divided into 10 mL glass tubes and centrifuged for 1 h at 2500 rcf. The resulting pellet was resuspended in 400 mL of 0.5% (v/v) sodium dodecyl sulfate (SDS) and subjected to ultrasonication using an SSE-1 Branson sonicator (Brookfield, CT, USA) for 2 min at 25% amplitude, with 9/9 s sonication/break cycles, and immediately transferred to 200 mL graduated cylinders and allowed to sediment for 1 h to remove the larger fractions. The upper fraction (100 mL) of each cylinder was collected and centrifuged to remove SDS. The resultant pellets were washed twice with Milli-Q water and twice with pure ethanol and dried under sterile air laminar flow. The dried pellets were weighed and resuspended in Milli-Q water at a concentration of 10 mg/mL. These suspensions were sonicated for 16 min at 10% amplitude in a cold-water bath, immediately frozen using liquid nitrogen, and transferred to a – 80 °C freezer until needed.

2.2. Ultracentrifugation optimization

To achieve the highest centrifugation efficiency, a 40-ppm suspension of non-labeled PSNPLs was prepared in Milli-Q water. The suspension was ultracentrifuged for 5, 15, 30, or 45 min at 13,200 rpm using a 5415 R Eppendorf centrifuge (Eppendorf AG, Hamburg, Germany).

The centrifugation yield was determined using an ultraviolet-visible (UV-Vis) spectrophotometer (ATI-UNICAM UV2; Thermo Fischer, Braunschweig, Germany). This was calculated by comparing the intensity between the non-centrifuged suspension, used as a reference ($A_{250\text{ nm}} 40\text{ ppm standard}$), and the supernatant of the centrifuged suspension at 250 nm ($A_{250\text{ nm}} (\text{supernatant of centrifugation } X \text{ min})$), which is within the range of the characteristic polystyrene wavelength, avoiding errors due to the saturation of the detector (Eq. 1).

$$\text{Centrifugation Yield (\%)} = \left(100 - \frac{A_{250\text{ nm}} (\text{supernatant of centrifugation } X \text{ min})}{A_{250\text{ nm}} 40\text{ ppm standard}}\right) \cdot 100 \quad (\text{Eq. 1})$$

2.3. Membrane centrifugation efficiency study

centrifugal Ultracel®– 100 K filter 1 × 105 MWCO (Merck KGaA, Darmstadt, Germany) were tested. A calibration curve was prepared using concentrations ranging 150 ppt to 50 ppb of 170 nm PSNPLs, and the remaining PSNPL present in the eluent was calculated. Four replicates of the centrifugation procedure were performed for 15 min at

3500 rpm. The separation yield was calculated by measuring the absorbance (at 250 nm) of the membrane eluent and interpolating the values on the PSNPLs calibration curve corresponding to $y = 0.0197x + 0.0271$, $r^2 = 0.9959$, as detailed in the [Supplementary Material](#) (SEQ1).

2.4. Labeling procedure

All preparations were performed by separately weighing NR, RhB, AL, Op, and iDP to obtain a final stock concentration of 1000 ppm. The NR and RhB solutions were prepared using 96% ethanol (Scharlab, Barcelona, Spain). For AL, Op, and iDP, the suspensions were prepared on “Ultrapure Type 1” (Milli-Q) 18.2 M Ω ·cm water (Merck KGaA, Darmstadt, Germany). PSNPLs at a fixed concentration of 40 ppm of PSNPLs was exposed to 400, 200, 100, and 50 ppm of each of the labeling solutions, regardless of water (AL, Op, and iDP) or 96% ethanol (NR and RhB), as previously described. The different mixtures were heated at 65 °C for 30 min on glass vials with constant agitation on an orbital agitator and incubator (Heidolph, Unimax1010) at 150 rpm. The stained particles were cleaned by performing ten ultra centrifugations for 45 min at 13,200 rpm, as described in the next section. The supernatant was removed from the pellet by decantation and further washes were performed with the corresponding solvent (Milli-Q water or ethanol, depending on the dye). The supernatants and resuspended pellets were analyzed using UV-Vis spectroscopy, as previously described, and fluorimetry analysis was performed. First, several concentrations of the strains were analyzed to determine the experimental excitation and emission wavelengths of each strain. Excitation fluorescence analysis was performed using a Cary Eclipse fluorescence spectrometer (Agilent, Santa Clara, CA, USA). Emission fluorimetry analysis was performed using the same parameters as in the excitation analysis; however, the initial scan wavelength was the excitation wavelength.

To study the cleaning efficiency, different supernatants were evaluated to determine the conditions that achieved the lowest possible fluorescence. Furthermore, to study the staining efficiency, the resuspended pellets of the stained PSNPLs were analyzed under the same conditions as previously described; however, the scan ranged from an excitation wavelength of 800 nm.

2.5. Agglomeration and resuspension study

To ensure that the agglomeration state of the stained PSNPLs remained negligible, the particles were heated at 65 °C for 45 min and ultracentrifuged for 45 min at 13,200 rpm ten times, reproducing the cleaning after the staining procedure. Subsequently, different resuspension procedures were applied to each one of the PSNPLs aliquots: no agitation (BC), orbital agitation (O) for 16 min at 350 rpm, vortex (V) for 16 min (Vortex-Vib, J.P SELECTA S.A., Barcelona, Spain), ultrasonic bath (BU) for 16 min (ULTR-3L2–001, Labbox Labware S.L, Barcelona, Spain), and ultrasonic probe (SU) at 10% of amplitude for 16 min in a cold bath (SSE-1 Branson Sonicator, Branson Ultrasonics Co., Brookfield, CT, USA). The average size of the resuspended aliquots was analyzed by Dynamic Light Scattering (DLS) using a Zetasizer® Ultra (Malvern Panalytical, Cambridge, UK) and compared with a freshly prepared standard of 170 nm polystyrene nanospheres at

40 ppm. In all cases, size distribution was evaluated using a DTS0012 cuvette under the conditions described in the following section. The data were processed and analyzed using GraphPad Prism software (GraphPad, San Diego, CA, USA).

2.6. The hydrodynamic behavior of labeled PSNPLs

The hydrodynamic behavior of the labeled PSNPLs was evaluated by measuring 100 ppm aliquots of labeled NPs in triplicate. To perform these measurements, the PSNPL parameters were established with a refractive index of 1.59. The parameters of Milli-Q water used as a dispersant were set as standards, considering a refractive index of 1.33 and a viscosity value of 0.8872. The sample size distribution was measured at a scattering collection angle of 174.7° using a DTS0012 cuvette, whereas the Z-potential was evaluated using DTS1070 cuvettes. The data obtained were analyzed as explained in the preceding section.

2.7. Cell culture

The THP1 leukemic monocyte cell line (Sigma-Aldrich) was selected based on its high ability to internalize MNPLs. Cells were maintained in filtered cap T-25 flasks (SPL Life Sciences, Pocheon-si, Gyeonggi-do, South Korea). The cellular suspensions were maintained at constant concentrations ranging $0.50\text{--}1.00 \times 10^6$ cells/mL at a maximum volume of 5 mL on Roswell Park Memorial Institute (RPMI) medium supplemented with 10% fetal bovine serum (FBS), 1% glutamine (Biowest, Nuaille, France), and 2.5 ppm of Plasmocin® (InvivoGen, CA, USA) at standard growing conditions of 37 °C, on humidified atmosphere with 5% CO₂, on a ICO150med CO₂ incubator (Mettler GmbH + Co KG, Schwabach, Germany).

2.8 Cell exposure to labeled PSNPLs

From the cell stock suspension, the required volumes at the concentration of 1.00×10^6 cell/mL were distributed by seeding 100 µL per well on U-type 96-well plates (SPL, LifeSciences, Pocheon-si, Gyeonggi-do, Republic of Korea). The particle working suspensions, prepared as previously described, were mixed with the previously seeded cells by gentle pipetting ten times. The exposed cells were maintained under the same conditions as in the maintenance procedure for 24 h and protected from light. Based on a large number of studies using polystyrene NPLs, this nanoplastic can be considered stable over time. Although stability should be a problem in long-term exposure, this was not the case because the study used acute exposure lasting for 24 h.

2.9. Cell viability test

To avoid interference caused by nNPs in the standard viability tests, the direct scoring of the number of viable cells after exposure, compared to those before exposure, was determined using the Beckman counter method. THP1 cells were exposed to 100 ppm of differently stained particles following the procedure described above. The cell viability was investigated using a 1:100 ISOFLOW dilution on a ZTM Coulter Counter (Beckman Coulter Inc., CA, USA). The average cell count was compared with that of untreated

controls, and values were analyzed using GraphPad Prism Software 7.0 (GraphPad, San Diego, CA, USA) by One-way analysis of variance (ANOVA) and contrasted with both unexposed and pristine-treated cells. For both cases the Dunnett post-test with a 95% confidence interval (CI) with $p \leq 0.05$ (*), ≤ 0.01 (**), and ≤ 0.001 (***) was used. Two experiments were performed in triplicates.

2.10. Flow cytometry analysis

Cells treated with labeled particles and the labeling elute resulting from a previously indicated membrane centrifugation efficiency study were cultured as described in the cell viability test section. Cells in 96 U-type well plates were washed twice by centrifugation at room temperature on a 5810 R device (Eppendorf, Hamburg, Germany) and resuspended in phosphate-buffered saline (PBS; 1X, Gibco, Thermo Fischer Scientific, Braunschweig, Germany). The samples were kept on ice and immediately analyzed using a Cytoflex LX flow cytometer (Beckman Coulter Inc., CA, USA). The setting conditions were set as a standard, and the array/gain of the detectors can be found in the [Supplementary Material \(Supplementary Table S1\)](#). A total of 5000 living cell events were recorded at a flow rate of 60 $\mu\text{L}/\text{min}$. Data from the positive signal channels were analyzed and compared with the controls.

2.11. Confocal microscopy analysis

THP1 cells, treated with labeled particles and the particles labeling elute, as previously described, were cultured on U-type 96-well plates for 24 h. Cells were then washed twice using 200 μL of PBS 1X. Final pellet resuspension was done on a pre-warmed RPMI-supplemented medium, and 300 μL of the cell suspension was transferred to a well on a μ -Slide, eight-well high Glass bottom (Ibidi GmbH, Gräfelfing, Germany). The cells were examined using a Leica TCS SP5 confocal microscope (Leica Microsystems CMS GmbH, Mannheim, Germany). Compatibility was tested using CellMask™ deep red and trihydrochloride trihydrate Hoechst 3334 solution, both diluted 1:10,000 for all labels except for Opticol labeled PSNPLs, where the compatibility was changed to CellMask Orange and DRAQ5 (Thermo Fischer Scientific, Braunschweig, Germany).

2.12. Simplified protocol and proof of concept

2.12.1. Fast protocol

As the potential effects of PET-NPLs are gaining attention in the scientific community, a proof-of-concept study was performed following the protocol developed for PS. Instead of pristine PSNPLs, “true-to-life” PET(Ti)-NPLs were stained. These titanium-doped PETNPLs were obtained from the degradation, through sanding, of opaque PET bottles containing titanium NPs (TiO_2NPs); consequently, the resulting MNPLs also contained embedded titanium. Briefly, PET(Ti)-NPLs were labeled by mixing 0.5 mL of the PET(Ti)-NPL suspension (at a concentration of 10,000 ppm) with 0.5 mL of Milli-Q water (containing 0.01 g of iDye PolyPink) in a 10 mL glass tube. The mixture was vigorously agitated by vortex and incubated for 2 h with a short vortexing every 30 min on a constant temperature digital block heater (VWR® Avantor® Inc., Philadelphia, USA). The particle-

label mix was resuspended in 9 mL of Milli-Q water and transferred onto an Amicon® Ultra-15 centrifugal Ultracel®– 100 K filter 1×10^5 MWCO (Merck KGaA, Darmstadt, Germany). A 15-min centrifugation was performed at 3453 rcf, and 9 mL of Milli-Q water was added to the V-shaped well; the wash was repeated four times. After washing, a volume ranging 100–160 μ L containing the labeled particles was recovered from the V-shaped well and aliquoted to volumes of 1000 μ L on Milli-Q water which were maintained covered from light at 4 °C. Irrespective of the desired biological application, it is highly advisable to evaluate the effectiveness of this method by running a lambda scan on a regular confocal microscope for particle aggregates. Alternatively, approaches that do not necessarily rely on NP aggregation, such as fluorescent nanotracking analysis (NTA) or fluorescent spectrometry, can also be used. Both proposals employ widely used, cost-efficient, and easy-to-use approaches.

2.12.2. Cell culture, treatment, and visualization

In this study, the human hepatic Huh-7 cell line was selected as a convenient experimental substitute for primary hepatocytes because the liver is one of the organs targeted by MNPLs pollutants. Huh-7 cells were cultured and seeded in filtered-cap T-25 flasks (SPL, Life Sciences Co. Ltd., Naechon-myeon, Republic of Korea) in Dulbecco's modified Eagle's medium (DMEM) supplemented with 10% fetal bovine serum (FBS) from Biowest (Nouaillé, France) and Plasmocin (InvivoGen, CA, USA). To proceed, 7000 cells were seeded and cultured on μ -slide eight-well high glass bottom (Ibidi GmbH, Gräfelfing, Germany) for 24 h before treatments. Culture media was removed by aspiration and replaced with 0.20 mL of freshly prepared iDye-PET(Ti)-NPLs suspension (100 μ g/mL) on pre-warmed DMEM at 37 °C and incubated for 24 h at standard growing conditions of 37 °C, in a humidified atmosphere with 5% CO₂ on an ICO150med CO₂ incubator (Memmert GmbH + Co KG, Schwabach, Germany). After 24 h of incubation with the iDye-PET(Ti)-NPLs suspension, cells were washed twice with 250 μ L of a pre-warmed medium. Finally, 300 μ L of pre-warmed medium was added to each well and the plates were investigated immediately after 5 min of incubation with CellMask™ deep red and trihydrochloride trihydrate Hoechst 3334 solution both diluted 1:10,000, on a Leica TCS SP5 confocal microscope (Leica Microsystems CMS GmbH, Mannheim, Germany).

3. Results and discussion

3.1. Ultracentrifugation optimization

First, ultracentrifugation conditions were established to separate PSNPLs from the supernatant. As expected, the results of centrifugation over time showed a significant decrease in the characteristic absorbance (at 250 nm) of PSNPLs (which indicated a decrease in the PSNPLs present in the supernatant) when the centrifugation time was increased (Fig. 1). The data indicate that the average intensity (absorbance in a.u.) decreased, from 2.69 at 0 min to 0.10 at 45 min. Consequently, the remaining PSNPL in the supernatant was reduced from 100% at 0 min to 66% at 5 min and to 4% at 45 min of centrifugation. Consequently, 45 min was chosen as the optimal centrifugation time to separate the stained/unstained NPLs from the supernatant.

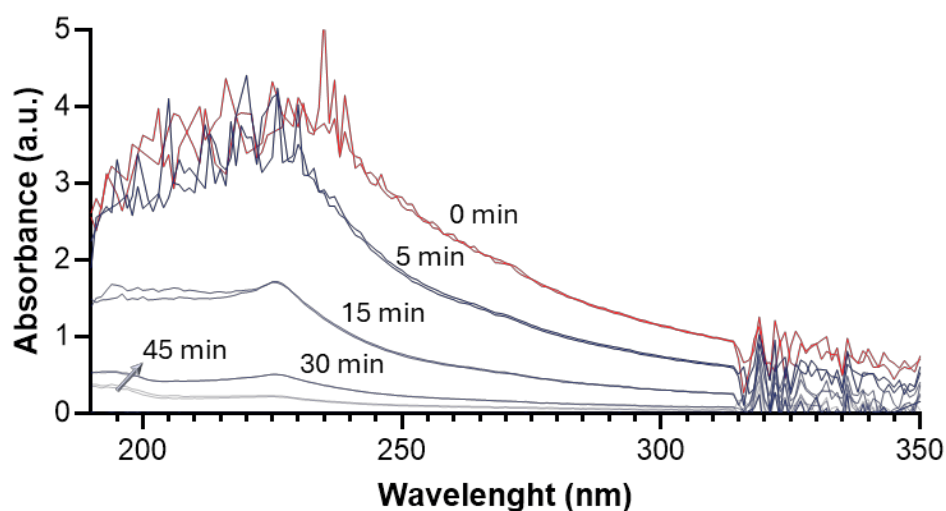


Fig. 1. The UV spectrum of each supernatant ranging 0–45 min of ultracentrifugation time at 13,200 rpm.

3.2. Membrane centrifugation efficiency study

As indicated in the [Supplementary Information \(Supplementary Fig. S1\)](#), the calibration curve for the analysis of PSNPLs showed a linear trend from 125 to 50 ppm. When using the calibration curve to evaluate the results from the four replicates performed with the Amicon® tubes, a concentration below the limit of detection was obtained. This indicates the non-significant presence of PSNPLs in the eluent, showing 100% retention efficiency of the membrane used. However, when the PSNPLs were resuspended in the membrane, an average loss of $17 \pm 8\%$ was observed. Therefore, this difference in absorbance can be attributed to the loss of particles stuck in the membrane or the walls of the tube, when trying to recover them from the membrane, after centrifugation. However, for the scope of the present study, membrane centrifugation was appropriate to ensure proper cleaning of the PSNPLs from the remaining staining in the supernatant when PSNPL labeling was used (see subsequent sections) to ensure separation from the supernatant in less time, even losing a higher amount. For subsequent analyses, the membranes were centrifuged whenever possible.

3.3. Staining and cleaning efficiency

To test the efficiency of the staining, different compounds were tested at different excitation and emission wavelengths, as shown in the [Supplementary Material \(Supplementary Table S2\)](#). The results obtained were within the range of those presented in the literature, except for Amarillo Luminoso and Opticol, for which no data were found in the open literature [21], [22]. Regarding the fluorescence yield, the chemical dyes (NR and RhB) showed significantly higher fluorescence intensities, even at lower concentrations, than the textile dyes used and the optical brightener. Regarding the different concentrations of the dyes tested for labeling PSNPLs, the highest intensity in all resuspended PSNPLs was observed with the ratio corresponding to the highest

concentration of the dye (corresponding to the ratio 10:1). Fig. 2 shows the emission spectra of the PSNPLs stained at 400 ppm, except for NR (200 ppm), which showed similar intensities.

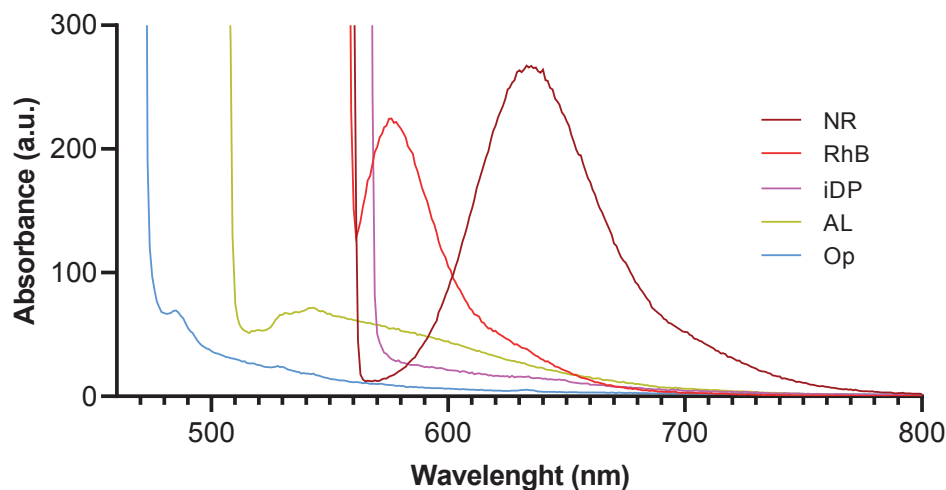


Fig. 2. Emission spectra of PSNPLs stained at 400 ppm (except for NR, which was stained at 200 ppm) with the different tested compounds. Legend abbreviations: Nile Red (NR), Rhodamine B (RhB), iDye PolyPink (iDP), Amarillo Luminoso (AL), and Opticol (Op).

Finally, concerning the cleaning of the PSNPLs to eliminate free dye, the procedures used were effective because the fluorescence intensity observed in the 10th wash supernatant was at least ten times lower than that of the stained PSNPLs. This fluorescence was colorless to the naked eye, except for NR and RhB, which showed a light red color with absorbance at the noise level when analyzed using UV-Vis spectrophotometry. Collectively, the results indicated that the ultracentrifugation cleaning procedure was reliable, and no free dye was detected in the visible spectrum at significant levels.

3.4. Agglomeration and resuspension study

The potential agglomeration levels of PSNPLs obtained using different resuspension approaches were evaluated by DLS and are graphically represented in Fig. 3a. The highest number of particles in all resuspension techniques had a diameter between 126–170 nm, which agreed with the results obtained in the blank of both DLS (named B) studies. The size distribution deviations were determined by considering the previously mentioned blank histograms (Fig. 3b). The ultrasonic probe exhibits the lowest deviation, followed by the ultrasonic bath, orbital, vortex, and centrifugation blanks.

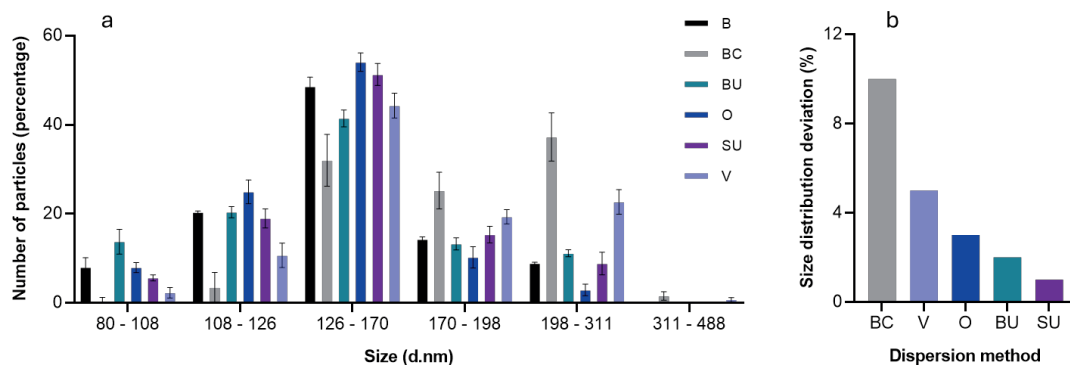


Fig. 3. (a) Size distribution histogram of the pristine PSNPL diameters obtained using DLS after different resuspension treatments. (b) Size distribution deviation expressed in percentages of the different resuspension techniques compared to the blank size distribution obtained using DLS. Legend abbreviations: DLS blank (B), centrifugation blank (BC), orbital (O), vortex (V), ultrasonic bath (BU), ultrasonic probe (SU).

The hydrodynamic behavior in terms of size distribution is depicted in Fig. 4 for all the stained particles evaluated. The Z-average values, based on intensity calculations, are 362 ± 5 nm for RhB, 363 ± 1 nm for AL, 309 ± 1 nm for Op, 352 ± 5 nm for iDP, and 539.50 nm for NR. The polydispersity indexes for 0.27, 0.25, 0.34, 0.62, and 0.70 for RhB, AL, OP, iDP, and NR, respectively.

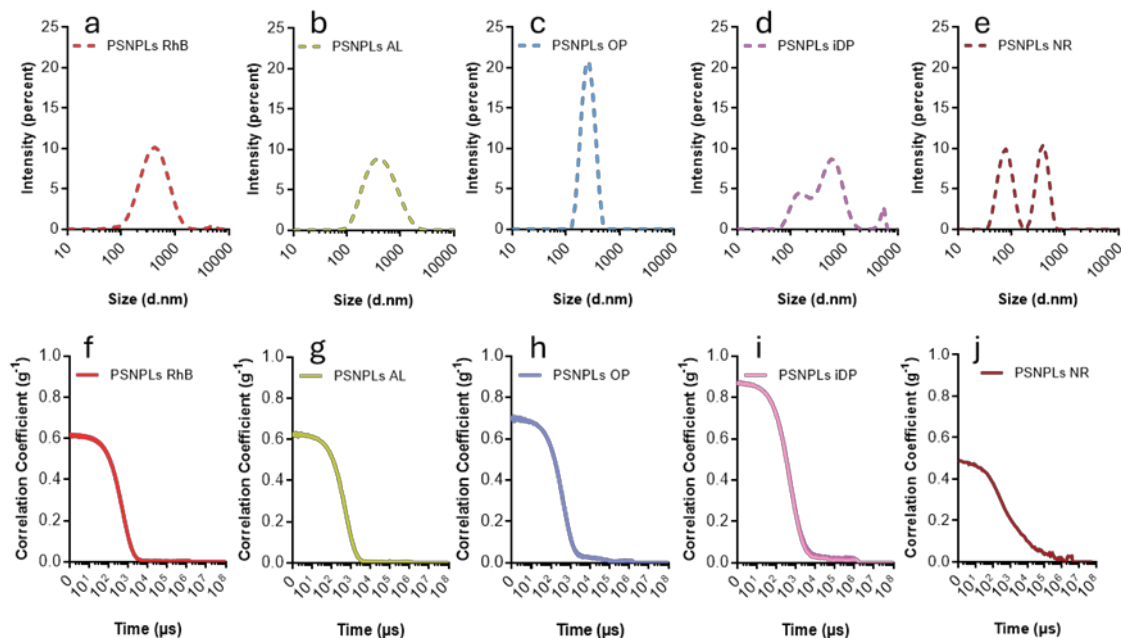


Fig. 4. Size distribution (using DLS) of PSNPLs for (a) RhB, (b) AL, (c) Op, (d) iDP, and (e) NR are represented as intensity percent. Correlation coefficients for all independent measurements are shown for RhB, AL, OP, iDP, and NR-stained PSNPLs on f, g, h, i, and j, respectively.

The obtained size distributions were consistent, and for all cases (except NR), the Z-average values were close to 350 nm, showing solid correlation coefficients. Notably, the more reliable values for correlation were those obtained when iDye PolyPink labeled particles were used, and the lower correlation was obtained for RhB and AL. In the case of NR-stained PSNPLs, the correlations and measurements were inconsistent and difficult to determine. These data indicate that the dispersion of iDye PolyPink-stained PSNPLs is the most suitable for future applications, especially if we consider that the typically described error in size estimation from fluorescent particles emitting in the range 600–700 nm is mild compared to Opticol, which is the only compound that does not emit in this range [23]. Even considering the relatively consistent values on the Z-average values, evidencing an agglomeration of particles related to the commercial information delivered by the manufacturer (170 ± 9 nm) the curves, for size distributions in percentage of intensity, describe the typically expected behavior for fluorescent samples. However, the fluorescent light emitted by some strains is non-coherent and can be recorded as noise, broadening the peaks [23]. This was observed for the RhB- and AL-stained NPs, which reduced their potential as candidates for labeling NPLs. With respect to the Z-potential, for all studied cases (Fig. 4a–d) the values were far from zero (summarized in Supplementary Table S3). Moreover, the values ranged -20 – (-46) mV which is an indicator that the suspensions are less prone to form aggregates. For RhB- and iDP-labeled NPLs, the measured values were close to -30 mV, which is typically the optimum value for particles in suspension to be considered stable monodispersions.

3.5 Cell viability

A relevant condition for dye selection is that it should not compromise cell viability. In our study, no significant decrease in cell viability was observed for any of the tested compounds in the human leukemia monocytic THP1 cells. This cell line has shown a significant ability to internalize PSNPLs [24], ensuring the uptake of labeled NPLs and supports the data indicating a lack of toxicity. However, small decreases in viability values were observed for RhB- and AL-stained PSNPLs; however, these decreases were not statistically significant, as indicated in Fig. 5. Notably, toxicity has been reported in A549 cells exposed to rhodamine-labeled silica NPs [25]. This means that the viability effects would not be a discriminating factor in the selection of the best compound to stain NPLs using this technique. However, it is tempting to advise against values deviating from the pointed line on the graph representing the values for untreated PSNPLs.

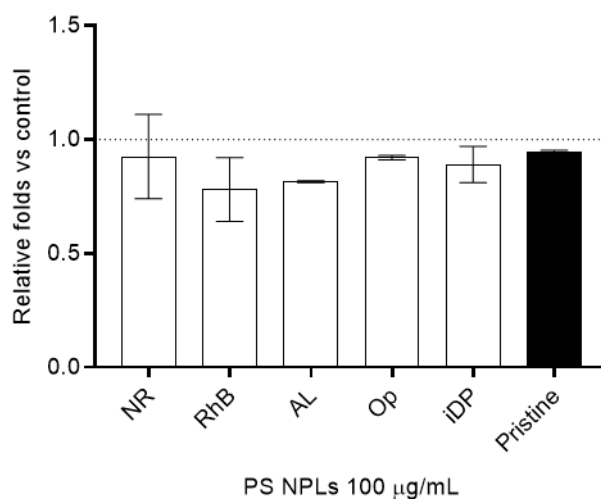


Fig. 5. Cell viability for THP1 cells after 24-h exposure to stained-PSNPLs. Nile Red (NR), Rhodamine B (RhB), Amarillo Luminoso (AL), Optical (Op), and i-Dye Poly Pink (iDP) NPs (100 $\mu\text{g/mL}$). Values are relative to the untreated cells (control, dotted line). Cells treated with unlabeled PSNPLs (pristine) are also included. No significant statistical differences were observed using the one-side ANOVA with Dunnett's post hoc test ($p \leq 0.05$).

3.6. Flow cytometry analysis

The use of non-destructive techniques, such as fluorescence-activated cell sorting (FACS), may be favored by the fluorescent labeling of MNPLs. Therefore, the evaluation of its suitability with the selected strains may provide an idea as to which of the labels used in this study may be the most suitable. Thus, THP1 cells exposed for 24 h to labeled NPLs were investigated using flow cytometry. The details of each of the investigated channels are depicted in the [Supplementary Material](#) ([Supplementary Figs. S2a–f](#) for the particle-staining eluent, and [Supplementary Figs. S2g–i](#) for labeled particles). The first significant finding was the lack of specificity for Nile Red, which has already been discussed by other authors [26], [27]. Thus, the high affinity of Nile Red for neutral lipids and other cellular components was demonstrated in our work. Despite previous reports on their usefulness, the use of Nile Red, as well as other stains with lipid affinity, should be considered a suboptimal approach when used in cellular backgrounds [28], [20]. Thus, THP1 cells treated with different eluents showed no signal ([Fig. 6](#)), with the exception of the NR eluent. Therefore, these results would indicate both the effectiveness of the cleaning process and the inconvenience of using Nile Red. Thus, if we consider this characteristic crucial, the use of Nile Red must be discarded when better alternatives are available. Another characteristic is that no signal was detected near the UV spectra when Nile Red was in its free form or when no PSNPL particles were present.

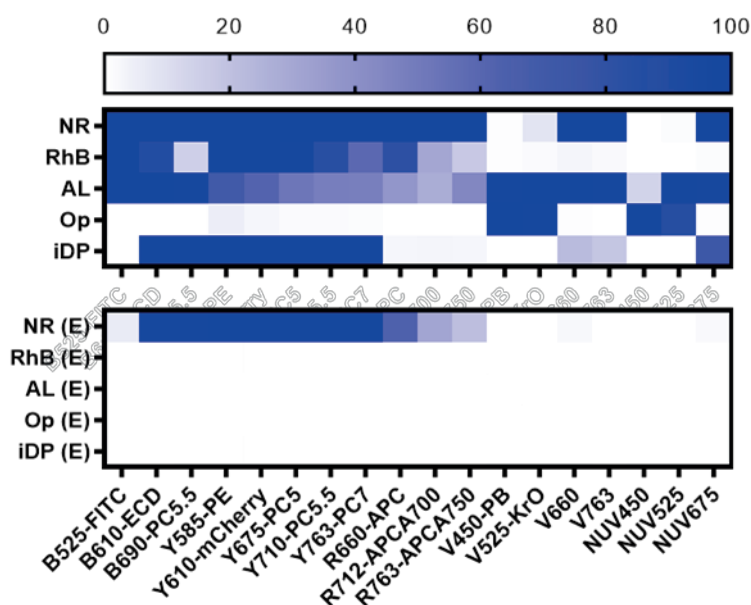


Fig. 6. Upper part: flow cytometry evaluation of the emission on THP1 cells exposed for 24 h to Nile red (NR)-, Rhodamine B (RhB)-, Amarillo Luminoso (AL)-, Opticol (OP)-, and Idye PolyPink (iDP)-labeled polystyrene NPs (100 $\mu\text{g/mL}$). Lower part: data from their correspondent eluent (E-suffix added in all cases) for control. The used laser excitation and the corresponding wavelengths are indicated as follows: blue (B), yellow (Y), red (R), violet (V), a near UV (NUV). The emissions are represented as the percentage of cells that emit at the corresponding wavelengths.

For AL-PSNPL-treated cells, emission was observed in all channels, and the signal was mild (less than 25%) only in the near ultraviolet (NUV)450 channel, where the shift was rounded to 13%. Moreover, the shift was at least 50% for 10 detectors. This may interfere with other signals emitted by other fluorochromes regularly used in biology as DRAQ5, Hoechst 33342 on nuclei, or Cellmask™ Deep Red for plasma membrane, and its use is inadvisable.

Moreover, because staining is persistent and difficult to remove, its inappropriate use may damage the microfluidic components of the cytometer. Notably, RhB- and iDP-labeled PSNPLs presented similar emissions, with the significant difference that internalized RhB-labeled PSNPLs emitted at 525 nm when excited with a blue laser and at 660 nm when excited with a red laser. In contrast, the internalized iDP-PSNPLs emit light at 675 nm when excited with an NUV laser. The differences between these two labels were minimal, and both results were almost equivalent. Finally, the Opticol-labeled PSNPLs presented a narrow emission spectrum (only at 450 and 525 nm) and only when excited with violet or near-UV lasers. Although Opticol appears to be useful in terms of compatibility, we will see further complications with this compound when complementary techniques are used. The results for RhB, iDP, and OP were confirmed and validated by repeating the experiments with adherent HeLa cells. These cells have been extensively used to study the effects of new materials, such as the label-free detection of metallic NPs [29], fluorescent nanopolymers [30], and carbon-based compounds [31]. Moreover,

these cells have been supported by sophisticated techniques such as stimulated emission depletion microscopy, which is useful for detecting fluorescence at wavelengths lower than 200 nm [32]. Detailed methods and information on the use of this cell line are available in the [Supplementary Material](#) (Supplementary Figs. S3.1 and 2), and the comparisons are depicted and summarized in [Supplementary Fig. S3.3](#).

3.7. Confocal microscopy

Internalization of the labeled NPs was assessed using confocal microscopy. For better visualization, despite the staining color, all labeled particles were represented in green, membranes in red, and nuclei in blue. Representative images of all the cases are shown in [Fig. 7](#). The first observation ([Fig. 7f](#)) shows that Amarillo luminoso seems to produce not only interference with several of the signals but also causes some sort of cell stress, since in all cases, the shape of the cells was not regular and consistently altered compared to the control ([Fig. 7g](#)). Although cell viability was reduced in the short-term treatment (24 h), this reduction was not statistically significant. However, prolonged exposure may induce cell viability inconveniences that were not studied further because no useful traits for this label were found. Further experiments were not performed using this dye.

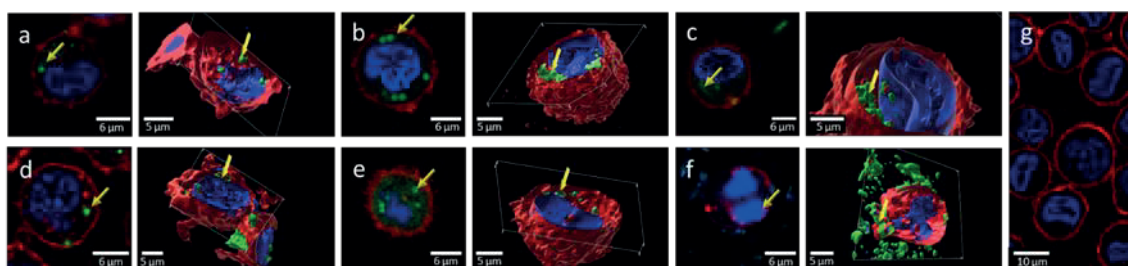


Fig. 7. Confocal Images of THP1 cells exposed for 24 h to commercially available (a) fluorescein labeled-PSNPLs, (b) Nile Red, (c) Rhodamine B, (d) Opticol, (e) i-Dye Poly Pink, and (f) Amarillo Luminoso PSNPLs (100 $\mu\text{g/mL}$). A digital reconstruction is presented at the right of each image. Yellow arrows indicate the presence of labeled NPs. Untreated THP1 cells are shown on (g), as controls.

Although emissions at the expected wavelengths were easily observed, difficulties arose when the signals from small PSNPL agglomerates or single particles were evaluated. Although these difficulties can be solved using the so-called nanoscopy methodology, which is a far-field microscopy technique that can generate images beyond diffraction-limited resolution, such as stimulated emission depletion (STED) microscopy [27], it can pose additional technical difficulties and a non-negligible increase in costs. In the case of NR-PSNPLs, owing to the previously explained non-specific staining, there are always uncertainties regarding the resulting images because the eluent can label the cells. Furthermore, since Nile Red presents an excitation wavelength shift from 450 to 560 nm by solvatochromism, its combined use with other stains or simultaneous scanning with B- and G-excitation filters may present scoring difficulties. No previous reports on RhB-labeled found in have been published. However, exposure to high concentrations of RhB

may result in non-specific staining along with loss of cellular integrity, as shown in Fig. 8a1, whereas no signals were observed at low concentrations (20 ppm) or with the eluent (Fig. 8a2 and 3, respectively).

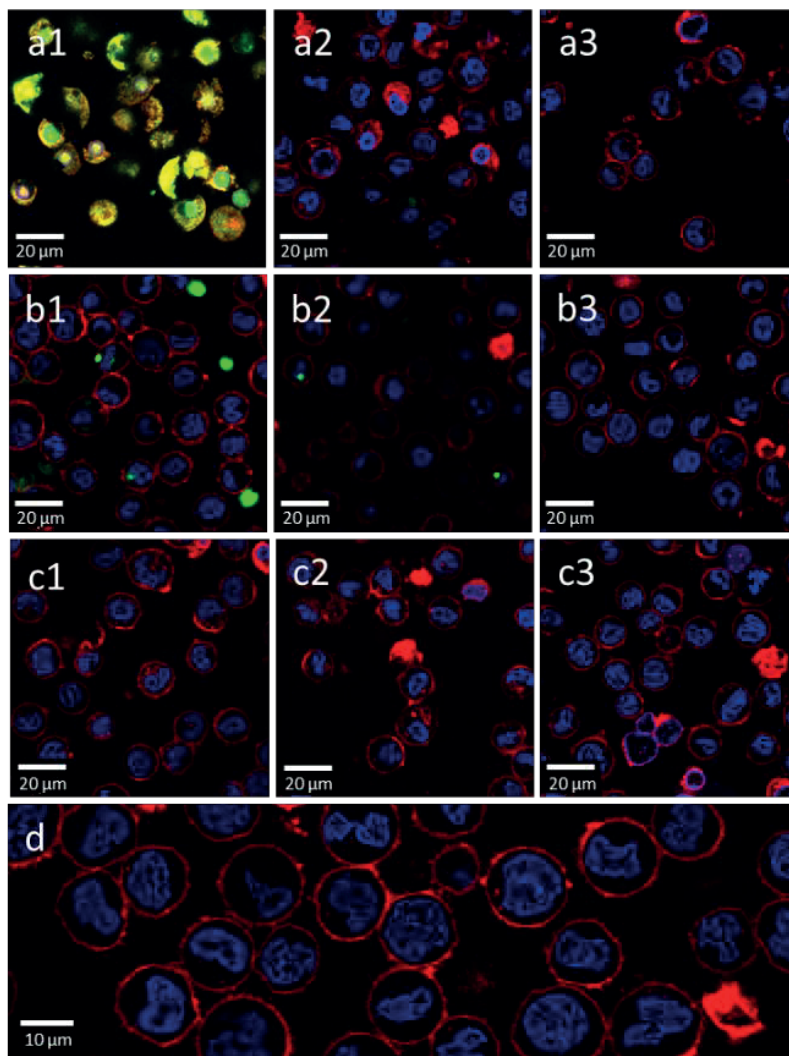


Fig. 8. Confocal Images of THP1 cells exposed for 24 h to pigments with no particles. (a1) Rhodamine B: 2000 ppm, (a2) 20 ppm, and (a3) eluent. (b1) Optical: 2000 ppm, (b2) 20 ppm, and a(b3) eluent. iDye PolyPink: (c1) 2000 ppm, (c2) 20 ppm, and (c3) eluent. (d) Untreated THP1 cells.

Although no effects on cell viability were observed when Optical labeling was used, non-specific fluorescence signals were observed in THP1 cells treated with the particle-free stain, including high (2000 ppm) and low (20 ppm) concentrations (Fig. 8b1 and 8b2, respectively). However, the formation of Optical hot spots was observed, suggesting the agglomeration of the compound. Furthermore, in agreement with the cytometry findings, no signals were detected in the eluent-treated cells (Fig. 8b3). As previously described, the compatibility of Optical with regularly used stains permitted its use with DRAQ5 and CellMask Orange. Interestingly, the problems described for the previous two strains were

not observed for the iDye PolyPink. Thus, no signals or detrimental visual effects on cell integrity were observed in any of the cases in which the cells were exposed to the iDye PolyPink dye or eluent (Fig. 8c1–3). Consequently, and for all the observations described above, we concluded that this labeling can be considered the most suitable alternative for tracking NPs on biological samples, not only because it does not generate cellular damage but also because it does not interfere with the channels used in confocal microscopy. Moreover, iDye-labeled PET and PS NPs have been reported to be used with Alexa Fluor 488 labeled secondary antibodies with no interference[33], [34]. It has been also successfully proven to work well with fluorescent compounds used for cytometry-based mitochondrial potential detection [35] and FITC-marked antibodies for macrophage polarization detection[36]. This versatility in compatibility was difficult or impossible with previously published protocols that use covalently bound FITC emission labeling [37] because the emission cannot be used with regular markers used for intracellular reactive oxygen species detection, such as DHE or DCFH-DA, owing to the overlapping of signals.

3.8. Simplified protocol for staining and proof of concept

Based on the above results, we selected iDye PolyPink as the dye that offers advantages for staining NPLs. Since the previous work was carried out using pristine PSNPLs, to support the proposal, this study has been extended by using a “true-to-life” NPL model such as PET(Ti)NPLs, stained with iDP (particles called iDP-PET(Ti)NPLs from now on). These Ti-doped PETNPLs were obtained by degrading milk PET bottles [20] and their toxicological profile *in vivo* has recently determined in *Drosophila* [38]. Differentiated human hepatoma (Huh-7) cells were used for this study. These cells have a high ability to internalize NPs and present a wide set of biological responses [39]. Fig. 9 shows the results of the internalization of the iDP-PET(Ti)NPLs by Huh-7 cells, where the hybrid nature of the iDP-PET(Ti)NPLs was easily observed.

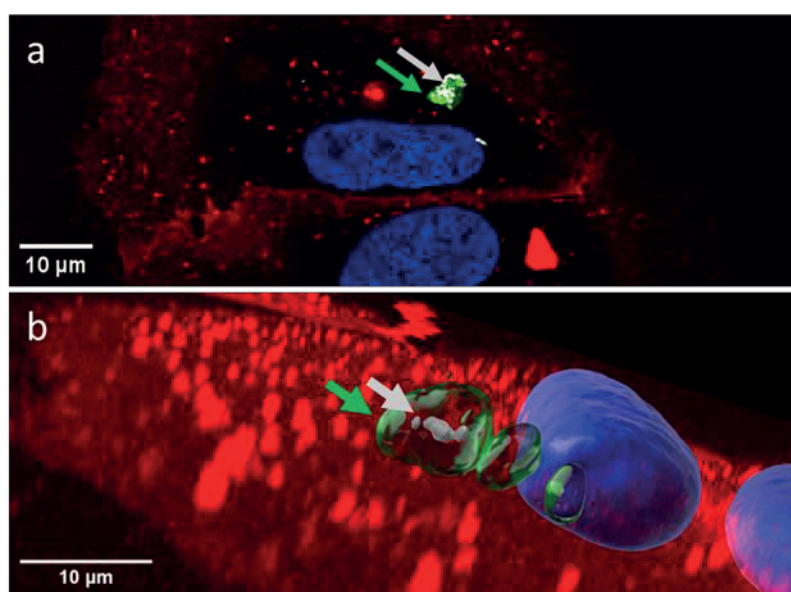


Fig. 9. (a) Confocal image of adherent Huh-7 cells exposed for 24 h to iDPPET(Ti)NPLs. (b) 3D reconstruction of the image. Colocalization of Ti signal acquired through reflection (grey arrows) and labeled nano polymers-metal (green arrows).

As demonstrated, the labeling of the PET moiety was always close to that of the doped titanium NPs, which is characteristic of PET opaque plastic. co-localization of the PET signal (labeled with iDP) and the reflection of Ti were visible in the interior of Huh-7 cells. This was always observed in the confocal images (as indicated in Fig. 9a), as well as in the 3D reconstruction (Fig. 9b), with a negligible background signal. This short study confirmed the effectiveness of the proposed simplified labeling protocol and its potential extension to other types of polymers and different cell types. Specifically, we determined the stability of the IDP labeling. Thus, IDP-labeled MNPLs were used after 8 months without the loss of fluorescence signals. This is another significant advantage of using the IDP.

Importantly, in parallel to this study, iDye PolyPink has been used to label different “true-to-life” nanoplastics aiming to confirm its advantages. Therefore, they have been used to label PET-NPLs resulting from the degradation of PET water bottles, PET(Ti)-NPLs from opaque milk bottles, and polylactic acid (PLA)-NPLs resulting from the release of PLA-teabags, when the process of simulating a cup of teabags. Thus, in *in vitro* studies, PET-labeled NPLs have been used to detect internalization into primary human nasal epithelial (HNEp) cells (Annangi et al., 2023). PET(Ti) labeled-NPLs have also been used to determine internalization in different hematopoietic cell lines, such as TK6 lymphoblasts, THP1 monocytes, and Raji-B lymphocytes [20]. Finally, iDye PolyPink was used to label NPLs from PLA bioplastics to determine their internalization into human intestinal cells such as Caco-2 and HT29, both as undifferentiated and differentiated cells, forming an *in vitro* model of the intestinal barrier [40]. Interestingly, iDye PolyPink labeling has been successfully applied to label PET and PET(Ti)-NPLs in an *in vivo* model, such as *Drosophila*, to demonstrate their uptake by enterocytes of the larval intestine or by hemocytes (with a function similar to lymphocytes in mammals) present in the hemolymph [41], [38].

4. Conclusions

As a general conclusion of our study, iDye PolyPink is proposed as a potentially suitable dye to label MNPLs, especially those “true-to-life” resulting from the laboratory degradation of plastic goods of different chemical origins. The evaluation of both widely distributed commercially available PSNPLs and true-to-life nanopolymers confirmed the suitability of the proposed protocol for more complex samples. Noncommercial MNPLs require a robust labeling protocol to confirm their internalization in studies aimed at determining their potential hazardous biological effects. Accordingly, this study provides a detailed and simple protocol for labeling true-to-life MNPLs.

This selection of iDye PolyPink was based on the non-optimum behavior of the other selected dyes in different assays. Thus, 1) for Rhodamine-B, no clear supernatant was obtained, showing a certain effect on treated cell viability, nonspecific staining in confocal

studies, and effects on cell integrity at high concentrations. 2) For Nile Red, a colored supernatant was observed despite the cleaning process. Furthermore, the lipophilic nature of the compound may induce nonspecific labeling in a lipid-rich environment, because lipid droplets are present inside the cell. In such cases, a simpler method to separate the dyed plastic signal from nonspecific staining may be required. 3) Amarillo Luminoso had the clear characteristic of being detectable in all fluorescence investigated channels, which in turn makes its use for biological applications highly disfavored due to its compatibility with fluorophores that are used daily. 4) Opticol presented non-specific fluorescence inside and outside cellular structures, which may have resulted in misinterpretation of the results. Consequently, more complex approaches are required to verify the signals obtained from labeled particles.

In summary, the goodness and compatibility of iDye-labeled nanoplastics with the standardized techniques used to determine their presence in both cells and tissues make the present approach useful for the proposed objectives.

Environmental implication

Environmental micro-/nanoplastics (MNPLs) are emerging pollutants of special concern, and determining their potential risks is essential. Although a large dataset has been obtained using pristine nano-polystyrene, it is not considered representative of the secondary MNPLs present in the environment. Consequently, obtaining true-to-life MNPLs resulting from the laboratory degradation of plastic goods seems to be an appropriate alternative to fill this gap. Notably, the use of such noncommercial MNPLs requires labeling to confirm their cell/tissue internalization. Although different dyes have been proposed for this purpose, there is a lack of comparative studies showing the advantages and disadvantages of each dye. In this study, after using a wide variety of assays to demonstrate their advantages and disadvantages, iDye PolyPink was proposed as the most suitable dye for labeling secondary MNPLs in studies aimed at identifying their internalization. Such labeling can be used in both in vivo/in vitro models to determine potential environmental and health hazards.

CRedit authorship contribution statement

Jessica Arribas Arranz: Methodology, Investigation. **Antonia Velázquez:** Supervision, Investigation. **Montserrat López-Mesas:** Writing – review & editing, Writing – original draft, Conceptualization. **Ricard Marcos:** Writing – review & editing, Conceptualization. **Michelle Morataya-Reyes:** Methodology, Investigation. **Fernando Carrillo-Navarrete:** Validation, Investigation. **Susana Pastor:** Supervision, Methodology, Investigation. **Karen Mejia-Carmona:** Supervision, Methodology. **Alba Hernández:** Writing – review & editing, Supervision, Conceptualization. **Victor Fuentes-Cebrian:** Validation, Investigation. **Camila Cazorla-Ares:** Validation, Investigation. **Lourdes Vela:** Validation, Methodology, Investigation. **Iris H. Valido:** Validation, Investigation. **Aliro Villacorta:** Writing – original draft, Methodology, Investigation.

Declaration of Competing Interest

The authors declare that they have no known competing financial interests or personal relationships that could have appeared to influence the work reported in this paper.

Data availability

Data will be made available on request.

Acknowledgments

A. Villacorta was supported by PhD fellowships from the National Agency for Research and Development (ANID), from the CONICYT PFCHA/DOCTORADO BECAS CHILE/2020–72210237. L. Vela was supported by a Ph.D. fellowship from the Fundación Carolina. M. Morataya-Reyes hold a Ph.D. FI fellowship from the Generalitat de Catalunya. A. Hernández was granted an ICREA ACADEMIA award. I.H. Valido was supported by “Ayudas Margarita Salas para la formación de jóvenes doctores”, Ministerio de Universidades (Spain). This project has received funding from the European Union’s Horizon 2020 Research and Innovation Programme under Grant Agreement No. 965196. This work was also partially supported by the Spanish Ministry of Science and Innovation [PID2020-116789, RB-C43], and by the Generalitat de Catalunya (2021-SGR-00731 and 2021-SGR-00723).

Appendix A. Supporting information

Supplementary data associated with this article can be found in the online version at doi.org/10.1016/j.jhazmat.2024.135134.

References

- [1] Bhat, M.A., Gedik, K., Gaga, E.O., 2023. Atmospheric micro (nano) plastics: future growing concerns for human health. *Air Qual Atmos Health* 16 (2), 233–262. <https://doi.org/10.1007/s11869-022-01272-2>.
- [2] Hartmann, N.B., Hüffer, T., Thompson, R.C., Hassellöv, M., Verschoor, A., Daugaard, A.E., et al., 2019. Are we speaking the same language? Recommendations for a definition and categorization framework for plastic debris. *Environ Sci Technol* 53 (3), 1039–1047. <https://doi.org/10.1021/acs.est.8b05297>.
- [3] Villacorta, A., Rubio, L., Alaraby, M., L’opez-Mesas, M., Fuentes-Cebrian, V., Moriones, O.H., et al., 2022. A new source of representative secondary PET nanoplastics. Obtention, characterization, and hazard evaluation. *J Hazard Mater* 439, 129593. <https://doi.org/10.1016/j.jhazmat.2022.129593>.
- [4] Domenech, J., Annangi, B., Marcos, R., Hernández, A., Catalán, J., 2023. Insights into the potential carcinogenicity of micro- and nano-plastics. *Mutat Res Rev Mutat Res* 791, 108453. <https://doi.org/10.1016/j.mrrev.2023.108453>.
- [5] Rubio, L., Marcos, R., Hernández, A., 2020. Potential adverse health effects of ingested micro- and nanoplastics on humans. Lessons learned from in vivo and in vitro mammalian models. *J Toxicol Environ B Crit Rev* 23 (2), 51–68. <https://doi.org/10.1080/10937404.2019.1700598>.
- [6] Xu, J.L., Lin, X., Wang, J.J., Gowen, A.A., 2022. A review of potential human health impacts of micro- and nanoplastics exposure. *Sci Total Environ* 851 (Pt 1), 158111. <https://doi.org/10.1016/j.scitotenv.2022.158111>.

- [7] Sohail, M., Urooj, Z., Noreen, S., Baig, M.M.F.A., Zhang, X., Li, B., 2023. Micro- and nanoplastics: contamination routes of food products and critical interpretation of detection strategies. *Sci Total Environ* 891, 164596. <https://doi.org/10.1016/j.scitotenv.2023.164596>.
- [8] Liang, J.L., Cao, G.X., Zheng, F.Y., Li, S.X., Liu, F.J., Lin, L.X., et al., 2022. Low-toxic, fluorescent labeled and size-controlled graphene oxide quantum dots@ polystyrene nanospheres as reference material for quantitative determination and in vivo tracing. *Chemosphere* 307 (Pt 4), 136094. <https://doi.org/10.1016/j.chemosphere.2022.136094>.
- [9] Zhang, H.J., Zhou, H.R., Pan, W., Wang, C., Liu, Y.Y., Yang, L., et al., 2023. Accumulation of nanoplastics in human cells as visualized and quantified by hyperspectral imaging with enhanced dark-field microscopy. *Environ Int* 179, 108134. <https://doi.org/10.1016/j.envint.2023.108134>.
- [10] Shruti, V.C., Pérez-Guevara, F., Roy, P.D., Kutralam-Muniasamy, G., 2022. Analyzing microplastics with Nile Red: emerging trends, challenges, and prospects. *J Hazard Mater* 423 (Pt B), 127171. <https://doi.org/10.1016/j.jhazmat.2021.127171>.
- [11] Dutta, S., Misra, A., Bose, S., 2024. Polyoxometalate nanocluster-infused triple IPN hydrogels for excellent microplastic removal from contaminated water: detection, photodegradation, and upcycling. *Nanoscale* 16 (10), 5188–5205. <https://doi.org/10.1039/d3nr06115a>.
- [12] Nalbene, L., Panebianco, A., Giarratana, F., Russell, M., 2021. Nile Red staining for detecting microplastics in biota: Preliminary evidence. *Mar Pollut Bull* 172, 112888. <https://doi.org/10.1016/j.marpolbul.2021.112888>.
- [13] Greenspan, P., Fowler, S.D., 1985. Spectrofluorometric studies of the lipid probe, Nile Red. *J Lipid Res* 26, 781–789.
- [14] Çelen Erdem, İ., Ünek, C., Akkus, Süt, P., Karabıyık Acar, Ö., Yurtsever, M., Şahin, F., 2023. Combined approaches for detecting polypropylene microplastics in crop plants. *J Environ Manag* 347, 119258. <https://doi.org/10.1016/j.jenvman.2023.119258>.
- [15] Mohan, M., Gaonkar, A.A., Pandya Nandappa, D., K.K., Vittal, R., Chakraborty, A., et al., 2023. Screening for microplastics in drinking water and its toxicity profiling in zebrafish. *Chemosphere* 341, 139882. <https://doi.org/10.1016/j.chemosphere.2023.139882>.
- [16] Gao, Z., Wontor, K., Cizdziel, J.V., 2022. Labeling microplastics with fluorescent dyes for detection, recovery, and degradation experiments. *Molecules* 27 (21), 7415. <https://doi.org/10.3390/molecules27217415>.
- [17] Aoki, H., 2022. Material-specific determination based on microscopic observation of single microplastic particles stained with fluorescent dyes. *Sens (Basel)* 22 (9), 3390. <https://doi.org/10.3390/s22093390>.
- [18] Tong, H., Jiang, Q., Zhong, X., Hu, X., 2021. Rhodamine B dye staining for visualizing microplastics in laboratory-based studies. *Environ Sci Pollut Res Int* 28 (4), 4209–4215. <https://doi.org/10.1007/s11356-020-10801-4>.
- [19] Le Quoc, P., Fokina, M.I., Martynova, D.M., Olekhovich, R.O., Uspenskaya, M.V., 2022. Method of manufacturing and staining microplastics for using in the biological experiments. *Environ Sci Pollut Res Int* 29 (44), 67450–67455. <https://doi.org/10.1007/s11356-022-22776-5>.
- [20] Villacorta, A., Vela, L., Morataya-Reyes, M., Llorens-Chiralt, R., Rubio, L., Alaraby, M., et al., 2023. Titanium-doped PET nanoplastics of environmental origin as a true-to-life model of nanoplatic. *Sci Total Environ* 880, 163151. <https://doi.org/10.1016/j.scitotenv.2023.163151>.
- [21] Karakolis, E.G., Nguyen, B., You, J.B., Rochman, C.M., Sinton, D., 2019. Fluorescent dyes for visualizing microplastic particles and fibers in laboratory-based studies. *Environ Sci Technol Lett* 6 (6), 334–340. <https://doi.org/10.1021/acs.estlett.9b00241>.
- [22] Maes, T., Jessop, R., Wellner, N., Haupt, K., Mayes, A.G., 2017. A rapid screening approach to detect and quantify microplastics based on fluorescent tagging with Nile Red. *Sci Rep* 7, 44501. <https://doi.org/10.1038/srep44501>.
- [23] Bhattacharjee, S., 2016. DLS and zeta potential - what they are and what they are not. *J Control Release* 235, 337–351. <https://doi.org/10.1016/j.jconrel.2016.06.017>.
- [24] Rubio, L., Barguilla, I., Domenech, J., Marcos, R., Hernández, A., 2020. Biological effects, including oxidative stress and genotoxic damage, of polystyrene nanoparticles in different

- human hematopoietic cell lines. *J Hazard Mater* 398, 122900. <https://doi.org/10.1016/j.jhazmat.2020.122900>.
- [25] Gualtieri, M., Skuland, T., Iversen, T.G., Låg, M., Schwarze, P., Bilaničová, D., et al., 2012. Importance of agglomeration state and exposure conditions for uptake and pro-inflammatory responses to amorphous silica nanoparticles in bronchial epithelial cells. *Nanotoxicology* 6 (7), 700–712. <https://doi.org/10.3109/17435390.2011.604441>.
- [26] Macairan, J.-R., Nguyen, B., Li, F., Tufenkji, N., 2023. Tissue clearing to localize microplastics via three-dimensional imaging of whole organisms. *Environ Sci Technol* 57 (23), 8476–8483. <https://doi.org/10.1021/acs.est.2c07209>.
- [27] Nguyen, B., Tufenkji, N., 2022. Single-particle resolution fluorescence microscopy of nanoplastics. *Environ Sci Technol* 56, 6426–6435. <https://doi.org/10.1021/acs.est.1c08480>.
- [28] Rodríguez-Hernández, A.G., Muñoz-Tabares, J.A., Aguilar-Guzmán, J.C., Vazquez-Duhalt, R., 2019. A novel and simple method for polyethylene terephthalate (PET) nanoparticle production. *Environ Sci Nano* 6 (7), 2031–2036. <https://doi.org/10.1039/c9en00365g>.
- [29] Chithrani, B.D., Ghazani, A.A., Chan, W.C.W., 2006. Determining the size and shape dependence of gold nanoparticle uptake into mammalian cells. *Nano Lett* 6 (4), 662–668. <https://doi.org/10.1021/nl052396o>.
- [30] Peñaloza, J.P., Márquez-Miranda, V., Cabaña-Brunod, M., Reyes-Ramírez, R., Llancahuen, F.M., Vilos, C., et al., 2017. Intracellular trafficking and cellular uptake mechanism of PHBV nanoparticles for targeted delivery in epithelial cell lines. *J Nanobiotechnol* 15 (1). <https://doi.org/10.1186/s12951-016-0241-6>.
- [31] Chaloupková, Z., Žárská, L., Belza, J., Poláková, K., 2023. Label-free detection and mapping of graphene oxide in single HeLa cells based on MCR-Raman spectroscopy. *Anal Methods* 15 (42), 5582–5588. <https://doi.org/10.1039/d3ay01122d>.
- [32] Liu, Y., Peng, Z., Peng, X., Yan, W., Yang, Z., Qu, J., 2021. Shedding new lights Into STED microscopy: emerging nanoprobe for imaging (Frontiers Media S.A.). *Front Chem* Vol. 9. <https://doi.org/10.3389/fchem.2021.641330>.
- [33] Annangi, B., Villacorta, A., Vela, L., Tavakolpournegari, A., Marcos, R., Hernández, A., 2023. Effects of true-to-life PET nanoplastics using primary human nasal epithelial cells. *Environ Toxicol Pharmacol* 100, 104140. <https://doi.org/10.1016/j.etap.2023.104140>.
- [34] Annangi, B., Villacorta, A., López-Mesas, M., Fuentes-Cebrian, V., Marcos, R., Hernández, A., 2023. Hazard assessment of polystyrene nanoplastics in primary human nasal epithelial cells, focusing on the autophagic effects. *Biomolecules* 13, 220. <https://doi.org/10.3390/biom13020220>.
- [35] Tavakolpournegari, A., Annangi, B., Villacorta, A., Banaei, G., Martin, J., Pastor, S., et al., 2023. Hazard assessment of different-sized polystyrene nanoplastics in hematopoietic human cell lines. *Chemosphere* 325, 138360. <https://doi.org/10.1016/j.chemosphere.2023.138360>.
- [36] Tavakolpournegari, A., Villacorta, A., Morataya-Reyes, M., Arribas Arranz, J., Banaei, G., Pastor, S., et al., 2024. Harmful effects of true-to-life nanoplastics derived from PET water bottles in human alveolar macrophages. *Environ Pollut* 348, 123823. <https://doi.org/10.1016/j.envpol.2024.123823>.
- [37] Magri, D., Sánchez-Moreno, P., Caputo, G., Gatto, F., Veronesi, M., Bardi, G., et al., 2018. Laser ablation as a versatile tool to mimic polyethylene terephthalate nanoplastic pollutants: characterization and toxicology assessment. *ACS Nano* 12 (8), 7690–7700. <https://doi.org/10.1021/acs.nano.8b01331>.
- [38] Alaraby, M., Villacorta, A., Abass, D., Hernández, A., Marcos, R., 2024. Titanium-doped PET nanoplastics, from opaque milk bottle degradation, as a model of environmental true-to-life nanoplastics. Hazardous effects on *Drosophila*. *Environ Pollut* 341, 122968. <https://doi.org/10.1016/j.envpol.2023.122968>.
- [39] Alsubaie, S.M., Ali, D., Almutairi, B.O., Almeer, R., Alarifi, S., 2022. Evaluation of cyto- and genotoxic influence of lanthanum dioxide nanoparticles on human liver cells. 15593258221128428 *Dose Response* 20 (3). <https://doi.org/10.1177/15593258221128428>.
- [40] Banaei, G., García-Rodríguez, A., Tavakolpournegari, A., Martín-Pérez, J., Villacorta, A., Marcos, R., et al., 2023. The release of polylactic acid nanoplastics (PLA-NPLs) from

commercial teabags. Obtention, characterization, and hazard effects of true-to-life PLA-NPLs. J Hazard Mater 458, 131899. <https://doi.org/10.1016/j.jhazmat.2023.131899>.

- [41] Alaraby, M., Villacorta, A., Abass, D., Hernández, A., Marcos, R., 2023. The hazardous impact of true-to-life PET nanoplastics in Drosophila. Sci Total Environ 863, 160954. <https://doi.org/10.1016/j.scitotenv.2022.160954>.

DISCUSSION

4. DISCUSSION

4.1. Main objective brief

The main objective of the Thesis was the obtention of true-to-life nanoplastics as representative models of secondary environmental nanoplastics for hazard assessment uses, enabling the thorough evaluation of their physicochemical properties, biological interactions, and potential hazards. The need to accurately understand the impact of nanoplastics on living organisms, particularly on humans, has become a significant challenge for the scientific community, as well as a growing concern for the public opinion and regulators. The development of true-to-life models, which better represent what is found in nature, is of extreme relevance due to the complexity of separating or isolating these materials from the complex matrices in which they are typically dispersed. To date, most studies have been conducted using plastic nanoparticles, traditionally composed of pristine materials such as polystyrene, which is commercially available in various sizes and surface functionalization, as well as stained with fluorochromes to facilitate their follow up in cells/organisms. While these models are excellent for understanding the dynamics of nanoplastics and their interactions, or for fine-tuning techniques, their greatest advantage can also be their biggest drawback—their inability to accurately represent what is found in the environment. As a result, most studies tend to reflect subcellular, cellular or organoid-level effects using models that may be considered overly restrictive in terms of subsequent interpretation. Therefore, the need to increase the complexity of biological models *in vitro* or the use of *in vivo* or *ex vivo* approaches must go together with the need to increase the complexity of MNPL models to uncover the true biological effects that may arise from exposure to the wide variety of forms and sizes of nanoplastics found in the environment.

It is important to acknowledge that the models proposed here lack significant diversity in terms of polymer matrices leaving aside the fact that one of them contains titanium. However, this is precisely the factor we aim to isolate to provide a first conceptual and functional approximation of environmental polymers or composites, enabling their tracking and quantification. In doing that, we push the boundaries of what is possible in terms of both technology and technique.

Additionally, the need to develop a simple method not only for tracking but also for quantifying the amount of nanoplastics within a cell has been one of the most significant challenges in the field. In that context, the obtention of metal-doped MNPLs looks like a promising tool to be used to identify/quantify the presence of MNPLs in a defined organ

of the exposed organism. Taking advantage of the presence of titanium dioxide nanoparticles in the opaque PET milk bottles, we succeed to obtain Ti-doped PET MNPLs to be used to such ends. Since the particulate nature of the material means that its distribution is heavily dependent on physicochemical factors, it becomes crucial to determine the amount of titanium per particle and, subsequently, the number of particles per cell, or per unit of area, mass of tissue, or organ, depending on the experimental approach being pursued.

This highlights the importance not only of chemical quantification but also of having a clear visual and technical aid to distinguish the signals of nanoplastics from the matrix in which they are embedded. As such, developing a process that is not only effective in staining nanoplastics but also non-toxic—both in terms of the procedure and the outcome—is essential. Moreover, this method should allow for the identification of nanoplastics in biological structures without causing significant alterations to the polymer matrix. Furthermore, it is important that these methods are not only compatible with each other but also with the typical tools and techniques commonly used in Biology.

For this reason, the efforts dedicated in this work have been directed towards the efficient production of an environmentally representative nanoplastic, namely true-to-life nanoplastics, as a model for studying the potential damage these materials may cause. To achieve this, we have focused on validating the production method and ensuring the ease of tracking these particles in human cells, alongside conducting preliminary toxicity studies.

4.2. The need for true-to-life nanoplastic and the strategy for PET nanoplastic production

There is an urgent necessity for changing the way we are carrying on experiments relate not only with the use of new approach methodologies but also the good understanding of the possible toxicants that we are exposed to. Therefore, understanding that when plastic goods leave the production line and encounters the environment simultaneously begins its degradation process, is crucial. During this degradation process, plastic is exposed to phenomena such as abrasion and fragmentation, which contribute to its breakdown.

The degradation process is exacerbated once these plastic goods have reached the end of their useful life and are disposed of, often in landfills. Inevitably, a significant fraction of plastic waste will end up in the ocean, where it will be subjected to additional forces that contribute to its breakdown, such as the abrasion caused by ocean waves

and the materials they carry, as well as collisions with rocks, plus salinity (Andrady, 2011). In addition, we must also consider complementary and persistent factors, such as exposure to radiation, which occurs throughout the entire lifespan of the plastic material and contributes to its breakdown. This process is known as photodegradation of plastic. It is important to note that the smaller the plastic fragment, the greater the surface area exposed to this factor, increasing the possible incidence of photodegradation as the fragment size decreases and is relevant to understand that not only direct but also indirect photolysis may influence the process through the interaction with photo-induced species such as ROS, $\cdot\text{OH}$ radicals, singlet oxygen species ($^1\text{O}_2$) among others (Kaing et al., 2024). Once the aforementioned environmental factors, among others, contributed to the fragmentation of plastics, there is a significant possibility that this process will continue, either through the progressive and constant actions already mentioned or by the inclusion of new factors. For example, interactions with organisms can further fragment the particles while getting introduced into the trophic chain, moving up to higher trophic levels and accumulating through a process of biomagnification (Wesch et al., 2016; Dawson et al., 2018). Exposure to plastic nanoparticles in aquatic organisms has demonstrated that damage caused by pristine polystyrene (PS) nanoparticles can exert sublethal effects, which by themselves can lead to the underestimation of potential hazards. The inclusion of more complex materials out of polystyrene, at least in terms of composition, has shown sublethal biological impacts at biochemical endpoints, such as oxidative stress, as well as behavioral changes, like reduced swimming distance in *Daphnia magna* (Masseroni et al., 2024). These effects have been previously described, and studies have investigated not only the type of polymer in the particles but also the contaminants they may carry (Renzi et al., 2019; Zimmermann et al., 2020). It is interesting to note that, in different *in vivo* models, a similar pattern emerges. Only very mild or entirely absent effects were observed when *Drosophila* larvae are exposed to polystyrene nanoparticles with the more pronounced related to the small size of the PSNPLs (Alaraby et al., 2022), whereas more significant effects can be observed when they are exposed to nanoplastics derived from the degradation of plastic bottles. In the last case, alterations in the gene expression of pathways related to oxidative stress could be observed (Alaraby et al., 2023, 2024). A common factor in each of the mentioned cases is the completion of what is known as the 'journey' of plastic particles inside the organisms, once ingested. In *Drosophila* these particles can make a complete passage from ingestion, interacting with structures such as the intestine components and its corresponding microbiota, to be uptake by enterocytes, and their subsequent translocation across the intestinal barrier into the hemolymph, where they interact with

hemocytes. Similarly, their interactions within the lumen and with the corresponding microbiota have also been investigated (Alaraby et al., 2022, 2023, 2024). This is relevant, as demonstrates by the observed effects not only at the cellular level but also within whole organisms. The translocation of nanoplastics across a barrier has been previously observed in *in vitro* models, specifically in co-cultures of human Caco-2 with HT-29 cells in inserts, along with human Raji-B lymphocyte models, and the ease with polystyrene nanoplastics (Domenech, et al., 2020) or true-to-life PLA nanoplastics (Banaei et al., 2023) can cross biological barriers appears to be beyond dispute. As there are no major differences in how these particles interact with various models, it becomes essential to understand the response to exposure from different nanoplastics that better represent what exists in the environment, at levels ranging from cellular to the entire organisms. This has led to the proposal of several alternatives for generating laboratory-made nanoplastics, and the method presented here aims, among other things, to accurately represent what exists not only in suspension but also in large bodies of water, and even closer to home, such as in the water bottles, we use daily.

4.3. True-to-life PET MNPLs obtention

There is growing interest in the study of the potential health effects of micro- and nanoplastics. The interest within the scientific community is like what was observed in the field of ecotoxicology with the emergence of nanomaterials (Krug, 2014). In fact, as shown by our own data (Fig. 3, Introduction), this interest is reflected in the increasing number of studies focused on plastic nanoparticles such as polystyrene nanoplastics. This, in combination with the need for new models of complex nanoplastics, have led to the different groups to try to generate different types of nanoplastics, with different methodologies, to use the generated material to move from the nano polystyrene studies into more representative ones. It has been also stated that to study the environmental hazard and risk assessment of nanomaterials a series of baseline characterization is needed (Hartmann et al., 2017) and the main gaps in this field has also been thoroughly described (Cunningham et al., 2023). However, the world of nanoplastics is always more complex and need to be addressed from the very base where for instance the contaminants that comes from the manufacturing process also needs to be considered.

There is no production of nanoparticles that is free from technological challenges. In our case, one of the main difficulties, arise from generating the appropriate particle size, was the contamination resulting from the process. Contamination in a production process is a critical point, especially when the goal is to control toxicity or assess the potential

hazard of a material. There are reports in the literature showing that particles which are theoretically identical can exhibit diverse characteristics or behaviors in terms of toxicity, depending on their surface coatings or directly on the production and stabilization processes (Egbuna et al., 2021) and those effects have been observed to be differential for both *in vitro* and *ex vivo* for nanoplastics (Arribas Arranz et al., 2024; Martín-Pérez et al., 2024). Moreover, the use of surfactants as stabilizers can result in false toxicity results (Pikuda et al., 2019) and therefore it is important to evaluate the physicochemical characteristics of plastic particles before any biological approach is even considered.

When considering the approach to generate MNPLs from plastic good, several factors were weighed. Among them, the purity of the material was prioritized, as previously discussed, along with the ease of use in any laboratory with relatively basic equipment. The method was designed to be accessible and user-friendly, requiring minimal specialized training or complex machinery. The use of complex technologies such as laser ablation, previously proposed in the literature (Magri et al., 2018), was dismissed not due to surface modification—which could be an advantage when considering aged PET exhibiting characteristics of photodegradation—but rather because the aim was to maintain an unaltered surface. This approach would allow for future comparison between untreated PET particles and those exposed to degradation conditions, thus isolating the effects of each scenario. As a result, adaptations of a previously described protocol (Rodríguez-Hernández et al., 2019) were implemented to obtain more consistently representative particles. The use of a rotary tool attached to a motor was a significant improvement in terms of efficiency, but it also introduced other challenges, such as overheating of the material, turning what initially seemed like an advantage into a critical step that needed careful control. Another challenge was selecting the appropriate material for the size reduction process. Initially, when aluminum oxide grinding stones or silicon carbide were used, traces of these materials were detected in the obtained MNPLs by conventional spectroscopy techniques, highlighting the need for an alternative approach. At this point, the use of diamond rotary heads helped overcome a potential future issue, as the toxicity of certain metals, including those used in plastic production processes, has been previously documented in the literature (Turner & Filella, 2021). The wide range of size and shape heterogeneity is clearly observed through electron microscopy, where larger fragments can be seen, either because of the aggregation or agglomeration during production or homogenization. While it is easy to conclude that these larger fragments are volumetrically significant, they represent less than 1% of the total particle count in all analyzed cases. Nevertheless, analyzing each production batch is crucial, and it is essential to have efficient dispersion methods that do not interfere with

subsequent experiments. Both SDS and NovaChem detergents have been shown to function effectively in this regard; nevertheless, they must be completely removed/avoided when conducting biological approaches. In contrast, the NanoGenotox approach (Nanogentox, 2011) results in both good dispersion and compatibility for biological applications.

The hydrodynamic stability of the particles investigated is more complex, and the answer to their hydrodynamic behavior is not as straightforward as one might expect, even considering that the zeta potential values are quite far from zero, which is typically an indicator of suspension stability (Hao et al., 2023). These issues are largely mitigated by performing a 0.5 μm pre-filtration before analyzing nanoplastic samples, mainly because light scattering (LS) is a technique that depends not only on the stability of the suspension but also on the degree of monodispersion. In turns, the narrow size distribution of the sample is influenced not only by the inherent size distribution characteristics but also by the stability of the suspension over time which largely depend on the environment. Similar behaviors to those described here have been observed in more recent experimental approaches, where the presence of microparticles or aggregates results in bimodal distributions when the hydrodynamic behavior is studied (Ducoli et al., 2024). This makes the study of environmentally representative samples using DLS one of the techniques to employ, but not the only one on which future experiments should solely rely. Undoubtedly, it must be complemented with techniques that better describe the submicrometric scale, such as nanoparticle tracking analysis or electron microscopy, whether scanning or transmission. Alternatively, when allowed by the technique, much finer approaches in terms of separation, such as asymmetric flow field-flow fractionation can be employed (Valido et al., 2023), as we have performed. Another important step is confirming the identity of the nanoplastic we are working with, and a direct way to obtain this information is using FTIR. In this way, we have identified the functional groups corresponding to the type of polymer while also confirming that no peaks unrelated to PET have been detected. This, combined with the EDS analysis, confirms that the presence of impurities is below the detection limits of the typical techniques used in regular laboratory settings. Therefore, the nanoplastics generated here are suitable for use in biological assays.

A widely used approach for detecting nanoparticles in cells is the observation of changes in the internal granularity (Vila et al., 2017). This same approach remains equally valid for nanoplastics and has even been used to describe changes in cell volume (Martín-Pérez et al., 2024). In our case, we observed that particle uptake is affected in the short term by the presence or absence of FBS, while internalization appears to be

concentration-dependent, without reaching a saturation point. Concentrations as high as 1 mg/mL for nanoplastics have been reported in the literature (DeLoid et al., 2021; Marcellus et al., 2024), indicating that we are far from the maximum possible concentration. Particle internalization was further confirmed using Nile Red staining, a process not without challenges, as this compound has a very high efficiency in labeling cells, and in many cases, the detection of particles was hindered by the fluorescence from intracellular lipid bodies. This highlights the need to develop a more efficient labeling technique, while also demonstrating the intracellular localization of the particles, which we complemented with electron microscopy images. Once again, this underscores the importance of using complementary techniques when interpreting results and exercising caution in drawing conclusions.

PET nanoplastics have been studied in terms of toxicity, particularly in the context of genotoxicity (Egbuna et al., 2021; Møller & Roursgaard, 2023). However, few approaches have been made using materials other than polystyrene, and currently there are a growing number of studies in which biological implications of PET nanoparticles are investigated, involving human nasal primary cells (Annangi, Villacorta, Vela, et al., 2023), alveolar basal epithelial A549 cells (Alzaben et al., 2023) alveolar macrophages (Tavakolpournegari et al., 2024), and Caco-2 intestinal barrier cells (Magri et al., 2018), along with a recent study involving the regulatory widely accepted *in vitro* Bhas 42 cell transformation assay (Domenech et al., 2024) among the more relevant in the field. In our preliminary approach, we have identified, in addition to internalization and changes at the cellular structural level, a very low reactivity in terms of cell survival, with only TK6 cells being slightly affected at concentrations so high as 200 µg/mL. Additionally, in THP1 cells exposed to sub-toxic levels, we were unable to detect genomic DNA breaks using the comet assay. While there were no significant changes in oxidative stress levels, a trend was observed. Altogether, this indicates the need for further investigations. This is clearer when we acknowledge that the scope of this study focuses on the particle itself and not on its effects and, therefore, refinements in cellular treatments, extended exposure times, or adjusted concentrations must undoubtedly be explored. Nevertheless, with respect to the main objective, we can assert beyond any reasonable doubt that our study has success obtaining an efficient method to produce PET nanoparticles to be used for biological studies aiming to detect potential harmful effects. This method refines the experimental techniques, minimizing the possibility of contamination, ensuring that any observed biological outcomes, if present, are specifically due to the material, its distribution, shape, composition, or interactions.

4.4. True-to-life titanium-doped PET MNPLs obtention

We have adopted a similar approach to take advantage of the availability of a material in the market that could fulfill two important needs. On one hand, there is a requirement for a material that can be doped with metals that are relatively safe, allowing for the tracking of nanoparticles in complex matrices. On the other hand, it must retain the properties of a nanoplastic, staying within the range where it maintains its nanoscale characteristics, such as Brownian motion and, of course, a high surface-area-to-volume ratio. These needs arise from the fact that, although there are studies that allow the tracking of nanoplastics, they predominantly rely on the properties of polystyrene plastic nanoparticles, which do not accurately represent what is found in the environment (Xu et al., 2022). Direct extrapolation from this data to more complex situations, such as human exposure risk assessments for nanoplastics, is therefore not possible. Once again, we are faced with a field of study that requires refinement.

In this chapter, we proposed the use of an adaptation of top-down methodologies employed for the production of both micro- (Lionetto et al., 2021; Pignattelli et al., 2021) and nanoplastics (Rodríguez-Hernández et al., 2019; Roursgaard et al., 2022; Alzaben et al., 2023). This approach takes advantage of the pre-embedded titanium nanoparticles within the polymeric matrix of commercial packaging products, typically used to limit gas transmission and provide protection against radiation for more sensitive products, such as those in the dairy industry (Tramis et al., 2021).

It is necessary to remark that a parallel study for tracing nanoplastics focused on fluorescence techniques was carried out within this study and even knowing that part of it is utilized in this chapter, we will delve deeper into it in the third chapter of this work. At this point, it is important to acknowledge that fluorescence-based technologies, while useful, cost-effective, and accessible for daily use, have significant limitations at the biological scale. They must be at least initially complemented by other techniques to be used reliably for decision-making or drawing conclusions in a complex field like nanotoxicology. For instance, an important drawback is the necessity of perform a pre-labeling step for MNPLs before their biological application, and even then, these labeled plastics are subject to the typical properties of fluorophores, such as photobleaching (Jensen, 2012; Demchenko, 2020; Kwak et al., 2024).

One of the main features to highlight is the quantity of material produced during the nanoplastic production process. It is also worth noting that the separation process is more efficient, with the larger fraction more easily settling at the bottom of the sedimentation cylinders, allowing the fraction exhibiting Brownian behavior to be better separated from the larger particles. This is likely due to the titanium nanoparticles' higher

density, which provides a greater mass-to-volume ratio. Nonetheless, the yield is sufficient to carry out not only the full set of physicochemical characterizations but also comprehensive toxicological evaluations, both *in vitro* and *in vivo*.

Since enough amounts were obtained, it was logical to proceed with its characterization. The first noticeable feature in electron microscopy use, beyond the irregular geometry, is the difference in electron density of the materials composing the nanoplastic. This variation in electron density is traditionally utilized in biological samples, such as in uranium-based negative staining for protein identification (Shirai, 2018). This allows for the differentiation of heavier atoms from lighter ones, but caution must be taken to avoid overlapping layers of lighter atoms, which can lead to errors for users unfamiliar with the technique, especially given the non-uniformity of the material.

It is important to remember that despite being catalogued as no longer safe by the EFSA Panel on Food Additives and Flavourings (EFSA., 2021), titanium dioxide NPs (E171) are still widely use as food additive and therefore its study has a dual impact. First, and possibly the most evident, is understanding how this additive, along with the nanoplastic derived from daily consumer packaging products, could affect human health. Second, as a direct consequence of the first and the goal of this particular work, is the development of a tool that allows for more accurate assessments of these impacts. Due to the ease of tracking through commonly used laboratory techniques, thanks to the ease of staining against a carbon-based background, such as biological samples or complex matrices(Mitrano et al., 2019; Hoppe et al., 2023), the use of metal-loaded nanoparticles has already been described as an alternative to this challenge. However, we understand that, as of today, the nanoplastics proposed here offer a promising solution and stands out as the first approach to metal-dopped true-to-life or environmentally representative composite model.

As a logical continuation from the first chapter, the hydrodynamic characterization in this case was carried out after the particles were subjected to the NanoGenotox dispersion protocol, which proved to be the most suitable. In addition, measurements were conducted using both DLS and MADLS, specifically employing angles that allow the detection of small, medium, and large particles separately, followed by averaging the values to obtain a theoretically more accurate result. However, the differences were not substantial, indicating good dispersion of the material. A noticeable change was observed in the surface potential of the particles, shifting from -33.10 which is considerable as a good value for maintaining the stability of colloidal suspensions (Lin et al., 2010) to -18.23. Despite this shift, the stability of the suspensions remained adequate, even when evaluated in high-conductivity media. This behavior, which differs

from non-doped particles, may explain why the separation in the sedimentation cylinder was more pronounced.

Regarding the identity of the nanocomposite, two approaches were used. As in the previous case, FTIR was the technique chosen to identify the chemical nature of the nanoparticles. This time, the analyses were carried out on PET films from both transparent and opaque packaging, as well as on the nanoparticles generated from them and the powder produced in the intermediate stages of production. The identity of the observed peaks was compared with the literature and corresponds to what is expected for PET polymers in each case. Additionally, through electron microscopy, we once again investigated differences in electron density and backscatter, and even within the polymeric structure, it was possible to identify Ti, concealed beneath a superficial polymer layer. This was complemented by an EDS detector, which confirmed the presence of Ti alone in both the analyzed particles and the general samples. This allowed us not only to confirm the quality of the manufacturing process in terms of being free from contaminants but also to verify once again that we successfully generated the desired particle. In combination with this confirmation, the Ti content was measured by mass spectroscopy, showing a decrease in the relative amount of Ti compared with the raw material. This indicates areas for control within the production process; however, for the purposes of biological studies, this does not present a significant drawback, and it will be more valuable to control the amount of titanium in the particles at the end of production than to focus on the Ti loss during the process.

Once we understood the material we were working with, we proceeded to label the nanoparticles for observation using confocal microscopy. We employed the method developed in parallel, which will be further discussed in the next chapter. However, it is worth mentioning here that the method proved efficient and easy to use. PET-Ti particles labeled with iDye were analyzed by confocal microscopy, both on their own and inside cells, determining their emission spectrum and confirming the colocalization of the fluorescent signal with the reflection generated by the Ti, once again verifying the hybrid nature of the material through an accessible technique. By utilizing the advantages of confocal microscopy, we were able to determine the presence of particles within human-derived THP1 monocytes, as well as the Ti within the PET. Additionally, we confirmed that, at concentrations of up to 100 $\mu\text{g/mL}$, the material did not cause a decrease in cell viability in any of the three hematopoietic cell lines used for evaluation (THP1, TK6 and Raji-B), which had previously been studied under similar conditions for various types of plastics (Rubio et al., 2020; Tavakolpournegari et al., 2023; Vela et al., 2023).

4.5. Research for a labelling efficient method for true-to-life MNPLs

Different approaches have been adopted to evaluate the presence of MNPLs interacting with cells from the use of highly technological and biocompatible graphene quantum dots (Liang et al., 2022) to hyperspectral imaging of labelled free nanoplastics interaction at single cell level (H. J. Zhang et al., 2023). Rather than delving into the advantages or disadvantages of the various methods that creatively address a fundamental problem in nanoscience—determining the location of particles to understand the effective dose, not just the applied dose—we have focused our efforts on proposing a viable alternative that allows us to label nanoparticles effectively.

The purification of nanoparticles has been described as essential for obtaining reliable and reproducible results in the field of biology, especially given that many findings depend on this technique, and nanotechnology is not an exception. Numerous research groups have made diverse attempts to increase the purity of their nanoparticle preparations, focusing on size and shape. These efforts include techniques such as magnetic flow field fractionation, chromatography, density gradient filtration, and gel electrophoresis, among others. However, these methodologies are mostly designed or suitable for hard nanoparticles, or at least not intended for use with soft nanoparticles, as they are typically focused on metallic nanoparticles (Robertson et al., 2016). Therefore, we aimed to present an easy-to-use, experimentally and budget friendly alternative that utilizes a regular centrifuge for the separation of nanoplastics. This method serves as a first step in isolating the labeled particles from the labeling solution, bypassing the need for dialysis. We established 45 min as an acceptable centrifugation time, acknowledging a loss of less than 4% of the sample. When larger centrifugation volumes are required, or a more efficient labeling technique is needed, membrane centrifugation is recommended. While it might initially seem that a greater quantity of particles could be lost due to material being trapped in the membranes, this method is more optimal in terms of time and labor. If the potential percentage of particle loss is kept in mind, membrane centrifugation can be a more viable option, which is, in fact, the approach we have chosen as the most appropriate.

A quick way to assess the behavior of particles after being subjected to a stressful procedure, such as centrifugation—especially under conditions where nanoparticles need to be centrifuged to induce precipitation—is to measure their hydrodynamic behavior. Various resuspension methods were tested, with sonication proving to be the most efficient. Numerous reports detail particle resuspension methods, but the most widely used and effective approach is, without a doubt, the application of energy through

sonication. This method forms the foundation of the most adopted resuspension protocol for working with nanoparticles in biological applications (Nanogenotox, 2011).

When evaluating the staining of the nanoparticles, it is important to note that all particles were effectively stained using adapted methodologies previously described for micro- and nanoplastics (Karakolis et al., 2019; Nguyen & Tufenkji, 2022). With the added particularity of testing at different levels of biological compatibility and labeling and therefore effectiveness. This means that even if the particles are effectively labeled, they may not necessarily be useful for biological applications. In this case, depending on their characteristics, they have been classified as either optimal, such as iDye, or suboptimal, like luminous yellow (Amarillo luminoso), whose fluorescence across multiple channels makes it less suitable for biological applications. In the case of Rhodamine B and Opticol, although initially useful, they cause alterations in cellular integrity or produce nonspecific signals at high concentrations, which can lead to erroneous conclusions if the necessary precautions are not taken.

This protocol has been presented as a simplified protocol, not only verified by using a different cellular model to demonstrate its versatility but also for its application with true-to-life PET-Ti nanocomposites. To exemplify this, we have observed in a hepatic cell model (HUH7) the presence of PET-Ti nanoplastics within the cell, with colocalized signals from both the labeled polymer and the reflection from the metal, making it possible to detect the particles clearly and easily within a biological matrix. This is seen as the signal of the metal inside the signal of the particle, which is itself inside the signal of the cell.

Ultimately, the proposed method, along with the previously developed particle production methodology, offers an advantage by facilitating the tracing and detection of nanoparticles using widely accessible and inexpensive techniques such as fluorescence microscopy, confocal microscopy, and flow cytometry. However, a cautionary note must be raised regarding the potential release of titanium nanoparticles from the mixed matrix, as signals from isolated titanium have been identified after passage through the intestines of *Drosophila* larvae (Alaraby et al., 2024). This is particularly relevant because detrimental effects caused by titanium nanoparticles have been previously reported in this organism (Carmona et al., 2015; Demir, 2020; Alaraby et al., 2021). This may be due to the potential detachment of titanium during the production process, possible effects resulting from interaction with the intestinal barrier, incomplete labeling, or the loss of staining in this concrete analyzed nanoplastic. While this is uncommon, it is something to consider, as similar effects are expected in emerging environmental contaminants. Therefore, we believe that the associated techniques to evaluate biological endpoints, in

combination with the hereby proposed methodologies, allow us to overcome what has been defined as general analytical challenges inherent to nanoplastic research (Kokalj et al., 2021).

4.6. Final remarks

Together, both PET and PET-Ti nanoplastics, along with the development of a reliable method for labeling nanoparticles, have been established as a foundation for studying the toxicity of nanomaterials within the framework of the European project PlasticHeal (*Innovative tools to study the impact and mode of action of micro and nanoplastics on human health: towards a knowledge base for risk assessment H2020-965196*). Among other important goals, this project aims to develop new methodologies and provide reliable scientific evidence to enable regulators to establish a solid knowledge base for the proper risk assessment of MNPLs.

PlasticHeal is part of the CUSP cluster, which brings together five European initiatives, fostering synergies by uniting multidisciplinary teams of scientists, industry stakeholders, and policymakers. The goal is to investigate the complex relationships between micro- and nanoplastics (MNPs) and human health, from early life to adulthood. This research also contributes to the project “*Desarrollo de NAMs para la evaluación de los efectos para la salud de contaminantes emergentes presentes en las aguas residuales (PID2020-116789RB-C43)*”. Consequently, these obtained nanoplastics and methodologies have been distributed, studied, and their effects evaluated by multiple groups throughout the consortium, with many studies nearing publication. Additionally, there are already existing publications and *in vitro* evaluation studies determining the effects of the obtained true-to-life MNPLs on human nasal epithelial cells (Annangi et al., 2023), in the evaluation of the cell transforming potential (Domenech et al., 2024) as well as on the effects induced in alveolar macrophages (Tavakolpournegari et al., 2024). Furthermore, *in vivo* studies have been done for PET in *Drosophila* and mice (Alaraby et al., 2023; Loret et al., 2023), as well as with PET-Ti (Alaraby et al., 2024). Furthermore, *ex vivo* studies using human whole blood have been conducted (Arribas Arranz et al., 2024) together with studies determining the effects resulting from the chemical aging degradation point of view (Douki et al., 2024). In addition of the use of the obtained true-to-life MNPLs, the proposed staining methodology have served for many of the above-mentioned studies along with the study of labelled PS, mainly for cytometry and confocal endpoints related with mitochondrial alterations (Annangi et al., 2023; Tavakolpournegari

et al., 2023) and to determine cell internalization of true-to-life PLA nanoparticles from commercial teabags (Banaei et al., 2023).

Throughout, this has highlighted the versatility, utility, and benefits of the materials and endpoints studied. Once again, it demonstrates that working in multidisciplinary teams enables science to achieve far more than could be accomplished in isolation and both the published articles and the use of the materials/protocols generated in the work that conduct to this Thesis by colleague's research, highlight the relevance of the task and the results reported in this Thesis.

CONCLUSIONS

5. CONCLUSIONS

5.1.

The main objective of this Thesis was achieved through the successful development of methods for producing PET and titanium-doped PET MNPL, coupled with detailed characterization and toxicological assessments in human cell models. The developed methodologies proved useful to advance in the understanding of the health risk associated to MNPLs human exposure.

5.2.

A reliable method to produce PET MNPLs derived from commercially available PET water bottles was developed. In addition, the physicochemical characteristics of the resulting material were thoroughly examined using a wide range of tools. Regarding its potential toxicity, no significant effects in cell viability were observed in human-derived THP1 and TK6 cells. A time/dose dependence uptake was observable, influenced by the use of FBS, indicating how the complexity of the culture media may influence the cell/particle interaction.

5.3

The method for PET MNPLs production was adapted and refined for the obtention of MNPLs from opaque PET milk bottles. The developed methodology yields quantifiable titanium-doped PETi MNPLs. Such particles were fully characterized by DLS, TEM, SEM-EDS confirming the well distributed presence of titanium particles embedded in the PET matrix, with a size distribution within the nano range, and with a diverse morphology from pointy to round edges. No toxicity of such true-to-life MNPLs was detectable in three hematopoietic cell lines tested despite the observable PET-Ti nanoplastic internalization.

5.4.

A reliable, cost-effective and easy to use method for staining true-to-life MNPLs was developed using iDye, with potential application both in *in vitro* and *in vivo* internalization studies. Fluorescence compatibility and lack of toxicity was verified using human-derived cells. The stained MNPLs was clearly visualized inside cells using fluorescence microscopy and fluorescence-based flow cytometry approaches.

REFERENCES

6.- REFERENCES

- Alaraby, M., Abass, D., Domenech, J., Hernández, A., & Marcos, R. (2022). Hazard assessment of ingested polystyrene nanoplastics in *Drosophila* larvae. *Environmental Science: Nano*, 9, 1845–1857. <https://doi.org/10.1039/d1en01199e>
- Alaraby, M., Hernández, A., & Marcos, R. (2021). Novel insights into biodegradation, interaction, internalization and impacts of high-aspect-ratio TiO₂ nanomaterials: A systematic in vivo study using *Drosophila melanogaster*. *Journal of Hazardous Materials*, 409. <https://doi.org/10.1016/j.jhazmat.2020.124474>
- Alaraby, M., Villacorta, A., Abass, D., Hernández, A., & Marcos, R. (2023). The hazardous impact of true-to-life PET nanoplastics in *Drosophila*. *Science of the Total Environment*, 863. <https://doi.org/10.1016/j.scitotenv.2022.160954>
- Alaraby, M., Villacorta, A., Abass, D., Hernández, A., & Marcos, R. (2024). Titanium-doped PET nanoplastics, from opaque milk bottle degradation, as a model of environmental true-to-life nanoplastics. Hazardous effects on *Drosophila*. *Environmental Pollution*, 341. <https://doi.org/10.1016/j.envpol.2023.122968>
- Alzaben, M., Burve, R., Loeschner, K., Møller, P., & Roursgaard, M. (2023). Nanoplastics from ground polyethylene terephthalate food containers: Genotoxicity in human lung epithelial A549 cells. *Mutation Research - Genetic Toxicology and Environmental Mutagenesis*, 892. <https://doi.org/10.1016/j.mrgentox.2023.503705>
- American Society for testing and materials International (ASTM). (n.d.-a). *ASTM D7611-13 Standard practice for coding plastic manufactured articles for resin identification*. *Guiding the Plastics Recycling Value Chain*. www.astm.org
- American Society for testing and materials International (ASTM). (n.d.-b). *Standard Practice for Coding Plastic Manufactured Articles for Resin Identification*. https://doi.org/10.1520/D7611_D7611M-20.20
- Andrady, A. L. (2011). Microplastics in the marine environment. In *Marine Pollution Bulletin* (Vol. 62, Issue 8, pp. 1596–1605). <https://doi.org/10.1016/j.marpolbul.2011.05.030>
- Annangi, B., Villacorta, A., López-Mesas, M., Fuentes-Cebrian, V., Marcos, R., & Hernández, A. (2023). Hazard Assessment of Polystyrene Nanoplastics in Primary Human Nasal Epithelial Cells, Focusing on the Autophagic Effects. *Biomolecules*, 13(2). <https://doi.org/10.3390/biom13020220>
- Annangi, B., Villacorta, A., Vela, L., Tavakolpournegari, A., Marcos, R., & Hernández, A. (2023). Effects of true-to-life PET nanoplastics using primary human nasal epithelial cells. *Environmental Toxicology and Pharmacology*, 100. <https://doi.org/10.1016/j.etap.2023.104140>
- Arribas Arranz, J., Villacorta, A., Rubio, L., García-Rodríguez, A., Sánchez, G., Llorca, M., Farre, M., Ferrer, J. F., Marcos, R., & Hernández, A. (2024). Kinetics and toxicity of nanoplastics in ex vivo exposed human whole blood as a model to understand their impact on human health. *Science of the Total Environment*, 948. <https://doi.org/10.1016/j.scitotenv.2024.174725>

- Attama, A. A., Reginald-Opara, J. N., Uronnachi, E. M., & Onuigbo, E. B. (2016). Nanomedicines for the Eye: Current Status and Future Development. In *Nanoscience in Dermatology* (pp. 323–336). Elsevier Inc. <https://doi.org/10.1016/B978-0-12-802926-8.00025-2>
- Bakelizer, T. (1993). *A national historic chemical landmark. The “Old Faithful” Bakelizer.*
- Banaei, G., García-Rodríguez, A., Tavakolpournegari, A., Martín-Pérez, J., Villacorta, A., Marcos, R., & Hernández, A. (2023). The release of polylactic acid nanoplastics (PLA-NPLs) from commercial teabags. Obtention, characterization, and hazard effects of true-to-life PLA-NPLs. *Journal of Hazardous Materials*, 458. <https://doi.org/10.1016/j.jhazmat.2023.131899>
- Barguilla, I., Domenech, J., Ballesteros, S., Rubio, L., Marcos, R., & Hernández, A. (2022). Long-term exposure to nanoplastics alters molecular and functional traits related to the carcinogenic process. *Journal of Hazardous Materials*, 438. <https://doi.org/10.1016/j.jhazmat.2022.129470>
- Bergmann, M., Collard, F., Fabres, J., Gabrielsen, G. W., Provencher, J. F., Rochman, C. M., van Seville, E., & Tekman, M. B. (2022). Plastic pollution in the Arctic. In *Nature Reviews Earth and Environment* (Vol. 3, Issue 5, pp. 323–337). Springer Nature. <https://doi.org/10.1038/s43017-022-00279-8>
- Billings, A., Jones, K. C., Pereira, M. G., & Spurgeon, D. J. (2021). Plasticisers in the terrestrial environment: Sources, occurrence and fate. In *Environmental Chemistry* (Vol. 18, Issue 3, pp. 111–130). CSIRO. <https://doi.org/10.1071/EN21033>
- Browne, M. A., Dissanayake, A., Galloway, T. S., Lowe, D. M., & Thompson, R. C. (2008). Ingested microscopic plastic translocates to the circulatory system of the mussel, *Mytilus edulis* (L.). *Environmental Science and Technology*, 42(13), 5026–5031. <https://doi.org/10.1021/es800249a>
- Cambridge dictionary. (2024). *Plastic, noun (substance) Cambridge dictionary.* <https://dictionary.cambridge.org/dictionary/english/plastic>
- Carmona, E. R., Escobar, B., Vales, G., & Marcos, R. (2015). Genotoxic testing of titanium dioxide anatase nanoparticles using the wing-spot test and the comet assay in *Drosophila*. *Mutation Research - Genetic Toxicology and Environmental Mutagenesis*, 778, 12–21. <https://doi.org/10.1016/j.mrgentox.2014.12.004>
- Cunningham, B. E., Sharpe, E. E., Brander, S. M., Landis, W. G., & Harper, S. L. (2023). Critical gaps in nanoplastics research and their connection to risk assessment. In *Frontiers in Toxicology* (Vol. 5). Frontiers Media S.A. <https://doi.org/10.3389/ftox.2023.1154538>
- Dawson, A. L., Kawaguchi, S., King, C. K., Townsend, K. A., King, R., Huston, W. M., & Bengtson Nash, S. M. (2018). Turning microplastics into nanoplastics through digestive fragmentation by Antarctic krill. *Nature Communications*, 9(1). <https://doi.org/10.1038/s41467-018-03465-9>
- DeLoid, G. M., Cao, X., Bitounis, D., Singh, D., Llopis, P. M., Buckley, B., & Demokritou, P. (2021). Toxicity, uptake, and nuclear translocation of ingested micro-nanoplastics in an in vitro model of the small intestinal epithelium. *Food and Chemical Toxicology*, 158(October), 112609. <https://doi.org/10.1016/j.fct.2021.112609>

- Demchenko, A. P. (2020). Photobleaching of organic fluorophores: Quantitative characterization, mechanisms, protection. In *Methods and Applications in Fluorescence* (Vol. 8, Issue 2). IOP Publishing Ltd. <https://doi.org/10.1088/2050-6120/ab7365>
- Demir, E. (2020). An in vivo study of nanorod, nanosphere, and nanowire forms of titanium dioxide using *Drosophila melanogaster*: toxicity, cellular uptake, oxidative stress, and DNA damage. *Journal of Toxicology and Environmental Health - Part A: Current Issues*, 83(11–12), 456–469. <https://doi.org/10.1080/15287394.2020.1777236>
- Domenech, J., de Britto, M., Velázquez, A., Pastor, S., Hernández, A., Marcos, R., & Cortés, C. (2021). Long-term effects of polystyrene nanoplastics in human intestinal Caco-2 cells. *Biomolecules*, 11(10). <https://doi.org/10.3390/biom11101442>
- Domenech, J., Hernández, A., Demir, E., Marcos, R., & Cortés, C. (2020). Interactions of graphene oxide and graphene nanoplatelets with the in vitro Caco-2/HT29 model of intestinal barrier. *Scientific Reports*, 10(1), 1–15. <https://doi.org/10.1038/s41598-020-59755-0>
- Domenech, J., Hernández, A., Rubio, L., Marcos, R., & Cortés, C. (2020). Interactions of polystyrene nanoplastics with in vitro models of the human intestinal barrier. *Archives of Toxicology*, 94(9), 2997–3012. <https://doi.org/10.1007/s00204-020-02805-3>
- Domenech, J., & Marcos, R. (2021). Pathways of human exposure to microplastics, and estimation of the total burden. In *Current Opinion in Food Science* (Vol. 39, pp. 144–151). Elsevier Ltd. <https://doi.org/10.1016/j.cofs.2021.01.004>
- Domenech, J., Villacorta, A., Ferrer, J. F., Llorens-Chiralt, R., Marcos, R., Hernández, A., & Catalán, J. (2024). In vitro cell-transforming potential of secondary polyethylene terephthalate and polylactic acid nanoplastics. *Journal of Hazardous Materials*, 469. <https://doi.org/10.1016/j.jhazmat.2024.134030>
- Douki, T., Bard, V., Boulée, M., & Carrière, M. (2024). Extensive HPLC-tandem mass spectrometry characterization of soluble degradation products of biodegradable nanoplastics under environmentally relevant temperature and irradiation conditions. *Environmental Science: Nano*. <https://doi.org/10.1039/d3en00960b>
- Ducoli, S., Federici, S., Cocca, M., Gentile, G., Zendrini, A., Bergese, P., & Depero, L. E. (2024). Characterization of polyethylene terephthalate (PET) and polyamide (PA) true-to-life nanoplastics and their biological interactions. *Environmental Pollution*, 343. <https://doi.org/10.1016/j.envpol.2023.123150>
- Ducoli, S., Federici, S., Nicsanu, R., Zendrini, A., Marchesi, C., Paolini, L., Radeghieri, A., Bergese, P., & Depero, L. E. (2022). A different protein corona cloaks “true-to-life” nanoplastics with respect to synthetic polystyrene nanobeads. *Environmental Science: Nano*, 9(4), 1414–1426. <https://doi.org/10.1039/d1en01016f>
- Egbuna, C., Parmar, V. K., Jeevanandam, J., Ezzat, S. M., Patrick-Iwuanyanwu, K. C., Adetunji, C. O., Khan, J., Onyeike, E. N., Uche, C. Z., Akram, M., Ibrahim, M. S., El Mahdy, N. M., Awuchi, C. G., Saravanan, K., Tijjani, H., Odoh, U. E., Messaoudi, M., Ifemeje, J. C., Olisah, M. C., ... Ibeabuchi, C. G. (2021). Toxicity of

- Nanoparticles in Biomedical Application: Nanotoxicology. In *Journal of Toxicology* (Vol. 2021). Hindawi Limited. <https://doi.org/10.1155/2021/9954443>
- European Commission. (2022). *Communication from the commission to the Eruopean Parliament, The Council, The European Economic an Social Committee an the Committee of the Regions. EU policy framework on biobased, biodegradable and compostable plastics.*
- Freinkel, S. (2011, May 29). A Brief History of Plastic's Conquest of the World. Cheap plastic has unleashed a flood of consumer goods. *Scientific American*.
- García-Rodríguez, A., Gutiérrez, J., Villacorta, A., Arribas Arranz, J., Romero-Andrada, I., Lacoma, A., Marcos, R., Hernández, A., & Rubio, L. (2024). Polylactic acid nanoplastics (PLA-NPLs) induce adverse effects on an in vitro model of the human lung epithelium: The Calu-3 air-liquid interface (ALI) barrier. *Journal of Hazardous Materials*, 475, 134900. <https://doi.org/10.1016/j.jhazmat.2024.134900>
- Garside, M. (2024). *Global plastic production 1950-2022.* <https://www.statista.com/statistics/282732/global>
- Geyer, R. (2020). Production, use, and fate of synthetic polymers. In *Plastic Waste and Recycling* (pp. 13–32). Elsevier. <https://doi.org/10.1016/b978-0-12-817880-5.00002-5>
- Gigault, J., El Hadri, H., Nguyen, B., Grassl, B., Rowencyk, L., Tufenkji, N., Feng, S., & Wiesner, M. (2021). Nanoplastics are neither microplastics nor engineered nanoparticles. In *Nature Nanotechnology* (Vol. 16, Issue 5, pp. 501–507). Nature Research. <https://doi.org/10.1038/s41565-021-00886-4>
- Goh, E. T., Kirby, G., Rajadas, J., Liang, X. J., & Tan, A. (2016). Accelerated Wound Healing Using Nanoparticles. In *Nanoscience in Dermatology* (pp. 287–306). Elsevier Inc. <https://doi.org/10.1016/B978-0-12-802926-8.00023-9>
- Gregory, M. R., & Andrady, A. L. (2003). Plastics in the marine environment. In *Plastics in the Marine Environment. In: Andrady, A.L., Ed., Plastics and the Environment* (Issue 1, pp. 379–401). <https://doi.org/10.1002/0471721557.ch10>
- Gwenzi, W., Simbanegavi, T. T., Marumure, J., & Makuvara, Z. (2022). Ecological health risks of emerging organic contaminants. In *Emerging Contaminants in the Terrestrial-Aquatic-Atmosphere Continuum: Occurrence, Health Risks and Mitigation* (pp. 215–242). Elsevier. <https://doi.org/10.1016/B978-0-323-90051-5.00011-0>
- Hales-Brittain, S. (2023, July). *It's Greek to Me: PLASTIC.* Bible & Archaeology (University of Iowa). <https://bam.sites.uiowa.edu/its-greek-me/plastic>
- Hao, Z., Li, C., Yu, J., Zhang, X., Ran, F., Dai, L., Shen, Z., Qiu, Z., & Wang, J. (2023). Lignin particles as green pore-forming agents for the fabrication of microporous polysulfone membranes. *International Journal of Biological Macromolecules*, 241. <https://doi.org/10.1016/j.ijbiomac.2023.124603>
- Hartmann, N. B., Ågerstrand, M., Lützhøft, H. C. H., & Baun, A. (2017). NanoCREDA transparent framework to assess' the regulatory adequacy of ecotoxicity data for nanomaterials – Relevance and reliability revisited. *NanoImpact*, 6, 81–89. <https://doi.org/10.1016/j.impact.2017.03.004>

- Hartmann, N. B., Hüffer, T., Thompson, R. C., Hassellöv, M., Verschoor, A., Daugaard, A. E., Rist, S., Karlsson, T., Brennholt, N., Cole, M., Herrling, M. P., Hess, M. C., Ivleva, N. P., Lusher, A. L., & Wagner, M. (2019). Are We Speaking the Same Language? Recommendations for a Definition and Categorization Framework for Plastic Debris. *Environmental Science and Technology*, 53(3), 1039–1047. <https://doi.org/10.1021/acs.est.8b05297>
- Hildebrandt, J., & Thünemann, A. F. (2023). Aqueous Dispersions of Polypropylene: Toward Reference Materials for Characterizing Nanoplastics. *Macromolecular Rapid Communications*, 44(6). <https://doi.org/10.1002/marc.202200874>
- Hoppe, M., Köser, J., Scheeder, G., Lamparter, A., Dorau, K., Grüger, L., Dierkes, G., & Schlich, K. (2023). Palladium-doped and undoped polystyrene nanoplastics in a chronic toxicity test for higher plants: Impact on soil, plants and ammonium oxidizing bacteria. *NanoImpact*, 32. <https://doi.org/10.1016/j.impact.2023.100484>
- International Union of Pure and Applied Chemistry. Subcommittee on Polymer Terminology., Jones, R. G., & International Union of Pure and Applied Chemistry. Commission on Macromolecular Nomenclature. (2009). *Compendium of polymer terminology and nomenclature : IUPAC recommendations, 2008*. Royal Society of Chemistry.
- ISO/TR 21960. (2020). *Plastics-Environmental aspects-State of knowledge and methodologies*.
- Jenner, L. C., Rotchell, J. M., Bennett, R. T., Cowen, M., Tentzeris, V., & Sadofsky, L. R. (2022). Detection of microplastics in human lung tissue using μ FTIR spectroscopy. *Science of the Total Environment*, 831. <https://doi.org/10.1016/j.scitotenv.2022.154907>
- Jensen, E. C. (2012). Types of Imaging, Part 2: An Overview of Fluorescence Microscopy. *Anatomical Record*, 295(10), 1621–1627. <https://doi.org/10.1002/ar.22548>
- Jensen, K. A., Kembouche, Y., Christiansen, E., Nicklas R, J., Håkan, W., Guiot, C., Spalla, O., & Witschger, O. (2011). *Final protocol for producing suitable manufactured nanomaterial exposure media*. Nanogenotox. https://www.anses.fr/en/system/files/nanogenotox_deliverable_5.pdf
- Kaing, V., Guo, Z., Sok, T., Kodikara, D., Breider, F., & Yoshimura, C. (2024). Photodegradation of biodegradable plastics in aquatic environments: Current understanding and challenges. *Science of The Total Environment*, 911(168539). <https://doi.org/https://doi.org/10.1016/j.scitotenv.2023.168539>
- Karakolis, E. G., Nguyen, B., You, J. B., Rochman, C. M., & Sinton, D. (2019). Fluorescent Dyes for Visualizing Microplastic Particles and Fibers in Laboratory-Based Studies. *Environmental Science and Technology Letters*, 6(6), 334–340. <https://doi.org/10.1021/acs.estlett.9b00241>
- Kau, D., Materić, D., Holzinger, R., Baumann-Stanzer, K., Schauer, G., & Kasper-Giebl, A. (2024). Fine micro- and nanoplastics concentrations in particulate matter samples from the high alpine site Sonnblick, Austria. *Chemosphere*, 352. <https://doi.org/10.1016/j.chemosphere.2024.141410>

- Kokalj, A. J., Hartmann, N. B., Drobne, D., Potthoff, A., & Kühnel, D. (2021). Quality of nanoplastics and microplastics ecotoxicity studies: Refining quality criteria for nanomaterial studies. *Journal of Hazardous Materials*, 415. <https://doi.org/10.1016/j.jhazmat.2021.125751>
- Krug, H. F. (2014). Nanosafety research-are we on the right track? In *Angewandte Chemie - International Edition* (Vol. 53, Issue 46, pp. 12304–12319). Wiley-VCH Verlag. <https://doi.org/10.1002/anie.201403367>
- Kwak, J. Il, Rhee, H., Kim, L., & An, Y.-J. (2024). In vivo visualization of environmentally relevant microplastics and evaluation of gut barrier damages in *Artemia franciscana*. *Journal of Hazardous Materials*, 478, 135596. <https://doi.org/10.1016/j.jhazmat.2024.135596>
- Liang, J. L., Cao, G. X., Zheng, F. Y., Li, S. X., Liu, F. J., Lin, L. X., Huang, X. G., Zhang, Z. H., Zheng, J. Y., & Huang, Q. Y. (2022). Low-toxic, fluorescent labeled and size-controlled graphene oxide quantum dots@polystyrene nanospheres as reference material for quantitative determination and in vivo tracing. *Chemosphere*, 307. <https://doi.org/10.1016/j.chemosphere.2022.136094>
- Lin, D., Tian, X., Wu, F., & Xing, B. (2010). Fate and Transport of Engineered Nanomaterials in the Environment. *Journal of Environmental Quality*, 39(6), 1896–1908. <https://doi.org/10.2134/jeq2009.0423>
- Lionetto, F., Corcione, C. E., Rizzo, A., & Maffezzoli, A. (2021). Production and characterization of polyethylene terephthalate nanoparticles. *Polymers*, 13(21). <https://doi.org/10.3390/polym13213745>
- Liu, W., Liao, H., Wei, M., Junaid, M., Chen, G., & Wang, J. (2024). Biological uptake, distribution and toxicity of micro(nano)plastics in the aquatic biota: A special emphasis on size-dependent impacts. In *TrAC - Trends in Analytical Chemistry* (Vol. 170). Elsevier B.V. <https://doi.org/10.1016/j.trac.2023.117477>
- Loret, T., Holme, S., Kuttykattil, A., Villacorta, A., Rodríguez-Garraus, A., Venus, T., Estrela-Lopis, I., JCatalán, J., Hernández, A., Marcos, R., & Bussy, C. (2023). 61 *Evaluation on the Toxicity, Alveolar Cell Accumulation and clearance of PET and PS Nanoplastics in Mouse Lungs*. https://academic.oup.com/annweh/article/67/Supplement_1/i53/7159439
- Magri, D., Sánchez-Moreno, P., Caputo, G., Gatto, F., Veronesi, M., Bardi, G., Catelani, T., Guarnieri, D., Athanassiou, A., Pompa, P. P., & Fragouli, D. (2018). Laser ablation as a versatile tool to mimic polyethylene terephthalate nanoplastic pollutants: Characterization and toxicology assessment. *ACS Nano*, 12(8), 7690–7700. <https://doi.org/10.1021/acsnano.8b01331>
- Marcellus, K. A., Bugiel, S., Nunnikhoven, A., Curran, I., & Gill, S. S. (2024). Polystyrene Nano- and Microplastic Particles Induce an Inflammatory Gene Expression Profile in Rat Neural Stem Cell-Derived Astrocytes In Vitro. *Nanomaterials*, 14(5). <https://doi.org/10.3390/nano14050429>
- Martín-Pérez, J., Villacorta, A., Banaei, G., Morataya-Reyes, M., Tavakolpournegari, A., Marcos, R., Hernández, A., & García-Rodríguez, A. (2024). Hazard assessment of nanoplastics is driven by their surface-functionalization. Effects in human-derived primary endothelial cells. *Science of the Total Environment*, 934. <https://doi.org/10.1016/j.scitotenv.2024.173236>

- Masseroni, A., Fossati, M., Ponti, J., Schirinzi, G., Becchi, A., Saliu, F., Soler, V., Collini, M., Della Torre, C., & Villa, S. (2024). Sublethal effects induced by different plastic nano-sized particles in *Daphnia magna* at environmentally relevant concentrations. *Environmental Pollution*, 343. <https://doi.org/10.1016/j.envpol.2023.123107>
- Materić, D., Peacock, M., Dean, J., Futter, M., Maximov, T., Moldan, F., Röckmann, T., & Holzinger, R. (2022). Presence of nanoplastics in rural and remote surface waters. *Environmental Research Letters*, 17(5). <https://doi.org/10.1088/1748-9326/ac68f7>
- Matsumoto, T., & Ochi, A. (1965). Polymerization of Styrene in Aqueous Solution 1965 Matsumoto-ochi. *高分子化学 (Polymer Chemistry)*, 22(244).
- Mitrano, D. M., Beltzung, A., Frehland, S., Schmiedgruber, M., Cingolani, A., & Schmidt, F. (2019). Synthesis of metal-doped nanoplastics and their utility to investigate fate and behaviour in complex environmental systems. *Nature Nanotechnology*, 14(4), 362–368. <https://doi.org/10.1038/s41565-018-0360-3>
- Mitrano, D. M., Wick, P., & Nowack, B. (2021). Placing nanoplastics in the context of global plastic pollution. In *Nature Nanotechnology* (Vol. 16, Issue 5, pp. 491–500). Nature Research. <https://doi.org/10.1038/s41565-021-00888-2>
- Møller, P., & Roursgaard, M. (2023). Exposure to nanoplastic particles and DNA damage in mammalian cells. In *Mutation Research - Reviews in Mutation Research* (Vol. 792). Elsevier B.V. <https://doi.org/10.1016/j.mrrev.2023.108468>
- Morand, S., & Lajaunie, C. (2018). Ecosystem Services for Health and Biodiversity. In *Biodiversity and Health* (pp. 133–146). Elsevier. <https://doi.org/10.1016/b978-1-78548-115-4.50009-3>
- Mulder, K., & Knot, M. (2001). PVC plastic: a history of systems development and entrenchment. In *Technology in Society* (Vol. 23). www.elsevier.com/locate/techsocDiscussion
- Nayanathara Thathsarani Pilapitiya, P. G. C., & Ratnayake, A. S. (2024). The world of plastic waste: A review. In *Cleaner Materials* (Vol. 11). Elsevier Ltd. <https://doi.org/10.1016/j.clema.2024.100220>
- Nguyen, B., & Tufenkji, N. (2022). Single-Particle Resolution Fluorescence Microscopy of Nanoplastics. *Environmental Science and Technology*, 56, 6426–6435. <https://doi.org/10.1021/acs.est.1c08480>
- Oxford dictionary. (2024). *Plastic, N., Sense 3.a.* *Oxford English Dictionary*. <https://doi.org/https://doi.org/10.1093/OED/8427312408>.
- Parkes. Alex. (1866). On, the Properties of Parkesine and its Application to the Arts and and Manufactures. *London Journal of the Society of Arts.* , 683, 384.
- Petersen, E. J., Barrios, A. C., Henry, T. B., Johnson, M. E., Koelmans, A. A., Montoro Bustos, A. R., Matheson, J., Roesslein, M., Zhao, J., & Xing, B. (2022). Potential Artifacts and Control Experiments in Toxicity Tests of Nanoplastic and Microplastic Particles. In *Environmental Science and Technology* (Vol. 56, Issue 22, pp. 15192–15206). American Chemical Society. <https://doi.org/10.1021/acs.est.2c04929>

- Petersen, E. J., Goss, G. G., von der Kammer, F., & Kennedy, A. J. (2021). New guidance brings clarity to environmental hazard and behaviour testing of nanomaterials. In *Nature Nanotechnology* (Vol. 16, Issue 5, pp. 482–483). Nature Research. <https://doi.org/10.1038/s41565-021-00889-1>
- Pignattelli, S., Broccoli, A., Piccardo, M., Feline, S., Terlizzi, A., & Renzi, M. (2021). Short-term physiological and biometrical responses of *Lepidium sativum* seedlings exposed to PET-made microplastics and acid rain. *Ecotoxicology and Environmental Safety*, 208, 111718. <https://doi.org/10.1016/j.ecoenv.2020.111718>
- PlasticsEurope. (2019). *Plastics-the Facts 2019. An analysis of European plastics production, demand and waste data*.
- Pradel, A., Catrouillet, C., & Gigault, J. (2023). The environmental fate of nanoplastics: What we know and what we need to know about aggregation. *NanoImpact*, 29. <https://doi.org/10.1016/j.impact.2023.100453>
- Reed, C. (2015). Dawn of the plasticene age. *New Scientist*, 225(3006), 28–32. [https://doi.org/10.1016/S0262-4079\(15\)60215-9](https://doi.org/10.1016/S0262-4079(15)60215-9)
- Renzi, M., Grazioli, E., & Blašković, A. (2019). Effects of Different Microplastic Types and Surfactant-Microplastic Mixtures Under Fasting and Feeding Conditions: A Case Study on *Daphnia magna*. *Bulletin of Environmental Contamination and Toxicology*, 103(3), 367–373. <https://doi.org/10.1007/s00128-019-02678-y>
- Reynaud, S., Aynard, A., Grassl, B., & Gigault, J. (2022). Nanoplastics: From model materials to colloidal fate. In *Current Opinion in Colloid and Interface Science* (Vol. 57). Elsevier Ltd. <https://doi.org/10.1016/j.cocis.2021.101528>
- Rist, S., & Hartmann, N. B. (2018). Aquatic ecotoxicity of microplastics and nanoplastics: Lessons learned from engineered nanomaterials. In *Handbook of Environmental Chemistry* (Vol. 58, pp. 25–49). Springer Verlag. https://doi.org/10.1007/978-3-319-61615-5_2
- Robertson, J. D., Rizzello, L., Avila-Olias, M., Gaitzsch, J., Contini, C., Mago, M. S., Renshaw, S. A., & Battaglia, G. (2016). Purification of Nanoparticles by Size and Shape. *Scientific Reports*, 6. <https://doi.org/10.1038/srep27494>
- Rodríguez-Hernández, A. G., Muñoz-Tabares, J. A., Aguilar-Guzmán, J. C., & Vazquez-Duhalt, R. (2019). A novel and simple method for polyethylene terephthalate (PET) nanoparticle production. *Environmental Science: Nano*, 6(7), 2031–2036. <https://doi.org/10.1039/c9en00365g>
- Roursgaard, M., Hezareh Rothmann, M., Schulte, J., Karadimou, I., Marinelli, E., & Møller, P. (2022). Genotoxicity of Particles From Grinded Plastic Items in Caco-2 and HepG2 Cells. *Frontiers in Public Health*, 10. <https://doi.org/10.3389/fpubh.2022.906430>
- Rubio, L., Barguilla, I., Domenech, J., Marcos, R., & Hernández, A. (2020). Biological effects, including oxidative stress and genotoxic damage, of polystyrene nanoparticles in different human hematopoietic cell lines. *Journal of Hazardous Materials*, 398(March), 122900. <https://doi.org/10.1016/j.jhazmat.2020.122900>

- Sánchez, A., Rodríguez-Viso, P., Domene, A., Orozco, H., Vélez, D., & Devesa, V. (2022). Dietary microplastics: Occurrence, exposure and health implications. *Environmental Research*, 212. <https://doi.org/10.1016/j.envres.2022.113150>
- Schwabl, P., Koppel, S., Konigshofer, P., Bucsics, T., Trauner, M., Reiberger, T., & Liebmann, B. (2019). Detection of various microplastics in human stool: A prospective case series. *Annals of Internal Medicine*, 171(7), 453–457. <https://doi.org/10.7326/M19-0618>
- Shirai, T. (2018). Protein structure analysis and validation. In *Encyclopedia of Bioinformatics and Computational Biology: ABC of Bioinformatics* (Vols. 1–3, pp. 512–519). Elsevier. <https://doi.org/10.1016/B978-0-12-809633-8.20282-3>
- Tavakolpournegari, A., Annangi, B., Villacorta, A., Banaei, G., Martin, J., Pastor, S., Marcos, R., & Hernández, A. (2023). Hazard assessment of different-sized polystyrene nanoplastics in hematopoietic human cell lines. *Chemosphere*, 325. <https://doi.org/10.1016/j.chemosphere.2023.138360>
- Tavakolpournegari, A., Villacorta, A., Morataya-Reyes, M., Arribas Arranz, J., Banaei, G., Pastor, S., Velázquez, A., Marcos, R., Hernández, A., & Annangi, B. (2024). Harmful effects of true-to-life nanoplastics derived from PET water bottles in human alveolar macrophages. *Environmental Pollution*, 348. <https://doi.org/10.1016/j.envpol.2024.123823>
- Teuten, E. L., Rowland, S. J., Galloway, T. S., & Thompson, R. C. (2007). Potential for plastics to transport hydrophobic contaminants. *Environmental Science and Technology*, 41(22), 7759–7764. <https://doi.org/10.1021/es071737s>
- Thompson, R. C., Olsen, Y., Mitchell, R. P., Davis, A., Rowland, S. J., John, A. W. G., McGonigle, D., & Russell, A. E. (2004). Lost at Sea: Where Is All the Plastic? *Science*, 304, 838–838. www.sciencemag.org/cgi/content/full/304/5672/838/
- Tramis, O., Garnier, C., Yus, C., Irusta, S., & Chabert, F. (2021). Enhancement of the fatigue life of recycled PP by incorporation of recycled opaque PET collected from household milk bottle wastes. *Waste Management*, 125, 49–57. <https://doi.org/10.1016/j.wasman.2021.02.006>
- Tsochatzis, E. D., Gika, H., Theodoridis, G., Maragou, N., Thomaidis, N., & Corredig, M. (2024). Microplastics and nanoplastics: Exposure and toxicological effects require important analysis considerations. In *Heliyon* (Vol. 10, Issue 11). Elsevier Ltd. <https://doi.org/10.1016/j.heliyon.2024.e32261>
- Turner, A., & Filella, M. (2021). Hazardous metal additives in plastics and their environmental impacts. In *Environment International* (Vol. 156). Elsevier Ltd. <https://doi.org/10.1016/j.envint.2021.106622>
- Valido, I. H., Fuentes-Cebrian, V., Hernández, A., Valiente, M., & López-Mesas, M. (2023). Validated method for polystyrene nanoplastic separation in aqueous matrices by asymmetric-flow field flow fraction coupled to MALS and UV–Vis detectors. *Microchimica Acta*, 190(8). <https://doi.org/10.1007/s00604-023-05851-7>
- Vela, L., Villacorta, A., Venus, T., Estrela-Lopis, I., Pastor, S., García-Rodríguez, A., Rubio, L., Marcos, R., & Hernández, A. (2023). The potential effects of in vitro digestion on the physicochemical and biological characteristics of polystyrene

- nanoplastics. *Environmental Pollution*, 329. <https://doi.org/10.1016/j.envpol.2023.121656>
- Vila, L., Marcos, R., & Hernández, A. (2017). Long-term effects of silver nanoparticles in caco-2 cells. *Nanotoxicology*, 11(6), 771–780. <https://doi.org/10.1080/17435390.2017.1355997>
- Wesch, C., Bredimus, K., Paulus, M., & Klein, R. (2016). Towards the suitable monitoring of ingestion of microplastics by marine biota: A review. In *Environmental Pollution* (Vol. 218, pp. 1200–1208). Elsevier Ltd. <https://doi.org/10.1016/j.envpol.2016.08.076>
- Woo, J. H., Seo, H. J., Lee, J. Y., Lee, I., Jeon, K., Kim, B., & Lee, K. (2023). Polypropylene nanoplastic exposure leads to lung inflammation through p38-mediated NF- κ B pathway due to mitochondrial damage. *Particle and Fibre Toxicology*, 20(1). <https://doi.org/10.1186/s12989-022-00512-8>
- Xu, J. L., Lin, X., Wang, J. J., & Gowen, A. A. (2022). A review of potential human health impacts of micro- and nanoplastics exposure. In *Science of the Total Environment* (Vol. 851). Elsevier B.V. <https://doi.org/10.1016/j.scitotenv.2022.158111>
- Younes, M., Aquilina, G., Castle, L., Engel, K. H., Fowler, P., Frutos Fernandez, M. J., Fürst, P., Gundert-Remy, U., Gürtler, R., Husøy, T., Manco, M., Mennes, W., Moldeus, P., Passamonti, S., Shah, R., Waalkens-Berendsen, I., Wölfle, D., Corsini, E., Cubadda, F., ... Wright, M. (2021). Safety assessment of titanium dioxide (E171) as a food additive. *EFSA Journal*, 19(5). <https://doi.org/10.2903/j.efsa.2021.6585>
- Yun, D. S., Lee, H. S., Jang, H. G., & Yoo, J. W. (2010). Controlling size and distribution for nano-sized polystyrene spheres. *Bulletin of the Korean Chemical Society*, 31(5), 1345–1348. <https://doi.org/10.5012/bkcs.2010.31.5.1345>
- Zalasiewicz, J., Waters, C. N., Ivar do Sul, J. A., Corcoran, P. L., Barnosky, A. D., Cearreta, A., Edgeworth, M., Gałuszka, A., Jeandel, C., Leinfelder, R., McNeill, J. R., Steffen, W., Summerhayes, C., Waprich, M., Williams, M., Wolfe, A. P., & Yonah, Y. (2016). The geological cycle of plastics and their use as a stratigraphic indicator of the Anthropocene. In *Anthropocene* (Vol. 13, pp. 4–17). Elsevier Ltd. <https://doi.org/10.1016/j.ancene.2016.01.002>
- Zhang, H. J., Zhou, H. R., Pan, W., Wang, C., Liu, Y. Y., Yang, L., Tsz-Ki Tsui, M., & Miao, A. J. (2023). Accumulation of nanoplastics in human cells as visualized and quantified by hyperspectral imaging with enhanced dark-field microscopy. *Environment International*, 179. <https://doi.org/10.1016/j.envint.2023.108134>
- Zhang, Y., Wang, S., Olga, V., Xue, Y., Lv, S., Diao, X., Zhang, Y., Han, Q., & Zhou, H. (2022). The potential effects of microplastic pollution on human digestive tract cells. *Chemosphere*, 291. <https://doi.org/10.1016/j.chemosphere.2021.132714>
- Zimmermann, L., Göttlich, S., Oehlmann, J., Wagner, M., & Völker, C. (2020). What are the drivers of microplastic toxicity? Comparing the toxicity of plastic chemicals and particles to *Daphnia magna*. *Environmental Pollution*, 267. <https://doi.org/10.1016/j.envpol.2020.115392>

ANNEXES

7. ANNEXES

7.1. The pdf of the published paper entitled *A new source of representative secondary PET nanoplastics. Obtention, characterization, and hazard evaluation*

Journal of Hazardous Materials 439 (2022) 129593



Contents lists available at ScienceDirect
Journal of Hazardous Materials
journal homepage: www.elsevier.com/locate/jhazmat



A new source of representative secondary PET nanoplastics. Obtention, characterization, and hazard evaluation

Aliro Villacorta^{a,b}, Laura Rubio^{a,c}, Mohamed Alaraby^{a,d}, Montserrat López-Mesas^e, Victor Fuentes-Cebrian^e, Oscar H. Moriones^{f,g}, Ricard Marcos^{a,*}, Alba Hernández^{a,*}

^a Group of Mutagenesis, Department of Genetics and Microbiology, Faculty of Biosciences, Universitat Autònoma de Barcelona, Cerdanyola del Vallès, Barcelona, Spain

^b Facultad de Recursos Naturales Renovables, Universidad Arturo Prat, Iquique, Chile

^c Nanobiology Laboratory, Department of Natural and Exact Sciences, Pontificia Universidad Católica Madre y Maestra, PUCMM, Santiago de los Caballeros, Dominican Republic

^d Zoology Department, Faculty of Sciences, Sohag University, 82524 Sohag, Egypt

^e GTS-UAB Research Group, Department of Chemistry, Faculty of Science, Universitat Autònoma de Barcelona, 08193 Bellaterra, Cerdanyola del Vallès, Spain

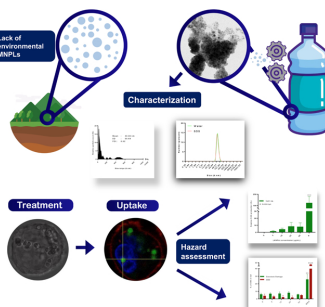
^f Institut Català de Nanociència i Nanotecnologia (ICN2-UAB-CSIC-BIST), Campus UAB, Bellaterra, 08193 Barcelona, Spain

^g Universitat Autònoma de Barcelona (UAB), Campus UAB, Bellaterra, 08193 Barcelona, Spain

HIGHLIGHTS

- A proposed method to get PET nanoplastic samples from plastic bottles is presented.
- Completed physicochemical characterization is provided.
- Cell uptake was evaluated following different methods.
- Different hazard effects were determined.
- The method is extrapolated to other plastic and avoids metal contamination.

GRAPHICAL ABSTRACT



ARTICLE INFO

Editor: Dr. T Meiping

Keywords:

Nanoplastics
Polyethylene terephthalate
Physicochemical characterization
Cell uptake
Cytotoxicity

ABSTRACT

Micro and nanoplastics (MNPLs) are emergent environmental pollutants requiring urgent information on their potential risks to human health. One of the problems associated with the evaluation of their undesirable effects is the lack of *representative samples*, matching those resulting from the environmental degradation of plastic wastes. To such end, we propose an easy method to obtain polyethylene terephthalate nanoplastics from water plastic bottles (PET-NPLs) but, in principle, applicable to any other plastic goods sources. An extensive characterization indicates that the proposed process produces uniform samples of PET-NPLs of around 100 nm, as determined by using AF4 and multi-angle and dynamic light scattering methodologies. An important point to be highlighted is that to avoid the metal contamination resulting from methods using metal blades/burrs for milling, trituration,

* Correspondence to: Group of Mutagenesis, Department of Genetics and Microbiology, Faculty of Biosciences, Universitat Autònoma de Barcelona, Campus of Bellaterra, 08193 Cerdanyola del Vallès, Barcelona, Spain.

E-mail addresses: ricard.marcos@uab.cat (R. Marcos), alba.hernandez@uab.cat (A. Hernández).

<https://doi.org/10.1016/j.jhazmat.2022.129593>

Received 10 March 2022; Received in revised form 4 July 2022; Accepted 11 July 2022

Available online 14 July 2022

0304-3894/© 2022 The Author(s). Published by Elsevier B.V. This is an open access article under the CC BY license (<http://creativecommons.org/licenses/by/4.0/>).

or sanding, we propose to use diamond burrs to produce metal-free samples. To visualize the toxicological profile of the produced PET-NPLs we have evaluated their ability to be internalized by cells, their cytotoxicity, their ability to induce oxidative stress, and induce DNA damage. In this preliminary approach, we have detected their cellular uptake, but without the induction of significant biological effects. Thus, no relevant increases in toxicity, reactive oxygen species (ROS) induction, or DNA damage -as detected with the comet assay- have been observed. The use of *representative* samples, as produced in this study, will generate relevant data in the discussion about the potential health risks associated with MNPLs exposures.

1. Introduction

Despite the multiple advantages of plastic materials, a very dramatic side-effect resulting from this big success is the increased presence of plastic wastes in the environment. Unfortunately, and considering the present capacities of recycling such wastes, this environmental catastrophe will still be increasing and remain for a long (Borrelle et al., 2020).

Once into the environment, plastic wastes degrade due to different abiotic (*i.e.*, photodegradation, physical abrasion, or hydrolysis) and biotic mechanisms (Ali et al., 2021a), generating a new source of contaminants: the micro/nanoplastics (MNPLs). With a size between less than 10 nm and a few mm, MNPLs can be highly mobilized by water and air and, consequently, they can be found in all the environmental niches on a global scale (Evangelidou et al., 2020; Batool et al., 2021). Another characteristic linked to the MNPLs' size is their potential to enter the food web as they can be easily uptaken by living organisms, including humans. In this way, they have become a new group of emergent contaminants with a potential human health risk. In fact, it has been demonstrated that at the nanoscale level MNPLs could exert important biological effects such as reactive oxygen species (ROS) generation, the activation of the immune system by inflammatory responses, and even more, genotoxic DNA damage (Rubio et al., 2020; Ballesteros et al., 2020; Rai et al., 2021).

It should be noted that environmental MNPLs have two different origins. One is associated with the abiotic/biotic degradation of big plastic sizes (macroplastics), as above indicated. In this case, these MNPLs are denominated secondary MNPLs. On the contrary, some MNPLs are synthesized at these small size ranges for specific purposes and are denominated primary MNPLs. One typical example of primary MNPLs is the micro/nanobeads used in exfoliating hand cleansers and facial scrubs. In fact, they are also intentionally added to other many products such as paints, coatings, and inks, or in construction, agriculture/horticulture, and medical products, among others. For these MNPLs, the estimated used amount in Europe is around 145,000 tons per year, and to minimize their impact on the environment and potentially on human health, a restriction on the intentionally-added-microplastic use has been proposed (ECHA, 2018). Regarding the environmental levels of secondary MNPLs they are very difficult to estimate. Nevertheless, it must be remembered that the world production of plastics on 2019 was 368 million tons, that its production is exponentially growing over time, that about 40 % was used for packaging (or single-use), and about 80 % is not properly recycled ending into the environment or landfills (PlasticsEurope 2019; Ali et al., 2021b).

Studies aiming to determine the potential hazard of MNPLs enface big challenges, one being the selection of environmentally representative MNPLs to be used as reference materials. Due to the impossibility of collecting real MNPLs from the environment, especially at the nano range, practically all available studies have used the only MNPLs type that is commercially available in a wide range of sizes, surface modifications, and labeling, which is polystyrene (PS) MNPLs. Hence, all our present knowledge on the potential risk of MNPLs for human health is basically limited to one polymer type. To avoid this bias, some recent alternatives have been proposed aiming at artificially degrade plastic items to obtain new sources of secondary MNPLs to be included in the hazard assessment studies. The pioneering study used the UV-laser

ablation process to obtain PET-NPLs (Magri et al., 2018). Others have used mechanical milling followed by sieve fractionation into MPLs fractions applied to agricultural plastics (a mulch film prepared biodegradable polymer polybutyrate adipate-co-terephthalate and low-density polyethylene (Astner et al., 2019). As well as the trituration of a few millimeters' of industrial PET pellets (Pignattelli et al., 2021). The use of mechanical ground approaches was also proposed to obtain PET-NPLs (Rodríguez-Hernández et al., 2019).

Two important aspects need to be pointed out regarding the so-far proposed alternative protocols to obtain MNPLs. First, polyethylene terephthalate (PET) is used in most of these approaches. This is because, as a thermoplastic polymer, PET do not undergo chemical reactions when heated, and can re-ground several times, what it is very useful for recycling purposes. This, among other reasons, is why PET is one of the major contributors to worldwide plastic wastes (Gwada et al., 2019). Second, many of the proposed methods to obtain degraded MNPLs, such as mechanical milling, allows only to obtain MPLs, but not NPLs. This is very relevant from the toxicological point of view, since it is considered that NPLs have the ability to cross biological primary barriers and, consequently, reach the different organs and tissues after an exposure (Zitouni et al., 2021).

According to the above indicated, it is clear that there is an urgent need to generate new representative MNPLs samples for further use in hazard evaluations (Balakrishnan et al., 2019). In this study, we thoroughly describe our in-house method to obtain PET-NPLs, provide exhaustive characterization of the obtained materials, and assess its usefulness in hazard assessment approaches by analyzing the cellular uptake, cytotoxicity, reactive oxygen (ROS) production, and DNA damage induction in human lymphoblastic cell line models after an acute exposure.

2. Materials and methods

2.1. PET-NPLs obtention

The PET raw material used to produce PET-NPLs was obtained from commercially available water plastic bottles. The developed procedure was adapted from the previously reported by Rodríguez-Hernández et al. (2019). A schematic overview of the used protocol is outlined in Fig. 1. Briefly, pieces of about 12 cm² from the bottom part of the water bottles were initially sanded with aluminum oxide/silicon carbide rotary burrs. Due to the observed metal-contamination (as explained in the Results section) a diamond rotary burr sander accessory, attached to a flexible shaft powered by a multitool Dremel 3000, was chosen for the sanding process. The obtained PET debris was passed through a 0.20 mm sieve (CISA R-92), and 4 g of the resulting material were dispersed in 40 mL of pre-heated (50 °C) trifluoroacetic acid (TFA, 90 % v/v), in a proportion of 10 mL TFA per gram of sieved PET, on a stirring plate at 100 rpm for 2 h. After a complete dispersion, the mixture was kept at room temperature overnight in continuous agitation. Next day, 40 mL of TFA 20 % (v/v) was added to the sample and the mixture was kept under constant and vigorous stirring for 24 h. After that, the obtained dispersion was distributed on six 10 mL glass tubes and centrifuged at 2500 RCF for 1 h. Once the supernatants were discarded, the obtained pellets were resuspended on 400 mL of 0.50 % sodium dodecyl sulfate (SDS) solution, vigorously mixed, and distributed into two 200 mL beakers, for

ultrasonication on an SSE-1 Branson sonicator. Sonication lasted for 2 min at 25% amplitude, in 9/9s sonication/break cycles. The volume of each beaker was transferred to a graduated cylinder, where sedimentation of larger particles took place for 1 h. The top 100 mL of the suspension (from each graduated cylinder) was collected and centrifuged as before for SDS elimination, and further washed twice with Milli-Q water and twice with pure ethanol, and let to dry. Pellets were then resuspended on Milli-Q at the desired final concentration, and sonicated at 10 % amplitude for 16 min in a cold-water bath, aliquoted, and immediately frozen on cryotubes in liquid nitrogen and stored at -80°C for further use. Each one of the cryotubes contains 1 mL of a concentration of 12.50 mg/mL.

2.2. Characterization of particle suspension

2.2.1. Scanning electron microscopy/Energy dispersive X-ray microscopy (SEM-EDS)

The stock solution was thawed on a warm bath at 37°C , and a working solution of 200 $\mu\text{g/mL}$ was prepared on Milli-Q water. A holey carbon grid was dipped into the working solution and water was allowed to evaporate overnight; additionally, a drop was placed on the Si holder. Then, particles in the grid were examined on a SEM Zeiss Merlin (Zeiss, Oberkochen, Germany) coupled with an X-Max 20 mm EDS system (Oxford Instruments, Oxford, UK). In addition to collecting SEM images, for the EDX analysis an area including the nanoparticle surface was selected, and the sample signal was collected and analyzed by the INCA Energy software.

2.2.2. Transmission electron microscopy (TEM)

A working solution of 200 $\mu\text{g/mL}$ was prepared on Milli-Q water and mounted on a holey carbon grid as described above. Particles in the grid were examined by TEM on a JEOL JEM 1400 instrument (JEOL LTD, Tokyo, Japan) operated at 120 kV. TEM imaging was analyzed for particle size distribution using ImageJ software 1.8.0.172 processing and analysis software.

2.2.3. Fourier transform infrared spectroscopy (FTIR)

To detect the functional groups, and to identify the samples as PET, these were analyzed by Fourier-transform infrared spectroscopy (FTIR),

as briefly indicated. A drop of particle suspension at a concentration of 1 mg/mL was placed on a gold mirror and let dry for one week inside a petri dish. Analysis was carried out on a Hyperion 2000 microspectrometer using the gold mirror as reference. This analysis was carried out at the Molecular Spectroscopy and Optical Microscopy facility at the Institut Català de Nanociència i Nanotecnologia (ICN2). To assess the composition, interferograms were analyzed and contrasted with previous reports.

2.2.4. Multi angle and dynamic light scattering (DLS-MADLS) and zeta potential

The indicative size of the colloid structures in suspension of the hypothetical hard sphere that behave similarly to the particle suspension of the PET-NPLs was analyzed using a Zetasizer® Ultra from Malvern Panalytical. A working solution of 1 mg/mL of PET-NPLs suspension was thawed and then diluted on Milli-Q water for further analysis at a concentration of 200 $\mu\text{g/mL}$. To investigate better the fraction on the nanoscale, avoiding the masking generated by, agglomerates or particles bigger in size, a sonication for 16 min at 10 % amplitude (as described above), and a filtration step with a 450 μm PES membrane Millex®-HP from Millipore express® was included. To visualize the influence of anionic surfactant as a dispersant of the sample the same procedure described was carried out maintaining the SDS 0.5 % v/v original concentration. Once prepared, the samples were placed on DTS1070 cuvette for surface charge determination by zeta potential measurements, for both water and SDS 0.5 % dispersant. DLS, MADLS and particle concentration measurement were carried out by placing 1.5 mL of the prepared solutions on DTS0012 cuvettes.

2.2.5. Asymmetric flow field flow fractionation (AF4)

The PET nanoparticles separation was performed using the AF2000 Asymmetric Flow FFF system from Postnova Analytics GmbH (Landsberg, Germany) with two PN1130 Isocratic Pumps, a Kloehe V6 Pump, a PN5300 Autosampler, a PEEK AF4 Channel with a 10 kDa regenerated cellulose membrane and a 350 μm height spacer. The mobile phase and the PET suspension were prepared in NovaChem Surfactant 100 (IES-MAT, Madrid, Spain) at 0.20 % (v/v). The size data (gyration radius, R_g) was obtained using a PN3609 MALS Detector (9 angles), calibrated with a 125 nm NIST Polystyrene Latex standard (Postnova Analytics GmbH),

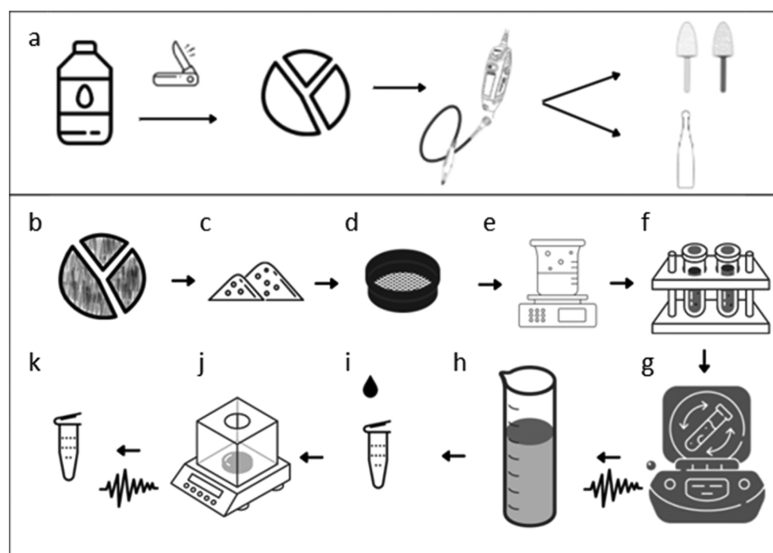


Fig. 1. Schematic representation of the fragmentation and grind process with the mixed burrs or the diamond covered burr (a). Representation of the fractioned pieces (b), PET powder obtained (c) that will be passed through the sieve (d), stirred, suspended, and heated at different concentrations of TFA (e), distributed on glass tubes (f) and centrifuged (g), washed and then resuspended on SDS, sonicated, and transferred to a cylinder for sedimentation (h) and then collected, washed (i), weighted (j), resuspended, sonicated and stored frozen until needed (k).

using the software AF2000 Software and used to calculate the geometric diameter (Dgeo) by dividing $2 \times R_g$ by the typical form factor of a sphere (0.78) (Lohrke et al., 2008). The method consisted in three steps, used a constant detector flow of 0.50 mL/min and injections of 20 μ L of samples of 1 mg/mL of PET-NPLs suspended in NovaChem 0.20 % were performed. The first step was a focusing step of 3 min with an injection flow of 0.20 mL/min, a cross-flow of 2.00 mL/min and a focus flow of 2.30 mL/min, the second was a separation step, with focus-flow of 0 mL/min, cross-flow from 2.00 mL/min exponential to 0.10 mL/min in 40 min and a final step at a constant flow of 0.10 mL/min of cross-flow during 20 min

2.3. Cell culture

Two human lymphoblastic cell lines were used to detect the potential biological effects of the obtained PET-NPLs, the THP-1 (monocytes) and the TK6 (lymphoblasts). Both cell lines were obtained from Sigma Aldrich (MO, USA) and grown in T-25 flasks containing Roswell Park Memorial Institute (RPMI) medium (Biowest, France) supplemented with 10 % fetal bovine serum (FBS), 1% glutamine (Biowest, France), and 2.5 μ g/mL of Plasmocin™ (InvivoGen, CA, USA). Cultures, with a density ranging from 5×10^5 and 1×10^6 cells were maintained at 37 °C in a humidified atmosphere of 5 % CO₂.

2.4. Cell uptake determination

To confirm the cell uptake of the obtained PET-NPLs, three different approaches have been used: flow cytometry (internal complexity), TEM (internalization), and confocal microscopy (Nile red staining).

2.4.1. Internal complexity

As an indicator of structural complexity of THP1 cells, once the PET-NPLs uptake takes place the orthogonal light scattering -commonly known as Side Scatter (SSC)- was evaluated at concentrations ranging from 0 to 50 μ g/mL after exposures lasting for 3 h. The highest concentration (50 μ g/mL) was tested in different scenarios in which PET-NPLs were added directly after being rapidly thawed from -80 °C on a 37 °C water bath, then vortexed and resuspended on RPMI media with or without FBS, vortexed again and applied directly to the culture and compared with regular culture conditions with and without FBS. Cells were analyzed by flow cytometry on a CytoFlex s and CytExpert software was used to properly collect means from 10,000 events on the live cell population. Data were analyzed using GraphPad Prism 7.0.

2.4.2. TEM analysis

Exposed cells were fixed in 2 % (w/v) paraformaldehyde and 2.5 % (v/v) glutaraldehyde (Merck, Darmstadt, Germany) in 0.10 M cacodylate buffer (Sigma-Aldrich, Steinheim, Germany) at pH 7.4. After that, cells were processed as already published (Rubio et al., 2016). Briefly, samples were post-fixed with osmium, dehydrated in ethanol, embedded in Epon, polymerized at 60 °C, and cut with an ultramicrotome. Finally, ultrathin sections placed in copper grids, were contrasted with conventional uranyl acetate and Reynolds's lead citrate solutions and observed using a Jeol 1400 (Jeol LTD) transmission electron microscope equipped with a CCD GATAN ES1000 W Erlangshen camera.

Nile Red stained particles and confocal visualization. Nile red staining of PET-NPLs was carried out following the procedure described in Rodríguez-Hernández et al. (2019) with some important modifications. Briefly, an aliquot (1 mg/mL) was centrifuged for 25 min at 16100 RCF. The supernatant was removed, and 1 mL of Nile red solution (0.50 % in DMSO) was added to the PET-NPLs pellet. The mixture was stirred at room temperature for 24 h (protected from light) at 200 rpm. Successive washes, at least twelve times, with ethanol in 0.10 M PBS, pH 7.40 and resuspended on RPMI supplemented media, prior to cell exposure. For confocal visualization, nuclei were stained using Hoechst 33342 (excitation of 405 nm and emission collected at 415–503), cell membranes

were dyed using Cellmask (excitation of 633 nm and emission collected at 645–786). For PET-NPLs labeled with Nile red, an excitation wavelength of 514 nm and emission collected at 546–628 was used. Images of each sample were obtained using a Leica TCS SP5 confocal microscope and processed using ImageJ processing and analysis software. version 1.8.0.172.

2.5. Cell viability assay

Cell viability after exposure to PET-NPLs, was determined using the Beckman counter method. To proceed, cells were seeded at a cell density of 5×10^5 cells/mL on 96 well plates and exposed to a range of concentrations from 0 up to 200 μ g/mL of PET-NPLs (200 μ g/mL per well). After the exposure time, cells were mixed and diluted 1:100 in ISOFLOW and counted with a ZTM series coulter-counter (Beckman Coulter Inc., CA, USA). The average number of cells counted in each treatment was compared with the average number of the untreated control cells. The results from the viability assay permit to determine the non-cytotoxic concentrations to be used in further experiments.

2.6. Reactive oxygen species (ROS) quantification

Due to the combined capacity of passively diffuse into the cell and being highly reactive, the reduced form of ethidium bromide (dihydroethidium, DHE) was used to detect cytosolic superoxide. Cellular suspensions were seeded on 96 U-type well plates at a cell density of 5×10^5 and treated with concentrations of 5, 10, 25, and 50 μ g/mL of PET-NPLs for 3 and 24 h. After the exposure, cells were centrifuged at 1000 rpm for 5 min, resuspended on 10 μ M DHE diluted on PBS 1X, to a final cell density of 1×10^6 , and incubated for 30 min at 37 °C. Cells were kept on ice for immediate analysis by using a flow cytometer (Beckman Coulter CytoFLEX S). A total number of 20000 events (single cells) were scored and evaluated using the CytExpert software.

2.7. DNA damage detection: The comet assay

The levels of DNA damage (DNA breaks) in both selected cell lines were evaluated using the published protocol (García-Rodríguez et al., 2019). Both, the overall DNA damage, and the oxidized DNA base levels were determined with the absence/presence of formamidopyrimidine DNA glycosylase (FPG) enzyme. This enzyme detects oxidized DNA bases, excise them, and generate a transient single-strand DNA break detected by the comet assay and denominated as specific oxidative DNA damage (ODD). THP1 cells were exposed to concentrations of 5, 10, 25, and 50 μ g/mL of PET-NPLs for 3 h. Treated cells were centrifuged at 0.30 RCF for 8 min at 4 °C. The obtained pellet was washed and resuspended on cold PBS 1x to get 10^6 cell density per mL. Cells were mixed 1:10 with 0.75 % low melting point agarose at 37 °C and dropped on triplicates onto GelBond® films (GBFs) (Life Sciences, Lithuania). GBFs containing the samples were treated overnight on cold lysis buffer at 4 °C and washed on successive 5 and 50 min of enzyme buffer immersion, immediately followed by 30 min incubation at 37 °C with FPG for the detection of ODD, or without FPG for the detection of general genotoxic damage. GBFs were subjected to electrophoresis (20 V, 300 mA, 4°C), washed twice with cold PBS 1X, fixed in absolute ethanol, and air-dried overnight at room temperature. After staining with SYBR Gold, GBFs were visualized in an epifluorescent microscope (Olympus BX50, Hamburg, Germany). The levels of DNA damage, as percentage of DNA in the tail, was quantified with the Komet 5.5 Image analysis system (Kinetic Imaging Ltd, Liverpool, UK). A total of 100 comet images randomly selected were analyzed per sample.

3. Results and discussion

3.1. Characterization of the obtained PET-NPL samples

3.1.1. Morphology and composition

To identify size, shape, and composition of the obtained PET-NPLs, SEM-EDS was used. In Figs. 2a and 2b (as well as in Fig. S1) SEM morphology of the obtained PET-NPLs is visualized. Surface irregularities of the produced particles can be easily observed on the copper and on the carbon sections of the holder. Not only the differences in size are noticeable, but also the holey structures that can be appreciated. This means that not only the particles are on the nanoscale, but also their surface/volume ratios are different than in a solid body. Interestingly, when energy dispersive X-ray microscopy was used, metal contamination resulting from the sanded process was detected. Thus, in the samples obtained using aluminum oxide/silicon carbide rotary burrs such elements were detected. This metal contamination was not present when a diamond rotary burr was used. This can be observed on Figs. 2c and 2d, and it is summarized on the included table (Fig. 2e). These findings raise an important alarm regarding the abrasive methods to be used in the case of mechanically produced MNPLs, mostly when the potential hazard of the obtained MNPLs need to be evaluated. Surprisingly, this potential metal contamination of the obtained samples is not taken into consideration in neither of the recent published papers using mechanical milling or the trituration of few millimeters' industrial pellets (Astner et al., 2019; Parolini et al., 2020; Lionetto et al., 2021; Pignattelli et al., 2021). The contamination by metals, as consequence of the mechanical milling of other polymers pellets, has also been detected by us, as indicated in Fig. S2, where the results of milling polylactic acid plastic' pellets are indicated. Therefore, from this point forward all the results presented in this study corresponds to the PET-NPLs produced with the diamond burr rotating tool.

From our data, a warning signal must be put to all the hazard data generated using MNPLs obtained using milling procedures, due to the potential metal associated contamination. It is well-know the toxic effects of metals, including those included during the manufacture of plastics (Turner and Filella, 2021).

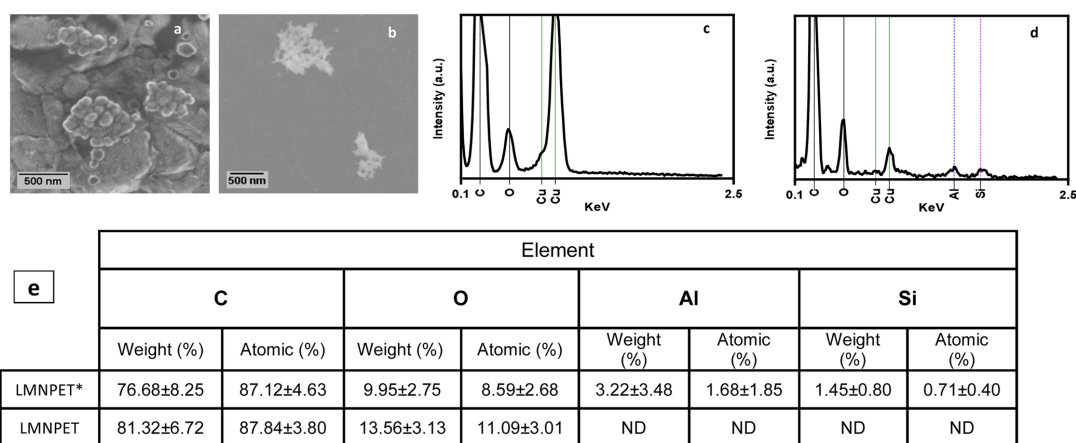
3.1.2. Dry state size distribution and shape

The TEM images of PET-NPLs reveal a polydisperse anisodiametric particles population with notorious lack of shape regularity. The Martin diameter was measured, and the relative percentage of particle size is represented in Fig. 3a using GraphPad Prism 7.0. The obtained average size of 40.08 nm presents a standard deviation of 55.68 nm and a polydispersity index of 0.52 evidencing the heterogeneity of the PET particles on the suspension produced by this method. Interestingly, the graphic shows a bimodal distribution with a big peak around 50 nm and a second small peak around 500 nm. As an overall, this means that our protocol produces PET particles inside the nano range.

Although the term MNPLs is increasingly used, no general agreement exists on the borders between microplastic and nanoplastic sizes. Engineered nanomaterials are classically considered to range between 1 and 100 nm, but this strict definition leaves out other sizes placed in the nano range. Although engineered materials are built at the desired size, secondary MNPLs are constituted by a wide range of sizes and shapes and some agreement is necessary to define the borders between MPLs and NPLs. At present, many authors consider that MNPLs range from few nm to several mm. To clarify the boundaries criteria, Hartmann et al. (2019) proposed to categorize MNPLs according to the conventional units of size: nano (1–1000 nm) and micro (1–1000 μ m). Nevertheless, to maintain the classical definition of nanomaterial/nanoplastic, they proposed to divide the nano range (1–1000 nm) between nanoplastics (1–100 nm) and submicron-plastics (100–1000 nm). Such classification needs to have the general agreement, mostly from those coming from the nanomaterials field. A close inspection of our TEM figures confirms the heterogeneity of the obtained material, which can be considered a realistic characteristic, thereby making it more representative from the environmental point of view. Thus, in addition of the small PET particles of around 50 nm (Fig. 3b), bigger sizes are also present, including rigid fibers (Figs. 3c, 3d), different large shapes (Fig. 3e), and agglomerates (Fig. 3f). Interestingly in Fig. 3f, it is evident that a high amount of PET in the nano range is contained in the agglomerates; nevertheless, the potential biological effects discussed further in this section do not seem to be highly affected by the presence of such agglomerates.

3.1.3. Chemical composition

To confirm the chemical identity of the obtained PET-NPL samples,



*Produced with aluminum oxide and silicon carbide burrs.

Fig. 2. Scanning electron microscopy results. Amorphous particle structures from a diverse range of geometry can be observed as aggregates metallic section of the holder (a) as in the polymer, where differences in sizes and shapes as well as holey structures can also be detected (b). Notorious differences on the EDS spectra are noticed according to the type of rotating burr utilized where only the diamond covered (c) was able to produce not contaminated samples (d). Aluminum contamination is marked on blue and silica on violet dashed lines, while copper signal marked with green solid lines corresponds to background signal produced by the copper grid holder. Summary of EDS for both conditions on the table at the bottom (e).

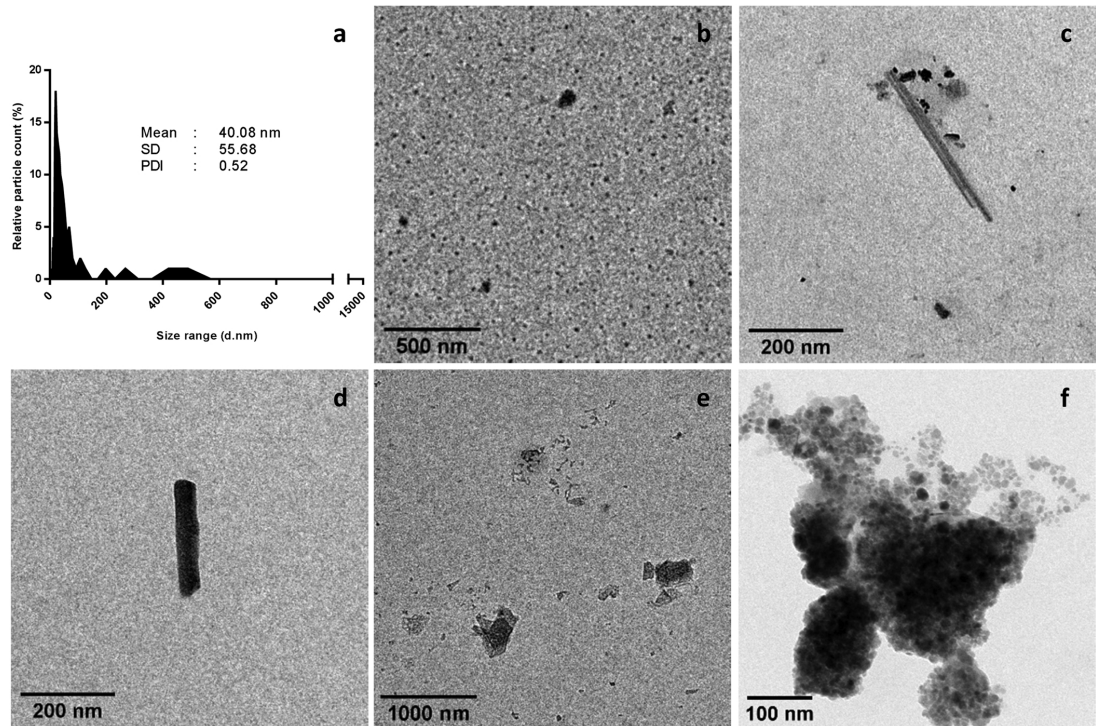


Fig. 3. PET-NPLs characterized by TEM. Size distribution of sizes was obtained from measures of more than 100 images showing a bimodal distribution, with the main peak with sizes around 50 nm, and a second peak with sizes around 400–500 nm (a). Fields with many small sized materials are observed (b), as well as some irregular shapes and fibers (c-e). Agglomerates permit to visualize the small sizes of their components (f).

FTIR analysis was carried out at the premises of the ICN2. To assess the composition of our samples the obtained interferograms were analyzed and contrasted with previous reports of the representative bands present

on PET spectrum (Andanson and Kazarian, 2008; Chen et al., 2013; Johnson et al., 2021), and then assigned as reported on Fig. 4. As observed, the obtained peaks match well with the expected, confirming

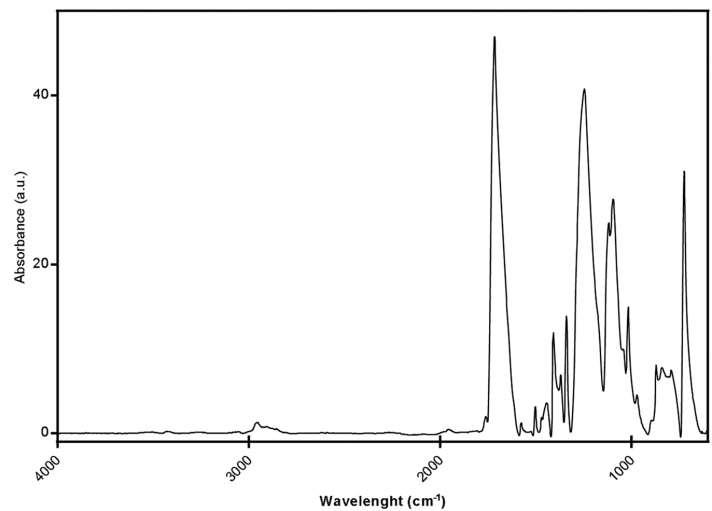


Fig. 4. FTIR spectra with the identity of principal peaks of the interferogram (a) and its assignment (b). Vertical lines indicate coincident peaks.

the PET nature of our samples.

3.1.4. Aqueous solution size distribution and zeta potential

From the bimodal distribution observable by TEM, we tried to reduce the content of the higher-size peak (including agglomerates) by using sonication and/or filtration. This approach is schematized on the [Supplementary Fig. S3](#). According to such approaches, we have observed that the best way to reduce agglomerates includes filtration and sonication. Thus, the characterization of such filtered/sonicated samples by a Zetasizer device is indicated in this section. Other combinations of filtration/sonication and dispersion procedures (Nanogenotox, 2011) are included in [Fig. S3](#). Hydrodynamic diameter measurements by using dynamic light scattering shows mild differences in the average size (of around 30 nm) between the suspension of nanoparticles in water, or with the addition of SDS. The obtained diameter (161.01 ± 3.94 nm) and polydispersity index (PI, 0.22) for aqueous dispersions, slightly differ from those observed using SDS, 129.01 ± 0.94 nm and 0.21, respectively. The corresponding signals, expressed as the mean of three independent measurements, are depicted in [Fig. 5a](#). The correlograms for each condition by triplicates are observed in [Fig. 5b](#). It is interesting to notice that for the mentioned measurements a fixed scattered collection angle of 174.7° was employed, but when the combination of three angles (174.7° , 90° , and 12.78°) are used, the differences or influence of the dispersion media is less noticeable. This can be observed on [Fig. 5c](#), where the curves for both conditions, are almost overlapping. Thus, DLS and even better MADLS are excellent tools for the initial characterization of the obtained PET-NPLs. Another important approach to describe the relative behavior of the particles in suspension is the zeta potential (ZP), which indicates the charge on the surface of the PET-NPLs and the stability of the colloid dispersion. In both cases, summarized on the table ([Fig. 5d](#)), the obtained ZP values can be considered as indicative of moderately stable to highly stable suspensions. It is important to remark the important influence of the sample sonication, prior to the characterization, as can be observed in the [Supplementary material \(Figs. S3 and S4\)](#). It is also remarkable that it is possible to calculate the number of particles from the intensity values ([Fig. 5d](#)). The obtained values indicate that the used protocol permits to obtain highly concentrated samples.

From the results obtained by the analysis of PET by AF4-MALS, after the void peak at 5 min, a large peak appeared, from min 10–35 with an increase of gyration radius from 30 nm up to 600 nm ([Fig. 6a](#)). The 90 % of PET size ranged from 40 nm up to 75 nm of gyration radius (103 up to 194 nm of Dgeo), being 5 % from 75 nm to 100 nm and the rest of the sample above 100 nm (Dgeo above 258 nm), as it can be seen in the Cumulative tendency in [Fig. 6b](#). Moreover, the differential distribution of the PET size, in [Fig. 6b](#), indicated the highest number of particles at

approximately 60 nm (155 nm of Dgeo), obtaining a weighted Dgeo of 145 ± 7 nm.

3.2. Cell uptake of PET-NPLs

To demonstrate the potential applicability of the obtained PET-NPLs, as a representative MNPLs material, it is important to find out whether it can be uptake by the cells after having applied a PET-NPLs dispersion and treatment protocol. Herein we have used three different approaches to confirm the cellular uptake in TK6 and THP1 cell models.

3.2.1. Internalization of PET-NPLs stained by Nile red by confocal microscopy

Nanoplastics, in opposition to metallic nanoparticles, are difficult to be visualized by confocal microscopy due to their lack of reflection. Hence, a staining is needed to explore its toxicokinetic behavior by imaging techniques. Among the different staining dyes available that can be applied to plastic particles after its synthesis/obtention, stand up the Nile red. It produced the best results when applied to virgin and weathered synthetic polymers and textile fibers, in comparison with other seven dyes (Prata et al., 2019). In fact, a recent review points out the main pros and cons of the use of the staining dye in the MNPLs context (Shruti et al., 2022). In our case, Nile red staining allowed us to visualize the internalized PET-NPLs inside cells. Due to its affinity for lipidic structures, Nile red signal could induce errors. Nevertheless, we have detected fluorescent signal into the nucleus ([Fig. 7a-c](#)) where not structures exist, confirming the usefulness of this staining. Further intracellular signals are indicated in [Fig. 7g-j](#), confirming the cell uptake. In fact, the use of Nile red staining was previously found to be useful to detect the cell uptake of other sources of in-house produced PET-NPLs (Rodríguez-Hernández et al., 2019).

3.2.2. Cell complexity as detected by flow cytometry

The first approach was an indirect one checking for structural cell changes due to PET-NPLs exposure. It is expected that cells internalizing PET-NPLs experience changes on their internal structures increasing their granularity, which can be assessed using flow cytometry. As cell granularity increase, an increment of side scattered light is expected, and this effect commonly known as cell-complexity can be observed on [Fig. 7e,f](#). This methodology has shown to be useful in detection cell uptake of different nanomaterials (Vila et al., 2017). From our results, we show that cell uptake is modulated by two factors, such as the exposure time and the presence/absence of FBS. As observed on [Fig. 7b](#), cell uptake increases with the exposure time showing higher uptake after exposures lasting for 3 h regarding the observed after 1 h exposure. In addition, PET-NPLs dispersed in culture media with or without FBS

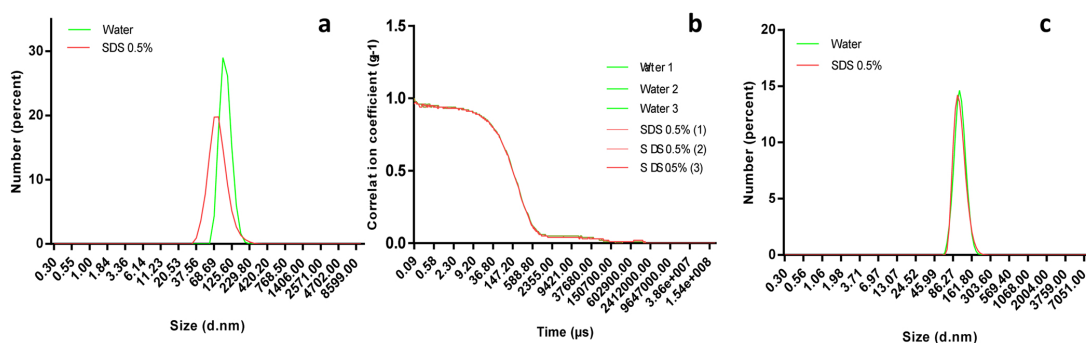


Fig. 5. Size distribution analysis by DLS. (a) Filtered and sonicated PET-NPLs samples were used with both water and SDS (0.5%) as dispersants, and 174.7° as the angle of scattering collection. (b) The correlation coefficients of the measurements. (c) Particle size distribution by using MADLS with three angles of scattering collection (174.7° , 90° , and 12.78°) with water or SDS (0.5 %) as dispersants.

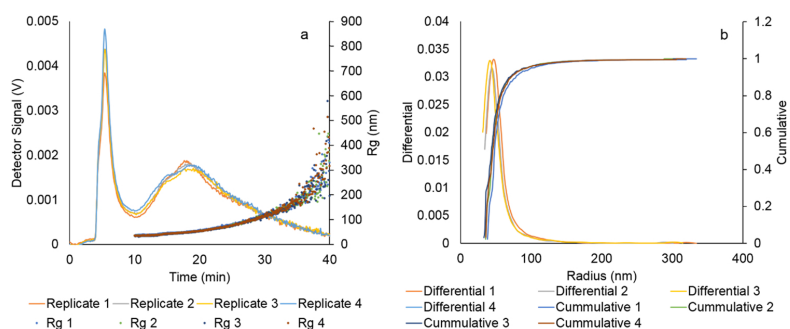


Fig. 6. AF4-MALS plots obtained for a 20 μL injection of 1 mg/mL of PET, (a) Fractogram (left axis: MALS 90° detector signal (V); right axis: Gyration Radius (Rg, nm)) and (b) Differential and Cumulative graphics.

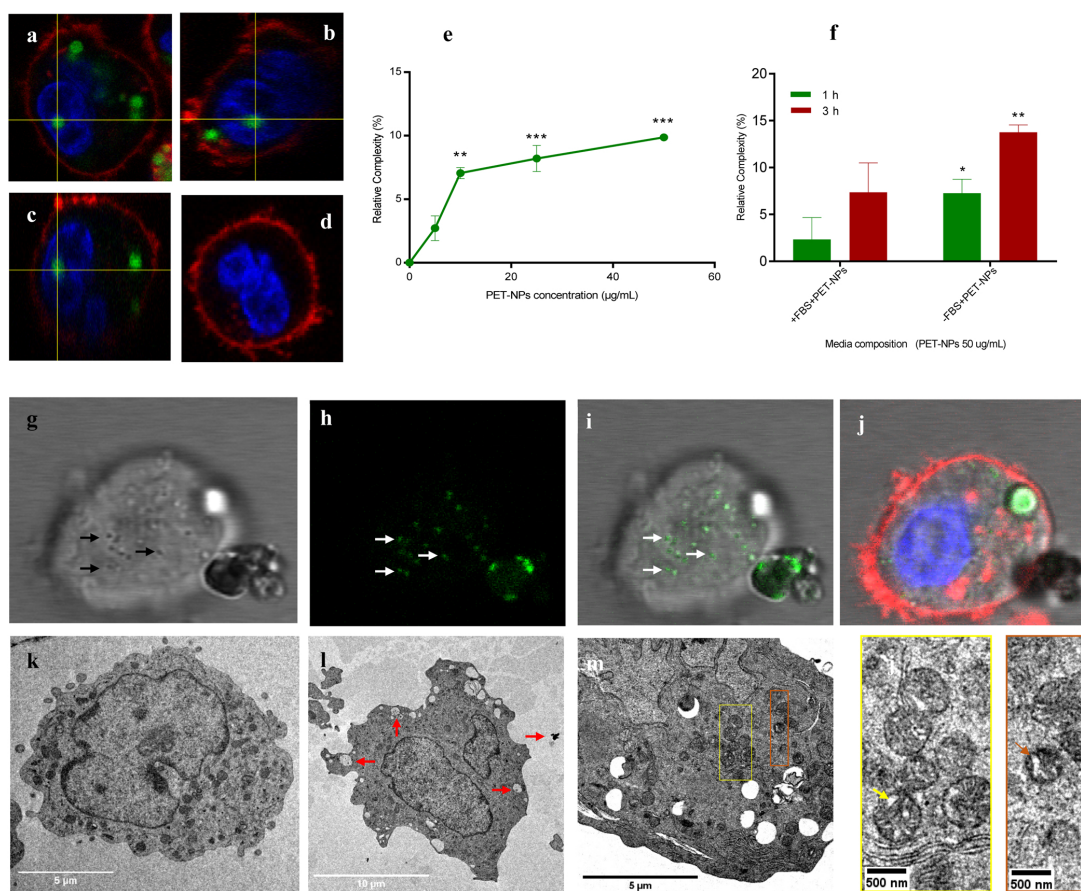


Fig. 7. Confocal orthogonal view of internalized Nile red stained PET-NPLs (green signal) on THP1 cells after 24 h exposure to 50 $\mu\text{g/mL}$ is presented as XY, YZ and XZ (a, b and c respectively) three dimensional views and d is the control. Small dot like structures is observed at the cytoplasm of THP1 cells (g) and fluorescence at 546–628 nm is collected on the same points. Merged images are visualized on i where also the big fluorescent structure corresponds to fluorescent agglomerates. Relative increment on complexity at early exposition to 50 $\mu\text{g/mL}$ of PET-NP on THP1 cells is represented on e (** $p < 0.018$, *** $p < 0.0009$ and **** $p < 0.0004$) and influence FBS on the media composition (f) (* $p < 0.0162$ and ** $p < 0.0087$). For both cases One-way ANOVA with Dunnett's post-test was used for the statistical analysis. TEM images show an increment on vacuoles at 5 (l) or 50 (m) $\mu\text{g/mL}$ of PET-NPs, relative to control (k), PET-NPs like structures are shown by the red arrows and mitochondrial abnormalities or holey mitochondrion are present only on PET-NPs treated cells (yellow and brown arrows).

are significantly different in terms of complexity, with a higher uptake in the absence of serum.

3.2.3. Cell uptake detection by TEM

TEM has successfully been applied to detect nanomaterials uptake by many cell types, including MNPLs (Vila et al., 2017; Cortés et al., 2020). Our TEM figures show substantial amounts of PET-NPLs incorporated into cytoplasmic vesicles (Fig. 7). Although no specific studies have been addressed to understand the cell uptake of PET-NPLs, their presence in the lysosomes of Caco-2 cells (Magri et al., 2021) can suggest that their uptake is by endocytosis, as previously demonstrated for PS-NPLs where that was considered as the main cellular absorption pathway (Magri et al., 2018; Cortés et al., 2020). Interestingly, we detect PETNPLs into mitochondria inducing some alterations. These effects have been also reported for PSNPLs (Cortés et al., 2020; Trevisan et al., 2020).

Taking all three approaches together, it seems clear that cells can uptake our lab-produced PET-NPLs.

3.3. Cytotoxicity

Cell viability curves were studied to determine the cytotoxic effects of PET-NPLs exposure on THP1 and TK6 cell-lines. As shown in Fig. 8 no significant cytotoxicity was observed up to the concentration of 100 µg/mL. Only mild effects were observed at the high concentration of 200 µg/mL of PET-NPLs on TK6, where the viability was compromised close to 80 % for exposures lasting for 48 h. Since our aim is to work with non-cytotoxic doses, the following experiments were carried out at concentrations up to 50 µg/mL.

This lack of toxicity of the obtained PET-NPLs agree with the reported for other secondary PET nanomaterials obtained using different methodological approaches (Magri et al., 2018; Dhaka et al., 2022). Although the toxic effects of MNPLs can depend on distinctive characteristics, i.e., the size, most of the studies agree with their lack of acute toxic effects. This has been proved when the effects of different MPLs (polyethylene, polypropylene, polyvinylchloride, and PET) were evaluated in three different cell lines (Stock et al., 2021). This means that other milder, sub-toxic cellular effects, and not cell death, must be selected as biomarker when evaluating the harmful effects associated with MNPLs exposure. Further efforts looking for different exposure scenarios, considering acute exposure to higher concentrations, repeated doses, or long-term exposures, are necessary to decipher the toxic effects of PET-NPLs obtained from environmental plastic samples.

3.4. ROS induction by PET-NPLs

The ability of our PET-NPLs to increase the intracellular levels of ROS was evaluated using the DHE detection assay, in THP1 cells. The results indicated in Fig. 9 show that exposures lasting for 3 h were unable to induce statistically significant differences in the ROS levels when

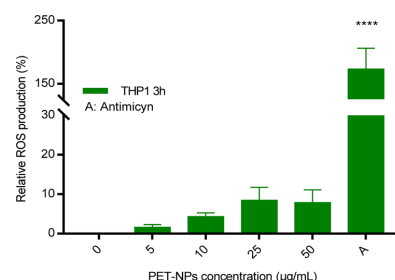


Fig. 9. Reactive oxygen species (ROS) induction in THP1 cells after PET-NPLs exposures lasting for 3 h at concentrations ranging from 0 to 50 µg/mL at 3 h exposition. Data is expressed as percentage of ROS production relative to the untreated control \pm SEM. One-way ANOVA with Dunnett's post-test was performed. Statistical significance indicated on the graph as **** $p < 0.0001$.

compared to untreated controls. Nevertheless, the positive control used (antimycin) induced important levels of ROS, confirming the goodness of the used protocol. Although one of the most recognized mechanisms of action of nanomaterials is the induction of ROS (Karkossa et al., 2021), MNPLs seem to have a different behavior. Recent results with real PET samples did not show ROS induction in human intestinal Caco-2 cells (Magri et al., 2021). This inability of PET-NPLs to induce oxidative stress *in vitro*, agree with many studies using PSNPLs as a model of MNPLs where exposure did not increase ROS levels in Caco-2 cells after acute exposures (Domenech et al., 2020) or after long-term exposures (Domenech et al., 2021). Nevertheless, the potential induction of oxidative stress seems to be dependent on the cell type as demonstrated with different hematopoietic cell lines where ROS was clearly observable (Rubio et al., 2020), as well as dependent on the particle size (Kik et al., 2021).

3.5. Genotoxic evaluation of PET-NPLs by using the comet assay

Among the different biomarkers evaluating health risk, those detecting genotoxicity stand out. This is because, due to the main role of DNA in cell functionality, DNA damage severely compromises human health (Carbone et al., 2020). Although the genotoxicity assays can evaluate both primary or fixed DNA damage, those detecting primary damage are much more sensitive. Thus, the comet assay is used to measures the induction of single/double DNA breaks as well as the induction of oxidative damage on the DNA bases. Its simplicity and sensitivity have spread its use in many fields, including the hazard assessment of nanomaterials (García-Rodríguez et al., 2019).

In our study, we have not been able to demonstrate the ability of our PET-NPLs to damage DNA, as indicated in Fig. 10. In addition to the lack of direct strand breaks (Fig. 10a) PET-NPLs exposure also did not induce oxidative damage on the DNA bases (Fig. 10b). These results agree with

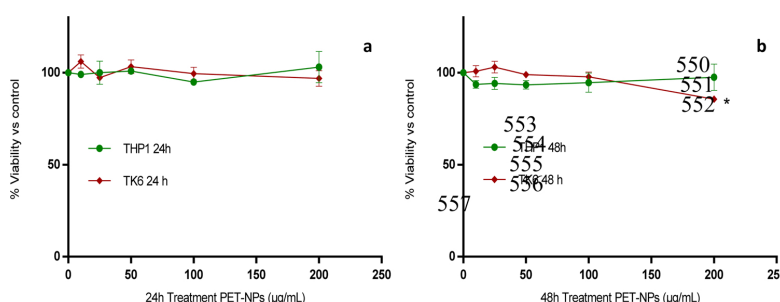


Fig. 8. Relative cell viability of THP1 (green) and TK6 (red) cell lines at concentrations ranging from 0 to 200 µg/mL, after PET-NPLs exposures lasting for 24 h (a) and 48 h (b). Data represented as percentage of living cells relative to the untreated control treatment at 24 (green) and 48 (blue) h of exposure. Data is expressed as percentage of cells relative to the untreated control \pm SEM. One-way ANOVA with Dunnett's post-test was used for the statistical analysis. Statistical significance indicated on the graph as * $p < 0.01$.

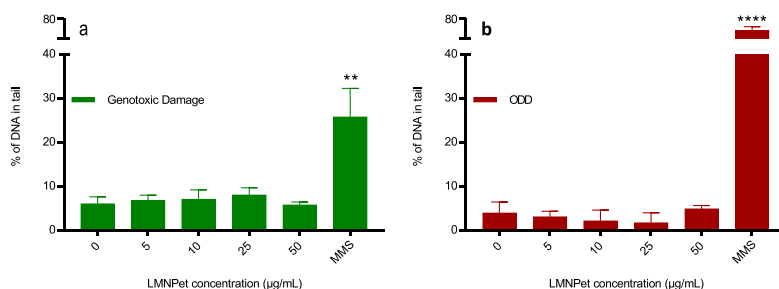


Fig. 10. THP1 genotoxic (a) and oxidative DNA damage (b) at concentrations ranging from 0 to 50 µg/mL and exposure lasting for 3 h. Damage is expressed as the percentage DNA in tail \pm SEM. One-way ANOVA with Dunnett's post-test was performed. Statistical significance indicated on the graph as ** $P < 0.01$ **** $p < 0.0001$, respectively. Methyl methanesulfonate (MMS) was used as a positive control.

our previous data showing that PET-NPLs were unable to induce oxidative stress. No other studies are using PET where the genotoxic potential was evaluated. Nevertheless, a few studies on the genotoxic potential of polystyrene MNPLs have been reported showing contradictory results. In *in vitro* studies, negative findings using the micronucleus assay were observed in the intestinal/placenta barrier cells exposed to 50/500 nm polystyrene NPLs (Hesler et al., 2020). Negative results were also reported in human intestinal Caco-2 cells exposed to 50 nm polystyrene NPLs both as a component of an *in vitro* barrier (Domenech et al., 2020) or after long-term exposures (Domenech et al., 2021). Nevertheless, positive effects were observed in sh27 fibroblasts using the micronucleus assay (Poma et al., 2019). This would indicate differences between cell types in both MNPLs uptake and genotoxic effects as reported when different types of human hematopoietic cell lines were used (Rubio et al., 2020).

As a summing up, we consider that the proposed method to obtain uniform and reproducible secondary NPLs from representative environmental plastic goods is adequate, since the nano sized fraction of the suspension is very high (about 95%). In addition, we consider that the obtained samples mimic the naturally occurring degradation phenomenon. The characterization of the working material by TEM showed a bimodal distribution in the nano range with most of the particles ranging around 50 nm. Simple filtering and sonication steps produce a uniform distribution around 100 nm when DLS and AF4 measurements are applied. We are confident that this methodology can be easily used to obtain NPLs from other plastics materials, scraping from the constrictions posed using pristine forms of commercial polystyrene NPLs. Materials resulting from environmentally representative plastics permit to answer the main open questions asking for the risks of environmental MNPLs resulting from degradation processes. As reported, our protocol using non-metallic burrs during the sanding process has a great advantage over those using metallic blades which contaminate the resulting MNPLs. Such metallic contamination would invalidate any approach aiming to evaluate the potential health risk of such types of MNPLs. It must be recalled that most of the studies evaluating the hazardous effects of MNPLs use sizes in the micro range. Although they can provide useful information, it must be remembered that plastic particles sized in the nano-range are more prone to cross epithelial barriers and, consequently, spread over the different tissues and organs. Accordingly, to be able to get nanoplastics -instead of microplastics- resulting from the degradation of representative environmental plastic pollutants can represent an important step to get more sound data answering about their potential effects on human health.

Although our hazard approach can be considered just as a preliminary one, it is important to highlight that the obtained PET-NPLs are easily internalized by the used cell models without important toxic or genotoxic effects. Due to the lack of gross biological effects, reported by many authors using different sized MNPLs, the use of methodological

approaches detecting other types of milder cell effects, out of cell death, should be used when evaluating the harmful effects associated with MNPLs exposure (Stock et al., 2021). In such a context, having the facility of easily obtaining different types of MNPLs can result very helpful. It is obvious that the original sources of the environmental commercial PET plastics can differ in factors such as crystallinity and plasticizer content. This can suppose differences in the obtained samples, hence differences in their induced biological effects. However, this should not necessarily be considered a problem but rather a challenge, since the obtained/evaluated samples are more representative of the environmentally MNPLs pollutants.

CRedit authorship contribution statement

RM and AH planned the experiments. AV, LR, MA, MLM, VFC, and OHM carried out the experimental part. AV analyzed the data, carried out the statistical analysis, and prepared tables/figures. AV, RM, and AH wrote the final manuscript.

Declaration of Competing Interest

The authors declare that they have no known competing financial interests or personal relationships that could have appeared to influence the work reported in this paper.

Data availability

Data will be made available on request.

Acknowledgments

A. Villacorta was supported by Ph.D. fellowships from the National Agency for Research and Development (ANID), CONICYT PFCHA / DOCTORADO BECAS CHILE / 2020 – 72210237. L. Rubio was supported by the Fondo Nacional de Innovación y Desarrollo Científico y Tecnológico (FONDOCYT) República Dominicana (Project 2018–2019-2B2–093). This project (PlasticHeal) has received funding from the European Union's Horizon 2020 research and innovation program under grant agreement No 965196. L. Rubio was supported by a contract Juan de la Cierva (IJC2020-26861/AEI/10.13039/501100011033).

Environmental Implication

In spite of the intrinsic interest in understanding the potential hazards associated with the environmental micro-/nanoplastics exposure, most of the studies use pristine commercial samples. Thus, a challenge is to get/evaluate environmental representative samples. In this context, we propose a method to obtain *real* environmental samples of

nanoplastics. Initially applied to PET water bottles, the proposed method is applicable to any source of environmental plastic goods. Interestingly, during the improvement of the method, we discover potential metal contamination resulting from other proposed milling procedures. Our method avoids such contamination, which benefits the ulterior hazard evaluations.

Appendix A. Supporting information

Supplementary data associated with this article can be found in the online version at doi:10.1016/j.jhazmat.2022.129593.

References

- Ali, M.U., Lin, S., Yousaf, B., Abbas, Q., Munir, M.A.M., Ali, M.U., Rasid, A., Zheng, C., Kuang, X., Wong, M.H., 2021b. Environmental emission, fate and transformation of microplastics in biotic and abiotic compartments: global status, recent advances and future perspectives. *Sci. Total Environ.* 791, 148422 <https://doi.org/10.1016/j.scitotenv.2021.148422>.
- Ali, S.S., Elsamahy, T., Koutra, E., Kornaros, M., El-Sheekh, M., Abdelkarim, E.A., Zhu, D., Sun, J., 2021a. Degradation of conventional plastic wastes in the environment: a review on current status of knowledge and future perspectives of disposal. *Sci. Total Environ.* 771, 144719 <https://doi.org/10.1016/j.scitotenv.2020.144719>.
- Andanson, J.M., Kazarian, S.G., 2008. In situ ATR-FTIR spectroscopy of poly(ethylene terephthalate) subjected to high-temperature treatment. *Macromol. Symp.* 265, 195–204. <https://doi.org/10.1002/masy.200850521>.
- Astner, A.F., Hayes, D.G., O'Neill, H., Evans, B.R., Pingali, S.V., Urban, V.S., Young, T.M., 2019. Mechanical formation of micro- and nano-plastic materials for environmental studies in agricultural ecosystems. *Sci. Total Environ.* 685, 1097–1106. <https://doi.org/10.1016/j.scitotenv.2019.06.241>.
- Balakrishnan, G., Dénél, M., Nicolai, T., Chassenieux, C., Lagarde, F., 2019. Towards more realistic reference microplastics and nanoplastics: preparation of polyethylene micro/nanoparticles with a biosurfactant. *Environ. Sci. Nano* 6, 315–324. <https://doi.org/10.1039/C8EN01005F>.
- Ballesteros, S., Domenech, J., Bargailla, I., Cortés, C., Marcos, R., Hernández, A., 2020. Genotoxic and immunomodulatory effects in human white blood cells after ex vivo exposure to polystyrene nanoplastics. *Environ. Sci. Nano* 7, 3431–3446. <https://doi.org/10.1039/D0EN00748J>.
- Batool, I., Qadir, A., Levermore, J.M., Kelly, F.J., 2021. Dynamics of airborne microplastics, appraisal and distributional behaviour in atmosphere; a review. *Sci. Total Environ.* 14, 150745 <https://doi.org/10.1016/j.scitotenv.2021.150745>.
- Borrelle, S.B., Ringma, J., Law, K.L., Monahan, C.C., Lebreton, L., McGivern, A., Murphy, E., Jambeck, J., Leonard, G.H., Hilleary, M.A., Eriksen, M., Possingham, H. P., De Frond, H., Gerber, L.R., Polidoro, B., Tahir, A., Bernard, M., Mallos, N., Barnes, M., Rochman, C.M., 2020. Predicted growth in plastic waste exceeds efforts to mitigate plastic pollution. *Science* 369, 1515–1518. <https://doi.org/10.1126/science.aba3656>.
- Carbone M., Arron ST, Beutler B, Bononi A, Cavenee W, Cleaver JE, Croce CM, D'Andrea A, Foulkes WD, Gaudino G, Groden JL, Henske EP, Hickson ID, Hwang PM, Kolodner RD, Mak TW, Malkin D, Monnat RJ Jr, Novelli F, Pass HI, Petrini JH, Schmidt LS, Yang H. Tumour predisposition and cancer syndromes as models to study gene-environment interactions. *Nat Rev Cancer*, 2020, 20(9): 533-549. doi: 10.1038/s41568-020-0265-y.
- Chen, Z., Hay, J.N., Jenkins, M.J., 2013. The thermal analysis of poly(ethylene terephthalate) by FTIR spectroscopy. *Thermochim. Acta* 552, 123–130. <https://doi.org/10.1016/j.tca.2012.11.002>.
- Cortés, C., Domenech, J., Salazar, M., Pastor, S., Marcos, R., Hernández, A., 2020. Nanoplastics as a potential environmental health factor: effects of polystyrene nanoparticles on human intestinal epithelial Caco-2 cells. *Environ. Sci. Nano* 7, 272–285. <https://doi.org/10.1039/C9EN00523D>.
- Dhaka, V., Singh, S., Anil, A.G., Sunil Kumar Naik, T.S., Garg, S., Samuel, J., Kumar, M., Ramamurthy, P.C., Singh, J., 2022. Occurrence, toxicity and remediation of polyethylene terephthalate plastics. A review. *J. Environ. Chem. Lett.* 13, 1–24. <https://doi.org/10.1007/s10311-021-01384-8>.
- Domenech, J., Hernández, A., Rubio, L., Marcos, R., Cortés, C., 2020. Interactions of polystyrene nanoplastics with *in vitro* models of the intestinal barrier. *Arch. Toxicol.* 94 (9), 2997–3012. <https://doi.org/10.1007/s00204-020-02805-3>.
- Domenech, J., de Brito, M., Velázquez, A., Pastor, S., Hernández, A., Marcos, R., Cortés, C., 2021. Long-term effects of polystyrene nanoplastics in human intestinal Caco-2 cells. *Biomolecules* 11, 1442. <https://doi.org/10.3390/biom11101442>.
- ECHA, (2018) European Chemicals Agency. Background document on the Opinion on the Annex XV report proposing restrictions on intentionally added microplastics. (<https://echa.europa.eu/documents/10162/2ddaab18-76d6-49a2-ec46-8350dabf5dc>).
- Evangelou, N., Grythe, H., Klimont, Z., Heyes, C., Eckhardt, S., Lopez-Aparicio, S., Stohl, A., 2020. Atmospheric transport is a major pathway of microplastics to remote regions. *Nat. Commun.* 11 (1), 3381. <https://doi.org/10.1038/s41467-020-17201-9>.
- García-Rodríguez, A., Rubio, L., Vila, L., Xamena, N., Velázquez, A., Marcos, R., Hernández, A., 2019. The comet assay as a tool to detect the genotoxic potential of nanomaterials. *Nanomaterials* 9, 1385. <https://doi.org/10.3390/nano9101385>.
- Gwada, B., Ogendi, G., Makindi, S.M., Trott, S., 2019. Composition of plastic waste discarded by households and its management approaches. *Glob. J. Environ. Sci. Manag.* 5, 83–94. <https://doi.org/10.22034/gjesm.2019.01.07>.
- Hartmann, N.B., Hüffer, T., Thompson, R.C., Hassellöv, M., Verschoor, A., Daugaard, A. E., Rist, S., Karlsson, T., Brennholt, N., Cole, M., Herring, M.P., Hess, M.C., Ivelva, N. P., Lusher, A.L., Wagner, M., 2019. Are we speaking the same language? Recommendations for a definition and categorization framework for plastic debris. *Environ. Sci. Technol.* 53 (3), 1039–1047. <https://doi.org/10.1021/acs.est.8b05297>.
- Hesler M, Aengenheister I, Ellinger B, Drexler R, Straskraba S, Jost C, Wagner S, Meier F, von Briesen H, Büchel C, Wick P, Buerki-Thurnherr T, Kohl Y. Multi-endpoint toxicological assessment of polystyrene nano- and microparticles in different biological models in vitro. *Toxicol In Vitro*, 2019, 61: 104610. doi: 10.1016/j.tiv.2019.104610.
- Johnson, L.M., Mecham, J.B., Krovi, S.A., Moreno Caffaro, M.M., Aravamudan, S., Kovach, A.L., Fennell, T.R., Mortensen, N.P., 2021. Fabrication of polyethylene terephthalate (PET) nanoparticles with fluorescent tracers for studies in mammalian cells. *Nanoscale Adv.* 3, 339–346. <https://doi.org/10.1039/D0NA00888E>.
- Karkossa, I., Bannuscher, A., Hellack, B., Wohlleben, W., Laloy, J., Stan, M.S., Dinischiotu, A., Wiemann, M., Luch, A., Haase, A., von Bergen, M., Schubert, K., 2021. Nanomaterials induce different levels of oxidative stress, depending on the used model system: comparison of *in vitro* and *in vivo* effects. *Sci. Total Environ.* 801, 149538 <https://doi.org/10.1016/j.scitotenv.2021.149538>.
- Kik, K., Bukowska, B., Krokosz, A., Sicińska, P., 2021. Oxidative properties of polystyrene nanoparticles with different diameters in human peripheral blood mononuclear cells (*In vitro* study). *Int. J. Mol. Sci.* 22 (9), 4406. <https://doi.org/10.3390/ijms22094406>.
- Lionetto, F., Corcione, C.E., Rizzo, A., Maffezzoli, A., 2021. Production and characterization of polyethylene terephthalate nanoparticles. *Polymers* 13 (21), 3745. <https://doi.org/10.3390/polym13213745>.
- Lohrke, J., Briel, A., Mäder, K., 2008. Characterization of superparamagnetic iron oxide nanoparticles by asymmetrical flow-field-flow-fractionation. *Nanomedicine* 3 (4), 437–452. <https://doi.org/10.2217/17435889.3.4.437>.
- Magri, D., Veronesi, M., Sánchez-Moreno, P., Tolardo, V., Bandiera, T., Pompa, P.P., Athanassiou, A., Fragouli, D., 2021. PET nanoplastics interactions with water contaminants and their impact on human cells. *Environ. Pollut.* 271, 116262 <https://doi.org/10.1016/j.envpol.2020.116262>.
- Magri, D., Sánchez-Moreno, P., Caputo, G., Gatto, F., Veronesi, M., Bardi, G., Catelani, T., Guarnieri, D., Athanassiou, A., Pompa, P.P., Fragouli, D., 2018. Laser ablation as a versatile tool to mimic polyethylene terephthalate nanoplastic pollutants: characterization and toxicology assessment. *ACS Nano* 12 (8), 7690–7700. <https://doi.org/10.1021/acsnano.8b01331>.
- Nanogenotox protocol. Final protocol for producing suitable manufactured nanomaterial exposure media. Nanogenotox, towards a method for detecting the potential genotoxicity of nanomaterials, 2011. (https://www.anses.fr/en/system/files/nanogenotox_deliverable_5.pdf). Accessed on 15/01/2022.
- Parolini, M., Ferrario, C., De Felice, B., Gazzotti, S., Bonasoro, F., Candia Carnevali, M.D., Ortenzi, M.A., Sugni, M., 2020. Interactive effects between sinking polyethylene terephthalate (PET) microplastics deriving from water bottles and a benthic grazer. *J. Hazard. Mater.* 398, 122848 <https://doi.org/10.1016/j.jhazmat.2020.122848>.
- Pignatelli, S., Broccoli, A., Piccardo, M., Felline, S., Terlizzi, A., Renzi, M., 2021. Short-term physiological and biometrical responses of *Lepidium sativum* seedlings exposed to PET-made microplastics and acid rain. *Ecotoxicol. Environ. Saf.* 208, 111718 <https://doi.org/10.1016/j.ecoenv.2020.111718>.
- PlasticsEurope, – The Facts 2018: An analysis of european plastics production, demand and waste data. (<https://plasticseurope.org/wp-content/uploads/2021/10/2018-Plastics-the-facts.pdf>).
- Prata, J.C., Reis, V., Matos, J.T.V., da Costa, J.P., Duarte, A.C., Rocha-Santos, T., 2019. A new approach for routine quantification of microplastics using Nile Red and automated software (MP-VAT). *Sci. Total Environ.* 690, 1277–1283. <https://doi.org/10.1016/j.scitotenv.2019.07.060>.
- Rai, P.K., Lee, J., Brown, R.J.C., Kim, K.H., 2021. Environmental fate, ecotoxicity biomarkers, and potential health effects of micro- and nano-scale plastic contamination. *J. Hazard. Mater.* 403, 123910 <https://doi.org/10.1016/j.jhazmat.2020.123910>.
- Rodríguez-Hernández, A.G., Muñoz-Tabares, J.A., Aguilar-Guzmán, J.C., Vazquez-Duhalt, R., 2019. A novel and simple method for polyethylene terephthalate (PET) nanoparticle production. *Environ. Sci. Nano* 6 (7), 2031–2036. <https://doi.org/10.1039/c9en00365g>.
- Rubio, L., Annangi, B., Vila, L., Hernández, A., Marcos, R., 2016. Antioxidant and anti-genotoxic properties of cerium oxide nanoparticles in a pulmonary-like cell system. *Arch. Toxicol.* 90, 269–278. <https://doi.org/10.1007/s00204-015-1468-y>.
- Rubio, L., Bargailla, I., Domenech, J., Marcos, R., Hernández, A., 2020. Biological effects, including oxidative stress and genotoxic damage, of polystyrene nanoparticles in different human hematopoietic cell lines. *J. Hazard. Mater.* 398, 122900 <https://doi.org/10.1016/j.jhazmat.2020.122900>.
- Shruti, V.C., Pérez-Guevara, F., Roy, P.D., Kutralam-Muniasamy, G., 2022. Analyzing microplastics with Nile Red: emerging trends, challenges, and prospects. *J. Hazard. Mater.* 423 (Pt B), 127171 <https://doi.org/10.1016/j.jhazmat.2021.127171>.
- Stock, V., Laurisch, C., Franke, J., Dönmez, M.H., Voss, L., Böhmert, L., Braeuning, A., Sieg, H., 2021. Uptake and cellular effects of PE, PP, PET and PVC microplastic particles. *Toxicol. Vitro* 70, 105021 <https://doi.org/10.1016/j.tiv.2020.105021>.
- Trevisan, R., Uozukukwu, D., Di Giulio, R.T., 2020. PAH sorption to nanoplastics and the Trojan horse effect as drivers of mitochondrial toxicity and PAH localization in zebrafish. *Front. Environ. Sci.* 8, 78. <https://doi.org/10.3389/fenvs.2020.00078>.

A. Villacorta et al.

Journal of Hazardous Materials 439 (2022) 129593

- Turner, A., Filella, M., 2021. Hazardous metal additives in plastics and their environmental impacts. *Environ. Int.* 156, 106622 <https://doi.org/10.1016/j.envint.2021.106622>.
- Vila, L., Rubio, L., Annangi, B., García-Rodríguez, A., Marcos, R., Hernández, A., 2017. Frozen dispersions of nanomaterials are a useful operational procedure in nanotoxicology. *Nanotoxicology* 11, 31–40. <https://doi.org/10.1080/17435390.2016.1262918>.
- Zitouni, N., Bousserhine, N., Missawi, O., Boughattas, I., Chèvre, N., Santos, R., Belbekhouche, S., Alphonse, V., Tisserand, F., Balmassiere, L., Dos Santos, S.P., Mokni, M., Guerbej, H., Banni, M., 2021. Uptake, tissue distribution and toxicological effects of environmental microplastics in early juvenile fish *Dicentrarchus labrax*. *J. Hazard. Mater.* 403, 124055 <https://doi.org/10.1016/j.jhazmat.2020.124055>.

7.1.1. Supplementary material corresponding to the article entitled *A new source of representative secondary PET nanoplastics. Obtention, characterization, and hazard evaluation* (

Lab-made PET nanoplastics. Obtention, characterization, and hazard evaluation

Aliro Villacorta^{1,2}, Laura Rubio³, Mohamed Alaraby^{1,4}, Montserrat López-Mesas⁵, Victor Fuentes-Cebrian⁵, Oscar H. Moriones^{6,7} Ricard Marcos^{1,§}, Alba Hernández^{1,§}

¹Group of Mutagenesis, Department of Genetics and Microbiology, Faculty of Biosciences, Universitat Autònoma de Barcelona, Cerdanyola del Vallès (Barcelona), Spain.

¹Group of Mutagenesis, Department of Genetics and Microbiology, Faculty of Biosciences, Universitat Autònoma de Barcelona, Cerdanyola del Vallès (Barcelona), Spain.

²Facultad de Recursos Naturales Renovables, Universidad Arturo Prat, Iquique, Chile.

³Nanobiology Laboratory, Department of Natural and Exact Sciences, Pontificia Universidad Católica Madre y Maestra, PUCMM, Santiago de los Caballeros, Dominican Republic.

⁴Zoology Department, Faculty of Sciences, Sohag University (82524), Sohag, Egypt.

⁵GTS-UAB Research Group, Department of Chemistry, Faculty of Science, Universitat Autònoma de Barcelona, 08193 Bellaterra, Cerdanyola del Vallès, Spain.

⁶Institut Català de Nanociència i Nanotecnologia (ICN2-UAB-CSIC-BIST), Campus UAB, Bellaterra, 08193 Barcelona, Spain.

⁷Universitat Autònoma de Barcelona (UAB), Campus UAB, Bellaterra, 08193 Barcelona, Spain.

[§]Corresponding authors at Group of Mutagenesis, Department of Genetics and Microbiology, Faculty of Biosciences, Universitat Autònoma de Barcelona, Campus of Bellaterra, 08193 Cerdanyola del Vallès (Barcelona), Spain.

E-mail: alba.hernandez@uab.cat (A. Hernández)

ricard.marcos@uab.cat (R. Marcos)

SUPPLEMENTARY FIGURES

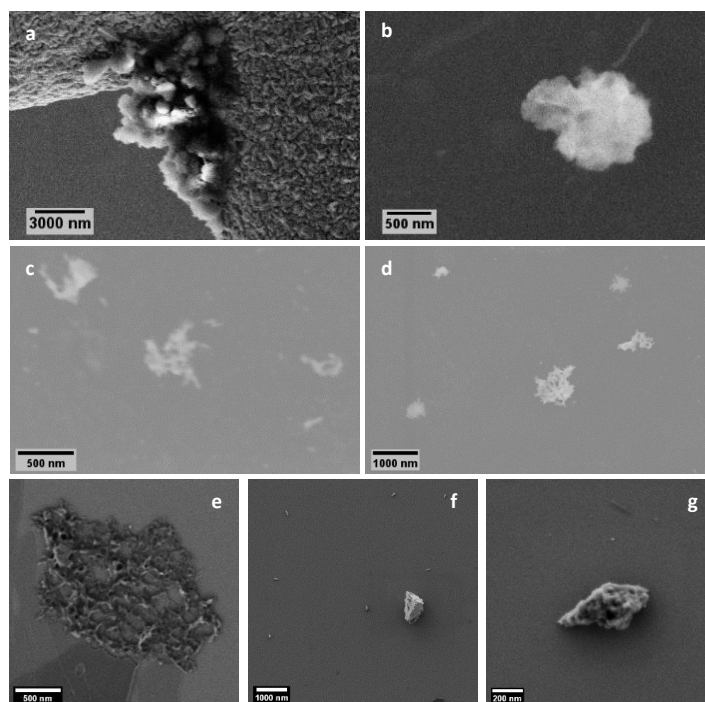


Figure S1.- SEM images of aggregates of particles on the border of the copper grid (a), and shape irregularities on the surface of the particle (b). Fields containing different PET particles are presented in (c) and (d). Particles dried on Si holder for better contrast show the same holey structures described in (e) and the polydispersity of the particles is observed in (f). A closer look at the rounded borders of the particle is visualized in (g).

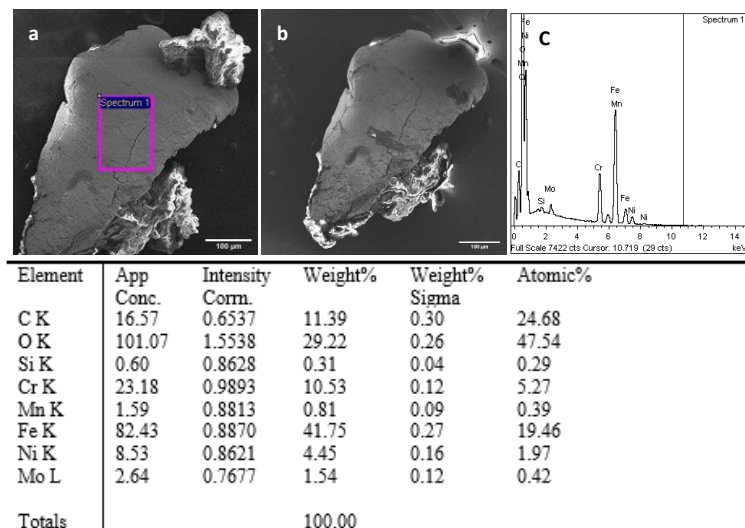
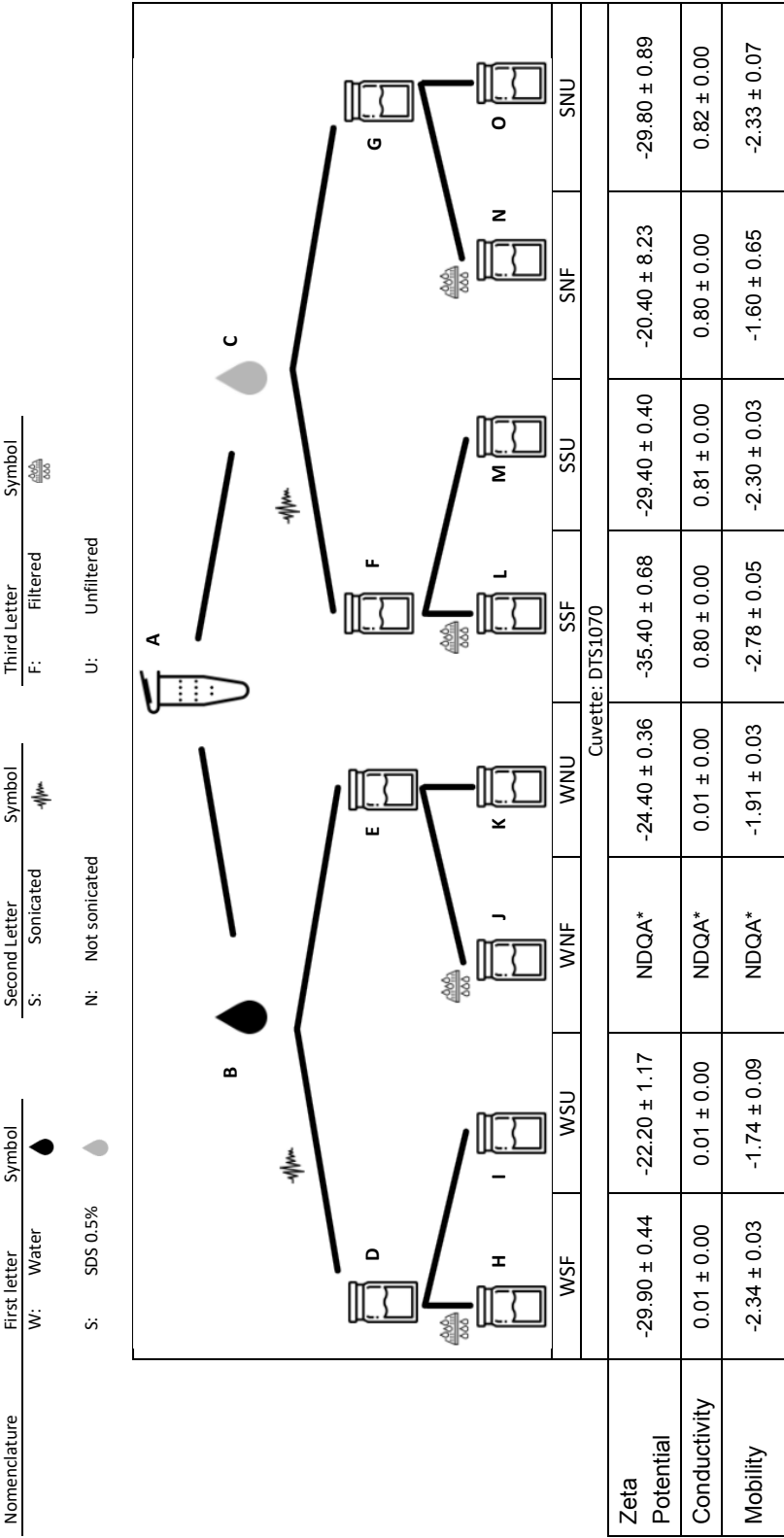


Figure S2.- SEM-EDS Imaging of polylactic acid PLA microplastics contamination previous (a) and after (b) EDS. Is important to notice the reduction in size or shrinking suffered for the polymers placed on the right side and top of the specimen during the beam of electron exposition while the non-polymeric contamination remains with no significant alterations. Raw EDS spectrum is presented (c), summarizing the element composition.



Z Average	139.0 ± 1.22	431.01 ± 100	NDQA*	4.34x10 ³ ± 1.47x10 ³	129.01 ± 3.26	416.99 ± 89.80	102.00 ± 43.60	4.89x10 ³ ± 1.94x10 ³
Polydispersity	0.15 ± 0.01	0.58 ± 0.17	NDQA*	0.97 ± 0.27	0.19 ± 0.02	0.54 ± 0.00	0.50 ± 0.26	0.97 ± 0.28

Cuvette: DTS0012

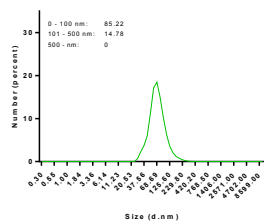
Z-Average	161.00 ± 3.90	0.00 ± 0.00	567.01 ± 312.00	4.03x10 ³ ± 1.85x10 ³	129.00 ± 0.94	528.01 ± 152	567.01 ± 312	4.32x10 ³ ± 1.13x10 ³
Polydispersity	0.22 ± 0.02	0.00 ± 0.00	0.46 ± 0.23	1.59 ± 0.30	0.21 ± 0.02	0.60 ± 0.07	0.46 ± 0.23	1.35 ± 0.56
Particle Concentration	8.68x10 ⁸	7.39x10 ⁹	NDQA*	3.72x10 ²¹	8.68x10 ⁸	6.10E+09	NDQA*	2.26x10 ¹⁸
Data quality guidance	No issues	Larger-sized population Except for 12.78 collector	Weak scattering	Mainly number fluctuation	No issues	Larger-sized population	Mainly number fluctuation & Weak scattering	Mainly number fluctuation

Figure S3. - Preparation for particle characterization. Scheme representing different steps for characterizing on aqueous solution **A** is the starting sample previously frozen on liquid nitrogen and stored at -80 °C which was thawed at 37°C on a water bath. **B** and **C** represent the aqueous suspension preparation on water (**black drop**) or 0.5% SDS (**gray drop**). **D** is the water dispersant working solution sonicated and **E** the not sonicated one. **F** is the SDS 0.5% dispersant working solution sonicated and **G** the not sonicated one. **H** and **L** represent the sonicated and filtered samples on water and SDS 0.5% respectively. **I** and **M** represent the sonicated and non-filtered samples on water and SDS 0.5% respectively. **J** and **N** represent the non-sonicated and filtered samples on water and SDS 0.5% respectively. And finally, **K** and **O** represent the non-sonicated and non-filtered samples on water and SDS 0.5% respectively. *NDQA: No data quality available.

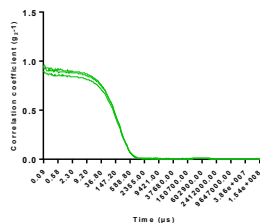
WSF (H)

Cuvette DTS1070

DLS

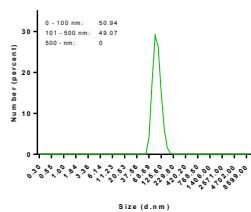


Correlogram

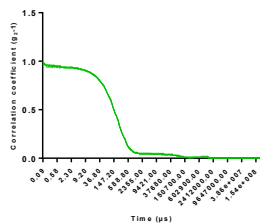


Cuvette DTS0012

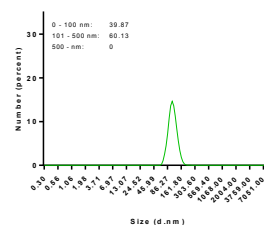
DLS



Correlogram



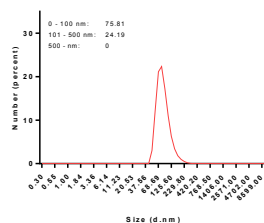
MADLS



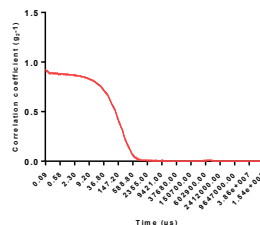
SSF (L)

Cuvette DTS1070

DLS

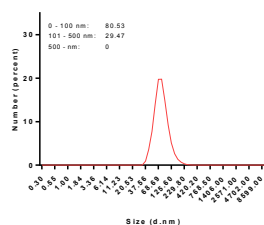


Correlogram

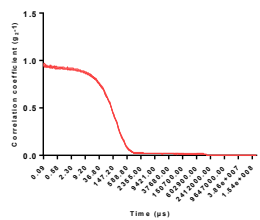


Cuvette DTS0012

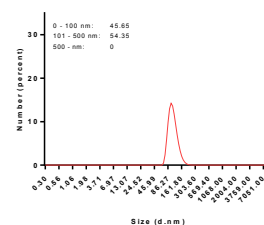
DLS

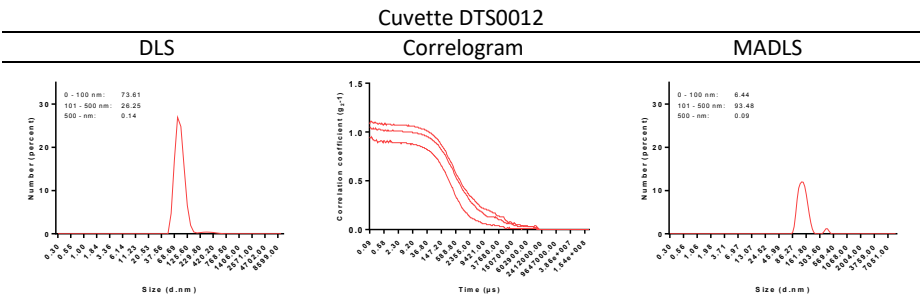
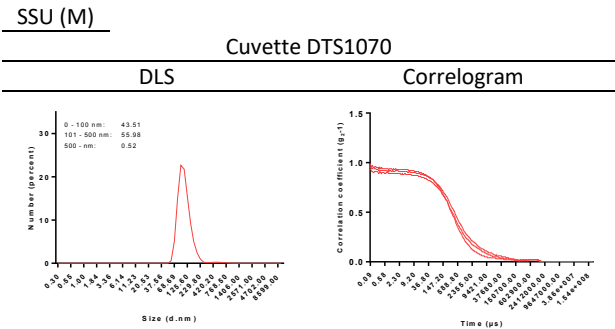
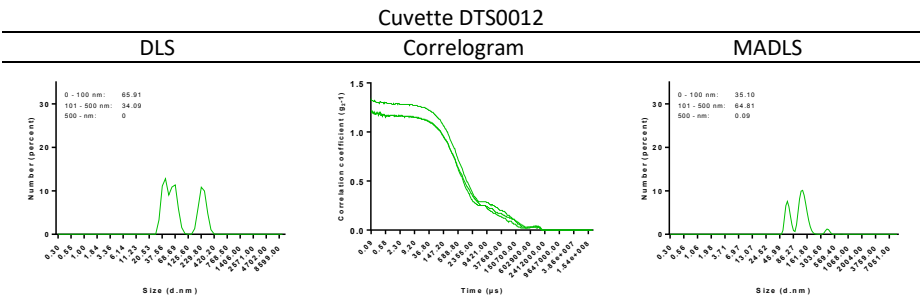
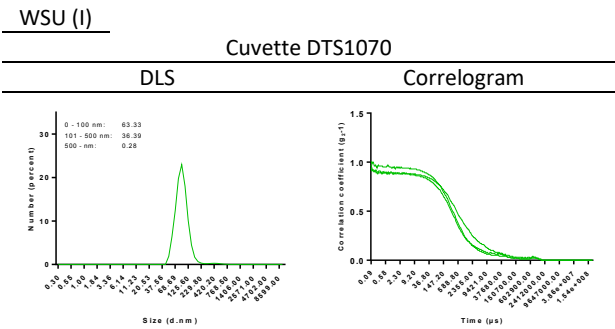


Correlogram



MADLS



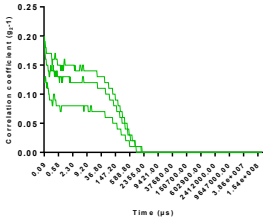
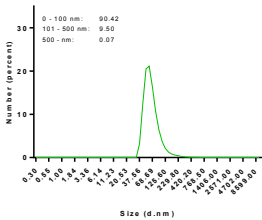


WNF (J)

Cuvette DTS1070

DLS

Correlogram

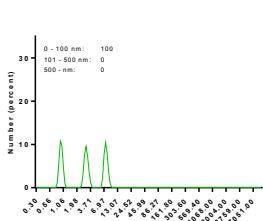
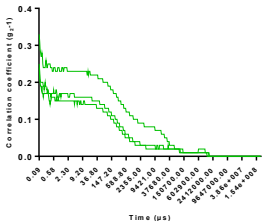
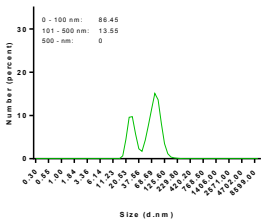


Cuvette DTS0012

DLS

Correlogram

MADLS

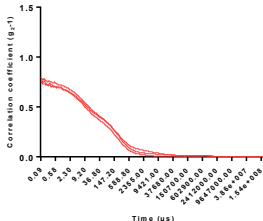
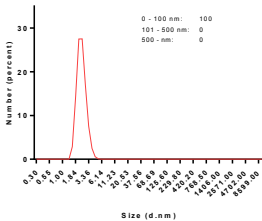


SNF (N)

Cuvette DTS1070

DLS

Correlogram

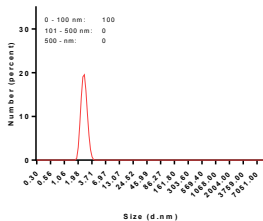
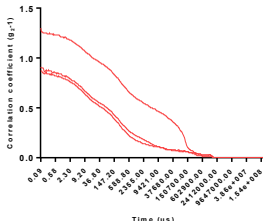
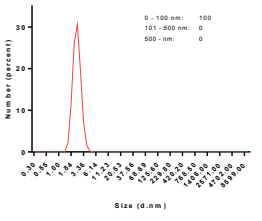


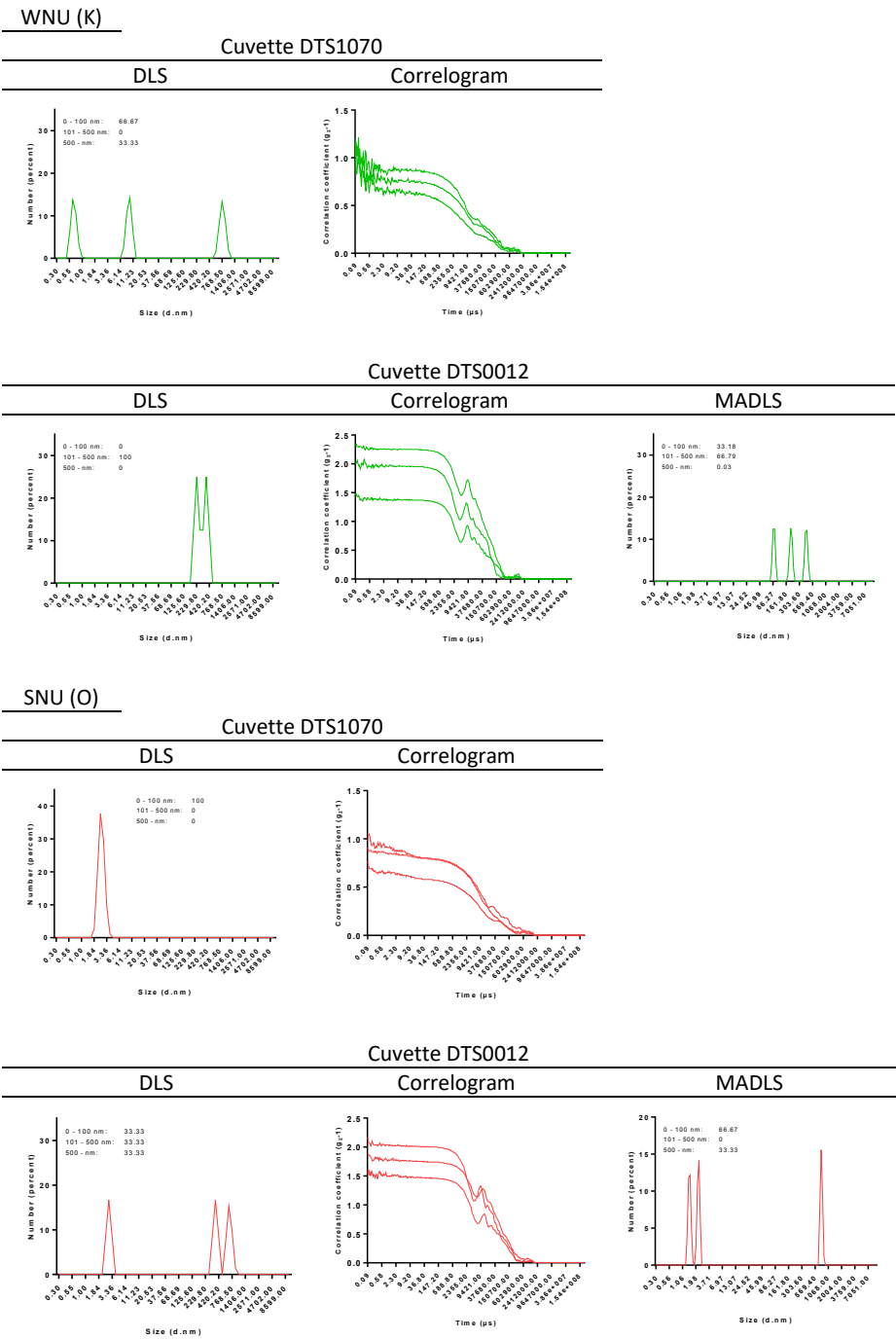
Cuvette DTS0012

DLS

Correlogram

MADLS





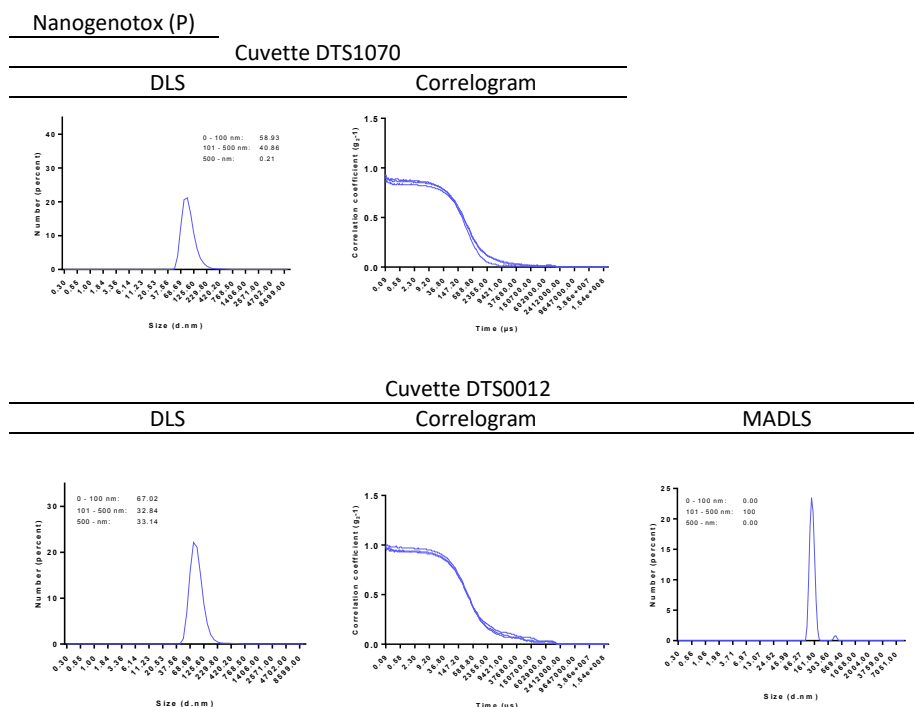


Figure S4.- As a continuation of the previous figure, the size distribution for **H, I, J, K, L, M, N,** and **O** conditions is indicated. The DLS and MADLS measurement, with their respective correlograms, are presented.

7.2. Pdf of the article entitled *Titanium-doped PET nanoplastics of environmental origin as a true-to-life model of nanoplastic*

Science of the Total Environment 880 (2023) 163151



Contents lists available at ScienceDirect

Science of the Total Environment

journal homepage: www.elsevier.com/locate/scitotenv



Titanium-doped PET nanoplastics of environmental origin as a true-to-life model of nanoplastic



Aliro Villacorta^{a,b}, Lourdes Vela^{a,c}, Michelle Morataya-Reyes^a, Raquel Llorens-Chiralt^d, Laura Rubio^a, Mohamed Alaraby^{a,e}, Ricard Marcos^{a,*}, Alba Hernández^{a,*}

^a Group of Mutagenesis, Department of Genetics and Microbiology, Faculty of Biosciences, Universitat Autònoma de Barcelona, Cerdanyola del Vallès, Barcelona, Spain

^b Facultad de Recursos Naturales Renovables, Universidad Arturo Prat, Iquique, Chile

^c Faculty of Health Sciences Eugenio Espejo, Universidad UTE, Quito, Ecuador

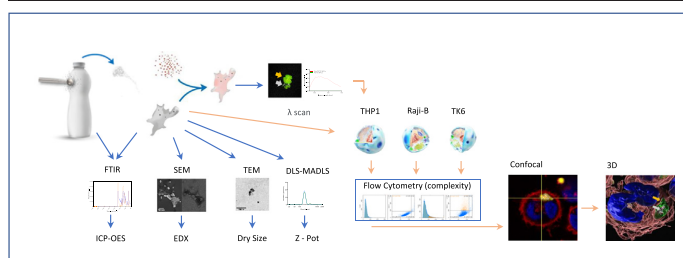
^d AIMPLAS, Plastics Technological Centre, Gustave Eiffel, 4, 46980 Paterna, Valencia, Spain

^e Zoology Department, Faculty of Sciences, Sohag University, 82524 Sohag, Egypt

HIGHLIGHTS

- Nanoplastics from opaque PET milk bottles have been obtained.
- The hybrid (PET/TiO₂NPs) nature of this material has been demonstrated.
- TEM/confocal microscopy showed the colocalization of both constituents.
- TEM(Ti)NPLs internalize differentially according to the used cell types.
- No toxic effects were observed for this true-to-life NPL.

GRAPHICAL ABSTRACT



ARTICLE INFO

Editor: Damià Barceló

Keywords:

PET(Ti) nanoplastics
Obtention
Characterization
Cell internalization

ABSTRACT

The increased presence of secondary micro/nanoplastics (MNPLs) in the environment requires urgent studies on their potentially hazardous effects on exposed organisms, including humans. In this context, it is essential to obtain representative MNPL samples for such purposes. In our study, we have obtained true-to-life NPLs resulting from the degradation, via sanding, of opaque PET bottles. Since these bottles contain titanium (TiO₂NPs), the resulting MNPLs also contain embedded metal. The obtained PET(Ti)NPLs were extensively characterized from a physicochemical point of view, confirming their nanosized range and their hybrid composition. This is the first time these types of NPLs are obtained and characterized. The preliminary hazard studies show their easy internalization in different cell lines, without apparent general toxicity. The demonstration by confocal microscopy that the obtained NPLs contain Ti samples offers this material multiple advantages. Thus, they can be used in *in vivo* approaches to determine the fate of NPLs after exposure, escaping from the existing difficulties to follow up MNPLs in biological samples.

1. Introduction

The extended use of plastic goods has results in global environmental pollution by plastic wastes, and their consequent environmental alarms (Chang et al., 2022). Although plastics have a relatively long life, degradation occurs through different physical-chemical-biological processes generating the so-called micro- and nanoplastics (MNPLs). At these sizes, and especially at the nano range, MNPLs can be easily internalized by organisms

* Corresponding authors at: Group of Mutagenesis, Department of Genetics and Microbiology, Faculty of Biosciences, Universitat Autònoma de Barcelona, Campus of Bellaterra, 08193 Cerdanyola del Vallès, Barcelona, Spain.

E-mail addresses: ricard.marcos@uab.cat (R. Marcos), alba.hernandez@uab.cat (A. Hernández).

<http://dx.doi.org/10.1016/j.scitotenv.2023.163151>

Received 30 January 2023; Received in revised form 13 March 2023; Accepted 25 March 2023

Available online 1 April 2023

0048-9697/© 2023 The Authors. Published by Elsevier B.V. This is an open access article under the CC BY license (<http://creativecommons.org/licenses/by/4.0/>).

(including humans) following different routes, finally resulting in a potential health hazard (Rubio et al., 2020a; Gigault et al., 2021; Wu et al., 2022). Thus, determining the potential hazard risks associated with MNPLs exposure is a hot and current topic.

Although great efforts have been devoted to evaluating the hazards associated with MNPLs exposure, the lack of representative environmental MNPLs is a big barrier to overcome. Consequently, most of the studies have been carried out with pristine commercial polystyrene (PS) samples that, despite their advantages (uniformity, different sizes, surface functionalization, and fluorescent staining), are not fully representative of the environmental MNPLs (Xu et al., 2022). Although PSMNPLs have been shown to be very useful for many purposes, the extrapolation of the obtained data is doubtful for human health risk assessment associated with MNPLs exposures (Brachner et al., 2020; Coffin et al., 2022). Consequently, the obtention of environmentally relevant (true-to-life) MNPLs is an urgent challenge to be achieved.

Due to the impossibility of getting enough uniform MNPLs just by picking up environmental samples, different protocols have been proposed by using the physical degradation of plastic goods, followed by the collection of the different fractions (containing MPLs or NPLs), and their ulterior characterization. Interestingly, most of the published proposals have used polyethylene terephthalate (PET) goods as the original source. This is mainly due to the high demand for this plastic type that is mainly used for packaging, including bottles for multiple purposes, although it is also a polymer widely used in the textile industry (PlasticsEurope, n.d.). Consequently, and because of the deficient recycling mechanisms and the lack of awareness on the part of society, they finally end up in the environment as plastic waste. Among the different experimental approaches, the UV-laser ablation process was first used to obtain PET-NPLs (Magri et al., 2018). Alternatively, mechanical milling is another fractionation process used to obtain mainly the MPLs fraction (Astner et al., 2019; Pignattelli et al., 2021; Lionetto et al., 2021). Furthermore, the use of mechanical ground approaches has also been proposed as an easy way to obtain PET-NPLs (Rodríguez-Hernández et al., 2019; Roursgaard et al., 2022; Villacorta et al., 2022).

Among the different types of PET bottles, we can distinguish between transparent and opaque PET ones. Opaque PET bottles are highly used many for packing milk because they provide the light protection that UHT milk requires and minimize gas permeability which, together with their low cost, are some of their advantages in front of other packaging options (Tramis et al., 2021). These characteristics of the opaque PET are due to the presence of titanium dioxide nanoparticles (TiO_2NPs) used as a filler, which also allows for reducing the bottle thickness. One of the common protocols to increase the compatibility of the fillers introduced in the plastics intend to modify their surfaces by increasing their hydrophilicity or hydrophobicity. This compatibility critically depends on the particle size of the filler because that can increase/decrease viscosity affecting the physical and chemical properties of the final compound. Since surface treatments can decrease the viscosity of the compound or masterbatch, modifications of the surface of fillers are becoming important because of its improvement in adhesion (Mozetič, 2019). Surface modifications can be achieved by the

chemical interaction of the fillers with compounds that possess functional groups, by chemical absorption on the surface of the particles of the filling material of some modifying agents, or by coating the filler particles with a suitable coupling agent (Fronza et al., 2019).

Aiming to obtain environmental representative MNPLs, we have used opaque PET bottles to obtain NPLs, following the protocol recently published (Villacorta et al., 2022). These true-to-life NPLs may help us to understand the complexity of the environmental MNPLs, while constituting unrivaled materials to be used to evaluate the potential health hazards of environmental MNPLs. Although different metals and metalloids like arsenic, cadmium, chromium (VI), and lead are normally used as plastic additives (Smith and Turner, 2020; Turner and Filella, 2021), they are present in amounts significantly less than TiO_2NPs in opaque PET bottles. The presence of such metals can suppose a potential concern from a toxicological perspective, not only for their possible leaching in environmental conditions but for their behavior in specific physicochemical conditions, such as the acidic environments encountered in the digestive tract of many animals, when MNPLs are unintentionally ingested. Beyond their potential toxicological profile, the obtention of titanium-doped MNPLs can represent a suitable true-to-life model to follow up their fate in complex matrices, including experimental *in vivo* models. Before determining the potential toxicity of MNPLs exposure, their cell uptake must be demonstrated and, if possible, quantified. These aspects have been the subject of recent reviews considering both the exposure route and the model organism used (Paul et al., 2020; Huang et al., 2022; Dusza et al., 2023).

Here we present our approach to obtain PET(Ti)NPLs, as well as their complete physico-chemical characterization. In addition, preliminary data on their behavior in human cells under *in vitro* exposure conditions is also reported. It is important to point out that this is the first report getting and analyzing NPLs from opaque PET bottles.

2. Materials and methods

2.1. PET(Ti) nanoplastics obtention

We have used commercially available opaque-PET bottles to produce PET nanoplastics containing titanium [PET(Ti)NPLs]. The used procedure was based on the recently published method designed to get PETNPLs from water bottles (Villacorta et al., 2022). The process is schematized in Fig. 1. Briefly, pieces of about 12 cm^2 were cut from the original opaque PET bottle and sanded with a diamond rotary burr accessory, taking particular attention not to overheat the surface by passing in only one direction and only once on the same area. The obtained opaque PET debris was passed through a 0.20 mm sieve and 4 g of the resulting material was dispersed on 40 mL of trifluoroacetic acid pre-heated to 50°C on a stirring plate at 100 rpm for 2 h and then kept under continuous agitation at room temperature overnight. The next day, 40 mL of TFA (20% , v/v) were added and the mixture was kept under constant stirring for 24 h more. The suspension was then passed through the 0.20 mm sieve, to eliminate the bigger pieces, and centrifuged at 2500 rcf for 1 h once distributed on six 10 mL glass tubes. The obtained pellets were resuspended on 400 mL

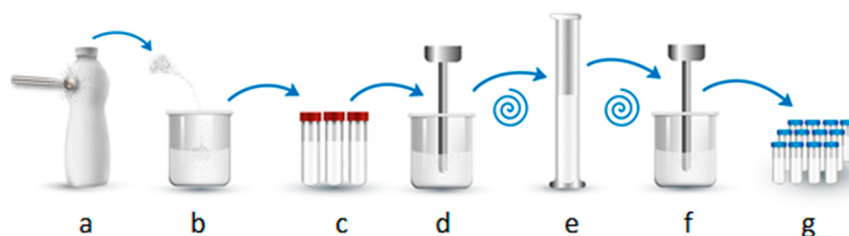


Fig. 1. Schematic representation of the PET(Ti)NPLs production. Opaque PET fragment from bottles were grinded until a powder is obtained, passed through the sieve (a), stirred, suspended, and heated at different concentrations of TFA (b), distributed on glass tubes and centrifuged (c), resuspended on SDS, sonicated (d), and transferred to a cylinder for sedimentation (e) and then collected, washed, weighted, resuspended and sonicated (f) and aliquots were prepared and stored frozen until needed (g).

of a 0.5 % sodium dodecyl sulfate (SDS) solution, vigorously mixed, distributed into two 200 mL beakers, and ultrasonicated on an SSE-1 Branson sonicator (Branson Ultrasonics Co., Brookfield, CT, USA) for 2 min at 25 % amplitude, in 9/9 s sonication/break cycles. The content of each beaker was transferred to a graduated cylinder to sediment for 1 h, to eliminate the bigger fraction. The top 100 mL of each cylinder were collected and centrifuged to eliminate SDS. Pellets were washed twice with Milli-Q water and twice with pure ethanol and dried under sterile air laminar flow. Pellets were then weighted and resuspended on Milli-Q water at concentrations of 10 mg/mL. Suspensions were then sonicated for 16 min at 10 % amplitude in a cold-water bath and stock solution aliquots of 1 mL were immediately frozen on cryotubes in liquid nitrogen and stored at -80°C for further use.

2.2. PET(Ti)NPLs characterization by transmission electron microscopy (TEM)

A carbon-covered copper grid was dipped into the working solution (200 $\mu\text{g/mL}$) and allowed to evaporate overnight. Particles in the grid were examined by TEM using a JEOL JEM 1400 instrument (JEOL Ltd., Tokyo, Japan) operated at 120 kV. TEM images were analyzed for particle size distribution by measuring the Martin diameter using the ImageJ software 1.8.0.172 and processed with the GraphPad Prism 7.0 software (GraphPad, San Diego, CA). The Savitzky-Golay-like filter was applied to smoothen the curve.

2.3. PET(Ti)NPLs characterization by scanning electron microscopy (SEM) & energy dispersive X-ray spectroscopy (EDS)

From the stock solution, a working solution of 200 $\mu\text{g/mL}$ was prepared by thawing in a warm bath at 37°C and diluted in Milli-Q water. The working solution was vigorously vortexed and 10 μL of the suspension were deposited on a silica holder. Water was evaporated from the sample and examined on an SEM Zeiss Merlin (Zeiss, Oberkochen, Germany) coupled with an X-Max 20 mm EDS system (Oxford Instruments, Oxford, UK). In addition to collecting SEM images, an area including the nanoparticle surface was selected for the EDX analysis, the signal was collected and analyzed by the INCA Energy software (INCA, Grinnell, IA, USA).

2.4. PET(Ti)NPLs characterization by multi-angle and dynamic light scattering (DLS-MADLS), and zeta potential

The indicative size of the colloid structures in the suspension of the PET (Ti)NPLs was determined using a Zetasizer® Ultra device from Malvern Panalytical (Cambridge, United Kingdom). To such end, a working solution of 100 $\mu\text{g/mL}$ of PET(Ti)NPLs was used. Additionally, to investigate the influence of the culture media in the nanoplastic dispersion, the same concentration was prepared by using the Nanogenotox dispersion protocol (Nanogenotox, 2011), and its behavior was evaluated on both Milli-Q water and on FBS supplemented RPMI (Roswell Park Memorial Institute) medium supplemented with 10 % fetal bovine serum (FBS), 1 % glutamine (Biowest, France), and 2.5 $\mu\text{g/mL}$ of Plasmocin™ 226 (InvivoGen, CA, USA).

2.5. PET(Ti)NPLs characterization by Fourier transform infrared spectroscopy (FTIR)

To detect functional groups, and to identify samples as PET, materials at different stages of the production process were used. Thus, pieces of original materials (water- and opaque-bottles), midterm production sanded material before acid exposure, and final nanoparticle samples were analyzed and compared. For PET(Ti)NPLs from the stock solutions (10 mg/mL), a drop was placed on a gold mirror and let dry for one week inside a Petri dish. For the solid samples, 3×3 cm pieces for both PET bottle types were cut directly from bottles. For the above-described materials (suspension and solids original samples), the analysis was carried out on a Vertex 80 device, while the dust of polymer-metal obtained from the sanded material was analyzed by using a Tensor 27 device. Both types of equipment

were from Bruker (Bruker Corporation, Billerica, Massachusetts, USA). To assess the composition, the obtained interferograms were analyzed and contrasted with previously reported data.

2.6. PET(Ti)NPLs characterization by mass spectroscopy

To determine the Ti content of the original PET source, 0.10 g of the PET (Ti) film was weighted on a Mettler Toledo XP205DR analytical balance (Mettler-Toledo S.A.E., Barcelona, Spain). This amount was dispersed in Milli-Q water to the same concentration than the stock PET(Ti) (10 mg/mL). In an independent way, 0.25 mL of the two dispersions were vigorously agitated and digested in 5 mL of a mixture (4 mL HNO_3 65 % (p/v) and 1 mL of HF 40 % (p/v)) in a microwave oven for 20 min at 260°C (ramp 25 min to reach 260°C). Samples were diluted on HNO_3 (1 % v/v) before injection. The Ti content of the samples was determined on an inductively coupled plasma optical emission spectrometer ICP-OES Agilent 5900 (Agilent Technologies, Santa Clara, CA, USA).

2.7. PET(Ti)NPLs labeling and confocal visualization

To visualize/identify PET(Ti)NPLs on confocal microscopy, the reflection property was used for the detection of Ti. To visualize PET, separately from Ti, samples were labeled with iDye Poly Pink (iDye), following an adaptation of the published protocols to dye microplastics (Karakolis et al., 2019; Nguyen and Tufenkji, 2022). Briefly, a working solution of 1 mL of PET(Ti)NPLs at the concentration of 5 mg/mL was prepared from the stock dispersion (10 mg/mL) and transferred into a 1.5 mL tube containing previously weighed 0.01 g of the textile dye (iDye) used for synthetic fibers. The mixture was vigorously vortexed and incubated for 2 h at 70°C on a glass tube. After cooling at room temperature, 9 mL of Milli-Q water was added to the suspension and then centrifuged at 4000 rpm on an Amicon® Ultra-15 centrifugal Ultracel®-100 K filter 1×10^5 MWCO for 15 min. This step was performed twice to remove the excess of iDye. The washed particles were then collected and suspended in the final volume of 1 mL of Milli-Q water and stored protected from light at 4°C until needed. Here on, these stained PET(Ti)NPLs are named iDyePET(Ti)NPLs. For their visualization in the confocal microscope, the particle suspension was diluted on Milli-Q water at a final concentration of 400 $\mu\text{g/mL}$ and two drops of 20 μL were placed on a slide, covered with a coverslip, and let dry inside the biosafety cabinet on air laminar flow. PET(Ti)NPLs were prepared similarly to be used as control. Both slides were examined by confocal microscopy using a Leica TCS SP5 confocal microscope. Excitation wavelength of 561 nm was set on an acousto-optic tunable filter (AOTF 561) and, emission spectra was collected between 580 and 700 nm (lambda scan begin bandwidth 575.00–585.00 nm to lambda scan end bandwidth 691.00–701.00 nm). Emission was analyzed using the Leica Application Suite X 3.7.5.24914 (Leica Microsystems CMS GmbH Wetzlar, Germany). Images were collected under the same conditions, further explained on Section 2.10.

2.8. Cell culture

To determine the cell internalization ability of PET(Ti)NPLs, three human hematopoietic cell lines were used. Thus, THP-1 monocytes, TK6 lymphoblasts, and Raji-B B-lymphocytes were selected as a widely distributed and accepted lymphoblastic human cell models. All three cell lines were purchased from Sigma Aldrich (MO, USA). Cells were grown in T-25 flasks on RPMI medium (Biowest, France) supplemented with 10 % FBS, 1 % glutamine (Biowest, France), and 2.5 $\mu\text{g/mL}$ of Plasmocin (InvivoGen, CA, USA). Cultures, with a density ranging from 5×10^5 to 1×10^6 cells, were maintained at 37°C in a humidified atmosphere of 5 % CO_2 .

2.9. PET(Ti)NPLs cell uptake (internal complexity), as determined by flow cytometry

To quantify cell internalization, the internal complexity of the exposed cells was used as an indicator of internal structural cell complexity and

determined by flow cytometry. To proceed, the three selected cell lines (TK6, Raji-B, and HTP-1) were grown on U-bottom 96 well plate at a cell density of 5×10^5 cells/mL on a final volume of 0.20 mL and treated with concentrations of 25, 50, and 100 $\mu\text{g/mL}$ for a 24 h period. Once PET(Ti)NPLs uptake takes place, the orthogonal light scattering – commonly known as Side Scatter (SSC) – was evaluated using a flow cytometer Cytoflex S (Beckman Coulter CytoFLEX S). A total number of 10,000 events (single cells) were scored and evaluated using the CytExpert software and data was processed using GraphPad Prism Software 7.0. (GraphPad, San Diego, CA).

2.10. PET(Ti)NPLs cell uptake determination by confocal microscopy

For the visualization of internalized PET(Ti)NPLs into the cells, confocal microscopy was used using the protocol recently described (Annangi et al., 2023). Nuclei were stained using Hoechst 33342 (excitation of 405 nm and emission collected at 415–503), and cell membranes were dyed using Cellmask (excitation of 633 nm and emission collected at 645–786). For iDyePET(Ti)NPLs, an excitation wavelength of 561 nm and emission collected at 570–630 were used. For the localization of Ti, reflection images were obtained in parallel. Images of each sample were obtained using a Leica TCS SP5 confocal microscope and processed using ImageJ processing and analysis software, version 265 1.8.0.172.

2.11. Cell viability effects of PET(Ti)NPLs in the used cell lines

To assess the cell viability of the three hematopoietic cell lines after exposure, cells were seeded on the same conditions as previously described at a cell density of 5×10^5 cells/mL on a final volume of 0.20 mL on U-bottom 96 well plates and treated with concentrations ranging from 0 to 100 $\mu\text{g/mL}$ for a 24 h period at standard conditions. Cells were then mixed and diluted 1:100 on ISOFLOW and counted with a ZTM coulter counter (Beckman Coulter Inc., CA, USA). The average number of cells counted on each treatment was compared with the average number of the untreated control cells and data was evaluated using GraphPad Prism Software 7.0. (GraphPad, San Diego, CA).

3. Results and discussion

The PET(Ti)NPLs samples obtained according to the protocol outlined in Fig. 1 were used for further characterization. It should be remarked the large amount of material obtained in the extraction process above described. The resulting 10 vials of 1 mL of the stock dispersion (10 mg/mL) were stored at -80°C . Working solutions were prepared following the Nanogenotox protocol and aliquoted in 10 vials containing 0.2 mL of a concentration of 5000 $\mu\text{g/mL}$. This means that a standard PET(Ti)NPLs production generate 100 vials of the working dispersion, which were stored at the same conditions until used. This is a large amount that permit to carry out several rounds of studies aiming to perform a complete characterization and they hazard evaluation. The original process

(Villacorta et al., 2022) has been used several times from PET water bottles to get more material to be spread among the PlasticHeal consortium, showing a very high repeatability.

3.1. Dry state size distribution and shape

TEM was used to determine the morphology and the size of the obtained PET(Ti)NPLs. The obtained figures were compared with those previously obtained from transparent PET bottles (Villacorta et al., 2022). In Fig. 2 it is indicated the morphology of PETNPLs (a) as compared with PET(Ti)NPLs (b and c). As observed, it is relatively easy to detect differences on the electrodensity of the sample when Ti is present. The presence of TiO_2NPs results in high-density points. Obviously, the degree of agglomeration can also be a factor modulating density. When the Martin diameter was measured for more than one hundred PET(Ti)NPLs figures, a mean size of 382.07 nm with a polydispersity index of 0.37 was obtained. Interestingly, the high electrodensity of TiO_2NPs also permitted to determine their size distribution inside the PET(Ti)NPLs complex, as indicated in Fig. 2d.

From the size distribution it is obvious that the average exceeds the range of the nanoparticles (or by extension of a nanoplastic) definition. The last recommendation of the European Commission state that, at least the 50 % of the particles contained in a dispersion must be in the nano-range, and at least one dimension must be in the 1–100 nm range (European Commission (EC), 2022). Nevertheless, this definition looks appropriated for the engineered nanomaterials, and by extension for the primary nanoplastics, but not seems adequate for secondary nanoplastics resulting from the degradation of macroplastic goods, were a large range of sizes and shapes are expected. To describe the new true-to-live obtained nanoplastics we propose to take into consideration the proposal of Hartmann et al. (2019). These authors propose to categorize MNPLs according to the conventional units of size: nano (1–1000 nm) and micro (1–1000 μm). Although the authors divide the nano range between nanoplastics (1–100 nm) and submicron-plastics (100–1000 nm), this division add more darkness than light. Thus, from the operational point of view our sample of PET(Ti)NPLs distribution falls into the nano range.

3.2. Dry state morphology and composition

To better identify the PET(Ti)NPLs morphology and composition, SEM-EDS methodologies were used. Fig. 3a and b show the observed morphologies. It must be noted that due to the high electrodensity of Ti, the morphological visualization of PET is affected, and the figure definitions are not optimal. It is important to note the morphology of the TiO_2NPs showing their nanorod shape. Considering the average length of the TiO_2NPs nanorod present in the PET(Ti)NPLs it is assumable the size distribution determined by TEM, since it is difficult to find PET structures not associated to TiO_2NPs .

As previously indicated, different metals and metalloids like arsenic, cadmium, chromium (VI), and lead are normally used as plastic additives

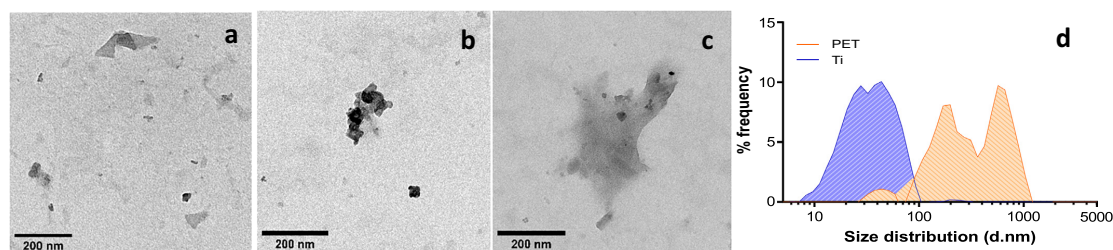


Fig. 2. TEM figures from in-house secondary PETNPLs (a) compared with PET(Ti)NPLs (b, c). The presence of TiO_2NPs is detected as a high density spots. Size distribution for PET(Ti)NPLs was determined, and a bimodal distribution was observed (orange). Due to the good detection of TiO_2NPs , their size distribution (Martin diameter) was also determined (blue).

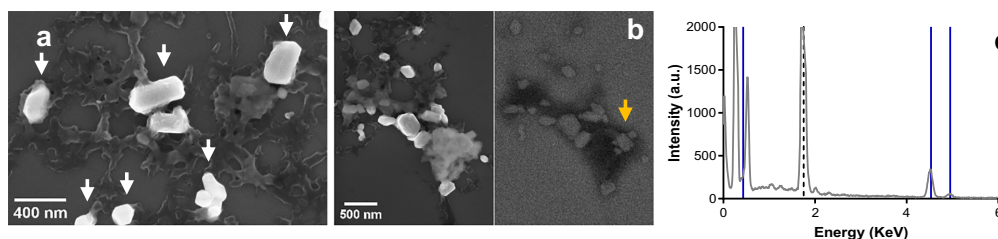


Fig. 3. SEM figures of PET(Ti)NPLs show TiO₂NPs embedded on nano-PET structures both on secondary electrons view (a), and both secondary (b, left) and backscattered (b, right) electrons. On (a) the white arrows indicate the TiO₂NPs, and on (b) the yellow arrow indicates the TiO₂NPs that are not easily visible due to the polymer covering. The EDS spectrum observed on (c), show the characteristic peaks of Ti remarked on blue, and the dashed line indicates the Si holder interference.

and, consequently, they can be found in their derived MNPLs (Turner and Filella, 2021). Nevertheless, the levels of titanium present in the MNPLs resulting from opaque bottles, like the obtained in this study, are very much high and impregnating the resulting MNPLs. This could suppose an associated hazard risk for such type of MNPLs. It should be remembered that Ti compound, and by extension TiO₂NPs, is a recognized food additive (E171), wide used in many food matrices (Cornu et al., 2022), were the E letter codes for substance that can be used as food additives. In addition to the multiple studies looking for potential hazards associated with E171 use, a recent publication from the panel on Food Additives and Flavorings from the European Food Safety Authority (EFSA) indicates that, “based on all the evidence available, E171 can no longer be considered as safe when used as a food additive” (EFSA Panel on Food Additives and Flavorings (FAF) et al., 2021).

Nevertheless, PET(Ti)NPLs samples can result very useful for specific purposes. The need to detect the fate of MNPLs in complex environmental matrices has been outlined as a special challenge. In the same way, to determine the fate of MNPLs in complex organisms like mammals is another important challenge. To overcome this problem, the use of metal-doped nanoplastics has been proposed (Mitrano et al., 2019; Clark et al., 2022). Nevertheless, these type of nanoplastics are far from the representative secondary MNPLs present in the environment. From this point of view our PET

(Ti)NPLs would cover two main aspects, i) are MNPLs containing metal that can be used to determine their fate in experimental mammalian models, and ii) are true-to-life representative environmental MNPLs.

3.3. PET(Ti)NPLs size distribution and zeta potential in aqueous solution

The hydrodynamic behavior of PET(Ti)NPLs dispersed on Milli-Q water, or following the Nanogenotox protocol, shows mild differences among them. Independently of these mild differences, they show that there is a need of standardized procedures when it comes to nanoplastic dispersions. At this point is relevant to point out that, independently of the dispersion used, all obtained values do not differ importantly from the values obtained when TEM approaches were used (382.07 nm).

As observed on Fig. 4a–d, in terms of size distribution in number percentage, the curves whether on water or RPMI supplemented media almost overlap, and the Z-average shows no significant differences except for the behavior of PET(Ti)NPLs on supplemented RPMI, when compared with water dispersion using the one-way ANOVA with Dunnett multiple comparison test with a significance of 0.05. These data indicate that the surface coating of the particles is relevant in terms of hydrodynamic behavior when complex matrices must be used. This not only apply for *in vitro* studies but mainly for *in vivo* studies, pointing out the need of establish

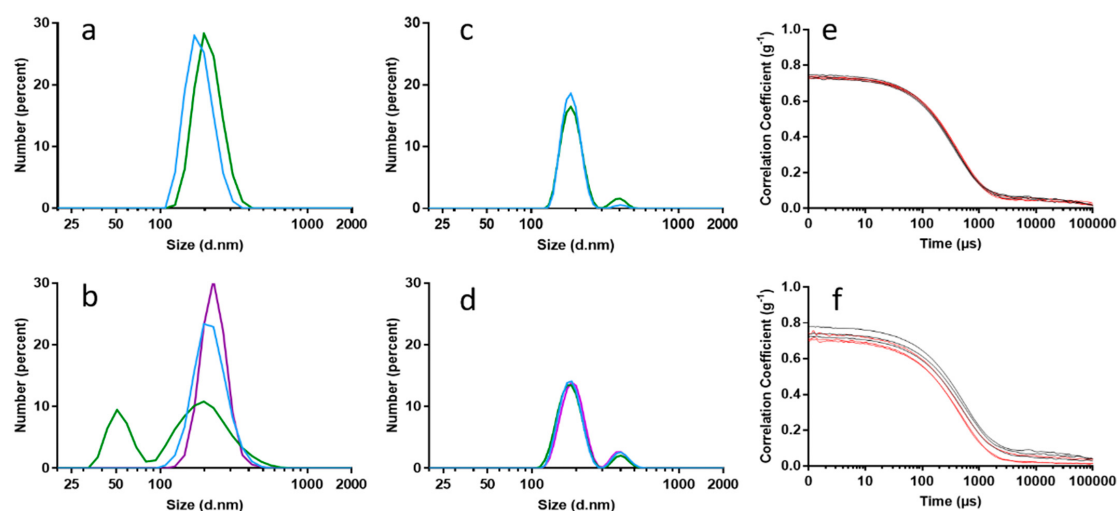


Fig. 4. Size distribution analysis of PET(Ti)NPLs on MilliQ water (a, c) and on supplemented RPMI media (b, d) are shown by DLS (a, b) and (MADLS) (c, d) on Milli-Q water (light blue line on all charts) and on the Nanogenotox dispersion protocol (green line on all charts). Additionally multiple narrow measurements (purple lines on b and d) are shown. All correlation measurements are shown at the right side of the corresponding line (e, f, respectively).

Table 1
Description of hydrodynamic measurements.

Sample	Z-average	PDI	Z-potential*
PET(Ti)NPLs — Milli-Q	308.00 ± 6.10	0.36	−33.10 (1)
PET(Ti)NPLs — Nanogenotox	320.00 ± 8.18	0.34	−18.23 (2)
PET(Ti)NPLs — RPMI — Nanogenotox	287.00 ± 16.10	0.40	−9.51 (3)
PET(Ti)NPLs — RPMI	357.00 ± 36.50 ^x	0.41	−6.96 (4)

* Significant differences in Z-potential values were determined by the one-way ANOVA analysis, with a Tukey's multiple comparison test. Comparisons were established between dispersion conditions (1–4) as follows: (1–2**) (1–3***), (1–4***), (2–3*), (2–4*), and (3–4^{ns}). [ns: non-significant; * $P < 0.05$, ** $P < 0.01$; *** $P < 0.001$]. ^x significant ($P < 0.05$) in comparison with Milli-Q water dispersion.

implemented dispersion protocols of nanoplastics as a good practice in terms of keeping the dispersed nanoplastics in the nanoscale range. This is a relevant key factor when different biological endpoints must be further tested. The differences in the Z-average when the BSA is added to the PET (Ti)NPLs dispersion and tested on supplemented RPMI culture medium may result in an electrostatic stabilization and this can be depicted not only in the already described changes but also in the Z-potential differences (Table 1) where the surface charge of the particle is dramatically shifted. In terms of significance, and regarding the Z-potential values, only PET(Ti)NPLs suspended on RPMI with or without the Nanogenotox protocol are not significantly different. When water dispersion values are compared with the other dispersion protocols, very significant differences for Z-potential values are observed. The particles dispersed in complex matrices tend to present a higher value of heterogeneity, which can be confirmed by observing that the values of this type of dispersion are above 0.40 in terms of the polydispersity index (PDI), while the dispersions in water do not exceed this value. In both cases, the values are not excessively low.

3.4. Chemical determination of the PET(Ti)NPLs and Ti content quantification

As the FTIR methodology is suitable for the analysis of films, suspensions, and powders, we have used this tool to confirm the chemical identity of our PET(Ti)NPLs. This approach was used not only for the characterization of the final nanomaterial product, but also for the original commercial material (opaque PET films) and for the PET(Ti) powder obtained in the mid-step part of the process of our PET(Ti)NPLS generation. The main reason of this sequential analysis was to demonstrate that not changes in the original chemical (PET) nature was produced in the nano PET obtaining process. As observed in the Fig. 5 no significant differences in the obtained spectra are observed, confirming that the different steps carried out in the process does not modify the PET chemical nature. Thus, we can observe

how the simultaneous determination of the organic component of the sample are consistent and correspond with the spectra of PET previously reported on literature (Chen et al., 2013; Johnson et al., 2021), as well as in our previous work (Villacorta et al., 2022).

As a control, regular commercially available PET samples, as well as the nanoparticles produced from their degradation are also presented (Figs. 5a, b). We assume that during the degradation process, a fraction of the original material is lost. We specifically ask if part of the titanium content could be lost during the process. To such end we determined the percentage of titanium in the original film and in the resulting nanoplastic. Results indicate that the titanium content of the opaque PET films was 3.83 %, which was reduced to 2.60 % in the resulting PET(Ti)NPLs. Results for ICP-OES for the resulting PET(Ti)NPLs were very consistent and the variability among replicates was low, never been higher than 1 µg/mL, and the relative standard deviation (RSD) was never higher than 7 %. On the other hand, for opaque PET film, the differences among replicates were never higher than 0.1 mg/g and the RSD was never higher than 0.6 %. We assume that during the different ultracentrifugation steps, some titanium (possibly due to its high weight) is lost. Nevertheless, a very important fraction remains associated to the final product of the degradation process. Although no indications on the potential leakage of titanium from the opaque bottles have been found, such plastic can suppose many problems entering in the recycling processes (Tramis et al., 2021).

3.5. PET(Ti)NPLs labeling and confocal visualization

In this study we successfully dye PET(Ti)NPLs with the commercially available textile dye *iDye Poly Pink* by heating the nanoplastic/dye mixture allowing the swelling of the polymer at the time that allowing the dye entering the polymeric matrix, achieving that within the polymeric matrix we can find both the titanium and the *iDye*. Particles were then resuspended and washed on Milli-Q water to remove the excess of pigment not attached to the particles, as previously described and depicted on Fig. 6a. *iDye*PET(Ti)NPLs shows a significant amount of fluorescence easily observed by confocal microscopy where fields with significant particle agglomerates were located and the emission collected (Fig. 6b, c, d). Consistent with previous reports (Karakolis et al., 2019) the fluorescence on PET was easily observed by this staining approach with the main difference that in our study we use nanoplastic instead of microplastics. In a recent study, authors shows that a commercially available dye (Atto 647N) can be used for similar approaches to stain different pristine NPLs (Nguyen and Tufenkji, 2022). It is necessary to remark that in our approach, in house made true-to-life nanoplastic have been used showing the suitability of our method not only for the type of polymer but also for size differences,

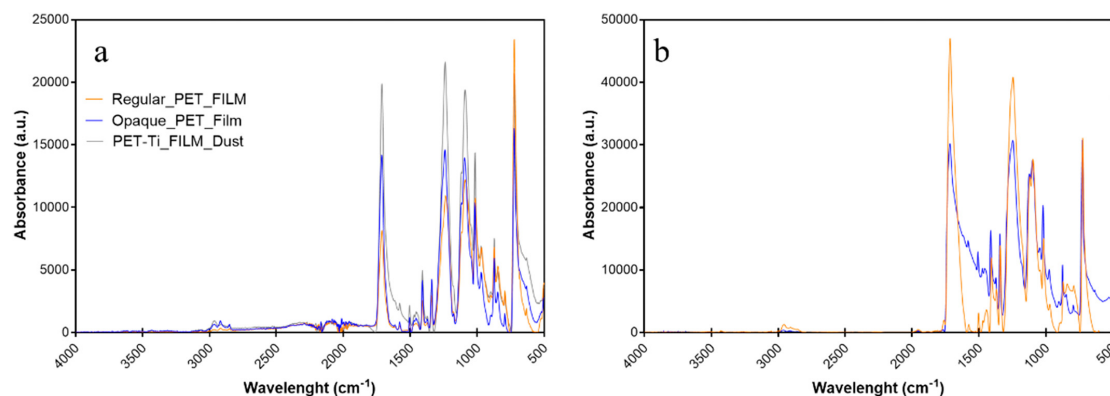


Fig. 5. FTIR spectra of the principal peaks of the interferogram. On the left chart (a) regular (orange), opaque PET (blue), and opaque PET dust produced from degradation process spectra are shown. On the right chart (b) PETNPLs (orange) from regular PET film and PET(Ti)NPLs (blue) from opaque PET are shown.

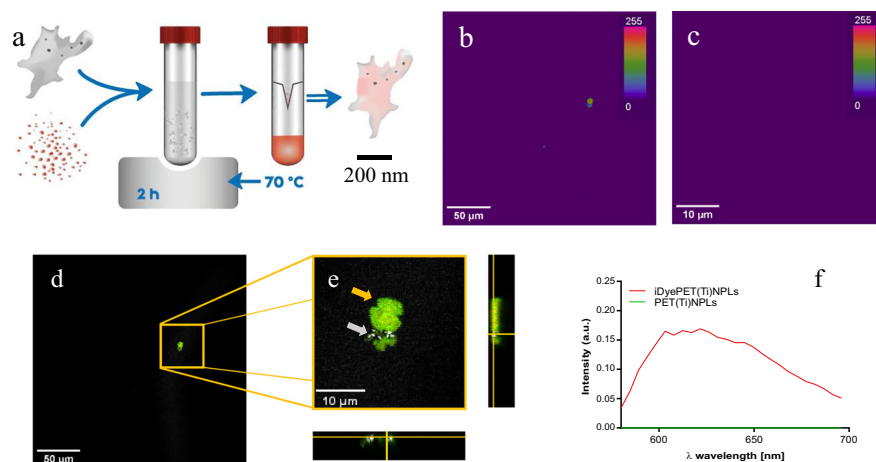


Fig. 6. a) Staining procedure: PET(Ti)NPLs were mixed with iDye Poly pink and heated at 70 °C for 2 h, then filtered, and finally resuspended. Labeling was evaluated by confocal microscopy acquiring images of the fluorescence where iDyePET(Ti)NPLs and PET(Ti)NPLs were observed agglomerated (b, c, respectively). d) When the signal for both iDye (yellow arrow) and Ti (grey arrow) were used, both signals appear together as indicative of the PET(Ti)NPLs identification. f) The emission spectra for both particles were collected and compared (green signal overlap the X-axis).

due to the polydisperse nature of our material. As shown in Fig. 6d, signals corresponding to PET and Ti co-localize, demonstrating the mixed nature of PET(Ti)NPLs. Finally, no fluorescence signal for iDye was detectable on fields where PET(Ti)NPLs were the only component.

3.6. Cellular uptake evaluation

The potential harmful effects induced by MNPLs exposure require their previous internalization. There are different approaches to measure such uptake, and in this study we have used both flow cytometry and confocal microscopy. By using flow cytometry, the intensity of the side-scattered light revealed that the particles were taken up in the cells, as initially proposed (Suzuki et al., 2007). This method has been used to detect the uptake of different nanomaterials including titanium nanoparticles, by measuring the complexity of the BEAS-2B cells (Vales et al., 2015). In our study, this method has been applied to different hematopoietic cell lines to determine potential differences according to the used cell type. If MNPLs can cross the protective barriers, they move to the general compartment (blood), interacting with their respective components. Thus, blood cells can be considered as a general target to be used to determine the potential effects of any exposure including MNPLs and more specifically PET(Ti)NPLs. The obtained results are indicated in Fig. 7, for three well-known leukocytic cell lines: TK6 lymphoblastic, Raji-B lymphocytes, and THP-1 monocytic cells (Rubio et al., 2020b). As observed, the PET(Ti)NPLs uptake differs among the cell lines, leukemic monocytes (THP-1) showing the highest increase on cell complexity after exposures lasting for 24 h, and at all tested concentrations. Contrary, the lymphoblastic TK6 show practically no uptake. This differential uptake was also reported for polystyrene NPLs using the same leukocytic cells (Rubio et al., 2020b), as well as for three different white peripheral blood cells (lymphocytes, monocytes, and polymorphonuclear cells) (Ballesteros et al., 2020). Accordingly, the complexity of the uptake response must be considered in the selection of the cells to be used in any experiment aiming to evaluate hazardous effects of MNPLs.

As indicated, cell uptake can also be determined by using confocal microscopy, as observed in Fig. 8. For this approach we focus our attention on THP-1 cells since this cell line showed the highest uptake in the flow cytometry approach. Interesting, we could colocalize both the signal coming from the emission of the iDye on the iDyePET(Ti)NPLs and the signal from Ti. This is observed when Fig. 8b and c are compared, indicating the

hybrid composition of the obtained PET(Ti)NPLs. The orthogonal views confirm the complex structures previously observed by using electronic microscopy (whether transmission or scanning) but this time inside a cell, as expected according to the complexity results obtained by flow cytometry. It is necessary to point out that not all the Ti remains attached to the PET MNPLs, since a fraction of the total is lost during the obtention process, as we describe on the Section 3.4, and quantify by ICP-OES. Nevertheless, the colocalization signals give relevant information supporting the mixed nature of the obtained true-to-life PET(Ti)NPLs.

3.7. PET(Ti)NPLs effects on cell viability

As a final approach in the exhaustive evaluation of the characteristics of the obtained true-to-life PET(Ti)NPLs, the harmful effects in different human cell lines were determined in terms of cell survival. The obtained results are depicted in Fig. 9.

Despite the previous results, showing notorious differences on the uptake among the different selected cell lines, no significant decreases on cell viability were noticeable for any tested concentration nor cell line. This would confirm that the obtained true-to-life NPLs are not toxic, at

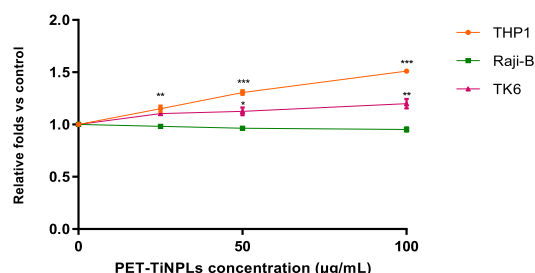


Fig. 7. Cellular internalization of PET(Ti)NPLs by Raji-B, TK6, and THP-1 cells after exposures lasting for 24 h. Graphs show the mean \pm SEM of three different experiments performed in duplicates. Complexity was compared with untreated cells using a One-way ANOVA analysis with Dunnett multiple comparisons post-test. (** $P < 0.01$; *** $P < 0.001$).

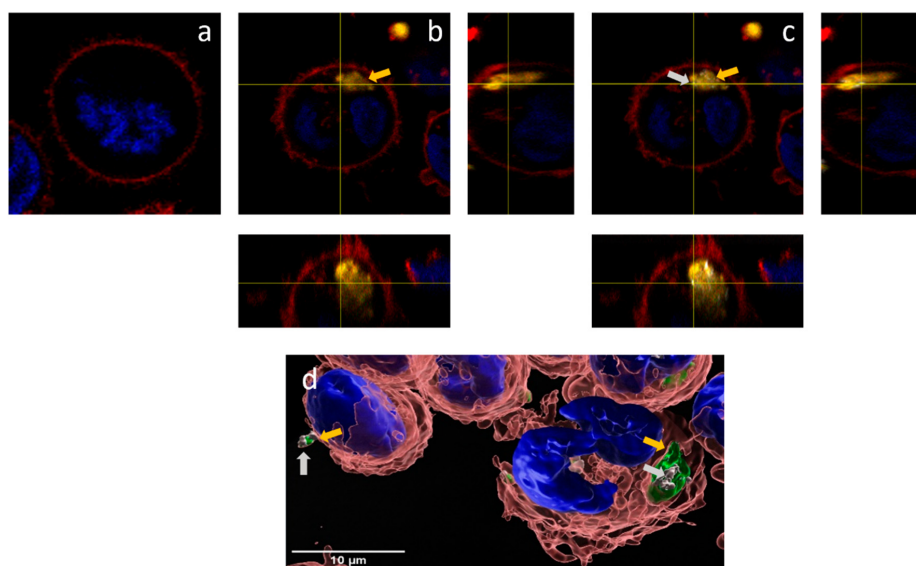


Fig. 8. Confocal microscopy uptake detection of iDyePET(Ti)NPLs in THP-1 cells, following 24 h exposure to 100 µg/mL. a) Control, untreated cells. b) Orthogonal view of THP1 cell with the Ti nanoparticles channel off and showing only iDye signal (yellow arrow). c) Co-localization of the Ti signal (grey arrow) with the PETNPLs emission. Arrows indicate both iDye and Ti signals. d) Imaris image reconstruction.

least in the used hematopoietic cell lines and detecting effects on cell viability. This would agree with previous experiments exposing these cell lines to polystyrene nanoparticles, where not viability effects were observed in that range of exposures lasting for 24 h, and only mild effects when concentrations range to high levels such as 200 µg/mL (Rubio et al., 2020b). The lack of effects on cell viability of PET(Ti)NPLs is like our previous report using true-to-life PETNPLs obtained from sanding water bottles material (Villacorta et al., 2022), and from other secondary nano PET particles obtained following other degradation procedures (Magri et al., 2018; Dhaka et al., 2022). Although the PET component is not considered as potentially toxic, what about the other component (TiO₂NPs)? It should be remembered that TiO₂NPs were authorized as a food additive (E171) in the EU, according to Annex II of Regulation (EC) No 1333/2008. A recent review conducted by the European Food Safety Authority (EFSA) on the safety of

TiO₂NP used as food additive concluded that not toxic/harmful were identified, but a concern on their potential genotoxicity cannot be ruled out (EFSA Panel on Food Additives and Flavourings (FAF) et al., 2021). Accordingly, our data would agree with the assumed non-harmful effects of PET(Ti)NPLs exposure. It is obvious that cell viability is just the first step in the evaluation of the potential toxicity of PET(Ti)NPLs. Consequently, further extensive studies using a wide set of biomarkers are required to rule out the existence of any type of harmful effects associated to the secondary MNPLs resulting from the degradation of opaque plastic goods.

4. Conclusions

True-to-life representative MNPLs, resulting from the degradation of environmental plastic waste, are urgently required to be used as a model for determining their potential hazards. In this context, the content of this study reports the obtention and characterization of MNPLs resulting from the degradation of opaque milk plastic bottles [PET(Ti)NPLs] which contain TiO₂NPs. This is the first study reporting the obtention/characterization of this type of MNPLs. In addition to the multiple physicochemical assays determining the hybrid chemical nature of the obtained material, size and shape confirmed their nano range size. The preliminary studies on their biological effects show an important but variable cell uptake, depending on the used cell line. Although no significant cell viability effects were observed in any of the used cell lines, further and complex studies are necessary to have a clear view of their potential health hazards. It must be pointed out that confocal microscopy images reported that both, in the dispersion media or internalized inside the cells, PET and Ti signals colocalize. This offers an important advantage to the obtained NPLs since they can be used in *in vivo* studies to demonstrate their fate inside the organism, thanks to the easy identification/localization/quantification of internalized Ti.

CRediT authorship contribution statement

RM and AH planned the experiments. AV, LV, MMR, RLC, LR, and MA carried out the experimental part. AV analyzed the data, carried out the

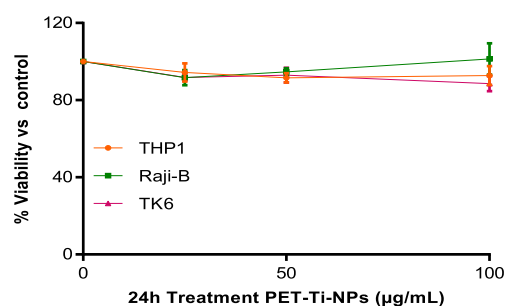


Fig. 9. Viability of hematopoietic THP-1, TK6, and Raji-B cells after exposures to PET(Ti)NPLs at concentrations ranging from 0 to 100 µg/mL for 24 h. The graph represents the viability relative to untreated cells. Graphs show the mean \pm SEM of three different experiments performed in duplicates. One-way ANOVA analysis with Dunnett multiple comparisons post-test with a confidence level of 95 % was performed.

statistical analysis, and prepared tables/figs. AV, RM, and AH wrote the final manuscript.

Data availability

Data will be made available on request.

Declaration of competing interest

The authors declare that they have no known competing financial interests or personal relationships that could have appeared to influence the work reported in this paper.

Acknowledgments

A. Villacorta was supported by PhD fellowships from the National Agency for Research and Development (ANID), CONICYT PFCHA/DOCTORADO BECAS CHILE/2020-72210237. L. Vela was supported by PhD fellowships from the Fundación Carolina. L. Rubio hold a postdoctoral Juan de la Cierva contract (IJC2020r26861/AEI/10.13039/501100011033). M. Alaraby hold a Maria Zambrano postdoctoral contract (code 693063) from the Spanish Ministerio de Universidades, funded by the European Union-Next GenerationEU, at the UAB. Morataya-Reyes hold a Ph.D. FI fellowship from the Generalitat de Catalunya, A. Hernández was granted an ICREA AC-ADEMIA award.

This project has received funding from the European Union's Horizon 2020 research and innovation programme under grant agreement No 965196. This work was partially supported by the Spanish Ministry of Science and Innovation (PID2020-116789, RB-C43) and the Generalitat de Catalunya (2021-SGR-00731).

We thank the Molecular Inorganic Nanoparticles Group at the *Institiut Català de Nanociència i Nanotecnologia* (ICN2-UAB-CSIC-BIST) at the UAB campus for using their premises.

References

- Annanig, B., Villacorta, A., López-Mesas, M., Fuentes-Cebrian, V., Marcos, R., Hernández, A., 2023. Hazard assessment of polystyrene nanoplastics in primary human nasal epithelial cells, focusing on the autophagic effects. *Biomolecules* 13, 220. <https://doi.org/10.3390/biom13020220>.
- Astner, A.F., Hayes, D.G., O'Neill, H., Evans, B.R., Pingali, S.V., Urban, V.S., Young, T.M., 2019. Mechanical formation of micro- and nano-plastic materials for environmental studies in agricultural ecosystems. *Sci. Total Environ.* 685, 1097–1106. <https://doi.org/10.1016/j.scitotenv.2019.06.241>.
- Ballesteros, S., Domenech, J., Barguilla, I., Cortés, C., Marcos, R., Hernández, R., 2020. Genotoxic and immunomodulatory effects in human white blood cells after ex vivo exposure to polystyrene nanoplastics. *Environ. Sci. Nano* 7, 3431–3446. <https://doi.org/10.1039/d0en00748j>.
- Brachner, A., Fragouli, D., Duarte, I.F., Farias, P.M.A., Dembski, S., Ghosh, M., Barisic, I., Zdziebko, D., Vanoirbeek, J., Schwabl, P., Neuhaus, W., 2020. Assessment of human health risks posed by nano- and microplastics is currently not feasible. *Int. J. Environ. Res. Public Health* 17 (23), 8832. <https://doi.org/10.3390/ijerph17238832>.
- Chang, X., Fang, Y., Wang, Y., Wang, F., Shang, L., Zhong, R., 2022. Microplastic pollution in soils, plants, and animals: a review of distributions, effects and potential mechanisms. *Sci. Total Environ.* 850, 157857. <https://doi.org/10.1016/j.scitotenv.2022.157857>.
- Chen, Z., Hay, J.N., Jenkins, M.J., 2013. The thermal analysis of poly(ethylene terephthalate) by FTIR spectroscopy. *Thermochim. Acta* 552, 123–130. <https://doi.org/10.1016/j.tca.2012.11.002>.
- Clark, N.J., Khan, F.R., Mitran, D.M., Boyle, D., Thompson, R.C., 2022. Demonstrating the translocation of nanoplastics across the fish intestine using palladium-doped polystyrene in a salmon gut-sac. *Environ. Int.* 159, 106994. <https://doi.org/10.1016/j.envint.2021.106994>.
- Coffin, S., Bouwmeester, H., Brander, S., Damdimopoulou, P., Gouin, T., Hermabessiere, L., Khan, E., Koelmans, A.A., Lemieux, C.L., Teerds, K., Wagner, M., Weisberg, S.B., Wright, S., 2022. Development and application of a health-based framework for informing regulatory action in relation to exposure of microplastic particles in California drinking water. *Microplast. Nanoplast.* 2 (1), 12. <https://doi.org/10.1186/s43591-022-00030-6>.
- Cornu, R., Béduneau, A., Martin, H., 2022. Ingestion of titanium dioxide nanoparticles: a definite health risk for consumers and their progeny. *Arch. Toxicol.* 96 (10), 2655–2686. <https://doi.org/10.1007/s00204-022-03334-x>.
- Dhaka, V., Singh, S., Anil, A.G., Sunil Kumar Naik, T.S., Garg, S., Samuel, J., Kumar, M., Ramamurthy, P.C., Singh, J., 2022. Occurrence, toxicity and remediation of polyethylene terephthalate plastics. A review. *Environ. Chem. Lett.* 20 (3), 1777–1800. <https://doi.org/10.1007/s10311-021-01384-8>.
- Dusza, H.M., van Boxel, J., van Duursen, M.B.M., Forsberg, M.M., Legler, J., Vähäkangas, K.H., 2023. Experimental human placental models for studying uptake, transport and toxicity of micro- and nanoplastics. *Sci. Total Environ.* 860, 160403. <https://doi.org/10.1016/j.scitotenv.2022.160403>.
- European Commission (EC), 2022. Recommendation on the nanoparticle definition. 10-6 https://ec.europa.eu/environment/chemicals/nanotech/pdf/C_2022_3689_1_EN_ACT_part1_v6.pdf.
- EFSA Panel on Food Additives and Flavourings (FAF)Younes, M., Aquilina, G., Castle, L., Engel, K.H., Fowler, P., Frutos Fernandez, M.J., Fürst, P., Gundert-Remy, U., Gürtler, R., Husøy, T., Manco, M., Mennes, W., Moldeus, P., Passamonti, S., Shah, R., Waalkens-Berendsen, I., Wölfe, D., Corsini, E., Cubadda, F., De Groot, D., FitzGerald, R., Gunnare, S., Gutleb, A.C., Mast, J., Mortensen, A., Oomen, A., Piersma, A., Plichta, V., Ulbrich, B., Van Loveren, H., Benford, D., Bignami, M., Bolognesi, C., Crebelli, R., Dusinska, M., Marcon, F., Nielsen, E., Schlatter, J., Vleminckx, C., Barmaz, S., Carli, M., Civitella, C., Girola, A., Rincon, A.M., Serafimova, R., Smeraldi, C., Tarazona, J., Tard, A., Wright, M., 2021. Safety assessment of titanium dioxide (E171) as a food additive. *EFSA J.* 19 (5), e06585. <https://doi.org/10.2903/j.efsa.2021.6585>.
- Fronza, B.M., Lewis, S., Shah, P.K., Barros, M.D., Giannini, M., Stansbury, J.W., 2019. Modification of filler surface treatment of composite resins using alternative silanes and functional nanogels. *Dent. Mater.* 35 (6), 928–936. <https://doi.org/10.1016/j.dental.2019.03.007>.
- Gigault, J., El Hadri, H., Nguyen, B., Grassl, B., Rowencyk, L., Tufenkij, N., Feng, S., Wiesner, M., 2021. Nanoplastics are neither microplastics nor engineered nanoplastics. *Nat. Nanotechnol.* 16 (5), 501–507. <https://doi.org/10.1038/s41565-021-00886-4>.
- Hartmann, N.B., Hüffer, T., Thompson, R.C., Hasselöv, M., Verschoor, A., Daugaard, A.E., Rist, S., Karlsson, T., Brennholt, N., Cole, M., Herrling, M.P., Hess, M.C., Ivleva, N.P., Lusher, A.L., Wagner, M., 2019. Are we speaking the same language? Recommendations for a definition and categorization framework for plastic debris. *Environ. Sci. Technol.* 53 (3), 1039–1047. <https://doi.org/10.1021/acs.est.8b05297>.
- Huang, D., Chen, H., Shen, M., Tao, J., Chen, S., Yin, L., Zhou, W., Wang, X., Xiao, R., Li, R., 2022. Recent advances on the transport of microplastics/nanoplastics in abiotic and biotic compartments. *J. Hazard. Mater.* 438, 129515. <https://doi.org/10.1016/j.jhazmat.2022.129515>.
- Johnson, L.M., Mecham, J.B., Krovi, S.A., Moreno Caffaro, M.M., Aravamudan, S., Kovach, A.L., Fennell, T.R., Mortensen, N.P., 2021. Fabrication of polyethylene terephthalate (PET) nanoparticles with fluorescent tracers for studies in mammalian cells. *Nanoscale Adv.* 3, 339–346. <https://doi.org/10.1039/D0NA00888E>.
- Karakolis, E.G., Nguyen, B., You, J.B., Rochman, C.M., Sinton, D., 2019. Fluorescent dyes for visualizing microplastic particles and fibers in laboratory-based studies. *Environ. Sci. Technol. Lett.* 6, 334–340. <https://doi.org/10.1021/acs.estlett.9b00241>.
- Lionetto, F., Corcione, C.E., Rizzo, A., Maffezzoli, A., 2021. Production and characterization of polyethylene terephthalate nanoparticles. *Polymers (Basel)* 13 (21), 3745. <https://doi.org/10.3390/polym13213745>.
- Magri, D., Sánchez-Moreno, P., Caputo, G., Gatto, F., Veronesi, M., Bardi, G., Catelani, T., Guarnieri, D., Athanassiou, A., Pompa, P.P., Fragouli, D., 2018. Laser ablation as a versatile tool to mimic polyethylene terephthalate nanoplastic pollutants: characterization and toxicology assessment. *ACS Nano* 12 (8), 7690–7700. <https://doi.org/10.1021/acsnano.8b01331>.
- Mitran, D.M., Beltzung, A., Frehland, S., Schmiedgruber, M., Cingolani, A., Schmidt, F., 2019. Synthesis of metal-doped nanoplastics and their utility to investigate fate and behaviour in complex environmental systems. *Nat. Nanotechnol.* 14 (4), 362–368. <https://doi.org/10.1038/s41565-018-0360-3>.
- Mozeš, M., 2019. Surface modification to improve properties of materials. *Materials (Basel)* 12 (3), 441. <https://doi.org/10.3390/ma12030441>.
- Nanogenotox, 2011. http://www.nanogenotox.eu/files/PDF/Deliverables/nanogenotox%20deliverable%203_wp4_%20dispersion%20protocol.pdf.
- Nguyen, B., Tufenkij, N., 2022. Single-particle resolution fluorescence microscopy of nanoplastics. *Environ. Sci. Technol.* 56 (10), 6426–6435. <https://doi.org/10.1021/acs.est.1c08480>.
- Paul, M.B., Stock, V., Cara-Carmona, J., Lisicki, E., Shopova, S., Fessard, V., Braeuning, A., Sieg, H., Böhmert, L., 2020. Micro- and nanoplastics -current state of knowledge with the focus on oral uptake and toxicity. *Nanoscale Adv.* 2 (10), 4350–4367. <https://doi.org/10.1039/d0na00539h>.
- Pignatelli, S., Broccoli, A., Piccardo, M., Feline, S., Terlizzi, A., Renzi, M., 2021. Short-term physiological and biometrical responses of *Lepidium sativum* seedlings exposed to PET-made microplastics and acid rain. *Ecotoxicol. Environ. Saf.* 208, 111718. <https://doi.org/10.1016/j.ecoenv.2020.111718>.
- PlasticsEurope, .. Plastics -The Facts 2021: An Analysis of European Plastics Production, Demand and Waste Data. (Accessed: on 13 September 2022); Available online <https://plasticseurope.org/wp-content/uploads/2021/12/Plastics-the-Facts-2021-web-final.pdf>.
- Rodríguez-Hernández, A.G., Muñoz-Tabares, J.A., Aguilar-Guzmán, J.C., Vazquez-Duhal, R., 2019. A novel and simple method for polyethylene terephthalate (PET) nanoparticle production. *Environ. Sci. Nano* 6 (7), 2031–2036. <https://doi.org/10.1039/c9en00365g>.
- Roursgaard, M., Hezareh Rothmann, M., Schulte, J., Karadimou, I., Marinelli, E., Möller, P., 2022. Genotoxicity of particles from grinded plastic items in Caco-2 and HepG2 cells. *Front. Public Health* 10, 906430. <https://doi.org/10.3389/fpubh.2022.906430>.
- Rubio, L., Marcos, R., Hernández, A., 2020. Potential adverse health effects of ingested micro- and nanoplastics on humans. Lessons learned from in vivo and in vitro mammalian models. *J. Toxicol. Environ. Health B. Crit. Rev.* 23 (2), 51–68. <https://doi.org/10.1080/10937404.2019.1700598>.
- Rubio, L., Barguilla, I., Domenech, J., Marcos, R., Hernández, A., 2020b. Biological effects, including oxidative stress and genotoxic damage, of polystyrene nanoplastics in different human hematopoietic cell lines. *J. Hazard. Mater.* 398, 122900. <https://doi.org/10.1016/j.jhazmat.2020.122900>.

- Smith, E.C., Turner, A., 2020. Mobilisation kinetics of Br, Cd, Cr, Hg, Pb, and Sb in microplastics exposed to simulated, dietary-adapted digestive conditions of seabirds. *Sci. Total Environ.* 733, 138802. <https://doi.org/10.1016/j.scitotenv.2020.138802>.
- Suzuki, H., Toyooka, T., Ibuki, Y., 2007. Simple and easy method to evaluate uptake potential of nanoparticles in mammalian cells using a flow cytometric light scatter analysis. *Environ. Sci. Technol.* 41, 3018–3024. <https://doi.org/10.1021/es0625632>.
- Tramis, O., Garnier, C., Yus, C., Irusta, S., Chabert, F., 2021. Enhancement of the fatigue life of recycled PP by incorporation of recycled opaque PET collected from household milk bottle wastes. *Waste Manag.* 125, 49–57. <https://doi.org/10.1016/j.wasman.2021.02.006>.
- Turner, A., Filella, M., 2021. Hazardous metal additives in plastics and their environmental impacts. *Environ. Int.* 156, 106622. <https://doi.org/10.1016/j.envint.2021.106622>.
- Vales, G., Rubio, L., Marcos, R., 2015. Long-term exposures to low doses of titanium dioxide nanoparticles induce cell transformation, but not genotoxic damage in BEAS-2B cells. *Nanotoxicology* 9 (5), 568–578. <https://doi.org/10.3109/17435390.2014.957252>.
- Villacorta, A., Rubio, L., Alaraby, M., López-Mesas, M., Fuentes-Cebrian, V., Moriones, O.H., Marcos, R., Hernández, A., 2022. A new source of representative secondary PET nanoplastics. Obtention, characterization, and hazard evaluation. *J. Hazard. Mater.* 439, 129593. <https://doi.org/10.1016/j.jhazmat.2022.129593>.
- Wu, P., Lin, S., Cao, G., Wu, J., Jin, H., Wang, C., Wong, M.H., Yang, Z., Cai, Z., 2022. Absorption, distribution, metabolism, excretion, and toxicity of microplastics in the human body and health implications. *J. Hazard. Mater.* 437, 129361. <https://doi.org/10.1016/j.jhazmat.2022.129361>.
- Xu, J.L., Lin, X., Wang, J.J., Gowen, A.A., 2022. A review of potential human health impacts of micro- and nanoplastics exposure. *Sci. Total Environ.* 17, 158111. <https://doi.org/10.1016/j.scitotenv.2022.158111>.

7.3. Pdf of the article entitled *Fluorescent labeling of micro/nanoplastics for biological applications with a focus on “true-to-life” tracking*

Journal of Hazardous Materials 476 (2024) 135134



Contents lists available at ScienceDirect

Journal of Hazardous Materials

journal homepage: www.elsevier.com/locate/jhazmat



Fluorescent labeling of micro/nanoplastics for biological applications with a focus on “true-to-life” tracking

Aliro Villacorta^{a,b,1}, Camila Cazorla-Ares^{c,1}, Victor Fuentes-Cebrian^c, Iris H. Valido^c, Lourdes Vela^{a,d}, Fernando Carrillo-Navarrete^e, Michelle Morataya-Reyes^a, Karen Mejia-Carmona^f, Susana Pastor^a, Antonia Velázquez^a, Jéssica Arribas Arranz^a, Ricard Marcos^a, Montserrat López-Mesas^{c,*}, Alba Hernández^{a,*}

^a Group of Mutagenesis, Department of Genetics and Microbiology, Faculty of Biosciences, Universitat Autònoma de Barcelona, Cerdanyola del Vallès 08193, Spain

^b Facultad de Recursos Naturales Renovables, Universidad Arturo Prat, Iquique, Chile

^c GTS Research Group, Department of Chemistry, Faculty of Science, Universitat Autònoma de Barcelona, Cerdanyola del Vallès 08193, Barcelona, Spain

^d Faculty of Health Sciences Eugenio Espejo, Universidad UTE, Quito, Ecuador

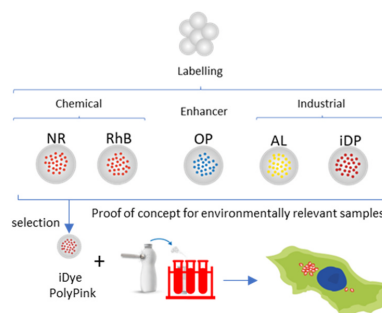
^e Institut d'Investigació Textil i Cooperació Industrial de Terrassa (INTEXTER) and Department of Chemical Engineering, Universitat Politècnica de Catalunya, Terrassa 08222, Barcelona, Spain

^f Institut Català de Nanociència i Nanotecnologia (ICN2-UAB-CSIC-BIST), Cerdanyola del Vallès, Spain

HIGHLIGHTS

- Advantages/disadvantages of five dyes to label nanoplastics (NPLs) were evaluated.
- A wide battery of assays was used for such determinations.
- iDye PolyPink was the dye showing more advantages.
- The advantages of labeling nanoplastics were extended to true-to-life NPLs.
- iDye PolyPink succeeded in staining titanium-doped PET-NPLs.

GRAPHICAL ABSTRACT



ARTICLE INFO

Keywords:

Micro/nanoplastics
Staining
Specificity

ABSTRACT

The increased environmental presence of micro-/nanoplastics (MNPLs) and the potential health risks associated with their exposure classify them as environmental pollutants with special environmental and health concerns. Consequently, there is an urgent need to investigate the potential risks associated with secondary MNPLs. In this context, using “true-to-life” MNPLs, resulting from the laboratory degradation of plastic goods, may be a sound approach. These non-commercial secondary MNPLs must be *labeled* to track their presence/journeys inside cells

* Correspondence to: Group of Mutagenesis, Department of Genetics and Microbiology, Faculty of Biosciences, and GTS Research Group, Department of Chemistry, Faculty of Science, both from Universitat Autònoma de Barcelona, Campus of Bellaterra, 08193 Cerdanyola del Vallès, Spain.

E-mail addresses: montserrat.lopez.mesas@uab.cat (M. López-Mesas), alba.hernandez@uab.cat (A. Hernández).

¹ Both authors contributed equally

<https://doi.org/10.1016/j.jhazmat.2024.135134>

Received 28 March 2024; Received in revised form 24 June 2024; Accepted 5 July 2024

Available online 8 July 2024

0304-3894/© 2024 The Author(s). Published by Elsevier B.V. This is an open access article under the CC BY license (<http://creativecommons.org/licenses/by/4.0/>).

iDye PolyPink
Cell-internalization tracking

or organisms. Because the cell internalization of MNPLs is commonly analyzed using fluorescence techniques, the use of fluorescent dyes may be a sound method to label them. Five different compounds comprising two chemical dyes (Nile Red and Rhodamine-B), one optical brightener (Opticol), and two industrial dyes (Amarillo Luminoso and iDye PolyPink) were tested to determine their potential for such applications. Using commercial standards of polystyrene nanoplastics (PSNPLs) with an average size of 170 nm, different characteristics of the selected dyes such as the absence of impact on cell viability, specificity for plastic staining, no leaching, and lack of interference with other fluorochromes were analyzed. Based on the overall data obtained in the wide battery of assays performed, iDye PolyPink exhibited the most advantages, with respect to the other compounds, and was selected to effectively label “true-to-life” MNPLs. These advantages were confirmed using a proposed protocol, and labeling titanium-doped PETNPLs (obtained from the degradation of milk PET plastic bottles), as an example of “true-to-life” secondary NPLs. These results confirmed the usefulness of iDye PolyPink for labeling MNPLs and detecting cell internalization.

1. Introduction

Large-scale production of synthetic organic polymers can be traced back to the 1950's. Since then, plastic production has progressively and steadily increased; consequently, a large amount of plastic waste has been continuously generated. Although environmental policies tend to reduce waste, a short-term scenario in which this situation could change is not feasible. In the environment, physicochemical or biologically mediated degradation processes of plastic waste produce secondary micro-/nanoplastics (MNPLs), which are considered environmental pollutants of emergent concern. Although the limits between microplastics (MPLs) and nanoplastics (NPLs) are still being investigated [1, 2], the smaller the size, the higher the probability of internalization into exposed organisms, including humans. As the definition of NPLs is a bit conflicting, this study considers NPLs in the range 1–1000 nm [3]. Multiple reviews have recently been published on the potential health risks associated with MNPL exposure, including oxidative stress, alterations in gene expression, genotoxicity, and carcinogenicity as potential effects associated with MNPL exposure [4–6]. However, the accurate determination of exposure (primarily at the NPLs level) requires further refinement and, consequently, the lack of exposure-effect information minimizes the relevance of the reported potential health risks [7]. In *in vitro/in vivo* experimental approaches, a growing interest exists in using “true-to-life” MNPLs resulting from the degradation of plastic goods because they are considered more representative of environmental plastic waste [3]. Accordingly, the use of these “true-to-life” MNPLs is a promising option, in opposition to the use of pristine polystyrene commercial MNPLs, to better define the potential risks associated with MNPL exposures owing to variations in their physicochemical properties. Notably, the confirmation that the used “true-to-life” (or any other used MNPLs) can internalize on cells/tissues should be a mandatory requirement in any published study. In this regard, significant advances have been made, pushing the boundaries of technology and techniques, demonstrating notable approaches such as the use of graphene oxide quantum dots to embed polystyrene (PS) microspheres by micro-emulsion polymerization [8] and hyperspectral imaging as a novel approach to studying the accumulation and distribution of NPs in human cells [9]. However, the development of techniques enabling three-dimensional (3D) analysis without detrimental or stressful effects at the cellular level and allowing, for instance, 3D reconstruction for future applications appears to be a secure path forward. Thus, it is necessary to “label” these “true-to-life” MNPLs in such a way that their presence can be easily detected to follow up on the presence of these plastics inside cell and /tissues. For such purposes, Nile Red staining has been extensively used to label MNPLs, showing multiple apparent advantages, including affordability and straightforward applications [10]. Although these advantages have been well-reported when environmental matrices are evaluated [11], problems arise with biological matrices [12], primarily because of the ability of Nile Red to stain intracellular lipid droplets/bodies. This ability to fluoresce strongly in lipophilic environments has been known for a long time and is why Nile Red was initially proposed to act as a lipid-specific stain [13]. In several

cases, Nile Red has been used to detect propylene microplastics in crop plants; however, the protocol assumes the destruction/digestion of the plants, which prevents the detection of *in situ* internalization [14]. Using Nile Red staining, polystyrene, polyethylene, and polyamide were detected in the bottled water samples. In addition, when zebrafish embryos were exposed to Nile red-stained polyethylene MPLs, their accumulation was observed in various organs [15]. Therefore, owing to the non-specific staining ability of Nile Red and its high cost, more specific MNPL staining is required.

Several studies have determined the potential usefulness of alternative dyes such as textile dyes. In a recent study, four textile dyes (Rit pink, Rit blue, iDye pink, and iDye blue) were compared with Nile Red using 17 different polymers [16]. The results indicated the low efficacy of blue dyes and similar efficacy of pink dyes for Nile Red. Another study compared the usefulness of fluorescein and Nile Red in detecting polystyrene, polypropylene, and polyethylene MNPLs [17]. Significant differences between dyes were observed, with fluorescein enabling the specific detection of polystyrene, whereas Nile Red showed the highest increase in fluorescence for polypropylene. Unfortunately, all of these studies were carried out in water dispersions, but did not use biological matrices, as required for biological studies. Furthermore, Rhodamine B has been demonstrated to successfully stain five types of microplastic polymers (polyethylene, polypropylene, polystyrene, polyvinyl chloride, and polyurethane) under laboratory conditions [18]. In addition, polyvinyl chloride MPLs were successfully stained, and their ingestion was demonstrated in the copepod (*Pseudocalanus spp*) gut [19]. All these studies highlight the relevance of staining MNPLs and the lack of consistent proposals for one of them.

The lack of harmonized and established protocols for MNPL labeling, to detect cell internalization, is an important inconvenience in the development and study of the effects of “true-to-life” MNPLs. To fill this gap, the present study was conducted using two textile dyes (Amarillo Luminoso Polyester GNH 400 for industrial use and iDye PolyPink for domestic use), an industrial optical brightener (Opticol UPR), and two chemical dyes (Nile Red and Rhodamine B) to determine their suitability. The study consisted of two parts. In the first step, a suitable protocol for staining commercial polystyrene nanoplastics (PSNPLs) is developed, avoiding interference from other typical labeling fluorescence compounds; the stained-PSNPLs are internalized into cells and their distribution is studied. In the second one, and as a *proof of concept*, the selected dye, following a simplified staining protocol, was evaluated for the labeling of titanium-labeled PET nanoplastics (PET-Ti-NPLs) resulting from the degradation of opaque PET plastic bottles, followed by the internalization into cells [20]. As a novelty, our proposal for the best labeling method for MNPLs is based on a deeper analysis of the pros and cons of the five selected dyes after analyzing their responses in a wide battery of assays.

2. Materials and methods

2.1. Reagents and standards

Commercial standards of polystyrene nanoplastics (PSNPLs) were obtained from Ted Pella Inc. (Redding, CA, USA). These nanospheres had an SEM/TEM certified size of 170 ± 9 nm and were provided in an aqueous stabilized suspension (for non-aggregation purposes) at a concentration of 0.1 % (w/v). The selected compounds were Nile Red (NR), Rhodamine B (RhB) (Merck KGaA, Darmstadt, Germany), Amarillo Luminoso Polyester GNH 400 (AL), Opticol UPR (Op) (Colorcenter, Terrassa, Spain), and iDye PolyPink (iDP) (Rupert, Gibbon & Spider, Inc., Healdsburg, CA, USA). For the second part of the study, “true-to-life” PET(Ti)-NPLs obtained as described below were used. Briefly, 12 cm² fragments from commercially available milk PET bottles were sanded using a diamond rotary burr to avoid overheating the surface of the polymer. The debris was sieved through a 0.20 mm mesh and 4 g of the fine material was dispersed in 40 mL of 90 % (v/v) trifluoroacetic acid (TFA) pre-heated to 50 °C on a stirring plate at 100 rpm for 2 h, followed by continuous agitation at room temperature overnight. Particles in suspension were sieved through a 0.20 mm mesh, and the eluent was divided into 10 mL glass tubes and centrifuged for 1 h at 2500 rcf. The resulting pellet was resuspended in 400 mL of 0.5 % (v/v) sodium dodecyl sulfate (SDS) and subjected to ultrasonication using an SSE-1 Branson sonicator (Brookfield, CT, USA) for 2 min at 25 % amplitude, with 9/9 s sonication/break cycles, and immediately transferred to 200 mL graduated cylinders and allowed to sediment for 1 h to remove the larger fractions. The upper fraction (100 mL) of each cylinder was collected and centrifuged to remove SDS. The resultant pellets were washed twice with Milli-Q water and twice with pure ethanol, and dried under sterile air laminar flow. The dried pellets were weighed and resuspended in Milli-Q water at a concentration of 10 mg/mL. These suspensions were sonicated for 16 min at 10 % amplitude in a cold-water bath, immediately frozen using liquid nitrogen, and transferred to a –80 °C freezer until needed.

2.2. Ultracentrifugation optimization

To achieve the highest centrifugation efficiency, a 40-ppm suspension of non-labeled PSNPLs was prepared in Milli-Q water. The suspension was ultracentrifuged for 5, 15, 30, or 45 min at 13,200 rpm using a 5415 R Eppendorf centrifuge (Eppendorf AG, Hamburg, Germany).

The centrifugation yield was determined using an ultraviolet-visible (UV-Vis) spectrophotometer (ATI-UNICAM UV2; Thermo Fischer, Braunschweig, Germany). This was calculated by comparing the intensity between the non-centrifuged suspension, used as a reference ($A_{250\text{ nm}} 40\text{ ppm standard}$), and the supernatant of the centrifuged suspension at 250 nm ($A_{250\text{ nm}}(\text{supernatant of centrifugation } X \text{ min})$), which is within the range of the characteristic polystyrene wavelength, avoiding errors due to the saturation of the detector (Eq. 1).

$$\text{Centrifugation Yield}(\%) = \left(1 - \frac{A_{250\text{ nm}}(\text{supernatant of centrifugation } X \text{ min})}{A_{250\text{ nm}} 40\text{ ppm standard}} \right) \cdot 100 \quad (1)$$

2.3. Membrane centrifugation efficiency study

To test another cleaning procedure, membranes Amicon® Ultra-15 centrifugal Ultracel®–100 K filter 1×10^5 MWCO (Merck KGaA, Darmstadt, Germany) were tested. A calibration curve was prepared using concentrations ranging 150 ppt to 50 ppb of 170 nm PSNPLs, and

the remaining PSNPL present in the eluent was calculated. Four replicates of the centrifugation procedure were performed for 15 min at 3500 rpm. The separation yield was calculated by measuring the absorbance (at 250 nm) of the membrane eluent and interpolating the values on the PSNPLs calibration curve corresponding to $y = 0.0197x + 0.0271$, $r^2 = 0.9959$, as detailed in the [Supplementary Material \(SEQ1\)](#).

2.4. Labeling procedure

All preparations were performed by separately weighing NR, RhB, AL, Op, and iDP to obtain a final stock concentration of 1000 ppm. The NR and RhB solutions were prepared using 96 % ethanol (Scharlab, Barcelona, Spain). For AL, Op, and iDP, the suspensions were prepared on “Ultrapure Type 1” (Milli-Q) 18.2 MΩ-cm water (Merck KGaA, Darmstadt, Germany). PSNPLs at a fixed concentration of 40 ppm of PSNPLs was exposed to 400, 200, 100, and 50 ppm of each of the labeling solutions, regardless of water (AL, Op, and iDP) or 96 % ethanol (NR and RhB), as previously described. The different mixtures were heated at 65 °C for 30 min on glass vials with constant agitation on an orbital agitator and incubator (Heidolph, Unimax1010) at 150 rpm. The stained particles were cleaned by performing ten ultra centrifugations for 45 min at 13,200 rpm, as described in the next section. The supernatant was removed from the pellet by decantation and further washes were performed with the corresponding solvent (Milli-Q water or ethanol, depending on the dye). The supernatants and resuspended pellets were analyzed using UV-Vis spectroscopy, as previously described, and fluorimetry analysis was performed. First, several concentrations of the strains were analyzed to determine the experimental excitation and emission wavelengths of each strain. Excitation fluorescence analysis was performed using a Cary Eclipse fluorescence spectrometer (Agilent, Santa Clara, CA, USA). Emission fluorimetry analysis was performed using the same parameters as in the excitation analysis; however, the initial scan wavelength was the excitation wavelength.

To study the cleaning efficiency, different supernatants were evaluated to determine the conditions that achieved the lowest possible fluorescence. Furthermore, to study the staining efficiency, the resuspended pellets of the stained PSNPLs were analyzed under the same conditions as previously described; however, the scan ranged from an excitation wavelength of 800 nm.

2.5. Agglomeration and resuspension study

To ensure that the agglomeration state of the stained PSNPLs remained negligible, the particles were heated at 65 °C for 45 min and ultracentrifuged for 45 min at 13,200 rpm ten times, reproducing the cleaning after the staining procedure. Subsequently, different resuspension procedures were applied to each one of the PSNPLs aliquots: no agitation (BC), orbital agitation (O) for 16 min at 350 rpm, vortex (V) for 16 min (Vortex-Vib, J.P SELECTA S.A., Barcelona, Spain), ultrasonic bath (BU) for 16 min (ULTR-3L2–001, Labbox Labware S.L, Barcelona, Spain), and ultrasonic probe (SU) at 10 % of amplitude for 16 min in a

cold bath (SSE-1 Branson Sonicator, Branson Ultrasonics Co., Brookfield, CT, USA). The average size of the resuspended aliquots was analyzed by Dynamic Light Scattering (DLS) using a Zetasizer® Ultra (Malvern Panalytical, Cambridge, UK) and compared with a freshly prepared standard of 170 nm polystyrene nanospheres at 40 ppm. In all cases, size distribution was evaluated using a DTS0012 cuvette under the

conditions described in the following section. The data were processed and analyzed using GraphPad Prism software (GraphPad, San Diego, CA, USA).

2.6. The hydrodynamic behavior of labeled PSNPLs

The hydrodynamic behavior of the labeled PSNPLs was evaluated by measuring 100 ppm aliquots of labeled NPs in triplicate. To perform these measurements, the PSNPL parameters were established with a refractive index of 1.59. The parameters of Milli-Q water used as a dispersant were set as standards, considering a refractive index of 1.33 and a viscosity value of 0.8872. The sample size distribution was measured at a scattering collection angle of 174.7° using a DTS0012 cuvette, whereas the Z-potential was evaluated using DTS1070 cuvettes. The data obtained were analyzed as explained in the preceding section.

2.7. Cell culture

The THP1 leukemic monocyte cell line (Sigma-Aldrich) was selected based on its high ability to internalize MNPLs. Cells were maintained in filtered cap T-25 flasks (SPL Life Sciences, Pocheon-si, Gyeonggi-do, South Korea). The cellular suspensions were maintained at constant concentrations ranging $0.50\text{--}1.00 \times 10^6$ cells/mL at a maximum volume of 5 mL on Roswell Park Memorial Institute (RPMI) medium supplemented with 10 % fetal bovine serum (FBS), 1 % glutamine (Biowest, Nuaillé, France), and 2.5 ppm of Plasmocin® (InvivoGen, CA, USA) at standard growing conditions of 37°C , on humidified atmosphere with 5 % CO_2 , on a ICO150med CO_2 incubator (Mettler GmbH + Co KG, Schwabach, Germany).

2.8. Cell exposure to labeled PSNPLs

From the cell stock suspension, the required volumes at the concentration of 1.00×10^6 cell/mL were distributed by seeding 100 μL per well on U-type 96-well plates (SPL, LifeSciences, Pocheon-si, Gyeonggi-do, Republic of Korea). The particle working suspensions, prepared as previously described, were mixed with the previously seeded cells by gentle pipetting ten times. The exposed cells were maintained under the same conditions as in the maintenance procedure for 24 h and protected from light. Based on a large number of studies using polystyrene NPLs, this nanoplastic can be considered stable over time. Although stability should be a problem in long-term exposure, this was not the case because the study used acute exposure lasting for 24 h.

2.9. Cell viability test

To avoid interference caused by nNPs in the standard viability tests, the direct scoring of the number of viable cells after exposure, compared to those before exposure, was determined using the Beckman counter method. THP1 cells were exposed to 100 ppm of differently stained particles following the procedure described above. The cell viability was investigated using a 1:100 ISOFLOW dilution on a ZTM Coulter Counter (Beckman Coulter Inc., CA, USA). The average cell count was compared with that of untreated controls, and values were analyzed using GraphPad Prism Software 7.0 (GraphPad, San Diego, CA, USA) by One-way analysis of variance (ANOVA) and contrasted with both unexposed and pristine-treated cells. For both cases the Dunnett post-test with a 95 % confidence interval (CI) with $p \leq 0.05$ (*), ≤ 0.01 (**), and ≤ 0.001 (***) was used. Two experiments were performed in triplicates.

2.10. Flow cytometry analysis

Cells treated with labeled particles and the labeling elute resulting from a previously indicated membrane centrifugation efficiency study were cultured as described in the cell viability test section. Cells in 96 U-type well plates were washed twice by centrifugation at room

temperature on a 5810 R device (Eppendorf, Hamburg, Germany) and resuspended in phosphate-buffered saline (PBS; 1X, Gibco, Thermo Fischer Scientific, Braunschweig, Germany). The samples were kept on ice and immediately analyzed using a Cytoflex LX flow cytometer (Beckman Coulter Inc., CA, USA). The setting conditions were set as a standard, and the array/gain of the detectors can be found in the [Supplementary Material \(Supplementary Table S1\)](#). A total of 5000 living cell events were recorded at a flow rate of 60 $\mu\text{L}/\text{min}$. Data from the positive signal channels were analyzed and compared with the controls.

2.11. Confocal microscopy analysis

THP1 cells, treated with labeled particles and the particles labeling elute, as previously described, were cultured on U-type 96-well plates for 24 h. Cells were then washed twice using 200 μL of PBS 1X. Final pellet resuspension was done on a pre-warmed RPMI-supplemented medium, and 300 μL of the cell suspension was transferred to a well on a $\mu\text{-Slide}$, eight-well high Glass bottom (Ibidi GmbH, Gräfelfing, Germany). The cells were examined using a Leica TCS SP5 confocal microscope (Leica Microsystems CMS GmbH, Mannheim, Germany). Compatibility was tested using CellMask™ deep red and trihydrochloride trihydrate Hoechst 3334 solution, both diluted 1:10,000 for all labels except for Opticol labeled PSNPLs, where the compatibility was changed to CellMask Orange and DRAQ5 (Thermo Fischer Scientific, Braunschweig, Germany).

2.12. Simplified protocol and proof of concept

2.12.1. Fast protocol

As the potential effects of PET-NPLs are gaining attention in the scientific community, a proof-of-concept study was performed following the protocol developed for PS. Instead of pristine PSNPLs, “true-to-life” PET(Ti)-NPLs were stained. These titanium-doped PETNPLs were obtained from the degradation, through sanding, of opaque PET bottles containing titanium NPs (TiO_2NPs); consequently, the resulting MNPLs also contained embedded titanium. Briefly, PET(Ti)-NPLs were labeled by mixing 0.5 mL of the PET(Ti)-NPL suspension (at a concentration of 10,000 ppm) with 0.5 mL of Milli-Q water (containing 0.01 g of iDye PolyPink) in a 10 mL glass tube. The mixture was vigorously agitated by vortex and incubated for 2 h with a short vortexing every 30 min on a constant temperature digital block heater (VWR® Avantor® Inc., Philadelphia, USA). The particle-label mix was resuspended in 9 mL of Milli-Q water and transferred onto an Amicon® Ultra-15 centrifugal Ultracel®–100 K filter 1×10^5 MWCO (Merck KGaA, Darmstadt, Germany). A 15-min centrifugation was performed at 3453 rcf, and 9 mL of Milli-Q water was added to the V-shaped well; the wash was repeated four times. After washing, a volume ranging 100–160 μL containing the labeled particles was recovered from the V-shaped well and aliquoted to volumes of 1000 μL on Milli-Q water which were maintained covered from light at 4°C . Irrespective of the desired biological application, it is highly advisable to evaluate the effectiveness of this method by running a lambda scan on a regular confocal microscope for particle aggregates. Alternatively, approaches that do not necessarily rely on NP aggregation, such as fluorescent nanotracking analysis (NTA) or fluorescent spectrometry, can also be used. Both proposals employ widely used, cost-efficient, and easy-to-use approaches.

2.12.2. Cell culture, treatment, and visualization

In this study, the human hepatic Huh-7 cell line was selected as a convenient experimental substitute for primary hepatocytes because the liver is one of the organs targeted by MNPLs pollutants. Huh-7 cells were cultured and seeded in filtered-cap T-25 flasks (SPL, Life Sciences Co. Ltd., Naechon-myeon, Republic of Korea) in Dulbecco's modified Eagle's medium (DMEM) supplemented with 10 % fetal bovine serum (FBS) from Biowest (Nuaillé, France) and Plasmocin (InvivoGen, CA, USA). To proceed, 7000 cells were seeded and cultured on $\mu\text{-slide}$ eight-

well high glass bottom (Ibidi GmbH, Gräfelfing, Germany) for 24 h before treatments. Culture media was removed by aspiration and replaced with 0.20 mL of freshly prepared iDye-PET(Ti)-NPLs suspension (100 µg/mL) on pre-warmed DMEM at 37 °C and incubated for 24 h at standard growing conditions of 37 °C, in a humidified atmosphere with 5 % CO₂ on an ICO150med CO₂ incubator (Mettler GmbH + Co KG, Schwabach, Germany). After 24 h of incubation with the iDye-PET(Ti)-NPLs suspension, cells were washed twice with 250 µL of a pre-warmed medium. Finally, 300 µL of pre-warmed medium was added to each well and the plates were investigated immediately after 5 min of incubation with CellMask™ deep red and trihydrochloride trihydrate Hoechst 3334 solution both diluted 1:10,000, on a Leica TCS SP5 confocal microscope (Leica Microsystems CMS GmbH, Mannheim, Germany).

3. Results and discussion

3.1. Ultracentrifugation optimization

First, ultracentrifugation conditions were established to separate PSNPLs from the supernatant. As expected, the results of centrifugation over time showed a significant decrease in the characteristic absorbance (at 250 nm) of PSNPLs (which indicated a decrease in the PSNPLs present in the supernatant) when the centrifugation time was increased (Fig. 1). The data indicate that the average intensity (absorbance in a.u.) decreased, from 2.69 at 0 min to 0.10 at 45 min. Consequently, the remaining PSNPL in the supernatant was reduced from 100 % at 0 min to 66 % at 5 min and to 4 % at 45 min of centrifugation. Consequently, 45 min was chosen as the optimal centrifugation time to separate the stained/unstained NPLs from the supernatant.

3.2. Membrane centrifugation efficiency study

As indicated in the [Supplementary Information \(Supplementary Fig. S1\)](#), the calibration curve for the analysis of PSNPLs showed a linear trend from 125 to 50 ppm. When using the calibration curve to evaluate the results from the four replicates performed with the Amicon® tubes, a concentration below the limit of detection was obtained. This indicates the non-significant presence of PSNPLs in the eluent, showing 100 % retention efficiency of the membrane used. However, when the PSNPLs were resuspended in the membrane, an average loss of 17 ± 8 % was observed. Therefore, this difference in absorbance can be attributed to the loss of particles stuck in the membrane or the walls of the tube, when trying to recover them from the membrane, after centrifugation. However, for the scope of the present study, membrane centrifugation was appropriate to ensure proper cleaning of the PSNPLs from the remaining staining in the supernatant when PSNPL labeling was used (see subsequent sections) to ensure separation from the supernatant in less time, even losing a higher amount. For subsequent analyses, the membranes

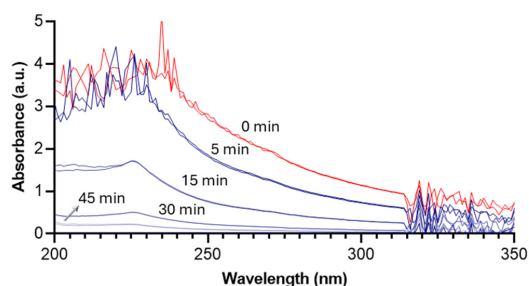


Fig. 1. The UV spectrum of each supernatant ranging 0–45 min of ultracentrifugation time at 13,200 rpm.

were centrifuged whenever possible.

3.3. Staining and cleaning efficiency

To test the efficiency of the staining, different compounds were tested at different excitation and emission wavelengths, as shown in the [Supplementary Material \(Supplementary Table S2\)](#). The results obtained were within the range of those presented in the literature, except for Amarillo Luminoso and Opticol, for which no data were found in the open literature [21,22]. Regarding the fluorescence yield, the chemical dyes (NR and RhB) showed significantly higher fluorescence intensities, even at lower concentrations, than the textile dyes used and the optical brightener. Regarding the different concentrations of the dyes tested for labeling PSNPLs, the highest intensity in all resuspended PSNPLs was observed with the ratio corresponding to the highest concentration of the dye (corresponding to the ratio 10:1). Fig. 2 shows the emission spectra of the PSNPLs stained at 400 ppm, except for NR (200 ppm), which showed similar intensities.

Finally, concerning the cleaning of the PSNPLs to eliminate free dye, the procedures used were effective because the fluorescence intensity observed in the 10th wash supernatant was at least ten times lower than that of the stained PSNPLs. This fluorescence was colorless to the naked eye, except for NR and RhB, which showed a light red color with absorbance at the noise level when analyzed using UV-Vis spectrophotometry. Collectively, the results indicated that the ultracentrifugation cleaning procedure was reliable, and no free dye was detected in the visible spectrum at significant levels.

3.4. Agglomeration and resuspension study

The potential agglomeration levels of PSNPLs obtained using different resuspension approaches were evaluated by DLS and are graphically represented in Fig. 3a. The highest number of particles in all resuspension techniques had a diameter between 126–170 nm, which agreed with the results obtained in the blank of both DLS (named B) studies. The size distribution deviations were determined by considering the previously mentioned blank histograms (Fig. 3b). The ultrasonic probe exhibits the lowest deviation, followed by the ultrasonic bath, orbital, vortex, and centrifugation blanks.

The hydrodynamic behavior in terms of size distribution is depicted in Fig. 4 for all the stained particles evaluated. The Z-average values, based on intensity calculations, are 362 ± 5 nm for RhB, 363 ± 1 nm for AL, 309 ± 1 nm for Op, 352 ± 5 nm for iDP, and 539.50 nm for NR. The polydispersity indexes for 0.27, 0.25, 0.34, 0.62, and 0.70 for RhB, AL, OP, iDP, and NR, respectively.

The obtained size distributions were consistent, and for all cases (except NR), the Z-average values were close to 350 nm, showing solid correlation coefficients. Notably, the more reliable values for correlation

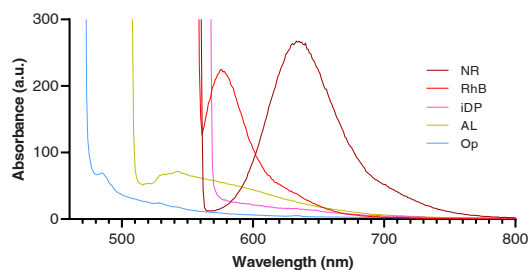


Fig. 2. Emission spectra of PSNPLs stained at 400 ppm (except for NR, which was stained at 200 ppm) with the different tested compounds. Legend abbreviations: Nile Red (NR), Rhodamine B (RhB), iDye PolyPink (iDP), Amarillo Luminoso (AL), and Opticol (Op).

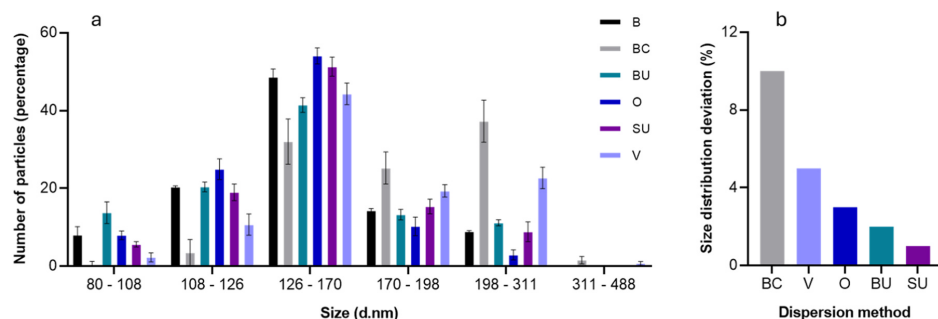


Fig. 3. (a) Size distribution histogram of the pristine PSNPL diameters obtained using DLS after different resuspension treatments. (b) Size distribution deviation expressed in percentages of the different resuspension techniques compared to the blank size distribution obtained using DLS. Legend abbreviations: DLS blank (B), centrifugation blank (BC), orbital (O), vortex (V), ultrasonic bath (BU), ultrasonic probe (SU).

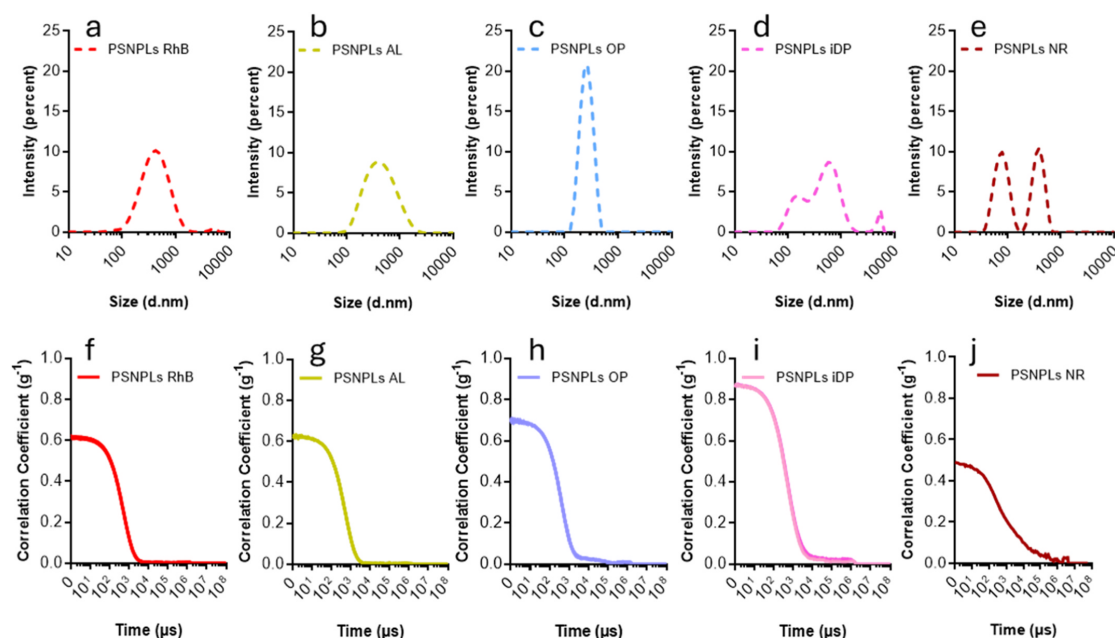


Fig. 4. Size distribution (using DLS) of PSNPLs for (a) RhB, (b) AL, (c) Op, (d) iDP, and (e) NR are represented as intensity percent. Correlation coefficients for all independent measurements are shown for RhB, AL, OP, iDP, and NR-stained PSNPLs on f, g, h, i, and j, respectively.

were those obtained when iDye PolyPink labeled particles were used, and the lower correlation was obtained for RhB and AL. In the case of NR-stained PSNPLs, the correlations and measurements were inconsistent and difficult to determine. These data indicate that the dispersion of iDye PolyPink-stained PSNPLs is the most suitable for future applications, especially if we consider that the typically described error in size estimation from fluorescent particles emitting in the range 600–700 nm is mild compared to Opticol, which is the only compound that does not emit in this range [23]. Even considering the relatively consistent values on the Z-average values, evidencing an agglomeration of particles related to the commercial information delivered by the manufacturer (170 ± 9 nm) the curves, for size distributions in percentage of intensity, describe the typically expected behavior for fluorescent samples. However, the fluorescent light emitted by some strains is non-coherent

and can be recorded as noise, broadening the peaks [23]. This was observed for the RhB- and AL-stained NPs, which reduced their potential as candidates for labeling NPLs. With respect to the Z-potential, for all studied cases (Fig. 4a–d) the values were far from zero (summarized in Supplementary Table S3). Moreover, the values ranged -20 – (-46) mV which is an indicator that the suspensions are less prone to form aggregates. For RhB- and iDP-labeled NPLs, the measured values were close to -30 mV, which is typically the optimum value for particles in suspension to be considered stable monodispersions.

3.5. Cell viability

A relevant condition for dye selection is that it should not compromise cell viability. In our study, no significant decrease in cell viability

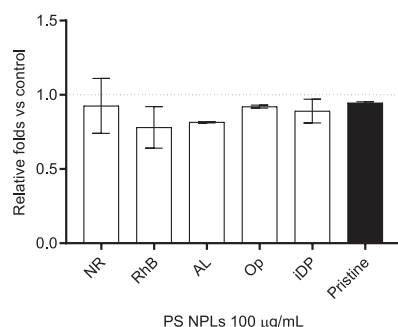


Fig. 5. Cell viability for THP1 cells after 24-h exposure to stained-PSNPLs. Nile Red (NR), Rhodamine B (RhB), Amarillo Luminoso (AL), Opticol (Op), and i-Dye Poly Pink (iDP) NPs (100 $\mu\text{g/mL}$). Values are relative to the untreated cells (control, dotted line). Cells treated with unlabeled PSNPLs (pristine) are also included. No significant statistical differences were observed using the one-side ANOVA with Dunnett's *post hoc* test ($p \leq 0.05$).

was observed for any of the tested compounds in the human leukemia monocytic THP1 cells. This cell line has shown a significant ability to internalize PSNPLs [24], ensuring the uptake of labeled NPLs and supports the data indicating a lack of toxicity. However, small decreases in viability values were observed for RhB- and AL-stained PSNPLs; however, these decreases were not statistically significant, as indicated in Fig. 5. Notably, toxicity has been reported in A549 cells exposed to rhodamine-labeled silica NPs [25]. This means that the viability effects would not be a discriminating factor in the selection of the best compound to stain NPLs using this technique. However, it is tempting to advise against values deviating from the pointed line on the graph representing the values for untreated PSNPLs.

3.6. Flow cytometry analysis

The use of non-destructive techniques, such as fluorescence-activated cell sorting (FACS), may be favored by the fluorescent labeling of MNPLs. Therefore, the evaluation of its suitability with the selected strains may provide an idea as to which of the labels used in this study may be the most suitable. Thus, THP1 cells exposed for 24 h to labeled NPLs were investigated using flow cytometry. The details of each of the investigated channels are depicted in the [Supplementary Material](#) (Supplementary Figs. S2a–f for the particle-staining eluent, and Supplementary Figs. S2g–l for labeled particles). The first significant finding was the lack of specificity for Nile Red, which has already been discussed by other authors [26,27]. Thus, the high affinity of Nile Red for neutral lipids and other cellular components was demonstrated in our work. Despite previous reports on their usefulness, the use of Nile Red, as well as other stains with lipid affinity, should be considered a suboptimal approach when used in cellular backgrounds [20,28]. Thus, THP1 cells treated with different eluents showed no signal (Fig. 6), with the exception of the NR eluent. Therefore, these results would indicate both the effectiveness of the cleaning process and the inconvenience of using Nile Red. Thus, if we consider this characteristic crucial, the use of Nile Red must be discarded when better alternatives are available. Another characteristic is that no signal was detected near the UV spectra when Nile Red was in its free form or when no PSNPL particles were present.

For AL-PSNPL-treated cells, emission was observed in all channels, and the signal was mild (less than 25 %) only in the near ultraviolet (NUV)450 channel, where the shift was rounded to 13 %. Moreover, the shift was at least 50 % for 10 detectors. This may interfere with other signals emitted by other fluorochromes regularly used in biology as.

DRAQ5, Hoechst 33342 on nuclei, or Cellmask™ Deep Red for plasma membrane, and its use is inadvisable.

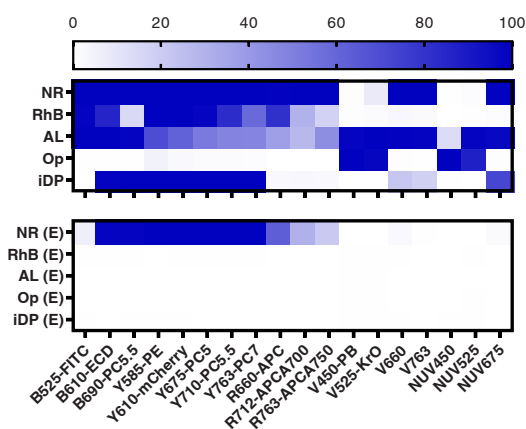


Fig. 6. Upper part: flow cytometry evaluation of the emission on THP1 cells exposed for 24 h to Nile red (NR)-, Rhodamine B (RhB)-, Amarillo luminoso (AL)-, Opticol (OP)-, and Idye PolyPink (iDP)-labeled polystyrene NPs (100 $\mu\text{g/mL}$). Lower part: data from their correspondent eluent (E-suffix added in all cases) for control. The used laser excitation and the corresponding wavelengths are indicated as follows: blue (B), yellow (Y), red (R), violet (V), and near UV (NUV). The emissions are represented as the percentage of cells that emit at the corresponding wavelengths.

Moreover, because staining is persistent and difficult to remove, its inappropriate use may damage the microfluidic components of the cytometer. Notably, RhB- and iDP-labeled PSNPLs presented similar emissions, with the significant difference that internalized RhB-labeled PSNPLs emitted at 525 nm when excited with a blue laser and at 660 nm when excited with a red laser. In contrast, the internalized iDP-PSNPLs emit light at 675 nm when excited with an NUV laser. The differences between these two labels were minimal, and both results were almost equivalent. Finally, the Opticol-labeled PSNPLs presented a narrow emission spectrum (only at 450 and 525 nm) and only when excited with violet or near-UV lasers. Although Opticol appears to be useful in terms of compatibility, we will see further complications with this compound when complementary techniques are used. The results for RhB, iDP, and OP were confirmed and validated by repeating the experiments with adherent HeLa cells. These cells have been extensively used to study the effects of new materials, such as the label-free detection of metallic NPs [29], fluorescent nanopolymers [30], and carbon-based compounds [31]. Moreover, these cells have been supported by sophisticated techniques such as stimulated emission depletion microscopy, which is useful for detecting fluorescence at wavelengths lower than 200 nm [32]. Detailed methods and information on the use of this cell line are available in the [Supplementary Material](#) (Supplementary Figs. S3.1 and 2), and the comparisons are depicted and summarized in [Supplementary Fig. S3.3](#).

3.7. Confocal microscopy

Internalization of the labeled NPs was assessed using confocal microscopy. For better visualization, despite the staining color, all labeled particles were represented in green, membranes in red, and nuclei in blue. Representative images of all the cases are shown in Fig. 7. The first observation (Fig. 7f) shows that Amarillo luminoso seems to produce not only interference with several of the signals but also causes some sort of cell stress, since in all cases, the shape of the cells was not regular and consistently altered compared to the control (Fig. 7g). Although cell viability was reduced in the short-term treatment (24 h), this reduction was not statistically significant. However, prolonged exposure may induce cell viability inconveniences that were not studied further

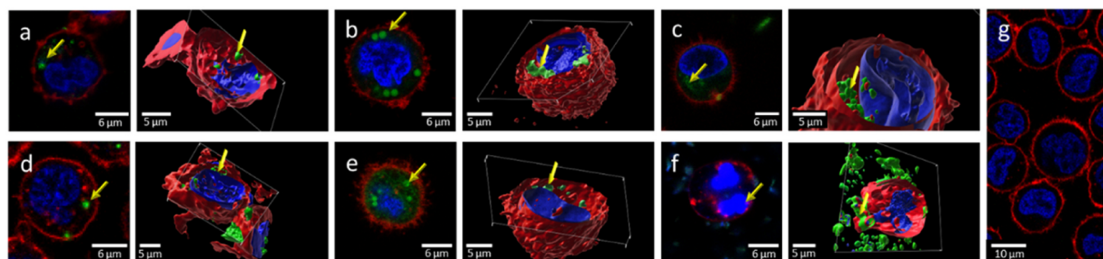


Fig. 7. Confocal Images of THP1 cells exposed for 24 h to commercially available (a) fluorescein labeled-PSNPLs, (b) Nile Red, (c) Rhodamine B, (d) Opticol, (e) i-Dye Poly Pink, and (f) Amarillo Luminoso PSNPLs (100 $\mu\text{g}/\text{mL}$). A digital reconstruction is presented at the right of each image. Yellow arrows indicate the presence of labeled NPs. Untreated THP1 cells are shown on (g), as controls.

because no useful traits for this label were found. Further experiments were not performed using this dye.

Although emissions at the expected wavelengths were easily observed, difficulties arose when the signals from small PSNPL

agglomerates or single particles were evaluated. Although these difficulties can be solved using the so-called nanoscopy methodology, which is a far-field microscopy technique that can generate images beyond diffraction-limited resolution, such as stimulated emission depletion

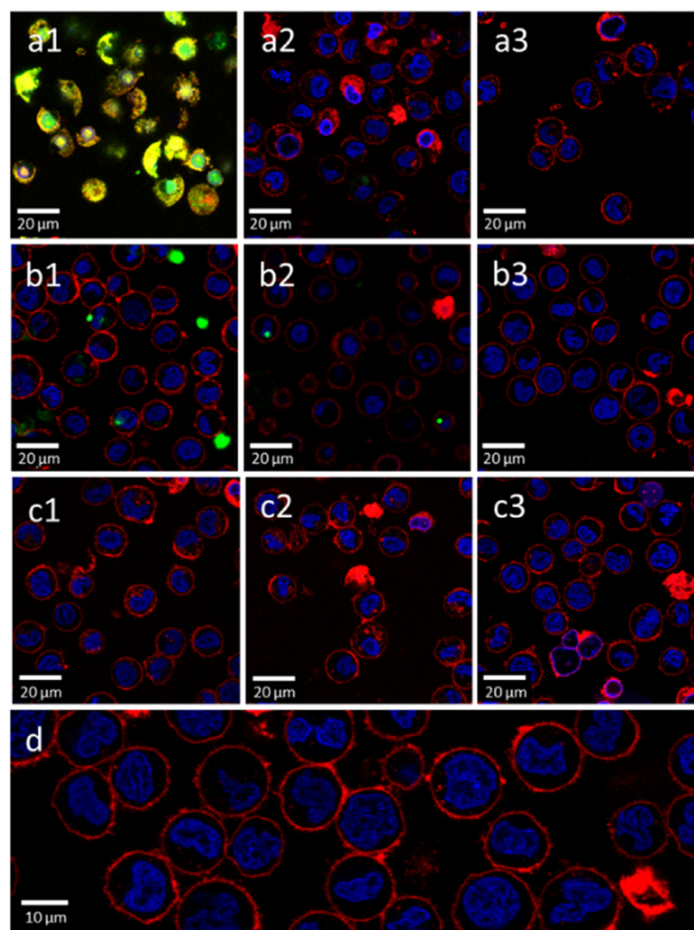


Fig. 8. Confocal Images of THP1 cells exposed for 24 h to pigments with no particles. (a1) Rhodamine B: 2000 ppm, (a2) 20 ppm, and (a3) eluent. (b1) Opticol: 2000 ppm, (b2) 20 ppm, and (a3) eluent. iDye PolyPink: (c1) 2000 ppm, (c2) 20 ppm, and (c3) eluent. (d) Untreated THP1 cells.

(STED) microscopy [27], it can pose additional technical difficulties and a non-negligible increase in costs. In the case of NR-PSNPLs, owing to the previously explained non-specific staining, there are always uncertainties regarding the resulting images because the eluent can label the cells. Furthermore, since Nile Red presents an excitation wavelength shift from 450 to 560 nm by solvatochromism, its combined use with other stains or simultaneous scanning with B- and G-excitation filters may present scoring difficulties. No previous reports on RhB-labeled found in have been published. However, exposure to high concentrations of RhB may result in non-specific staining along with loss of cellular integrity, as shown in Fig. 8a1, whereas no signals were observed at low concentrations (20 ppm) or with the eluent (Fig. 8a2 and 3, respectively).

Although no effects on cell viability were observed when Optical labeling was used, non-specific fluorescence signals were observed in THP1 cells treated with the particle-free stain, including high (2000 ppm) and low (20 ppm) concentrations (Fig. 8b1 and 8b2, respectively). However, the formation of Optical hot spots was observed, suggesting the agglomeration of the compound. Furthermore, in agreement with the cytometry findings, no signals were detected in the eluent-treated cells (Fig. 8b3). As previously described, the compatibility of Optical with regularly used stains permitted its use with DRAQ5 and CellMask Orange. Interestingly, the problems described for the previous two strains were not observed for the iDye PolyPink. Thus, no signals or detrimental visual effects on cell integrity were observed in any of the cases in which the cells were exposed to the iDye PolyPink dye or eluent (Fig. 8c1–3). Consequently, and for all the observations described above, we concluded that this labeling can be considered the most suitable alternative for tracking NPs on biological samples, not only because it does not generate cellular damage but also because it does not interfere with the channels used in confocal microscopy. Moreover, iDye-labeled PET and PS NPs have been reported to be used with Alexa Fluor 488 labeled secondary antibodies with no interference [33,34]. It has been also successfully proven to work well with fluorescent compounds used for cytometry-based mitochondrial potential detection [35] and FITC-marked antibodies for macrophage polarization detection [36]. This versatility in compatibility was difficult or impossible with previously published protocols that use covalently bound FITC emission labeling [37] because the emission cannot be used with regular markers used for intracellular reactive oxygen species detection, such as DHE or DCFH-DA, owing to the overlapping of signals.

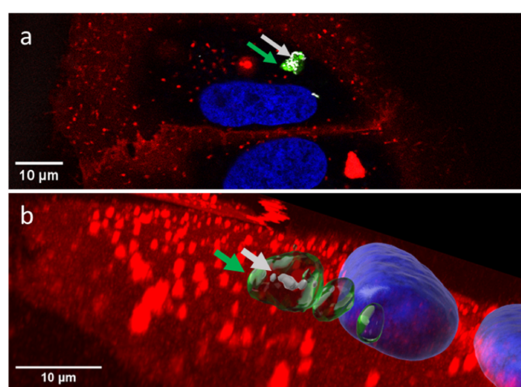


Fig. 9. (a) Confocal image of adherent Huh-7 cells exposed for 24 h to iDP-PET (Ti)NPLs. (b) 3D reconstruction of the image. Colocalization of Ti signal acquired through reflection (grey arrows) and labeled nano polymers-metal (green arrows).

3.8. Simplified protocol for staining and proof of concept

Based on the above results, we selected iDye PolyPink as the dye that offers advantages for staining NPLs. Since the previous work was carried out using pristine PSNPLs, to support the proposal, this study has been extended by using a “true-to-life” NPL model such as PET(Ti)NPLs, stained with iDP (particles called iDP-PET(Ti)NPLs from now on). These Ti-doped PETNPLs were obtained by degrading milk PET bottles [20] and their toxicological profile *in vivo* has recently determined in *Drosophila* [38]. Differentiated human hepatoma (Huh-7) cells were used for this study. These cells have a high ability to internalize NPs and present a wide set of biological responses [39]. Fig. 9 shows the results of the internalization of the iDP-PET(Ti)NPLs by Huh-7 cells, where the hybrid nature of the iDP-PET(Ti)NPLs was easily observed.

As demonstrated, the labeling of the PET moiety was always close to that of the doped titanium NPs, which is characteristic of PET opaque plastic. co-localization of the PET signal (labeled with iDP) and the reflection of Ti were visible in the interior of Huh-7 cells. This was always observed in the confocal images (as indicated in Fig. 9a), as well as in the 3D reconstruction (Fig. 9b), with a negligible background signal. This short study confirmed the effectiveness of the proposed simplified labeling protocol and its potential extension to other types of polymers and different cell types. Specifically, we determined the stability of the iDP labeling. Thus, iDP-labeled MNPLs were used after 8 months without the loss of fluorescence signals. This is another significant advantage of using the iDP.

Importantly, in parallel to this study, iDye PolyPink has been used to label different “true-to-life” nanoplastics aiming to confirm its advantages. Therefore, they have been used to label PET-NPLs resulting from the degradation of PET water bottles, PET(Ti)-NPLs from opaque milk bottles, and polylactic acid (PLA)-NPLs resulting from the release of PLA-teabags, when the process of simulating a cup of teabags. Thus, in *in vitro* studies, PET-labeled NPLs have been used to detect internalization into primary human nasal epithelial (HNEp) cells (Annangi et al., 2023). PET(Ti) labeled-NPLs have also been used to determine internalization in different hematopoietic cell lines, such as TK6 lymphoblasts, THP1 monocytes, and Raji-B lymphocytes [20]. Finally, iDye PolyPink was used to label NPLs from PLA bioplastics to determine their internalization into human intestinal cells such as Caco-2 and HT29, both as undifferentiated and differentiated cells, forming an *in vitro* model of the intestinal barrier [40]. Interestingly, iDye PolyPink labeling has been successfully applied to label PET and PET(Ti)-NPLs in an *in vivo* model, such as *Drosophila*, to demonstrate their uptake by enterocytes of the larval intestine or by hemocytes (with a function similar to lymphocytes in mammals) present in the hemolymph [38,41].

4. Conclusions

As a general conclusion of our study, iDye PolyPink is proposed as a potentially suitable dye to label MNPLs, especially those “true-to-life” resulting from the laboratory degradation of plastic goods of different chemical origins. The evaluation of both widely distributed commercially available PSNPLs and true-to-life nanoplastics confirmed the suitability of the proposed protocol for more complex samples. Noncommercial MNPLs require a robust labeling protocol to confirm their internalization in studies aimed at determining their potential hazardous biological effects. Accordingly, this study provides a detailed and simple protocol for labeling true-to-life MNPLs.

This selection of iDye PolyPink was based on the non-optimum behavior of the other selected dyes in different assays. Thus, 1) for Rhodamine-B, no clear supernatant was obtained, showing a certain effect on treated cell viability, nonspecific staining in confocal studies, and effects on cell integrity at high concentrations. 2) For Nile Red, a colored supernatant was observed despite the cleaning process. Furthermore, the lipophilic nature of the compound may induce nonspecific labeling in a lipid-rich environment, because lipid droplets

are present inside the cell. In such cases, a simpler method to separate the dyed plastic signal from nonspecific staining may be required. 3) Amarillo Luminoso had the clear characteristic of being detectable in all fluorescence investigated channels, which in turn makes its use for biological applications highly disfavored due to its compatibility with fluorophores that are used daily. 4) Opticol presented non-specific fluorescence inside and outside cellular structures, which may have resulted in misinterpretation of the results. Consequently, more complex approaches are required to verify the signals obtained from labeled particles.

In summary, the goodness and compatibility of iDye-labeled nanoplastics with the standardized techniques used to determine their presence in both cells and tissues make the present approach useful for the proposed objectives.

Environmental implication

Environmental micro-/nanoplastics (MNPLs) are emerging pollutants of special concern, and determining their potential risks is essential. Although a large dataset has been obtained using pristine nanoplastics, it is not considered representative of the secondary MNPLs present in the environment. Consequently, obtaining true-to-life MNPLs resulting from the laboratory degradation of plastic goods seems to be an appropriate alternative to fill this gap. Notably, the use of such noncommercial MNPLs requires labeling to confirm their cell/tissue internalization. Although different dyes have been proposed for this purpose, there is a lack of comparative studies showing the advantages and disadvantages of each dye. In this study, after using a wide variety of assays to demonstrate their advantages and disadvantages, iDye Poly-Pink was proposed as the most suitable dye for labeling secondary MNPLs in studies aimed at identifying their internalization. Such labeling can be used in both *in vivo*/*in vitro* models to determine potential environmental and health hazards.

CRedit authorship contribution statement

Jéssica Arribas Arranz: Methodology, Investigation. **Antonia Velázquez:** Supervision, Investigation. **Montserrat López-Mesas:** Writing – review & editing, Writing – original draft, Conceptualization. **Ricard Marcos:** Writing – review & editing, Conceptualization. **Michelle Morataya-Reyes:** Methodology, Investigation. **Fernando Carrillo-Navarrete:** Validation, Investigation. **Susana Pastor:** Supervision, Methodology, Investigation. **Karen Mejía-Carmona:** Supervision, Methodology. **Alba Hernández:** Writing – review & editing, Supervision, Conceptualization. **Victor Fuentes-Cebrian:** Validation, Investigation. **Camila Cazorla-Ares:** Validation, Investigation. **Lourdes Vela:** Validation, Methodology, Investigation. **Iris H. Valido:** Validation, Investigation. **Aliro Villacorta:** Writing – original draft, Methodology, Investigation.

Declaration of Competing Interest

The authors declare that they have no known competing financial interests or personal relationships that could have appeared to influence the work reported in this paper.

Data availability

Data will be made available on request.

Acknowledgments

A. Villacorta was supported by PhD fellowships from the National Agency for Research and Development (ANID), from the CONICYT PFCCHA/DOCTORADO BECAS CHILE/2020-72210237. L. Vela was supported by a Ph.D. fellowship from the Fundación Carolina. M.

Morataya-Reyes hold a Ph.D. FI fellowship from the Generalitat de Catalunya. A. Hernández was granted an ICREA ACADEMIA award. I.H. Valido was supported by “Ayudas Margarita Salas para la formación de jóvenes doctores”, Ministerio de Universidades (Spain).

This project has received funding from the European Union’s Horizon 2020 Research and Innovation Programme under Grant Agreement No. 965196. This work was also partially supported by the Spanish Ministry of Science and Innovation [PID2020-116789, RB-C43], and by the Generalitat de Catalunya (2021-SGR-00731 and 2021-SGR-00723).

Appendix A. Supporting information

Supplementary data associated with this article can be found in the online version at [doi:10.1016/j.jhazmat.2024.135134](https://doi.org/10.1016/j.jhazmat.2024.135134).

References

- [1] Bhat, M.A., Gedik, K., Gaga, E.O., 2023. Atmospheric micro (nano) plastics: future growing concerns for human health. *Air Qual Atmos Health* 16 (2), 233–262. <https://doi.org/10.1007/s11869-022-01272-2>.
- [2] Hartmann, N.B., Hüffer, T., Thompson, R.C., Hassellöv, M., Verschoor, A., Daugaard, A.E., et al., 2019. Are we speaking the same language? Recommendations for a definition and categorization framework for plastic debris. *Environ Sci Technol* 53 (3), 1039–1047. <https://doi.org/10.1021/acs.est.8b05297>.
- [3] Villacorta, A., Rubio, L., Alaraby, M., López-Mesas, M., Fuentes-Cebrian, V., Moriones, O.H., et al., 2022. A new source of representative secondary PET nanoplastics. Obtention, characterization, and hazard evaluation. *J Hazard Mater* 439, 129593 <https://doi.org/10.1016/j.jhazmat.2022.129593>.
- [4] Domenech, J., Annangi, B., Marcos, R., Hernández, A., Catalán, J., 2023. Insights into the potential carcinogenicity of micro- and nano-plastics. *Mutat Res Rev Mutat Res* 791, 108453. <https://doi.org/10.1016/j.mrrev.2023.108453>.
- [5] Rubio, L., Marcos, R., Hernández, A., 2020. Potential adverse health effects of ingested micro- and nanoplastics on humans. Lessons learned from *in vivo* and *in vitro* mammalian models. *J Toxicol Environ Health B Crit Rev* 23 (2), 51–68. <https://doi.org/10.1080/10937404.2019.1700598>.
- [6] Xu, J.L., Lin, X., Wang, J.J., Gowen, A.A., 2022. A review of potential human health impacts of micro- and nanoplastics exposure. *Sci Total Environ* 851 (Pt 1), 158111. <https://doi.org/10.1016/j.scitotenv.2022.158111>.
- [7] Sohail, M., Urooj, Z., Noreen, S., Baig, M.M.F.A., Zhang, X., Li, B., 2023. Micro- and nanoplastics: contamination routes of food products and critical interpretation of detection strategies. *Sci Total Environ* 891, 164596. <https://doi.org/10.1016/j.scitotenv.2023.164596>.
- [8] Liang, J.L., Cao, G.X., Zheng, F.Y., Li, S.X., Liu, F.J., Lin, L.X., et al., 2022. Low-toxic, fluorescent labeled and size-controlled graphene oxide quantum dots@ polystyrene nanospheres as reference material for quantitative determination and *in vivo* tracing. *Chemosphere* 307 (Pt 4), 136094. <https://doi.org/10.1016/j.chemosphere.2022.136094>.
- [9] Zhang, H.J., Zhou, H.R., Pan, W., Wang, C., Liu, Y.Y., Yang, L., et al., 2023. Accumulation of nanoplastics in human cells as visualized and quantified by hyperspectral imaging with enhanced dark-field microscopy. *Environ Int* 179, 108134. <https://doi.org/10.1016/j.envint.2023.108134>.
- [10] Shrutli, V.C., Pérez-Guevara, F., Roy, P.D., Kutralam-Muniasamy, G., 2022. Analyzing microplastics with Nile Red: emerging trends, challenges, and prospects. *J Hazard Mater* 423 (Pt B), 127171. <https://doi.org/10.1016/j.jhazmat.2021.127171>.
- [11] Dutta, S., Misra, A., Bose, S., 2024. Polyoxometalate nanocluster-infused triple IPN hydrogels for excellent microplastic removal from contaminated water: detection, photodegradation, and upcycling. *Nanoscale* 16 (10), 5188–5205. <https://doi.org/10.1039/d3nr06115a>.
- [12] Nalbonte, L., Panebianco, A., Giarratana, F., Russell, M., 2021. Nile Red staining for detecting microplastics in biota: Preliminary evidence. *Mar Pollut Bull* 172, 112888. <https://doi.org/10.1016/j.marpolbul.2021.112888>.
- [13] Greenspan, P., Fowler, S.D., 1985. Spectrofluorometric studies of the lipid probe, Nile Red. *J Lipid Res* 26, 781–789.
- [14] Çelen Erdem, İ., Ünek, C., Akkış, S., Karabiyik Acar, Ö., Yurtsever, M., Şahin, F., 2023. Combined approaches for detecting polypropylene microplastics in crop plants. *J Environ Manag* 347, 119258. <https://doi.org/10.1016/j.jenvman.2023.119258>.
- [15] Mohan, M., Gaonkar, A.A., Pandayanda Nanjappa, D., K.K. Vittal, R., Chakraborty, A., et al., 2023. Screening for microplastics in drinking water and its toxicity profiling in zebrafish. *Chemosphere* 341, 139882. <https://doi.org/10.1016/j.chemosphere.2023.139882>.
- [16] Gao, Z., Wontor, K., Cizdziel, J.V., 2022. Labeling microplastics with fluorescent dyes for detection, recovery, and degradation experiments. *Molecules* 27 (21), 7415. <https://doi.org/10.3390/molecules27217415>.
- [17] Aoki, H., 2022. Material-specific determination based on microscopic observation of single microplastic particles stained with fluorescent dyes. *Sens (Basel)* 22 (9), 3390. <https://doi.org/10.3390/s22093390>.
- [18] Tong, H., Jiang, Q., Zhong, X., Hu, X., 2021. Rhodamine B dye staining for visualizing microplastics in laboratory-based studies. *Environ Sci Pollut Res Int* 28 (4), 4209–4215. <https://doi.org/10.1007/s11356-020-10801-4>.

- [19] Le Quoc, P., Fokina, M.I., Martynova, D.M., Olekhovich, R.O., Uspenskaya, M.V., 2022. Method of manufacturing and staining microplastics for using in the biological experiments. *Environ Sci Pollut Res Int* 29 (44), 67450–67455. <https://doi.org/10.1007/s11356-022-22776-5>.
- [20] Villacorta, A., Vela, L., Morataya-Reyes, M., Llorens-Chiralt, R., Rubio, L., Alaraby, M., et al., 2023. Titanium-doped PET nanoplastics of environmental origin as a true-to-life model of nanoplastic. *Sci Total Environ* 880, 163151. <https://doi.org/10.1016/j.scitotenv.2023.163151>.
- [21] Karakolis, E.G., Nguyen, B., You, J.B., Rochman, C.M., Sinton, D., 2019. Fluorescent dyes for visualizing microplastic particles and fibers in laboratory-based studies. *Environ Sci Technol Lett* 6 (6), 334–340. <https://doi.org/10.1021/acs.estlett.9b00241>.
- [22] Maes, T., Jessop, R., Wellner, N., Haupt, K., Mayes, A.G., 2017. A rapid screening approach to detect and quantify microplastics based on fluorescent tagging with Nile Red. *Sci Rep* 7, 44501. <https://doi.org/10.1038/srep44501>.
- [23] Bhattacharjee, S., 2016. DLS and zeta potential - what they are and what they are not. *J Control Release* 235, 337–351. <https://doi.org/10.1016/j.jconrel.2016.06.017>.
- [24] Rubio, L., Barguilla, I., Domenech, J., Marcos, R., Hernández, A., 2020. Biological effects, including oxidative stress and genotoxic damage, of polystyrene nanoparticles in different human hematopoietic cell lines. *J Hazard Mater* 398, 122900. <https://doi.org/10.1016/j.jhazmat.2020.122900>.
- [25] Gualtieri, M., Skuland, T., Iversen, T.G., Låg, M., Schwarze, P., Bilanićová, D., et al., 2012. Importance of agglomeration state and exposure conditions for uptake and pro-inflammatory responses to amorphous silica nanoparticles in bronchial epithelial cells. *Nanotoxicology* 6 (7), 700–712. <https://doi.org/10.3109/17435390.2011.604441>.
- [26] Macairan, J.-R., Nguyen, B., Li, F., Tufenkji, N., 2023. Tissue clearing to localize microplastics via three-dimensional imaging of whole organisms. *Environ Sci Technol* 57 (23), 8476–8483. <https://doi.org/10.1021/acs.est.2c07209>.
- [27] Nguyen, B., Tufenkji, N., 2022. Single-particle resolution fluorescence microscopy of nanoplastics. *Environ Sci Technol* 56, 6426–6435. <https://doi.org/10.1021/acs.est.1c08480>.
- [28] Rodríguez-Hernández, A.G., Muñoz-Tabares, J.A., Aguilar-Guzmán, J.C., Vázquez-Duhalt, R., 2019. A novel and simple method for polyethylene terephthalate (PET) nanoparticle production. *Environ Sci Nano* 6 (7), 2031–2036. <https://doi.org/10.1039/c9en00365g>.
- [29] Chithrani, B.D., Ghazani, A.A., Chan, W.C.W., 2006. Determining the size and shape dependence of gold nanoparticle uptake into mammalian cells. *Nano Lett* 6 (4), 662–668. <https://doi.org/10.1021/nl052396o>.
- [30] Peñaloza, J.P., Márquez-Miranda, V., Cabaña-Brunod, M., Reyes-Ramírez, R., Llancahuen, F.M., Vilos, C., et al., 2017. Intracellular trafficking and cellular uptake mechanism of PHBV nanoparticles for targeted delivery in epithelial cell lines. *J Nanobiotechnol* 15 (1). <https://doi.org/10.1186/s12951-016-0241-6>.
- [31] Chaloupková, Z., Žárská, L., Belza, J., Poláková, K., 2023. Label-free detection and mapping of graphene oxide in single HeLa cells based on MCR-Raman spectroscopy. *Anal Methods* 15 (42), 5582–5588. <https://doi.org/10.1039/d3ay01122d>.
- [32] Liu, Y., Peng, Z., Peng, X., Yan, W., Yang, Z., Qu, J., 2021. Shedding new lights Into STED microscopy: emerging nanoprobe for imaging (Frontiers Media S.A.). *Front Chem* Vol. 9. <https://doi.org/10.3389/fchem.2021.641330>.
- [33] Annangi, B., Villacorta, A., Vela, L., Tavakolpournegari, A., Marcos, R., Hernández, A., 2023. Effects of true-to-life PET nanoplastics using primary human nasal epithelial cells. *Environ Toxicol Pharmacol* 100, 104140. <https://doi.org/10.1016/j.etap.2023.104140>.
- [34] Annangi, B., Villacorta, A., López-Mesas, M., Fuentes-Cebrian, V., Marcos, R., Hernández, A., 2023. Hazard assessment of polystyrene nanoplastics in primary human nasal epithelial cells, focusing on the autophagic effects. *Biomolecules* 13, 220. <https://doi.org/10.3390/biom13020220>.
- [35] Tavakolpournegari, A., Annangi, B., Villacorta, A., Banaei, G., Martin, J., Pastor, S., et al., 2023. Hazard assessment of different-sized polystyrene nanoplastics in hematopoietic human cell lines. *Chemosphere* 325, 138360. <https://doi.org/10.1016/j.chemosphere.2023.138360>.
- [36] Tavakolpournegari, A., Villacorta, A., Morataya-Reyes, M., Arribas Arranz, J., Banaei, G., Pastor, S., et al., 2024. Harmful effects of true-to-life nanoplastics derived from PET water bottles in human alveolar macrophages. *Environ Pollut* 348, 123823. <https://doi.org/10.1016/j.envpol.2024.123823>.
- [37] Magri, D., Sánchez-Moreno, P., Caputo, G., Gatto, F., Veronesi, M., Bardi, G., et al., 2018. Laser ablation as a versatile tool to mimic polyethylene terephthalate nanoplastic pollutants: characterization and toxicology assessment. *ACS Nano* 12 (8), 7690–7700. <https://doi.org/10.1021/acsnano.8b01331>.
- [38] Alaraby, M., Villacorta, A., Abass, D., Hernández, A., Marcos, R., 2024. Titanium-doped PET nanoplastics, from opaque milk bottle degradation, as a model of environmental true-to-life nanoplastics. Hazardous effects on *Drosophila*. *Environ Pollut* 341, 122968. <https://doi.org/10.1016/j.envpol.2023.122968>.
- [39] Alsubaie, S.M., Ali, D., Almutairi, B.O., Almeer, R., Alarifi, S., 2022. Evaluation of cyto- and genotoxic influence of lanthanum dioxide nanoparticles on human liver cells, 15593258221128428 Dose Response 20 (3). <https://doi.org/10.1177/155932582211284>.
- [40] Banaei, G., García-Rodríguez, A., Tavakolpournegari, A., Martín-Pérez, J., Villacorta, A., Marcos, R., et al., 2023. The release of polylactic acid nanoplastics (PLA-NPLs) from commercial teabags. Obtention, characterization, and hazard effects of true-to-life PLA-NPLs. *J Hazard Mater* 458, 131899. <https://doi.org/10.1016/j.jhazmat.2023.131899>.
- [41] Alaraby, M., Villacorta, A., Abass, D., Hernández, A., Marcos, R., 2023. The hazardous impact of true-to-life PET nanoplastics in *Drosophila*. *Sci Total Environ* 863, 160954. <https://doi.org/10.1016/j.scitotenv.2022.160954>.

7.3.1. Supplementary material of the article entitled *Fluorescent labeling of micro/nanoplastics for biological applications with a focus on “true-to-life” tracking*

Fluorescent labeling of micro/nanoplastics for biological applications with a focus on “true-to-life” tracking

Aliro Villacorta^{a,b,#}, Camila Cazorla-Ares^{c,#}, Victor Fuentes-Cebrian^c, Iris H. Valido^c, Lourdes Vela^{a,d}, Fernando Carrillo-Navarrete^e, Michelle Morataya-Reyes^a, Karen Mejia-Carmona^f, Susana Pastor^a, Antonia Velázquez^a, Jessica Arribas Arranz^a, Ricard Marcos^a, Montserrat López-Mesas^{c,*}, Alba Hernández^{a,*}

^aGroup of Mutagenesis, Department of Genetics and Microbiology, Faculty of Biosciences, Universitat Autònoma de Barcelona, Cerdanyola del Vallès, 08193, Spain.

^bFacultad de Recursos Naturales Renovables, Universidad Arturo Prat, Iquique, Chile.

^cGTS Research Group, Department of Chemistry, Faculty of Science, Universitat Autònoma de Barcelona, Cerdanyola del Vallès, 08193, Barcelona, Spain.

^dFaculty of Health Sciences Eugenio Espejo, Universidad UTE, Quito, Ecuador.

^eInstitut d'Investigació Tèxtil i Cooperació Industrial de Terrassa (INTEXTER) and Department of Chemical Engineering, Universitat Politècnica de Catalunya, Terrassa, 08222, Barcelona, Spain.

^fInstitut Català de Nanociència i Nanotecnologia (ICN2-UAB-CSIC-BIST), Cerdanyola del Vallès Spain.

SUPPLEMENTARY MATERIAL

Table S1. Array and gain of the detectors used for the detection of fluorescence signal on percolate product of the nanoplastic labelling procedures.

Channel	Gain
FSC	50
SSC	50
Violet	1
B525-FITC	88
B610-ECD	132
B690-PC5.5	301
Y585-PE	150
Y610-mCherry	121
Y675-PC5	127
Y710-PC5.5	143
Y763-PC7	669
R660-APC	487
R712-APCA700	464
R763-APCA750	841
V450-PB	65
V525-KrO	39
V660	213
V763	389
NUV450	85
NUV525	119
NUV675	179

Table S2. Max. excitation (nm) and Max. emission (nm) wavelengths for the compounds used in this study.

Compounds	λ_{exc} (nm)	λ_{em} (nm)
Nile Red	554	635
Rhodamine B	552	575
Amarillo Luminoso	500	544
i-Dye Poly Pink	560	584
Opticol	464	484

Table S3. Z-average size values, polydispersity indexes and Z-potential for all dyed particles investigated in this study. *Stand for single repetition.

PSNPLs	Z-Average	PDI	Z-Pot
NR	539.00* \pm 0.00	0.69	46.10 \pm 7.75
RhB	362.00 \pm 4.80	0.27	-31.20 \pm 0.64
AL	363.00 \pm 0.89	0.25	-40.30 \pm 0.26
Op	309.00 \pm 1.42	0.34	-22.60 \pm 0.73
iDP	352.00 \pm 5.44	0.62	-28.30 \pm 1.59

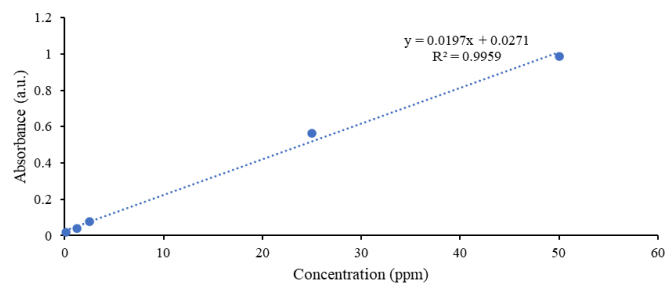
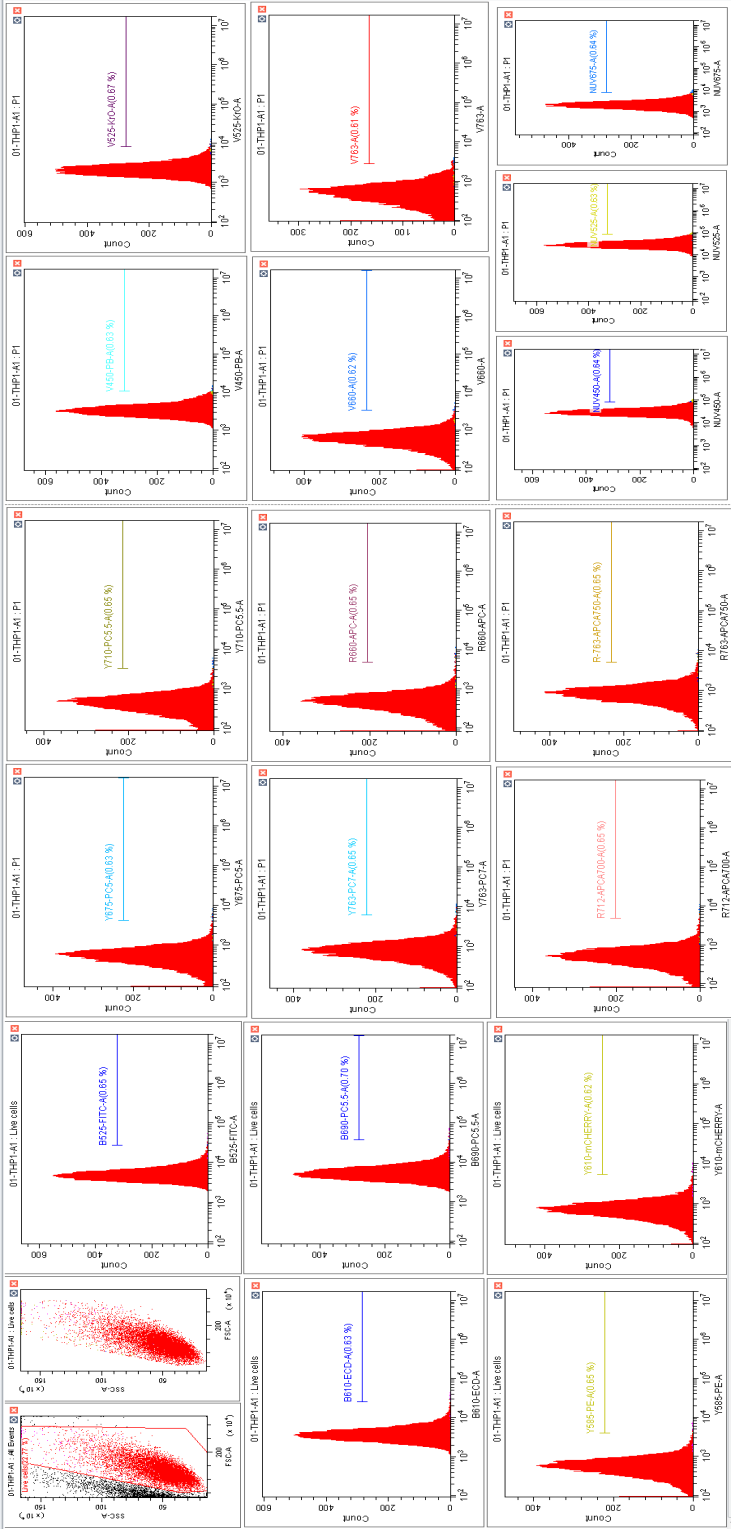


Figure S1. Calibration curve of PSNPLs dispersions in water by UV-Vis spectroscopy.

SEQ1. Equation for the concentration of NPLs on the concentration basis.

$$\text{Separation Yield (\%)} = \left(\frac{C_{\text{before centrifugation}} - C_{\text{after centrifugation}}}{C_{\text{before centrifugation}}} \right) \cdot 100$$

Figure S2. Eluent and particle evaluation by Flow Cytometry. I. Role of eluent (S2a-f)



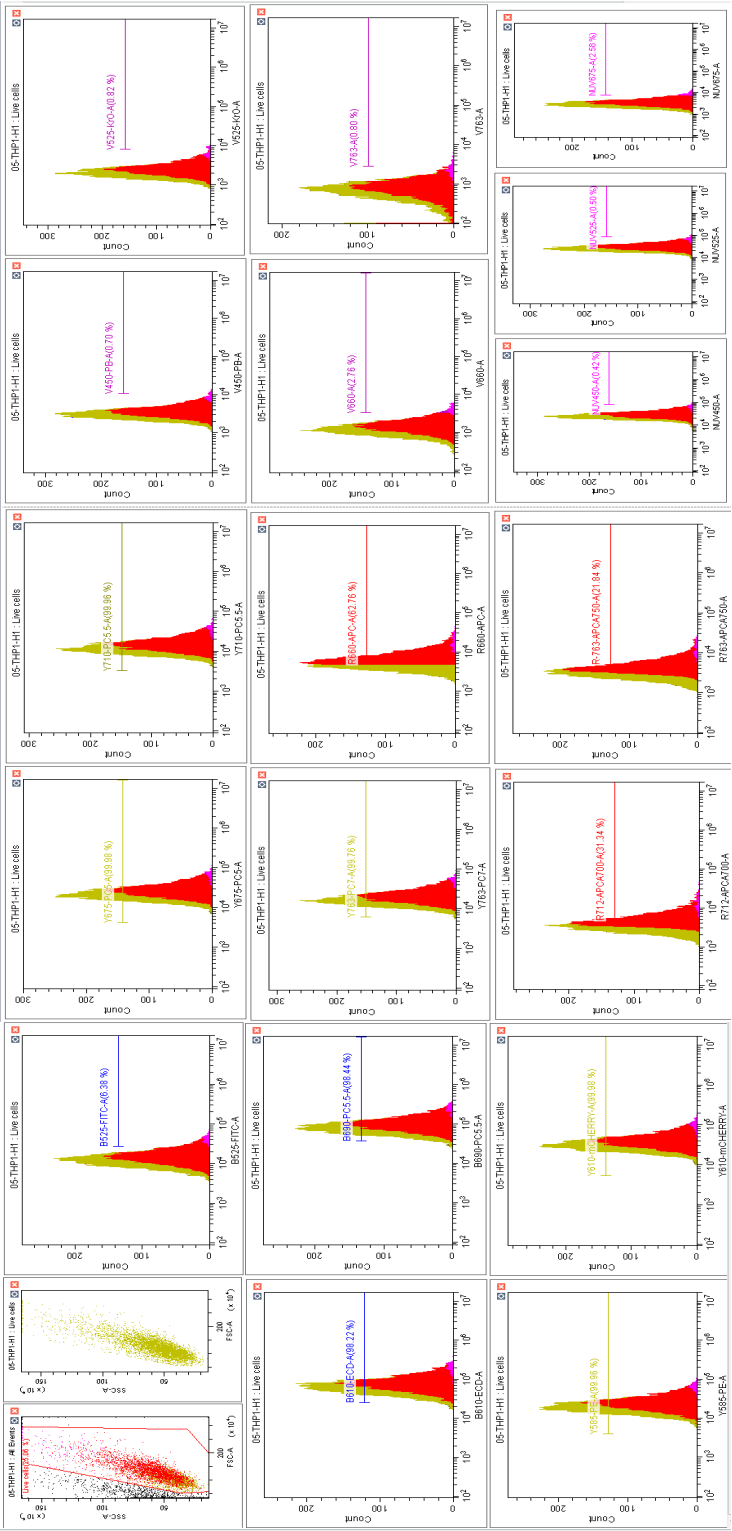


Figure S2b. THP1 cells exposed for 24 h to 100 µg/mL of NR-PSNPLs labeling eluent.

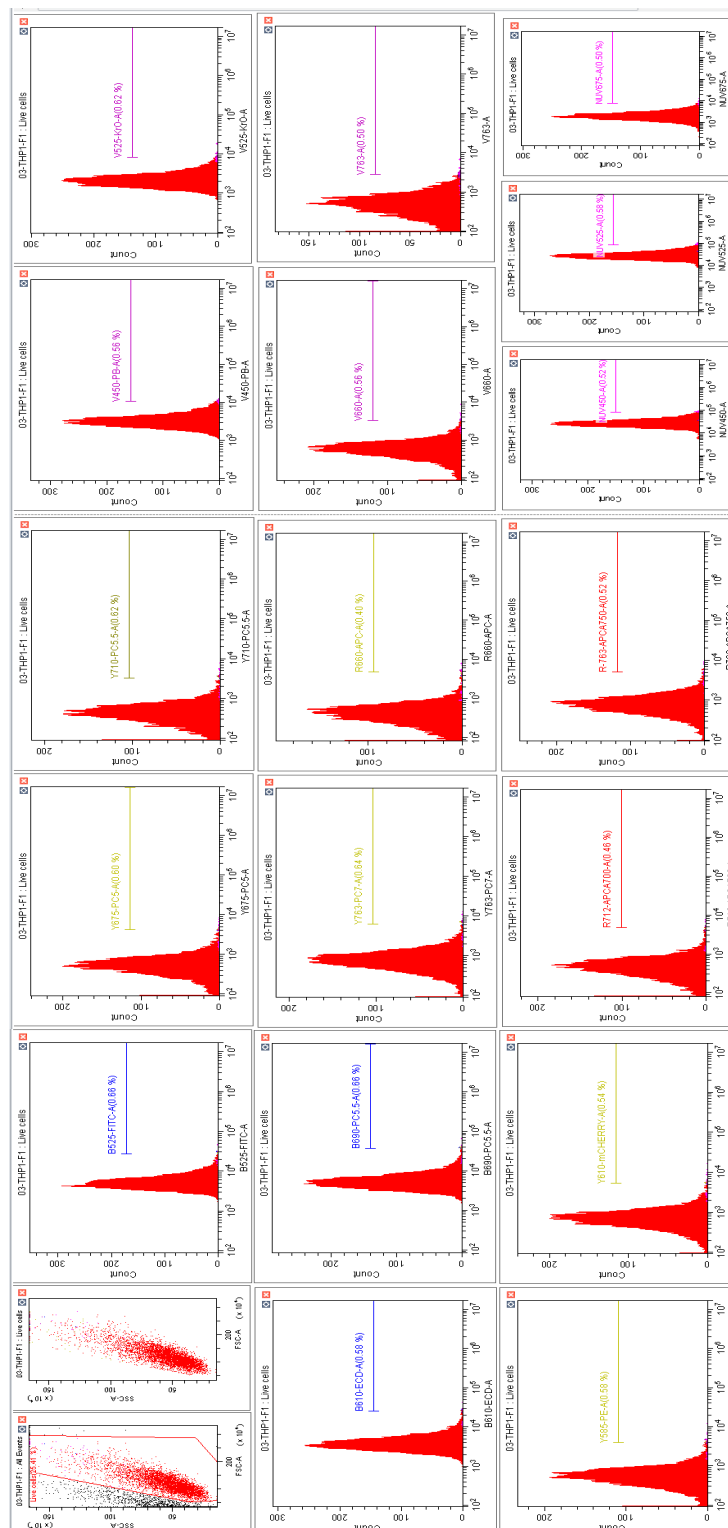


Figure S2c. THP1 cells exposed for 24 h to 100 $\mu\text{g/mL}$ of RhB-PSNPLs labeling eluent.

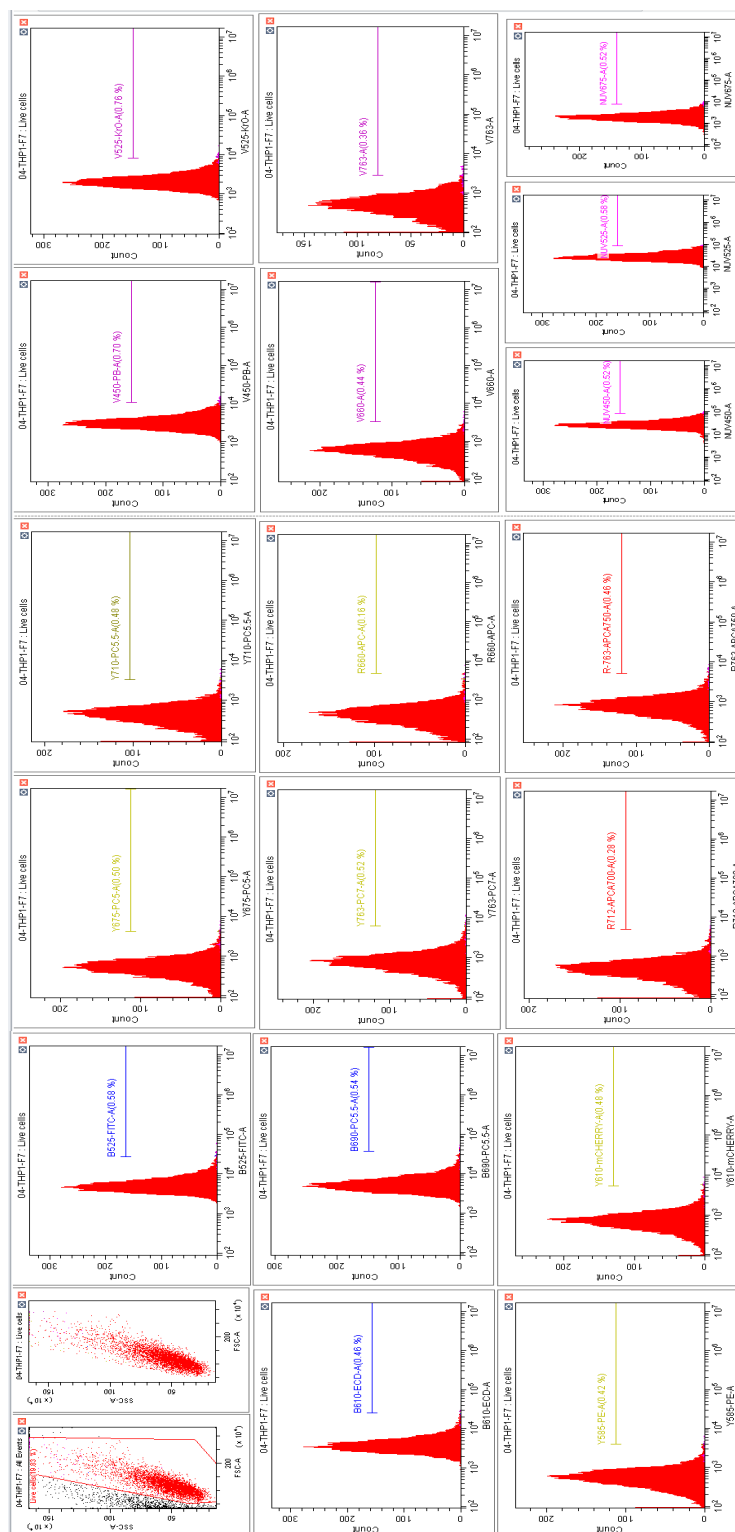


Figure S2d. THP1 cells exposed for 24 h to 100 µg/mL of ALPSNPLs labelling eluent.

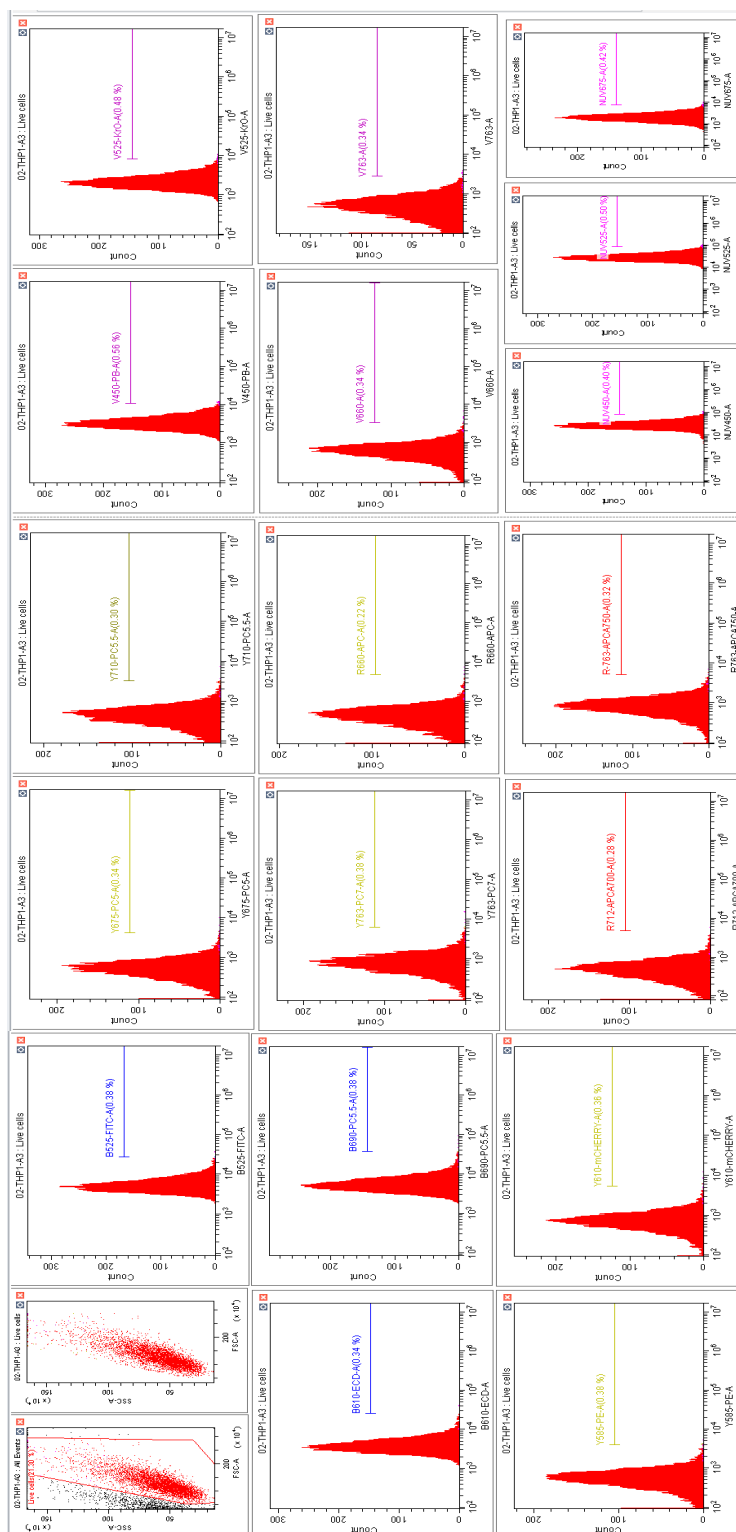


Figure S2e. THP1 cells exposed for 24 h to 100 $\mu\text{g/mL}$ of O-PSNPLs labeling eluent.

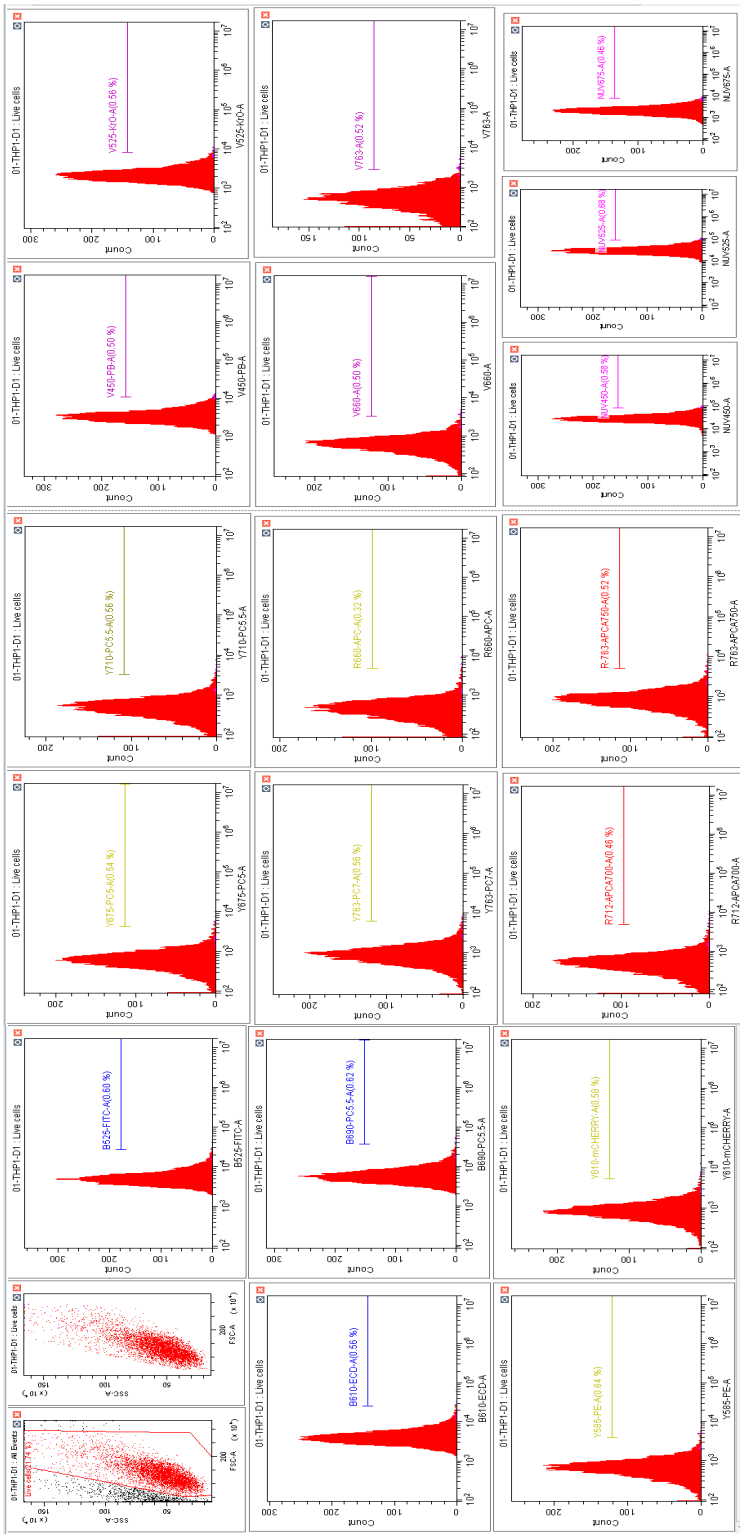


Figure S2f. THP1 cells were exposed for 24 h to 100 µg/mL of P-PSNPLs labeling eluent.

Figure S2. Eluent and particle evaluation by Flow Cytometry. II. Role of particle (**S2g-I**)

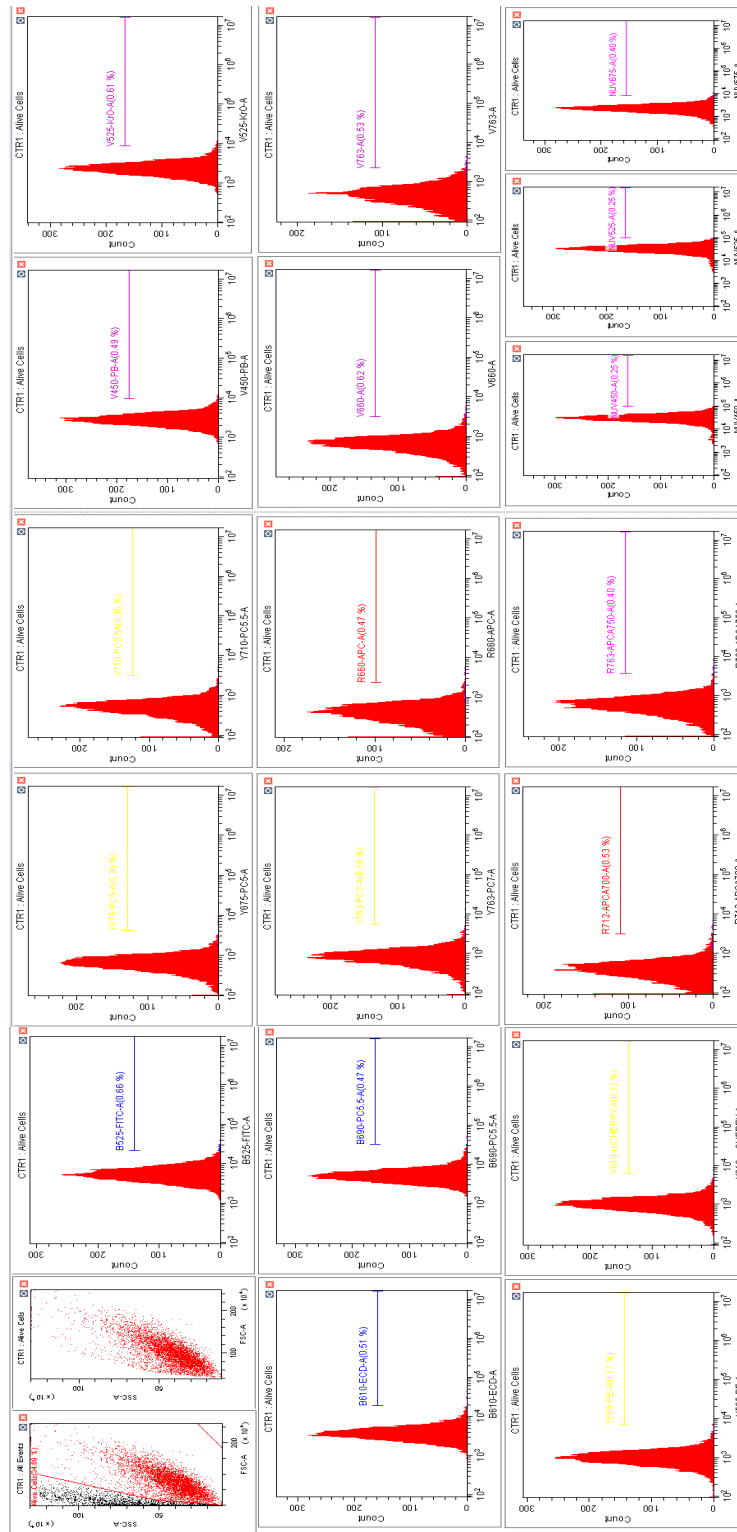
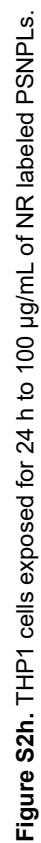


Figure S2g. THP1 cells control



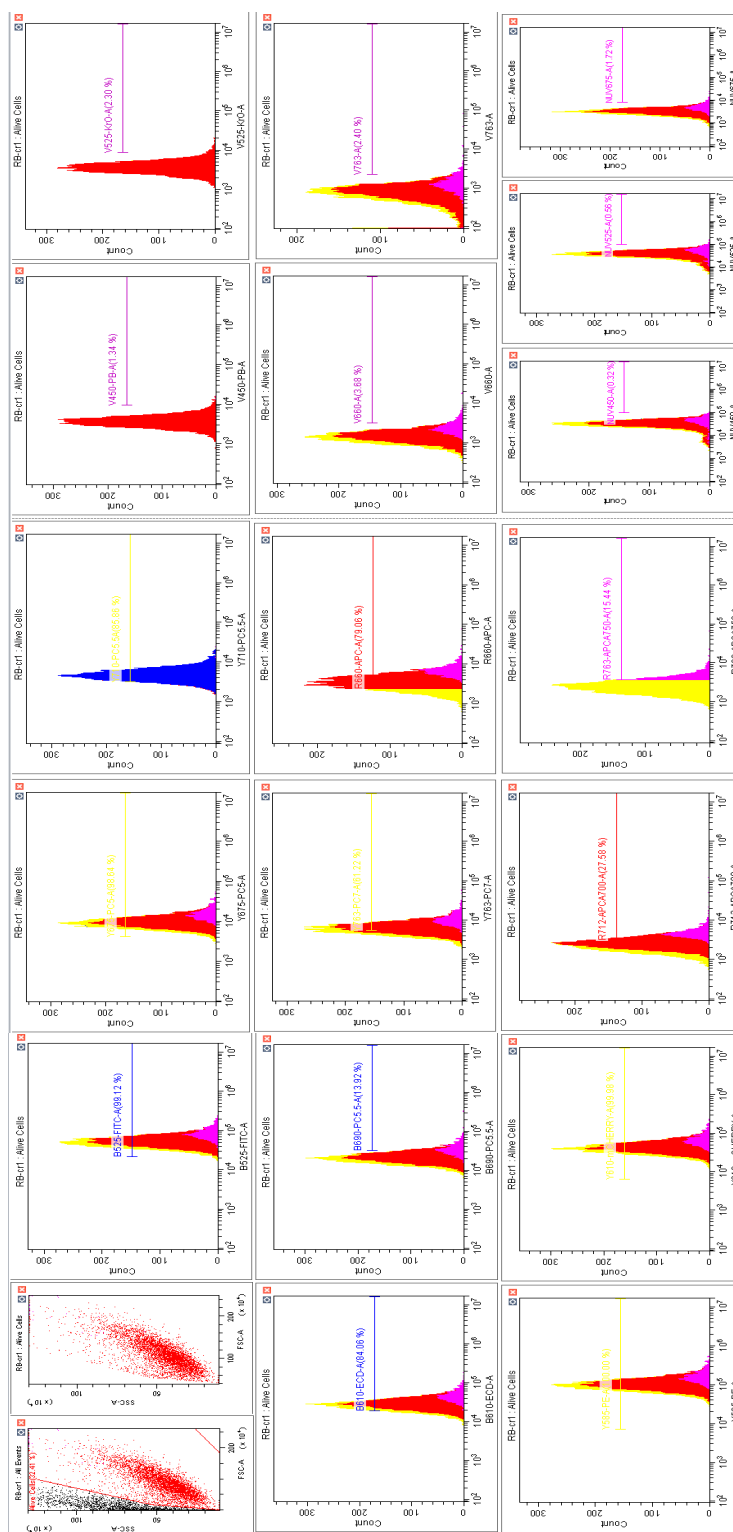


Figure S2i. THP1 cells exposed for 24 h to 100 $\mu\text{g/mL}$ of RhB -labeled PSNPLs.

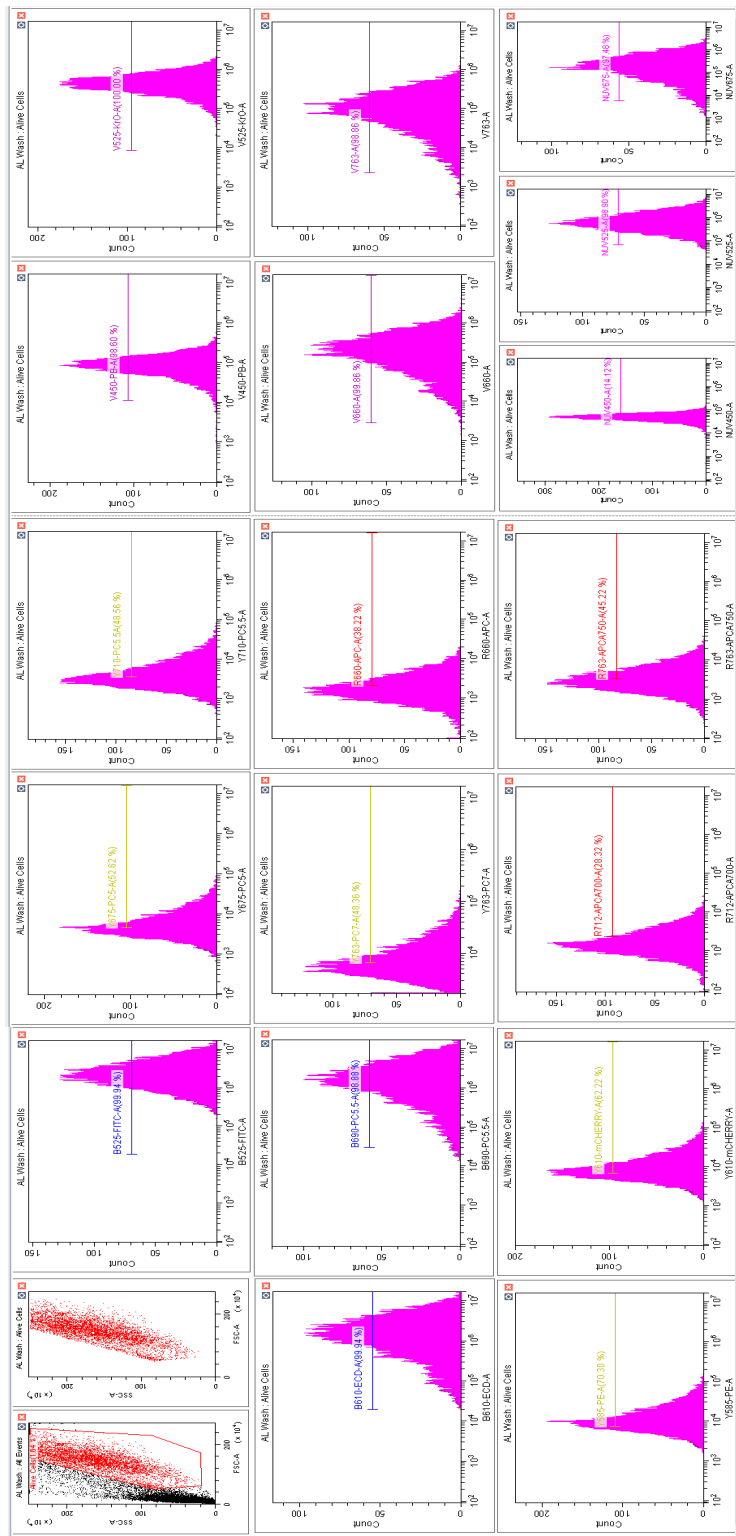


Figure S2j. THP1 cells exposed for 24 h to 100 µg/mL of AL-labeled PSNPLs.

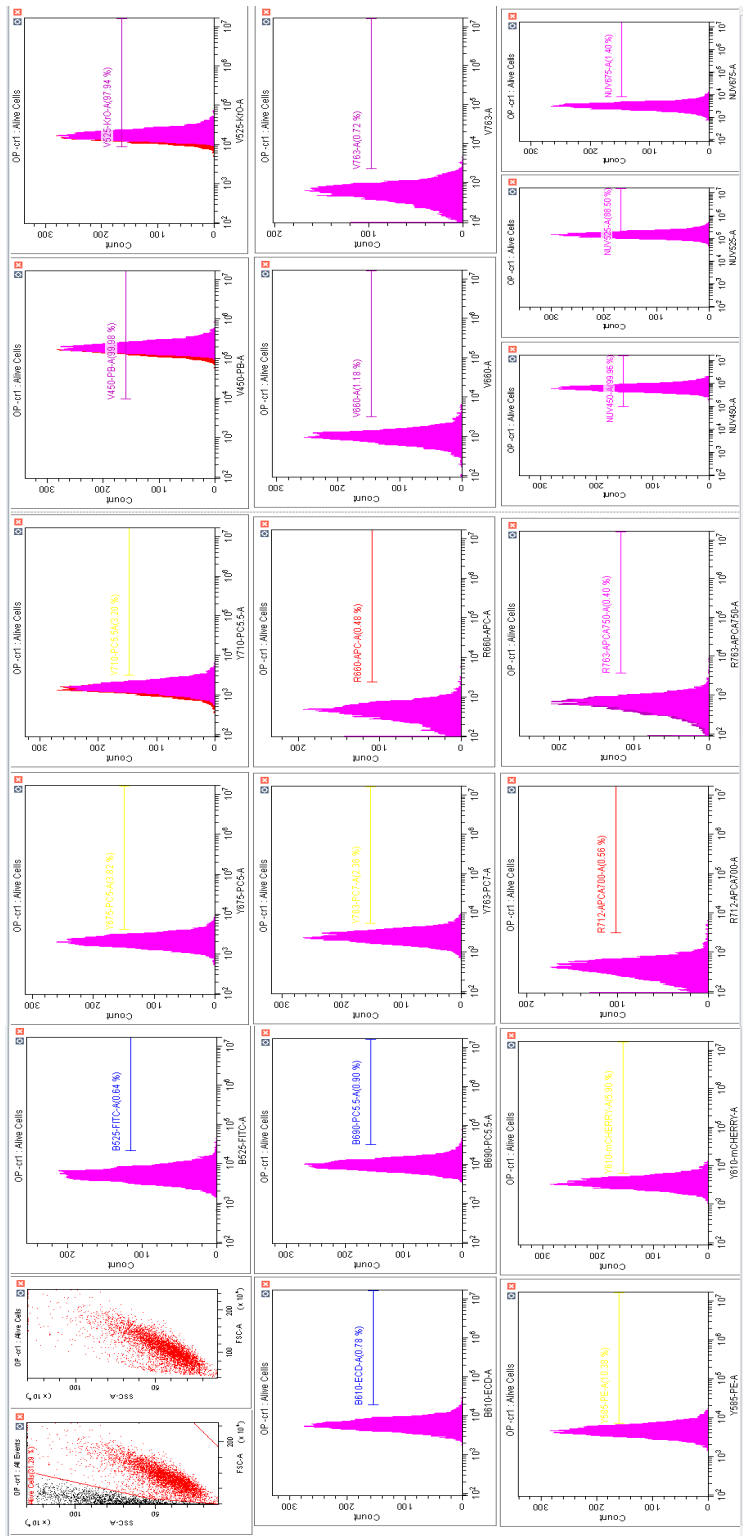


Figure S2k. THP1 cells exposed for 24 h to 100 µg/mL of O-labeled PSNPLs.

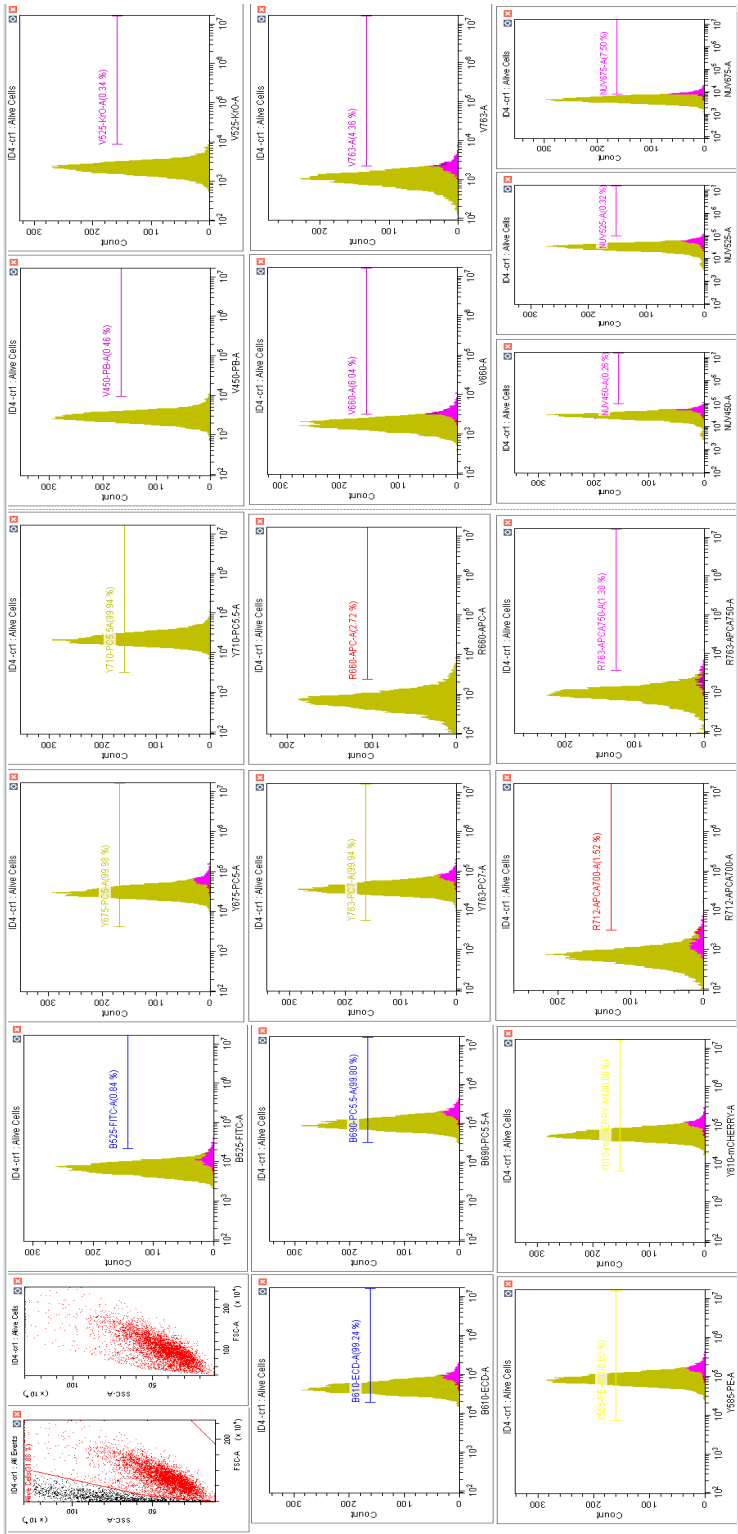


Figure S2I. THP1 cells exposed for 24 h to 100 µg/mL of P labelled PSNPLs.

Figure S3. Results from the studies carried out using HeLa cells

Figure S3.1. Exposure conditions for HeLa cells

- *Cell culture & treatment*

HeLa immortalized human cervix adenocarcinoma cells were obtained from "Centro Nacional de Investigaciones Oncológicas" CNIO (Madrid, Spain). Cells were maintained in culture on filtered cap T-25 flasks (SPL, Life Sciences. Pocheon-si, Gyeonggi-do, Republic of Korea), on Dulbecco's Modified Eagle's medium (DMEM) supplemented with 10% fetal bovine serum (FBS), purchased on Biowest (France), and Plasmocin (InvivoGen, CA, USA), respectively. For ¹²⁵I-labelled-NPLs exposures 50,000 cells per well were seeded and cultured on flat bottom 6 wells plates for 24 h. Then the media was removed by aspiration and replaced with 1.5 mL of freshly prepared particle suspension (100 µg/mL) on previously described medium, pre warmed at 37 °C and incubated for 24 h prior to flow cytometry analysis. Similarly, for confocal visualization, 7,000 cells were seeded and cultured on µ-Slide 8 well ^{high} Glass bottom, purchased on ibidi GmbH (Gräfelfing, Germany) for 24 h prior to treatments carried out as previously described. For both cases, cells were maintained at standard growing conditions of 37 °C, in humidified atmosphere with 5% CO₂ (Carbueros Metálicos, Cornellà de Llobregat, Spain) on a ICO150med CO₂ incubator (Memmert GmbH + Co KG Schwabach, Germany).

- *Flow cytometry preparation*

After the 24 h incubation with the different fluorescent NPLs, cells were washed twice with 1 mL of phosphate-buffered saline (PBS 1X), purchased on Gibco, Thermo Fischer Scientific (Massachusetts, USA). Cells were then trypsinized using 1x Trypsin (Biowest, France) on PBS and incubated for 5 min at standard conditions. Cells were then resuspended by gently pipetted up and down 4 times and then 5% 250 µL of FBS 5% on PBS was used as inactivator. Cells were then transferred to cytometry tubes and kept on ice protected from light to immediately be investigated using a Cytotoflex LX flow cytometer (Beckman Coulter INC., CA. USA).

- *Confocal microscopy preparation*

After the 24 h incubation with the different fluorescent NPLs, cells were washed twice with 1 mL of phosphate-buffered saline (PBS 1X), purchased on Gibco, Thermo Fischer Scientific (Massachusetts, USA). 250 µL of pre-warmed medium was added to each well and the plates were investigated immediately on a Leica TCS SP5 confocal microscope (Leica Microsystems CMS GmbH, Mannheim, Germany).

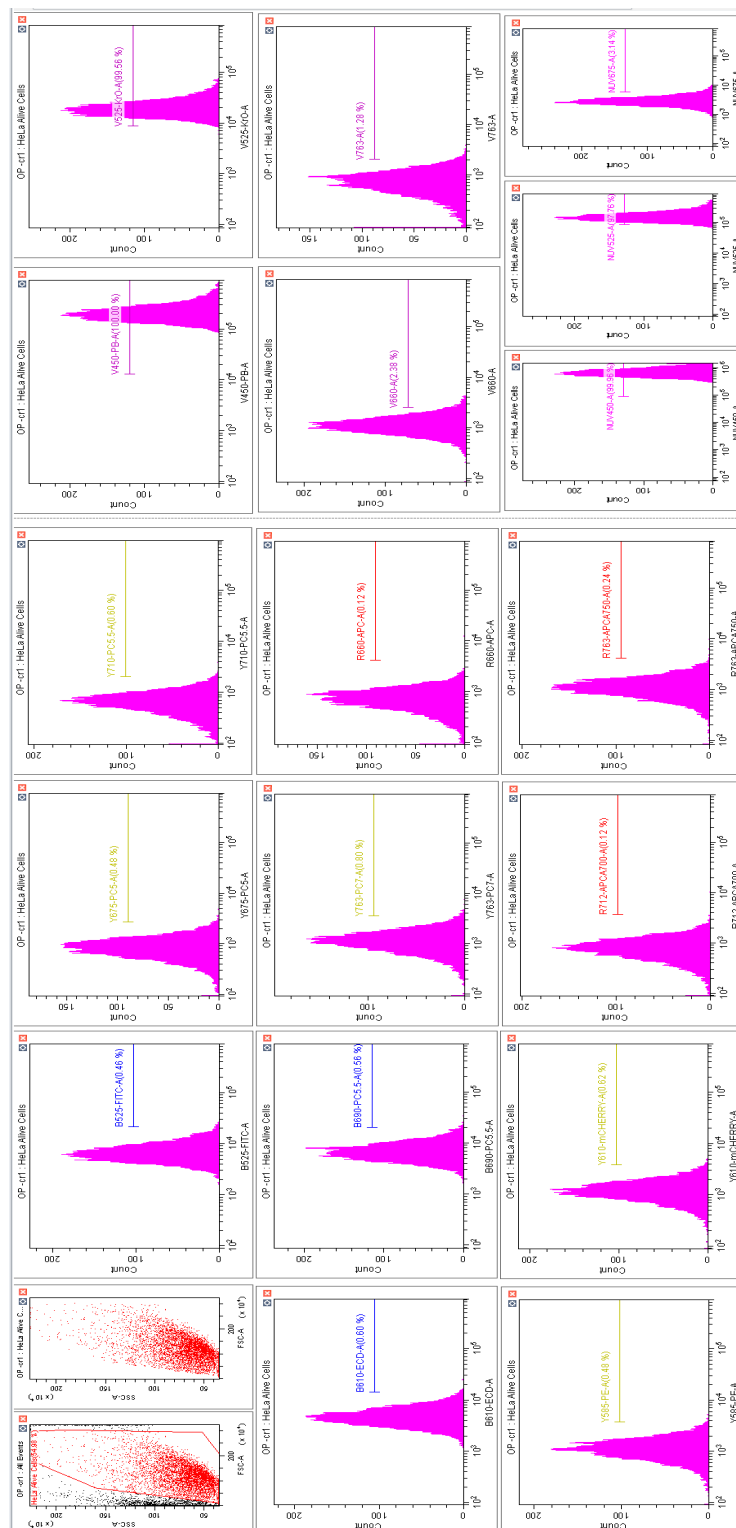


Figure S3.2b. HeLa cells exposed for 24 h to 100 $\mu\text{g/mL}$ of optical (Op)-labeled PSNPLs

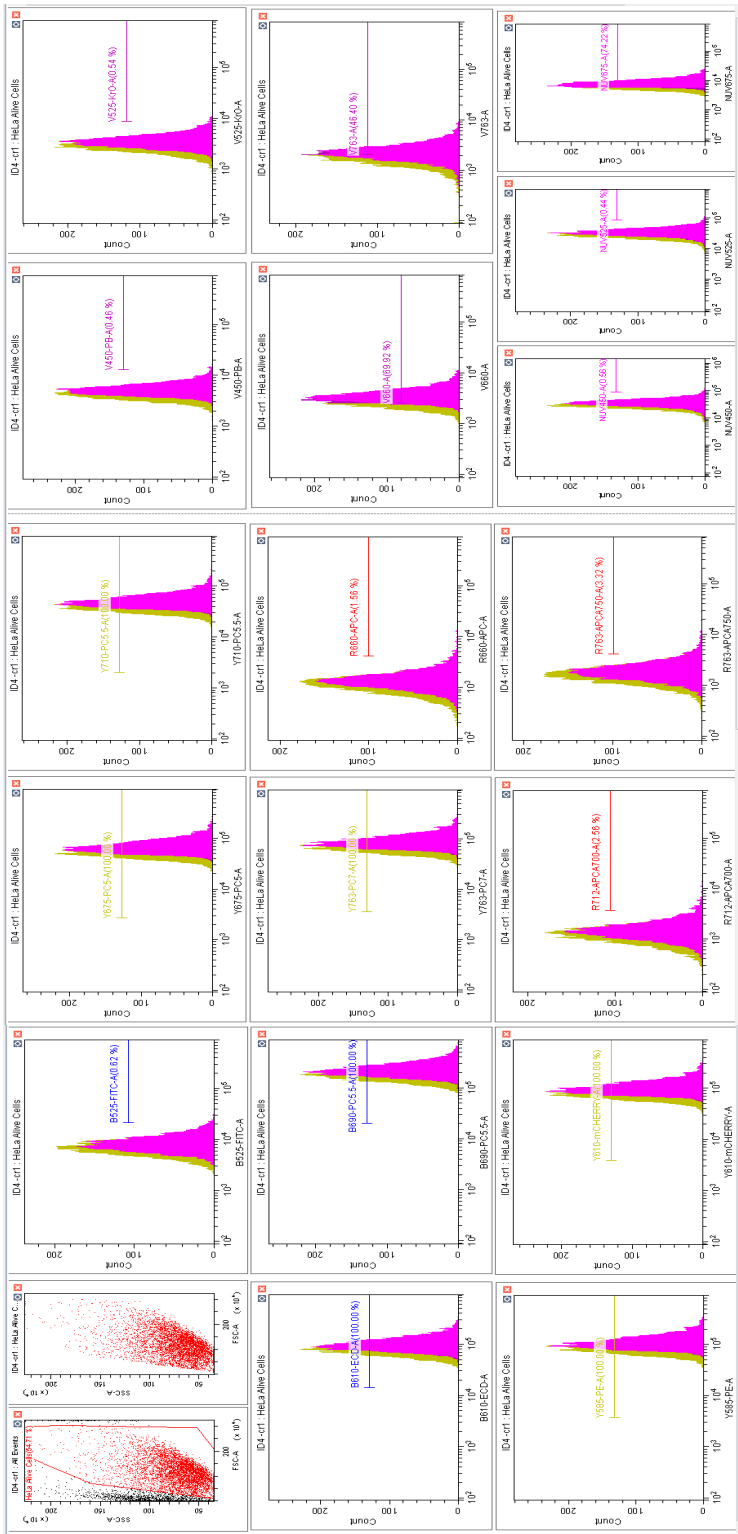


Figure S3.2c. HeLa cells exposed for 24 h to 100 µg/mL of iDye PolyPink (iDP)-labeled PSNPLs

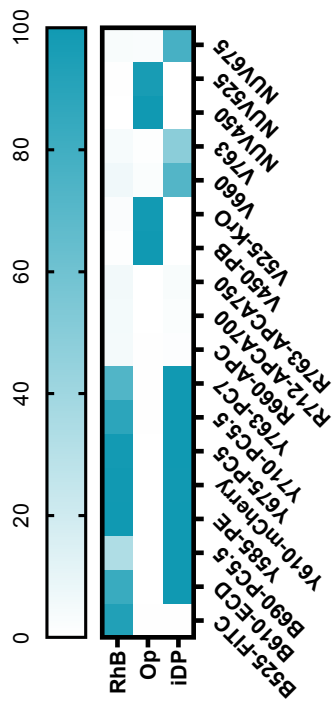


Figure S3.3. Flow cytometry evaluation of the emission on HeLa cells exposed for 24 h to rhodamine-B (RhB), optical (Op) and iDye PolyPink (iDP)-labeled PSNPLs at concentrations of 100 µg/mL evaluated by blue (B), yellow (Y), red (R), violet (V), and near UV (NUV) laser excitation and the corresponding wavelengths. The emissions are presented as the percentage of cells that emit at the corresponding wavelengths.

